WASHINGTON UNIVERSITY

SCHOOL OF ENGINEERING AND APPLIED SCIENCE
DEPARTMENT OF CIVIL ENGINEERING

ANALYTICAL METHOD FOR DETERMINING SEISMIC RESPONSE OF COOLING TOWERS ON FOOTING FOUNDATIONS

First Interim Report

NSF Grant No. PFR-7900012

by

Osama El-Shafee

and

Phillip L. Gould

Research Report No. 55 Structural Division Sept. 1979

ANALYTICAL METHOD FOR DETERMINING SEISMIC RESPONSE OF COOLING TOWERS ON FOOTING FOUNDATIONS

First Interim Report

NSF Grant No. PFR-7900012

by

Osama El-Shafee

and

Phillip L. Gould

Research Report No. 55 Structural Division Sept. 1979

i.a

50272-101

REPORT DOCUMENTATION PAGE

1. REPORT NO. NSF/RA-790165

2.

3. Recipient's Accession No. PB301308

4. Title and Subtitle
Analytical Method for Determining Seismic Response of Cooling Towers on Footing Foundations, First Interim Report

5. Report Date
September, 1979

6.

7. Author(s)
O. El-Shafee, P. L. Gould

8. Performing Organization Rept. No.
55

9. Performing Organization Name and Address
Washington University
School of Engineering and Applied Science
Department of Civil Engineering
St. Louis, Missouri 63011

10. Project/Task/Work Unit No.

11. Contract(C) or Grant(G) No.
(C)
(G) PFR7900012

12. Sponsoring Organization Name and Address
Engineering and Applied Science (EAS)
National Science Foundation
1800 G Street, N.W.
Washington, D.C. 20550

13. Type of Report & Period Covered
First interim

14.

15. Supplementary Notes

16. Abstract (Limit: 200 words)
A finite element model was developed to analyze shells of revolution under dynamic loading with soil-structure interaction effects. The model consists of high-precision rotational shell finite elements, representing the axisymmetric shell, supported on an equivalent boundary system, representing the soil medium. The substructure method is used to model the shell and soil components. In addition to the seismic analysis capability of the proposed model, it is also applicable to other dynamic loads such as wind. The dynamic behavior of a hyperboloidal cooling tower is studied using the proposed model. Dynamic properties are studied and stress analysis is carried out for a variety of soil conditions. The appendices include high precision rotational shell elements, details of stiffness matrix for an isoparametric solid element, a listing of the SUBASE Program, and modifications and additions for the User's Manual of the SHORE-III Program.

17. Document Analysis a. Descriptors
Dynamic tests
Loading (structural)
Model tests
Rotation
Soil structure
Cooling towers
Analyzing
Shells (structural forms)

b. Identifiers/Open-Ended Terms
Finite element model
SUBASE Program
SHORE-III Program
Shells of revolution

c. COSATI Field/Group

18. Availability Statement
NTIS

19. Security Class (This Report)

20. Security Class (This Page)

21. No. of Pages
228

22. Price
A11-A01

(See ANSI-Z39.18) See Instructions on Reverse OPTIONAL FORM 272 (4-77)
(Formerly NTIS-35)
Department of Commerce

ABSTRACT

A finite element model has been developed to analyze shells of revolution under dynamic loading with soil-structure interaction effects. The model consists of high-precision rotational shell finite elements, representing the axisymmetric shell, supported on an equivalent boundary system, representing the soil medium. The substructure method is used to model the shell and soil components. In addition to the seismic analysis capability of the proposed model, it is also applicable to other dynamic loads such as wind. The dynamic behaviour of a hyperboloidal cooling tower shell on discrete supports with a ring footing is studied using the proposed model. Dynamic properties are studied and stress analysis is carried out for a variety of soil conditions.

TABLE OF CONTENTS

TABLE OF CONTENTS
(continued)

TABLE OF CONTENTS
(continued)

LIST OF TABLES

LIST OF FIGURES

LIST OF FIGURES
(continued)

LIST OF FIGURES
(continued)

LIST OF FIGURES
(continued)

DYNAMIC ANALYSIS OF SHELLS OF REVOLUTION-SOIL SYSTEMS

1. INTRODUCTION

1.1 GENERAL

Recently, considerable effort has been made by researchers to obtain more realistic mathematical models for thin shells of revolution under dynamic loads. Without the foundation interaction in structure response, the dynamic model, in general, is expected to be inadequate. It is well known that the response of structures to dynamic loads will be influenced by deformability of the foundation. The significance of foundation interaction in structure response depends on the properties of the structure relative to the foundation.

Although a great deal of attention has been devoted to nuclear containment structures, dams and multistory buildings (1,2,3)*, the influence of the surrounding medium on the dynamic response of large towers and shells of revolution

* The numbers in parentheses in the text indicate references in the Bibliography.

has apparently not been studied extensively. For massive structures like large shells, part of the structure energy is dissipated into the supporting medium by radiation of waves and by hysteretic action in the medium itself, causing in most cases a significant reduction in the structure response. The importance of this factor increases with increasing intensity of ground shaking (4).

In the present report, a numerical method is presented for the dynamic analysis of axisymmetric shell structures resting on viscoelastic soil layers over rock of infinite horizontal extent. The approach used in this research is tempered by the availability and potential of the high precision rotational shell finite element model (5,6,7). With this factor in mind, the authors of this research report developed a compatible representation of the soil medium with the existing shell element formulation, suitable for any type of dynamic analysis.

1.2 REVIEW OF PAST WORK

It is useful to review the existing knowledge of soil-structure interaction by citing some of the studies carried out by different authors. One can divide the works into three general categories: the approaches to soil-structure interaction, methods and techniques, and parameters and applications. Among the last category, there does not appear sufficient studies on the interaction between the axisymmetric shells and the foundation system.

Before dealing with each of the above categories, it is suitable to introduce the work which is cited for the purpose of assessing the state of the art. A survey of the soil effect on the design of the nuclear power plants has been performed by the Ad Hoc Group on Soil-Structure Interaction (1). This paper provides some general insight which may be useful for the specific problem at hand. Veletsos (4) outlined a simple, practically oriented procedure for studying the effects of ground shock and earthquake motions on structure-foundation systems. The procedure is fairly straight forward and it is believed that considerable insight for understanding the general nature of the problem may be gained from such work. A limitation of this analysis is that it is only applicable for structures which may be modeled by a rigid foundation mat supported at the surface of a homogeneous half-space. An additional limitation of the procedure is the assumption of a linear response for the super structure.

1.2.1 Approaches to Soil-Structure Interaction

The basic alternative approaches to deal with the soil-structure interaction problem can be divided into complete interaction and inertial interaction analysis (1). The second approach neglects kinematic interaction and basically does not explicitly account for the variation of the input ground motion with the depth below the surface. The essential difference between the idealized complete interaction analysis and the inertial interaction analysis lies in the treatment of embedded structures. For embedded structures, the complete interaction analysis is clearly superior from a theoretical viewpoint, but its principal limitation is the cost of analysis.

Vaish and Chopra (2) classified the complete interaction analysis into a combined model and a substructure model. In the combined model, the entire structure-soil medium is modeled as a combined system subjected to an excitation at some assumed or actual boundary location such as the soil-rock interface. In the substructure model, the system is separated into substructures. Then the foundation medium is represented as an elastic half-space and is interfaced with the structure through a set of common coordinates at the boundary of the structure and the soil.

1.2.2 Methods and Techniques

Numerical techniques, and in particular, the finite element technique, have usually been used to carry out the complete interaction analysis, while inertial interaction analysis has generally been based on analytical solutions. These solutions are based on the soil being represented as a viscoelastic half-space or an elastic half space.

A complete interaction analysis for circular footings on layered media is presented by Kausel, Roësset and Waas (8) using a transmitting boundary to represent the far field. Dynamic analysis of rigid circular footings resting on a homogeneous, elastic half space has been carried out by Luco and Westmann (9). In this work numerical results for the analytical solution have been presented for the torsional, vertical, rocking and horizontal oscillations of the rigid disc.

Various approximate methods of superposition for the interaction problem have been recently proposed (10,11,12, 13,14). The methods have differed in the way in which modal damping is calculated, Novak (10), Rainer (12), and Roësset, Whitman and Dobry (13) assigned weighted values of damping based on the energy ratio criterion for evaluation of equivalent modal damping in composite elastic and inelastic structures, whereas Tsai (14) calculated the modal damping by matching the exact and normal modal solutions of the amplitude transfer function for a certain structure location. Bielak (11) assumed that the modal damping can be approximated based on some simplified soil-structure models and the appropriate soil properties.

Clough and Mojtahedi (15) concluded that the most efficient procedure, in case of non-proportional damping system, is to express the response in terms of undamped modal coordinates and to integrate directly the resulting coupled equations.

1.2.3 Parameters and Applications

The actual properties of the soil medium play the primary role in assessing the actual influence of soil-structure interaction on the structure response. Recently, Pandya and Setlur (16) have defined four cases which provide a range of soil properties useful for comparative analysis and subsequent generalization. It is the opinion of these authors that soil flexibility or compliance is the most important parameter in the soil-structure interaction phenomenon, and that a given flexibility can be realized by a non-unique combination of the basic parameters such as soil depth, shear modulus, etc.

Penzien (17) suggests a system of a non-linear spring and viscous dashpots to represent the soil model for determining the soil properties. In this model, Penzien choses a non-linear elastic spring with hysteresis characteristics to represent the immediate deformation characteristics of the soil structure under cyclic loading and a viscous dashpot in parallel with the spring, to represent the internal damping within the soil, while the creep behavior of the soil is represented by a viscous element in series with the spring-dashpot combination.

An evaluation of the effects of the foundation damping on the seismic response of simple building-foundation systems is presented by Veletsos and Nair (18). The supporting medium is modeled as a linear viscoelastic half space. This study shows that a consideration of the effect of energy dissipation by hysteretic action in the soil is to increase the overall damping of the structure-foundation system and to reduce the deformation of the structure.

In the approach taken by Scanlan (19), the seismic wave effect is studied by generalizing the input function in the time domain so as to account for the travel time of the passing wave over the plan dimension of the structural foundation. His study is based on a rigid foundation-soil spring model and suggests that a passing earthquake may excite both lateral and rotational displacements even for a structure which is symmetrical in plan and properties. The study suggests an inherent self-diminishing feature to earthquake excitation relative to the particular of a given design.

Akiyoshi (20) has proposed a new viscous boundary for shear waves in a one-dimensional discrete model that absorbs the whole energy of the wave traveling toward the boundary. Akiyoshi concluded that the mesh spacing less than one-sixth the wavelength of a sinusoidal wave should be used to obtain the allowable numerical solutions. The limitation of the proposed method is that it is restricted to the case of lumped mass-spring models.

The approaches and methods reviewed above have been applied to different types of structures. Reference was made previously to three papers dealing with the nuclear containment structures, dams and multistory buildings (1, 2,3). The analysis of a tall chimney, including foundation interaction, for the effects of gusting wind, vortex shedding and earthquake is studied by Novak (10). This study shows that the general trend of the soil-structure interaction effects is to reduce the response to dynamic loads. The effect of embedment and the influence of internal damping is investigated by Kousel (21) for circular foundation on layered media. The case of two-dimensional rigid foundation of semi-elliptical cross-section is studied by Luco, Wong and Trifunac (22) to examine the effects of the embedment depth and the angle of incidence of the seismic waves on the response of the foundation. This study shows that rocking and torsional motion of the foundation is generated in addition to translation.

1.3 SCOPE AND AIM

The aim of the present investigation is to develop a more realistic mathematical model for the dynamic analysis of shells of revolution by including the soil effect as a new factor which should influence the dynamic behavior of such structures. With this proposed model, it is possible to study the effect of the soil condition on the dynamic response of large towers like reinforced concrete cooling towers. In addition to the seismic analysis capability of the proposed model, it is also applicable to other dynamic loads like wind forces. This wide capability may provide better understanding to the dynamic behavior of the axi-symmetric shells and shell-like structures.

A basic theoretical background is furnished in Chapter 2. In this chapter, the wave propagation equations in the soil medium are presented and Hamilton's principle is specialized and adapted for the specific problem discussed in this report. The finite element formulations for the soil model are presented in Chapter 3 in which the energy absorbing boundary is formulated to represent the far field. The proposed dynamic model for the shell of revolution-soil system is presented in Chapter 4, along with the computer implementation. To examine the equivalent boundary system (EBS) which represents the soil medium, a parametric study is carried out in Chapter 5 in which the effect of the lower boundary and mesh size is examined. The effect of the driving frequency and the soil model behaviour in higher Fourier harmonics are studied in the same chapter. The dynamic behaviour of a cooling tower shell on a ring footing is studied, with the aid of the proposed model in Chapter 5. The dynamic analysis includes dynamic properties and stress analysis study for a variety of soil conditions. Summary and conclusions of the work are presented in Chapter 6.

It is hoped that the present work will provide some insight to the dynamic behavior of shells of revolution under wind or seismic loading which may, in turn, aid in providing a basis for rationally evaluating the footing option in the list of alternative foundations for large towers. Considerable economic benefits may be anticipated from this added option in the form of savings on foundation costs and reduced internal design forces due to the possible ameliorating effect of interaction.

2. BASIC FORMULATIONS FOR THE SOIL MODEL

2.1 INTRODUCTION

A considerable amount of work has been carried out in recent years to obtain improved solutions for the dynamic response of a rigid circular plate resting on a stratum or an elastic half space (23-26). In these studies, analytical or closed form solutions are presented, with relaxed boundary conditions which seem to introduce very little error. The solution of this problem is of great interest for its application in geophysics and engineering, and particularly, for its importance in foundation and earthquake engineering.

Despite their mathematical elegance, closed form solutions have a major drawback: they apply to ideally elastic, homogeneous, isotropic half spaces, an abstraction that seldom approaches reality. Soils are usually non-homogenous; their properties vary with depth; they are stratified in layers; and underground water adds further complications to their physical nature. Thus, the analyst must rely on experimental or numerical techniques.

In the approach used here, the problem is divided into a number of uncoupled two dimensional problems by representing an asymmetric loading or displacement pattern by a Fourier series about the vertical axis. Due to the orthogonality of Fourier series, each term in the loading series produces a displacement set in the same mode as the prescribed loading or displacement field, so long as the problem is linear. In the present chapter, the basic formulation for the wave propagation problem in a layered medium is presented for a general mode ($J \geq 0$). However, if one considers the foundation to be a rigid concentric ring footing, only the first two modes in the series are needed to describe the general motion of the footing acting on the free surface of a soil stratum. These are $j = 0$ for vertical and torsional excitation (axisymmetric modes), and $j = 1$ for rocking and swaying (antisymmetric modes).

2.2 DISPLACEMENTS AND LOADS

Let any point in the soil medium be described by the coordinates r, z, θ as shown in Figure 1. In the cylindrical coordinate system, the displacements in the radial, vertical and tangential directions are denoted by u, w, θ, respectively, while the loads in these directions are denoted by P_r, P_z and P_θ. They can always be expressed in Fourier series by

$$u = \sum_{j=0}^{\infty} (\bar{u}_s^j \cos j\theta + \bar{u}_a^j \sin j\theta)$$

$$w = \sum_{j=0}^{\infty} (\bar{w}_s^j \cos j\theta + \bar{w}_a^j \sin j\theta)$$

$$v = \sum_{j=0}^{\infty} (-\bar{v}_s^j \sin j\theta + \bar{v}_a^j \cos j\theta) \qquad (2\text{-}1)$$

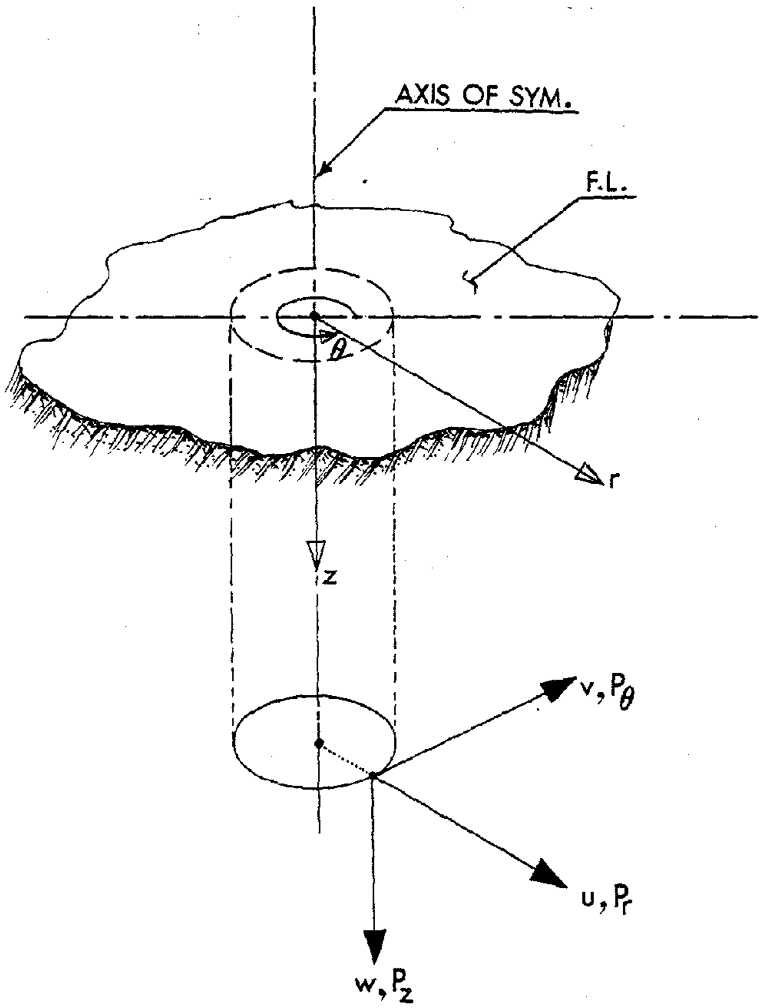

Figure 1. Coordinate System

and,

$$P_r = \sum_{j=0}^{\infty} (\bar{P}^j_{r_s} \cos j\theta + \bar{P}^j_{r_a} \sin j\theta)$$

$$P_z = \sum_{j=0}^{\infty} (\bar{P}^j_{z_s} \cos j\theta + \bar{P}^j_{z_a} \sin j\theta)$$

$$P_\theta = \sum_{j=0}^{\infty} (-\bar{P}^j_{\theta_s} \sin j\theta + \bar{P}^j_{\theta_a} \cos j\theta)$$

where the modal amplitudes with subscript s, a are referred to as the symmetric and antisymmetric displacement (load) components. Equations (2-1) may be rewritten in matrix form as

$$\left[\begin{array}{c} u \\ w \\ \hline v \end{array}\right] = \sum_{j=0}^{\infty} \left[\begin{array}{cc} \bar{u}^j_s & \bar{u}^j_a \\ \bar{w}^j_s & \bar{w}^j_a \\ \hline \bar{v}^j_a & -\bar{v}^j_s \end{array}\right] \left[\begin{array}{c} \cos j\theta \\ \\ \sin j\theta \end{array}\right] \tag{2-2}$$

with similar expressions for the loads. An alternative notation could be

$$u = \sum_j \bar{u} e^{ij\theta}$$

$$w = \sum_j \bar{w} e^{ij\theta}$$

and

$$v = \sum_j \bar{v} e^{ij\theta} \tag{2-3}$$

but since the modal amplitudes are complex for complex moduli, the latter notation is not advantageous.

The negative sign introduced in the sine term for the tangential components has the effect of yielding the same wave equations for both the symmetric and anti-symmetric components (same stiffness matrix in the finite element formulation).

The displacement vector of Equation (2-2) is written in partition form to separate the in-plane components (u,w) from the out-of-plane component (v). The modal displacement vector is then

$$u = \{\bar{u}_1 \,\vdots\, \bar{u}_2\} \tag{2-4}$$

where $\bar{u}_1 = \{\bar{u}, \bar{w}\}$

and $\bar{u}_2 = \bar{v}$ (2-5)

2.3 COMPATIBILITY EQUATIONS

The small strain and rotation-displacement relations expressed in cylindrical coordinates are

$$\begin{aligned}
\varepsilon_{rr} &= \frac{\partial u}{\partial r} \\
\varepsilon_{zz} &= \frac{\partial w}{\partial z} \\
\varepsilon_{\theta\theta} &= \frac{u}{r} + \frac{1}{r}\frac{\partial v}{\partial \theta} \\
\gamma_{zr} &= \frac{\partial u}{\partial z} + \frac{\partial w}{\partial r}
\end{aligned} \tag{2-6}$$

$$\gamma_{r\theta} = \frac{1}{r}\frac{\partial u}{\partial \theta} + \frac{\partial v}{\partial r} - \frac{v}{r}$$

$$\gamma_{\theta z} = \frac{\partial v}{\partial z} + \frac{1}{r}\frac{\partial w}{\partial \theta}$$

and the Fourier Expansions are

$$\begin{aligned}
\varepsilon_{rr} &= \sum_{j=0}^{\infty} (\bar{\varepsilon}^j_{rr_s} \cos j\theta + \bar{\varepsilon}^j_{rr_a} \sin j\theta) \\
\varepsilon_{zz} &= \sum_{j=0}^{\infty} (\bar{\varepsilon}^j_{zz_s} \cos j\theta + \bar{\varepsilon}^j_{zz_a} \sin j\theta) \\
\varepsilon_{\theta\theta} &= \sum_{j=0}^{\infty} (\bar{\varepsilon}^j_{\theta\theta_s} \cos j\xi + \bar{\varepsilon}^j_{\theta\theta_a} \sin j\theta) \\
\gamma_{zr} &= \sum_{j=0}^{\infty} (\bar{\gamma}^j_{zr_s} \cos j\theta + \bar{\gamma}^j_{zr_a} \sin j\theta) \\
\gamma_{r\theta} &= \sum_{j=0}^{\infty} (-\bar{\gamma}^j_{r\theta_s} \sin j\theta + \bar{\gamma}^j_{r\theta_a} \cos j\theta) \\
\gamma_{\theta z} &= \sum_{j=0}^{\infty} (-\bar{\gamma}^j_{\theta z_s} \sin j\theta + \bar{\gamma}^j_{\theta z_a} \cos j\theta)
\end{aligned} \tag{2-7}$$

where the modal amplitudes are related by

$$\begin{aligned}
\bar{\varepsilon}_{rr} &= \bar{u},r \\
\bar{\varepsilon}_{zz} &= \bar{w},z \\
\bar{\varepsilon}_{\theta\theta} &= \frac{1}{r}(\bar{u}-j\bar{v}) \\
\bar{\gamma}_{zr} &= \bar{u},_z + \bar{w},_r \\
\bar{\gamma}_{r\theta} &= \frac{1}{r}(j\bar{u}-\bar{v}+r\bar{v},_r) \\
\bar{\gamma}_{\theta z} &= j\bar{w}/r + v,z
\end{aligned} \tag{2-8}$$

The above equation may be expressed in matrix form as

$$\bar{\varepsilon} = A\bar{u} \tag{2-9}$$

where $\bar{\varepsilon} = \{\bar{\varepsilon}_{rr}, \bar{\varepsilon}_{zz}, \bar{\varepsilon}_{\theta\theta}, \bar{\gamma}_{zr} | \bar{\gamma}_{r\theta}, \bar{\gamma}_{\theta z}\}$ (2-10)

and A is the partitioned matrix operator

$$A = \left[\begin{array}{cc|c} \frac{\partial}{\partial r} & 0 & 0 \\ 0 & \frac{\partial}{\partial z} & 0 \\ \frac{1}{r} & 0 & -\frac{j}{r} \\ \frac{\partial}{\partial z} & \frac{\partial}{\partial r} & 0 \\ \hline \frac{j}{r} & 0 & r\frac{\partial}{\partial r}\left(\frac{1}{r}\right) \\ 0 & \frac{j}{r} & \frac{\partial}{\partial z} \end{array}\right] \tag{2-11}$$

It is convenient to write Equation (2-9) in the partitioned form

$$\left[\begin{array}{c} \bar{\varepsilon}_1 \\ \hline \bar{\varepsilon}_2 \end{array}\right] = \left[\begin{array}{c|c} A_{11} & jA_{12} \\ \hline jA_{21} & A_{22} \end{array}\right] \left[\begin{array}{c} \bar{u}_1 \\ \hline \bar{u}_2 \end{array}\right] \tag{2-12}$$

2.4 CONSTITUTIVE EQUATIONS

The stresses can be expanded in the same way as the strains and the modal components of stresses and strains are related by

$$\bar{\sigma} = D\bar{\varepsilon} \tag{2-13}$$

For cross-anisotropy, D(the constitutivity matrix) is restricted to be a function of r and z only. In the present study, only material-with properties not varying with θ will be considered. Matrix D for an isotropic material is given by

$$D = \left[\begin{array}{cccc|cc} \lambda+2\mu & \lambda & \lambda & 0 & & \\ \lambda & \lambda+2\mu & \lambda & 0 & & 0 \\ \lambda & \lambda & \lambda+2\mu & 0 & & \\ 0 & 0 & 0 & \mu & & \\ \hline & & & & \mu & 0 \\ & & 0 & & 0 & \mu \end{array}\right]$$

$$= \left[\begin{array}{c|c} D_1 & 0 \\ \hline 0 & D_2 \end{array}\right] \tag{2-14}$$

where λ and μ are the Lamé constants (complex in general). They are related to Young's modulus, Poisson's ratio and shear modulus through

$$\lambda = \frac{\nu E}{(1+\nu)(1-2\nu)} = \frac{2\nu G}{1-2\nu}$$

$$\mu = \frac{E}{2(1+\nu)} = G \qquad (2\text{-}15)$$

The modal stresses is defined by

$$\bar{\sigma} = \{\bar{\sigma}_1 : \bar{\sigma}_2\}$$

where $\bar{\sigma}_1 = \{\bar{\sigma}_{rr}, \bar{\sigma}_{zz}, \bar{\sigma}_{\theta\theta}\ \bar{\sigma}_{zr}\}$ (2-16)

and $\bar{\sigma}_2 = \{\bar{\sigma}_{r\theta}, \bar{\sigma}_{\theta z}\}$

while the true stresses are given by

$$\sigma_1 = \sum_{j=0}^{\infty} (\bar{\sigma}_{1s}^{j}\ \bar{\sigma}_{1a}^{j}) \begin{bmatrix} \cos j\theta \\ \sin j\theta \end{bmatrix}$$

$$\sigma_2 = \sum_{j=0}^{\infty} (\bar{\sigma}_{2s}^{j}\ \bar{\sigma}_{2a}^{j}) \begin{bmatrix} -\sin j\theta \\ \cos j\theta \end{bmatrix} \qquad (2\text{-}17)$$

The partitioning of this matrix into the submatrices D_1 and D_2 is consistent with that of the stresses and strains, and it follows that

$$\bar{\sigma}_1 = D_1\ \bar{\varepsilon}_1$$

$$\bar{\sigma}_2 = D_2\ \bar{\varepsilon}_2 \qquad (2\text{-}18)$$

2.5 WAVE EQUATIONS

The general equations of wave propagation expressed in cylindrical coordinates are (27)

$$\ddot{u} = \frac{1}{\rho}[(\lambda+2\mu)\frac{\partial\Delta}{\partial r} - \frac{\mu}{r}\frac{\partial}{\partial\theta}(\frac{\partial}{\partial r}(rv) - \frac{\partial u}{\partial\theta}) + \mu\frac{\partial}{\partial z}(\frac{\partial u}{\partial z} - \frac{\partial w}{\partial r})]$$

$$\ddot{w} = \frac{1}{\rho}[(\lambda+2\mu)\frac{\partial\Delta}{\partial z} - \frac{\mu}{r}\frac{\partial}{\partial r}\, r(\frac{\partial u}{\partial z} - \frac{\partial w}{\partial r}) + \frac{\mu}{r}\frac{\partial}{\partial\theta}(\frac{\partial w}{r\partial\theta} - \frac{\partial v}{\partial z})]$$

$$\ddot{v} = \frac{1}{\rho}[(\lambda+2\mu)\frac{1}{r}\frac{\partial\Delta}{\partial\theta} - \mu\frac{\partial}{\partial z}(\frac{1}{r}\frac{\partial w}{\partial\theta} - \frac{\partial v}{\partial z}) + \mu\frac{\partial}{\partial r}(\frac{\partial}{\partial r}(rv) - \frac{\partial u}{\partial\theta})]$$

(2-19)

where

$$\Delta = \text{volumetric change}$$
$$= \varepsilon_{rr} + \varepsilon_{zz} + \varepsilon_{\theta\theta}$$
$$= -\frac{1}{r}\frac{\partial(ru)}{\partial r} + \frac{\partial w}{\partial z} + \frac{1}{r}\frac{\partial v}{\partial\theta} \qquad (2\text{-}20)$$

For harmonic excitations with frequency Ω, the modal Fourier expansion of Equation (2-19) can be expressed by

$$\sum_{j=0}^{\infty}\bar{u}\begin{bmatrix}\cos j\theta\\ \sin j\theta\end{bmatrix} = \frac{-1}{\rho\Omega^2}\sum_{j=0}^{\infty}[(\lambda+2\mu)\frac{\partial}{\partial r}(\frac{\bar{u}}{r} + \frac{\partial\bar{u}}{\partial r} - \frac{j}{r}\bar{v} + \frac{\partial\bar{w}}{\partial z}) + \frac{\mu j}{r}(\frac{j\bar{w}}{r} - \frac{\partial\bar{v}}{\partial z}) + \mu\frac{\partial}{\partial z}(\frac{1}{r}\frac{\partial(r\bar{v})}{\partial r} - \frac{j\bar{u}}{r})]\begin{bmatrix}\cos j\theta\\ \sin j\theta\end{bmatrix}$$

$$\sum_{j=0}^{\infty}\bar{w}\begin{bmatrix}\cos j\theta\\ \sin j\theta\end{bmatrix} = \frac{-1}{\rho\Omega^2}\sum_{j=0}^{\infty}[(\lambda+2\mu)\frac{\partial}{\partial z}(\frac{\bar{u}}{r} + \frac{\partial\bar{u}}{\partial r} - \frac{j}{r}\bar{v} + \frac{\partial\bar{w}}{\partial z}) - \frac{\mu}{r}\frac{\partial}{\partial r}(\frac{\partial(r\bar{v})}{\partial r} - j\bar{u}) - \frac{\mu j}{r}(\frac{j}{r}\bar{w} - \frac{\partial\bar{v}}{\partial z})]\begin{bmatrix}\cos j\theta\\ \sin j\theta\end{bmatrix}$$

$$\sum_{j=0}^{\infty} \bar{v} \begin{bmatrix} -\sin j\theta \\ \cos j\theta \end{bmatrix} = \frac{-1}{\rho\Omega^2} \sum_{j=0}^{\infty} [(\lambda+2\mu) \frac{j}{r}(\frac{\bar{u}}{r} + \frac{\partial \bar{u}}{\partial r} - \frac{j\bar{v}}{r} + \frac{\partial \bar{w}}{\partial z})$$

$$- \mu\frac{\partial}{\partial z}(\frac{j\bar{w}}{r} - \frac{\partial \bar{v}}{\partial z}) + \mu \frac{\partial}{\partial r}(\frac{\partial \bar{u}}{\partial z} - \frac{\partial \bar{w}}{\partial r})] \begin{bmatrix} -\sin j\theta \\ \cos j\theta \end{bmatrix} \tag{2-21}$$

For an arbitrary j, it follows that

$$\bar{u} = \frac{-1}{\rho\Omega^2} [(\lambda+2\mu)\frac{\partial}{\partial r}(\frac{\bar{u}}{r} + \frac{\partial \bar{u}}{\partial r} - \frac{j}{r}\bar{v} + \frac{\partial \bar{w}}{\partial z}) + \mu \frac{j}{r}(\frac{\partial \bar{u}}{\partial z} - \frac{\partial \bar{w}}{\partial r})$$

$$+ \frac{\mu}{r}\frac{\partial}{\partial z}(\frac{\partial (r\bar{v})}{\partial r} - j\bar{u})]$$

$$\bar{w} = \frac{-1}{\rho\Omega^2} [(\lambda+2\mu)\frac{\partial}{\partial z}(\frac{\bar{u}}{r} + \frac{\partial \bar{u}}{\partial r} - \frac{j}{r}\bar{v} + \frac{\partial \bar{w}}{\partial z}) - \frac{\mu}{r}\frac{\partial}{\partial r}(\frac{\partial (r\bar{v})}{\partial r} - j\bar{u})$$

$$- \frac{\mu j}{r}(\frac{j}{r}\bar{w} - \frac{\partial \bar{v}}{\partial z})]$$

$$\bar{v} = \frac{-1}{\rho\Omega^2} [(\lambda+2\mu)\frac{j}{r}(\frac{\bar{u}}{r} + \frac{\partial \bar{u}}{\partial r} - \frac{j\bar{v}}{r} + \frac{\partial \bar{w}}{\partial z}) - \mu \frac{\partial}{\partial z}(\frac{j}{r}\bar{w} - \frac{\partial \bar{v}}{\partial z})$$

$$+ \mu \frac{\partial}{\partial r}(\frac{\partial \bar{u}}{\partial z} - \frac{\partial \bar{w}}{\partial r})] \tag{2-22}$$

which shall be called the Modal Wave Equations (MWE). They are only functions of r and z, with the parameter j = 0, 1, 2,...dependent on the Fourier decomposition of the loadings or prescribed displacements. The general solution of MWE is (28)

$$\bar{u} = e^{i\Omega t}[(kAe^{-\ell z}-mCe^{-mz})\frac{\partial H_j^{(2)}(kr)}{\partial r} + \frac{j}{r} B\, H_j^{(2)}(kr)e^{-mz}]$$

$$\bar{w} = e^{i\Omega t}[(Cke^{-mz}-\ell Ae^{-\ell z})k\, H_j^{(2)}(kr)]$$

$$\bar{v} = e^{i\Omega t}[(kAe^{-\ell z}-mCe^{-mz})\frac{j}{r}\, H_j^{(2)}(kr) + B\,\frac{\partial H_j^{(2)}(kr)}{\partial r}\, e^{-mz}]$$

(2-23)

in which $H_j^{(2)}(kr)$ are second Hankel functions of order j (order of Fourier component), A, B, C are integration constants, k is an arbitrary parameter (wave number), and

$$\ell = \pm\sqrt{k^2 - \frac{\Omega^2}{v_p{}^2}}$$

$$m = \pm\sqrt{k^2 - \frac{\Omega^2}{v_s^2}} \qquad (2\text{-}24)$$

and

$$\frac{1}{v_p} = \sqrt{\frac{\rho}{\lambda+2\mu}}$$

$$\frac{1}{v_s} = \sqrt{\frac{\rho}{\mu}}$$

where v_p and v_s are the compression and shear wave velocities, respectively.

In the particular solutions given by (2-23), analagous expressions containing first Hankel functions $H_j^{(1)}(kr)$ have been omitted, since they correspond, in combination with the factor $e^{i\Omega t}$, to waves travelling from infinity towards the origin and thus must be disregarded in accordance with Sommerfeld's radiation principle (29). (Sources confined to the vicinty of the origin). For this reason, the index (2) and the argument (kr) in the Hankel functions will be dropped.

The solution of the modal wave equations may be written as

$$\bar{u} = e^{i\Omega t}(f_1(z)H_j' + f_3(z)\frac{j}{r}H_j)$$

$$\bar{w} = kf_2(z)H_j\ e^{i\Omega t} \tag{2-25}$$

$$\bar{v} = e^{i\Omega t}(f_1(z)\frac{j}{r}H_j + f_3(z)H_j')$$

where $H_j' = \frac{\partial}{\partial r} H_j^{(2)}(kr)$

and

$$f_1(z) = kAe^{-\ell z} - mCe^{-mz}$$

$$f_2(z) = kCe^{-mz} - \ell Ae^{-\ell z} \tag{2-26}$$

$$f_3(z) = Be^{-mz}$$

Dropping the time dependent term $e^{i\Omega t}$ from (2-25) together with (2-26) one gets

$$\bar{Y} = HF \tag{2-27}$$

where $\bar{Y}$ is the modal displacement without the time dependent term, and

$$F = \{f_1, f_2, f_3\}$$

and

$$H = \begin{bmatrix} H_j' & 0 & \frac{j}{r} H_j \\ 0 & kH_j & 0 \\ \frac{j}{r} H_j & 0 & H_j' \end{bmatrix} \tag{2-28}$$

In the above equation F is only a function of z while H is a function of r and the harmonic number j.

Also, expressions for the strains and stresses in terms of the functions f_i will be needed later. Substituting (2-27) into (2-8) results in

$$\bar{\varepsilon}_{rr} = f_1\, H_j'' + f_3\, \frac{j}{r}\, (H_j' - \frac{H_j}{r})$$

$$\bar{\varepsilon}_{zz} = f_2' \cdot k \cdot H_j$$

$$\bar{\varepsilon}_{\theta\theta} = f_1\left(\frac{H_j'}{r} - \frac{j^2}{r^2} H_j\right) + f_3 \frac{j}{r}\left(\frac{H_j}{r} - H_j'\right)$$

$$\bar{\gamma}_{zr} = f_1' H_j' + f_2 k H_j' + f_3' \frac{j}{r} H_j \tag{2-29}$$

$$\bar{\gamma}_{r\theta} = f_1 \frac{j}{r}\left(2H_j' - \frac{H}{r}\right) + f_3\left(\frac{j^2}{r^2} H_j - \frac{1}{r} H_j' + H_j''\right)$$

$$\bar{\gamma}_{\theta z} = f_1' \frac{j}{r} H_j + f_2 k \frac{j}{r} H_j + f_3' H_j'$$

and with

$$\bar{\Phi} = (f_2' - kf_1)k H_j \tag{2-30}$$

the stresses follow as

$$\begin{aligned}
\bar{\sigma}_{rr} &= 2\mu\varepsilon_{rr} + \lambda\bar{\Phi} \\
\bar{\sigma}_{zz} &= 2\mu\varepsilon_{zz} + \lambda\bar{\Phi} \\
\bar{\sigma}_{\theta\theta} &= 2\mu\varepsilon_{\theta\theta} + \lambda\bar{\Phi} \\
\bar{\sigma}_{zr} &= \mu\gamma_{zr} \\
\bar{\sigma}_{r\theta} &= \mu\gamma_{r\theta} \\
\bar{\sigma}_{\theta z} &= \mu\gamma_{\theta z}
\end{aligned} \tag{2-31}$$

The modal wave equations (2-22) may be expressed in matrix form using Equations (2-25) through (2-28) as

$$H \cdot Z = 0 \tag{2-32}$$

where H is given by (2-28) and Z is a vector depends only on z

$$\mathbf{Z} = \begin{bmatrix} z_1 \\ z_2 \\ z_3 \end{bmatrix} = \begin{bmatrix} (\lambda+2\mu)(kf_2'-k^2f_1)+\mu(f_1''-kf_2')+\rho\Omega^2 f_1 \\ (\lambda+2\mu)(f_2''-kf_1')+\mu k(f_1'-kf_2)+\rho\Omega^2 f_2 \\ \mu(f_3''-k^2f_3)\ +\rho\Omega^2 f_3 \end{bmatrix} \qquad (2\text{-}33)$$

The above form of MWE is suitable for the finite element formulations as we will discuss later.

2.6 PRINCIPLE OF VIRTUAL DISPLACEMENTS

In dynamics, the generalization of the principle of virtual displacements into a law of kinetics by use of D'Aambert's principle is referred to as Hamilton's principle. For nonconservative systems, the principle states that the work performed by the applied external loads and inertial forces during an arbitrary virtual displacement field that is consistent with the constraints is equal to the change in strain energy plus the energy dissipated by internal friction during that virtual displacement.

Hamilton's principle shall be specialized and adapted for the specific problem discussed in this report in which the coordinate system is cylindrical, and the viscoelastic constants are complex. By applying two Fourier transformations, one in the time domain, and one in the θ

coordinate, the principle of virtual displacements for axisymmetric systems subjected to a general harmonic excitation shall be developed.

A general form of Hamilton's principle in elasticity is

$$\int_{t_0}^{t_1}\left[\int_V \delta\varepsilon_{ij}\sigma_{ij}dV - \int_V \delta u_i(b_i-\rho\ddot{u}_i)dV - \int_S \delta u_i p_i dA\right]dt = 0 \tag{2-34}$$

where $\delta\varepsilon_{ij}$ is the virtual strain field corresponding to the displacement field δu_i which is consistent with the constraints and vanishes at the time t_0 and t_1. The term $\delta\varepsilon_{ij}\,\sigma_{ij}$ represents the change in strain energy as well as the energy lost due to internal friction. S corresponds to that portion of the boundary where the forces are prescribed.

Since the prescribed virtual displacements are arbitrary, a set of displacements can be chosen of the form

$$\left.\begin{aligned} \delta u_i(x,t) &= \delta\tilde{u}_i(x)\cdot\delta(t) \\ \delta\varepsilon_{ij}(x,t) &= \delta\tilde{\varepsilon}_{ij}(x)\cdot\delta(t) \end{aligned}\right\} t_0 \le t \le t_1 \tag{2-35}$$

where x stands for the coordinate system,

$$x = (x_1,\ x_2,\ x_3) \tag{2-36}$$

and $\delta(t)$ is the Dirac delta function. Substitution in (2-34) and integration over the time domain yields

$$\int_V \delta\tilde{\varepsilon}_{ij}\sigma_{ij}\, dV - \int_V \delta\tilde{u}_i(b_i-\rho\ddot{u}_i)dV - \int_S \delta\tilde{u}_i\, p_i dA = 0 \tag{2-37}$$

where σ_{ij}, b_i, u_i and p_i are evaluated at the time t.

Alternatively, it is possible to arrive at this result starting from the equilibrium equations (wave equation) and the boundary force equations, and constraining the time variable to remain constant while the virtual displacements are applied, that is, the real motion is stopped while the virtual displacements are performed; however, the inertial forces must be assumed to persist. In other words, it is assumed that the performance of the virtual displacements consumes no time (30).

Applying a Fourier transformation (FT) to (2-37) and defining

$$\tilde{\sigma}_{ij}(\Omega) = FT(\sigma_{ij}(t)),\ \tilde{b}_i(\Omega) = FT(b_i(t)),\ \tilde{p}_i(\Omega) = FT(p_i(t)),$$

$$\tilde{u}_i(\Omega) = FT(u_i(t)),\ -\Omega^2\tilde{u}_i(\Omega) = FT(\ddot{u}_i(t)) \tag{2-38}$$

yields

$$\int_V \delta\tilde{\varepsilon}_{ij}\tilde{\sigma}_{ij}\, dV - \int_V \delta\tilde{u}_i(\tilde{b}_i+\rho\Omega^2\tilde{u}_i)dV - \int_S \tilde{p}_i\, \delta\tilde{u}_i dA = 0 \tag{2-39}$$

where the transformed quantities are in general complex.

For real elastic moduli, the stresses will be real and in phase with the strains and displacements whereas, for complex moduli, they will be complex and there will be a phase lag between these two quantities. The relation between the transformed stresses $\tilde{\sigma}_{ij}$ and strains $\tilde{\varepsilon}_{ij}$ is given by equation (2-13).

An alternate form of equation (2-39) is obtained using integration by parts, resulting in

$$\int_V \delta\tilde{u}_i(\tilde{\sigma}_{ij,j} + \tilde{b}_i + \rho\Omega^2\tilde{u}_i)dV + \int_S \delta\tilde{u}_i(\tilde{p}_i - n_j\tilde{\sigma}_{ij})dA = 0 \tag{2-40}$$

which, for arbitrary variations of the virtual displacements δu_i yields the body and boundary equilibrium equations. Using the stress-strain relation, the term in parenthesis in the first integral becomes the wave equation, which shall be useful later on. Switching now from tensor to matrix notation and dropping the superscript ~ with the implicit understanding that the applied forces (displacements) are harmonic, equation (2-39) becomes

$$\int_V \delta\varepsilon^T\sigma dV - \int_V \delta u^T(b+\rho\Omega^2 u)dV - \int_S \delta u^T p dA = 0 \qquad (2\text{-}41)$$

For a cylindrically orthotropic (cross anisotropic) material, integration w/r to θ, with $dV = rdrd\theta dz$, and using

$$\int_0^{2\Pi} \sin m\theta \sin n\theta \, d\theta = (\delta_{mn} - \delta_{m\theta}\ \delta_{n\theta})\Pi = \begin{cases} \Pi \text{ for } m=n\neq 0 \\ 0 \text{ otherwise} \end{cases}$$

$$\int_0^{2\Pi} \cos m\theta \cos n\theta \, d\theta = (\delta_{mn} + \delta_{m\theta}\delta_{n\theta})\Pi = \begin{cases} \Pi \text{ for } m=n\neq 0 \\ 2\Pi \text{ for } m=n=0 \\ 0 \text{ otherwise} \end{cases}$$

$$\int_0^{2\Pi} \sin m\theta \cos n\theta \, d\theta = 0 \qquad \text{for any values of m and n}$$

yields for the principle of virtual displacements

$$\iint \delta\bar{\varepsilon}^T D\ \bar{\varepsilon}\ rdrdz - \iint \rho\Omega^2\ \delta\bar{u}^T\bar{u}rdrdz$$

$$= \int_S \delta\bar{u}^T\bar{p}rds \qquad (2\text{-}42)$$

where the superscript bar refers to the Fourier modal amplitude. Similarly, by substituting Equation (2-32) into Equation (2-40), we find

$$\iint \delta\bar{u}^T\cdot H\cdot Z\cdot rdrdz + \int \delta\bar{u}^T(\bar{p}-\bar{\sigma}^*)rds = 0 \qquad (2\text{-}43)$$

where $\bar{\sigma}^* = \{n_j \bar{\sigma}_{ij}\}$ are the projection of the modal stresses on the unit outward boundary normal nj

$H \cdot Z =$ the modal wave equation (2-32).

Equation (2-43) is preferable over equation (2-42) or (2-41) when using the principle of virtual displacements to define the eigenvalue problem for the viscoelastic energy absorbing boundary since it does not require a cumbersome integration of products of the Hankel functions over the coordinate r.

3. FINITE ELEMENT FORMULATIONS

3.1 INTRODUCTION

Numerical techniques have been used successfully in the stress analysis of many complex structures. In particular, the finite element technique has been the major tool for analyzing different types of structures such as solids of revolution (31,32) and shells of revolution (5,6,7,33,34). These two classes of structures are of special importance in modelling the axisymmetric shell-soil system. The use of highly efficient rotational shell finite elements to model the superstructure suggested that the soil medium be represented in a similar manner. A main problem in this case is to account for the proper boundary conditions at the edges of a finite domain which will not introduce undesirable reflections of waves into the region of interest. A possible solution is to place the boundaries at a substantial distance from the footing if there is internal dissipation of energy in the soil. This approach requires a very large number of elements and is therefore expensive.

This chapter presents the finite element model used to represent the soil medium where axisymmetrical isoparametric quadratic solid elements with transmitting vertical boundaries placed directly at the outer edge of the structure are employed (Figure 2). With the energy transmitting boundary, the finite element region is reduced to minimum, resulting in a high order sophisticated model with comparatively few elements as has been the continuing objective in previous investigations at Washington University.

The formulation of the rotational shell elements is presented elsewhere (6,7,35), and for completeness, the outlines of the derivation of these highly efficient elements is presented in Appendix 8.1.

3.2 SOLID ELEMENT FORMULATIONS

The core region of Figure 2 is modelled by means of axisymmetric isoparametric quadratic solid elements. For each nodal circle there are three degrees-of-freedom; two of them are in-plane, u and w, while the third, v, is out-of-plane. These in-plane and out-of-plane degrees-of-freedom are separated in the formulations of the element stiffness and mass matrices. The name "isoparametric" derives from use of the same interpolation functions to define the element shape as are used to define the displacements within the element (36).

If ϕ denotes the expansion vector for the isoparametric formulation, see Figure 3,

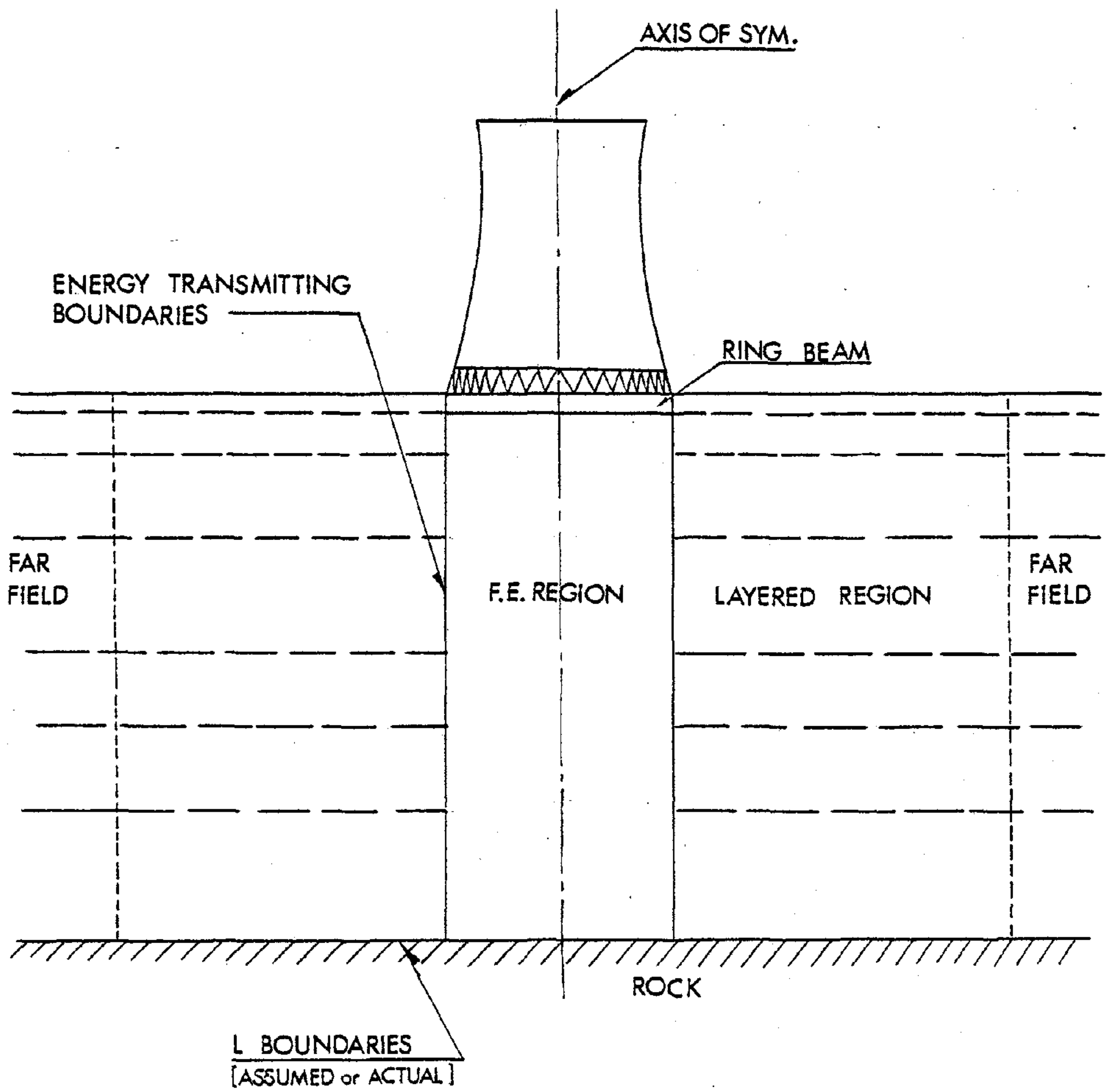

Figure 2. Finite Element Model for the Soil Medium

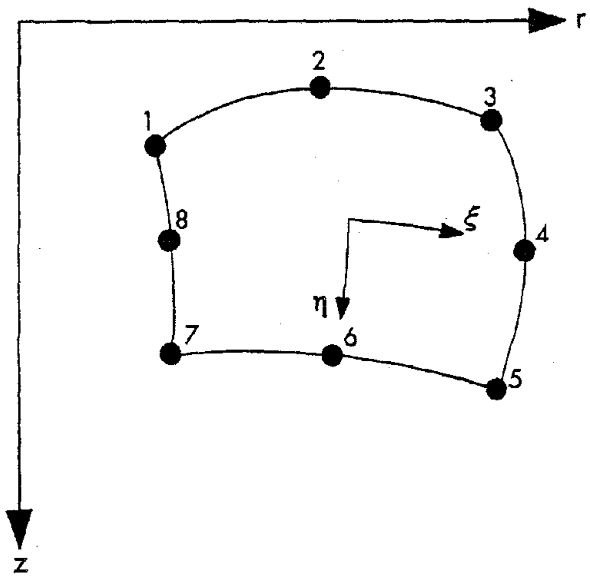

Figure 3. Isoparametric Quadratic Solid Element

$$
\begin{aligned}
r &= \sum_{i=1}^{n} \phi_i r_i \\
z &= \sum_{i=1}^{n} \phi_i z_i
\end{aligned}
\tag{3-1}
$$

where n = number of nodes per element.

In vector notation

$$
\begin{aligned}
r &= \phi^T r_o \\
z &= \phi^T z_o
\end{aligned}
\tag{3-2}
$$

$$
\begin{aligned}
\text{where } r_o &= \{r_1,\ r_2, \ldots r_n\} \\
z_o &= \{z_1,\ z_2, \ldots z_n\}
\end{aligned}
\tag{3-3}
$$

Using the same expansions for the displacements,

$$u = \Phi^T u_o \tag{3-4}$$

where

$$u = \begin{bmatrix} \bar{u} \\ \bar{w} \\ \bar{v} \end{bmatrix} \quad , \; u_o^T = \{\bar{u}_1, \bar{u}_2, \ldots, \bar{u}_n, \bar{w}_1, \bar{w}_2, \ldots, \bar{w}_n, \bar{v}_1, \bar{v}_2, \ldots, \bar{v}_n\}$$

and $$\Phi^T = \begin{bmatrix} \phi^T & & 0 \\ & \phi^T & \\ 0 & & \phi^T \end{bmatrix} \tag{3-5}$$

In equation (3-4), Φ^T is called the expansion matrix. From (2-10) and (3-4), one can write

$$\underset{6\times 1}{\begin{bmatrix} \underset{4\times 1}{\bar{\varepsilon}_1} \\ \hdashline \underset{2\times 1}{\bar{\varepsilon}_2} \end{bmatrix}} = \underset{6\times 3}{\left[\begin{array}{c:c} \underset{4\times 2}{A_{11}} & \underset{4\times 1}{A_{12}} \\ \hdashline \underset{2\times 2}{A_{21}} & \underset{2\times 1}{A_{22}} \end{array}\right]} \underset{3\times 3n}{\begin{bmatrix} \phi^T & & \\ & \phi^T & \\ & & \phi^T \end{bmatrix}} \underset{3n\times 1}{\begin{bmatrix} \bar{u}_1 \\ \bar{u}_2 \\ \vdots \\ \bar{u}_n \\ \bar{w}_1 \\ \bar{w}_2 \\ \vdots \\ \bar{w}_n \\ \hdashline \bar{v}_1 \\ \bar{v}_2 \\ \vdots \\ \bar{v}_n \end{bmatrix}} \qquad (3\text{-}6)$$

or $\bar{\varepsilon} = B\ u_o$

$$\text{where } B = \underset{6\times 3n}{\left[\begin{array}{c:c} \underset{4\times 2n}{b_{11}} & \underset{4\times n}{b_{12}} \\ \hdashline \underset{2\times 2n}{b_{21}} & \underset{2\times n}{b_{22}} \end{array}\right]} \qquad (3\text{-}7)$$

Substitution into equation (2-42) gives

$$\sum_{\text{elements}} \delta u_o^T \{\int\int (B^T D B - \rho\Omega^2 \Phi\Phi^T) u_o r\,dr\,dz - \int \Phi \bar{p} r\,ds\} = 0 \qquad (3\text{-}8)$$

For the k<u>th</u> element, the consistent mass matrix M_k, the stiffness matrix K_k and the load vector P_k are defined as:

$$M_k = \int\int \rho \Phi \Phi^T \, rdrdz$$
$$K_k = \int\int B^T DB \, rdrdz \qquad (3\text{-}9)$$
$$P_k = \int \Phi \bar{P} \, rds$$

3.2.1 Isoparametric Formulations

For quadratic elements, the total number of nodes per element n equals to eight and the shape functions $\phi_i = g_i$ $(i=1,\ldots,8)$ may be chosen as functions of the dimensionless coordinates ξ and η. In Table 1 the expressions for g_i, $g_{i,\xi}$ and $g_{i,\eta}$ are given.

The Jacobian is defined by

$$\text{Jac} = \begin{bmatrix} g_{1,\xi} g_{2,\xi} g_{3,\xi} g_{4,\xi} g_{5,\xi} g_{6,\xi} g_{7,\xi} g_{8,\xi} \\ g_{1,\eta} g_{2,\eta} g_{3,\eta} g_{4,\eta} g_{5,\eta} g_{6,\eta} g_{7,\eta} g_{8,\eta} \end{bmatrix} \begin{bmatrix} r_1 & z_1 \\ r_2 & z_2 \\ r_3 & z_3 \\ r_4 & z_4 \\ r_5 & z_5 \\ r_6 & z_6 \\ r_7 & z_7 \\ r_8 & z_8 \end{bmatrix}$$

$$\text{or Jac} = \begin{bmatrix} \sum_{i=1}^{8} g_{i,\xi} r_i & \sum_{i=1}^{8} g_{i,\xi} z_i \\ \sum_{i=1}^{8} g_{i,\eta} r_i & \sum_{i=1}^{8} g_{i,\eta} z_i \end{bmatrix} \qquad (3\text{-}10)$$

The inverse of the Jacobian IJ is, then, given by

$$IJ = \begin{bmatrix} IJ_{11} & IJ_{12} \\ IJ_{21} & IJ_{22} \end{bmatrix}$$

Table 1. Shape Functions and First Derivatives for Expansion Vector

i	g_i	$g_{i,\xi}$	$g_{i,\eta}$
1	$-\frac{1}{4}(1-\xi)(1-\eta)(1+\xi+\eta)$	$\frac{1}{4}(1-\eta)(2\xi+\eta)$	$\frac{1}{4}(1-\xi)(2\eta+\xi)$
2	$\frac{1}{2}(1-\xi^2)(1-\eta)$	$-\xi(1-\eta)$	$-\frac{1}{2}(1-\xi^2)$
3	$\frac{1}{4}(1+\xi)(1-\eta)(\xi-\eta-1)$	$\frac{1}{4}(1-\eta)(2\xi-\eta)$	$\frac{1}{4}(1+\xi)(2\eta-\xi)$
4	$\frac{1}{2}(1+\xi)(1-\eta^2)$	$\frac{1}{2}(1-\eta^2)$	$-\eta(1+\xi)$
5	$\frac{1}{4}(1+\xi)(1+\eta)(\xi+\eta-1)$	$\frac{1}{4}(1+\eta)(2\xi+\eta)$	$\frac{1}{4}(1+\xi)(2\eta+\xi)$
6	$\frac{1}{2}(1-\xi^2)(1+\eta)$	$-\xi(1+\eta)$	$\frac{1}{2}(1-\xi^2)$
7	$\frac{1}{4}(1-\xi)(1+\eta)(\eta-\xi-1)$	$\frac{1}{4}(1+\eta)(2\xi-\eta)$	$\frac{1}{4}(1-\xi)(2\eta-\xi)$
8	$\frac{1}{2}(1-\xi)(1-\eta^2)$	$-\frac{1}{2}(1-\eta^2)$	$-\eta(1-\xi)$

where

$$IJ_{11} = \left(\sum_{i=1}^{8} g_{i,\eta} z_i\right) / |Jac|$$

$$IJ_{12} = -\left(\sum_{i=1}^{8} g_{i,\xi} z_i\right) / |Jac|$$

$$IJ_{21} = -\left(\sum_{i=1}^{8} g_{i,\eta} r_i\right) / |Jac| \tag{3-11}$$

and

$$IJ_{22} = \left(\sum_{i=1}^{8} g_{i,\xi} r_i\right) / |Jac|$$

where $|Jac|$ is the determinant of the Jacobian matrix of equation (3-10). The inverse of the Jacobian is necessary for the transformation from r-z coordinates to ξ-η natural coordinates,

$$(\ \ )_{,r} = IJ_{11} \cdot (\ \ )_{,\xi} + IJ_{12} \cdot (\ \ )_{,\eta}$$

$$(\ \ )_{,z} = IJ_{21} \cdot (\ \ )_{,\xi} + IJ_{22} \cdot (\ \ )_{,\eta} \tag{3-12}$$

3.2.2 Element Mass and Stiffness Matrices

Using partitioned form of the B, D and Φ matrices we get:

$$M_k = \begin{bmatrix} m & 0 & 0 \\ 0 & m & 0 \\ 0 & 0 & m \end{bmatrix}_{24\times 24}$$

where $$m_{8\times 8} = \iint \rho\phi\phi^T \, rdrdz \tag{3-13}$$

and $$K_k = \left[\begin{array}{c|c} K_1 & K_2 \\ \hline K_2^T & K_3 \end{array}\right]_{24\times 24}$$

where
$$\begin{aligned} K_1 &= \iint (b_{11}^T D_1 b_{11} + b_{21}^T D_2 b_{21}) \, rdrdz \\ K_2 &= \iint (b_{11}^T D_1 b_{12} + b_{21}^T D_2 b_{22}) \, rdrdz \\ K_3 &= \iint (b_{22}^T D_2 b_{22} + b_{12}^T D_1 b_{12}) \, rdrdz \end{aligned} \tag{3-14}$$

From (3-7), the submatrices b_{11}, b_{12}, b_{21} and b_{22} are given by (See Appendix 8.2).

$$b_{11} = \begin{bmatrix} g_{1,r} & g_{2,r} & \cdots\cdots g_{8,r} & 0 & 0 \cdots\cdots 0 \\ 0 & 0 & \cdots\cdots 0 & g_{1,z} & g_{2,z} \cdots\cdots g_{8,z} \\ g_{1/r} & g_{2/r} & \cdots\cdots g_{8/r} & 0 & 0 \cdots\cdots 0 \\ g_{1,z} & g_{2,z} & \cdots\cdots g_{8,z} & g_{1,r} & g_{2,r} \cdots\cdots g_{8,4} \end{bmatrix}_{4\times 16} \tag{3-15-a}$$

$$b_{12} = \frac{-j}{r} \begin{bmatrix} 0 & 0 \cdots\cdots\cdots 0 \\ 0 & 0 \cdots\cdots\cdots 0 \\ g_1 & g_2 \cdots\cdots\cdots g_8 \\ 0 & 0 \cdots\cdots\cdots 0 \end{bmatrix}_{4\times 8} \tag{3-15-b}$$

$$b_{21} = \frac{j}{r} \begin{bmatrix} g_1 & g_2 \cdots\cdots g_8 & 0 & 0 \cdots\cdots 0 \\ 0 & 0 \cdots\cdots 0 & g_1 & g_2 \cdots\cdots g_8 \end{bmatrix}_{2\times 16} \tag{3-15-c}$$

$$b_{22} = \begin{bmatrix} r\frac{\partial}{\partial r}(g_{1/r}) & r\frac{\partial}{\partial r}(g_{2/r}) \cdots\cdots r\frac{\partial}{\partial r}(g_{8/r}) \\ g_{1,z} & g_{2,z} \cdots\cdots\cdots g_{8,z} \end{bmatrix}_{2\times 8} \tag{3-15-d}$$

and $\phi\phi^T$ is given by:

$$\phi\phi^T = \begin{bmatrix} g_1^2 & g_1 g_2 & g_1 g_3 \cdots\cdots g_1 g_8 \\ g_2 g_1 & g_2^2 & g_2 g_3 \quad\quad g_2 g_8 \\ g_3 g_1 & g_3 g_2 & g_3^2 \cdots\cdots g_3 g_8 \\ \vdots & \vdots & \vdots \quad\quad\quad \vdots \\ g_8 g_1 & g_8 g_2 & g_8 g_3 \cdots\cdots g_8^2 \end{bmatrix}_{8\times 8} \tag{3-16}$$

With RG defined as

$$RG = \sum_{i=1}^{8} g_i r_i \qquad (3\text{-}17)$$

and $$\iint(\quad)\,r\,dr\,dz = \int_{-1}^{1}\int_{-1}^{1}(\quad)\,RG \det Jac\, d\xi\, d\eta \qquad (3\text{-}18)$$

the mass matrix M_k and the stiffness matrix K_k are obtained for a general Fourier harmonic j; however, M_k is independent of j as one can see from equations (3-13) and (3-16).

The integration in each element is carried out by means of four points Gaussian integration with the dimensionless coordinates ξ, η. Since in the Gaussian quadrature scheme, there are no points on the boundary of the elements, no problems are encountered with the singularity of the integrand of the symmetry axis (r=0) for those elements adjacent to it.

The details of the isoparametric formulation for the element stiffness matrix is presented in Appendix 8.2.

3.3 THE BOUNDARIES

It is assumed that the finite element region has a fixed lower boundary, which may be true if we are dealing with a stratum over rock of infinite horizontal extent. The lower boundary location factor will be studied in case of a deep stratum or half space.

Now, for the total mass matrix M, total stiffness matrix K, and the total load vector P we have the following equation

$$(K - \Omega^2 M)u = P \tag{3-19}$$

where u stands for the total nodal displacements.

The above equation needs to be modified to include the effect of the far field on the stiffness of the core region. This can be achieved by considering the equilibrium of the vertical boundaries of the core region. If the core region of Figure 2 is removed and replaced by equivalent distributed forces corresponding to the internal stresses, the dynamic equilibrium of the far-field will be preserved. Since no other prescribed forces act on the far-field, the displacements at the boundary and at any other point in the far-field will be uniquely defined in terms of these boundary forces. The relation between these boundary forces and the corresponding boundary displacements is the dynamic boundary matrix to be added to the total dynamic stiffness matrix of equation (3-19).

For a consistent boundary (8), it is always possible to express the displacements in the far-field in terms of eigenfunctions corresponding to the natural modes of wave propagation in the stratum. The general solution to the problem is given by Equation (2-23) where k is an undetermined parameter of the wave number. In an unbounded medium, any value of k, and thus any wave length, is admissible; for a layered stratum, however, only a discrete set of values of k (each one with a corresponding propagation mode) will satisfy the boundary condition. At a given frequency, Ω, there are thus, an infinite but discrete set of propagation modes and wave numbers k, which can be found by solving a transcendental eigenvalue problem. For each eigenfunction one can determine the distribution of stresses up to a multiplicative constant, the participation factor of the mode. Combining these modal stresses so as to match any given distribution of stresses at the boundary, one can compute the participation factors and, correspondingly, the dynamic stiffness function relating boundary stresses to boundary displacements.

The solution of the actual transcendental eigenvalue problem for the continuum problem is difficult and time consuming requiring, in general, search procedures. A discrete eigenvalue problem can be obtained by substituting the actual dependence of the displacements on the z variable, as given by Equations (2-25) and (2-26), by an assumed expansion consistent with that used for the finite elements. The result is an algebraic eigenvalue problem with a finite number of eigenvectors and eigenvalues, for which efficient numerical solutions are available.

3.3.1 Wave Numbers and Modes of Propagation

Consider the toroidal section of the far-field limited by two cylindrical surfaces of radii r_o and r_1, as shown in Figure 4. The stratum is discretized in horizontal layers, the interfaces of which match the nodal circles of the finite element mesh in the core region. For the n<u>th</u> layer there are three nodes i, i+1, i+2, for the i<u>th</u> node the three degrees of freedom are:

$$x_i = \{x_1, x_2, x_3\}_i \tag{3-20}$$

The exact values for these three nodal displacements are given by Equation (2-25),

$$x_i = H \cdot F_i$$

and for the layer number n,

$$x_n = \{x_{1_i}, x_{2_i}, x_{3_i} : x_{1_{i+1}}, x_{2_{i+1}}, x_{3_{i+1}} : x_{1_{i+2}}, x_{2_{i+2}}, x_{3_{i+2}}\} \tag{3-21}$$

Approximate solution for the nodal displacements may be obtained using the same expansions as for the coordinates and displacements in the finite element region

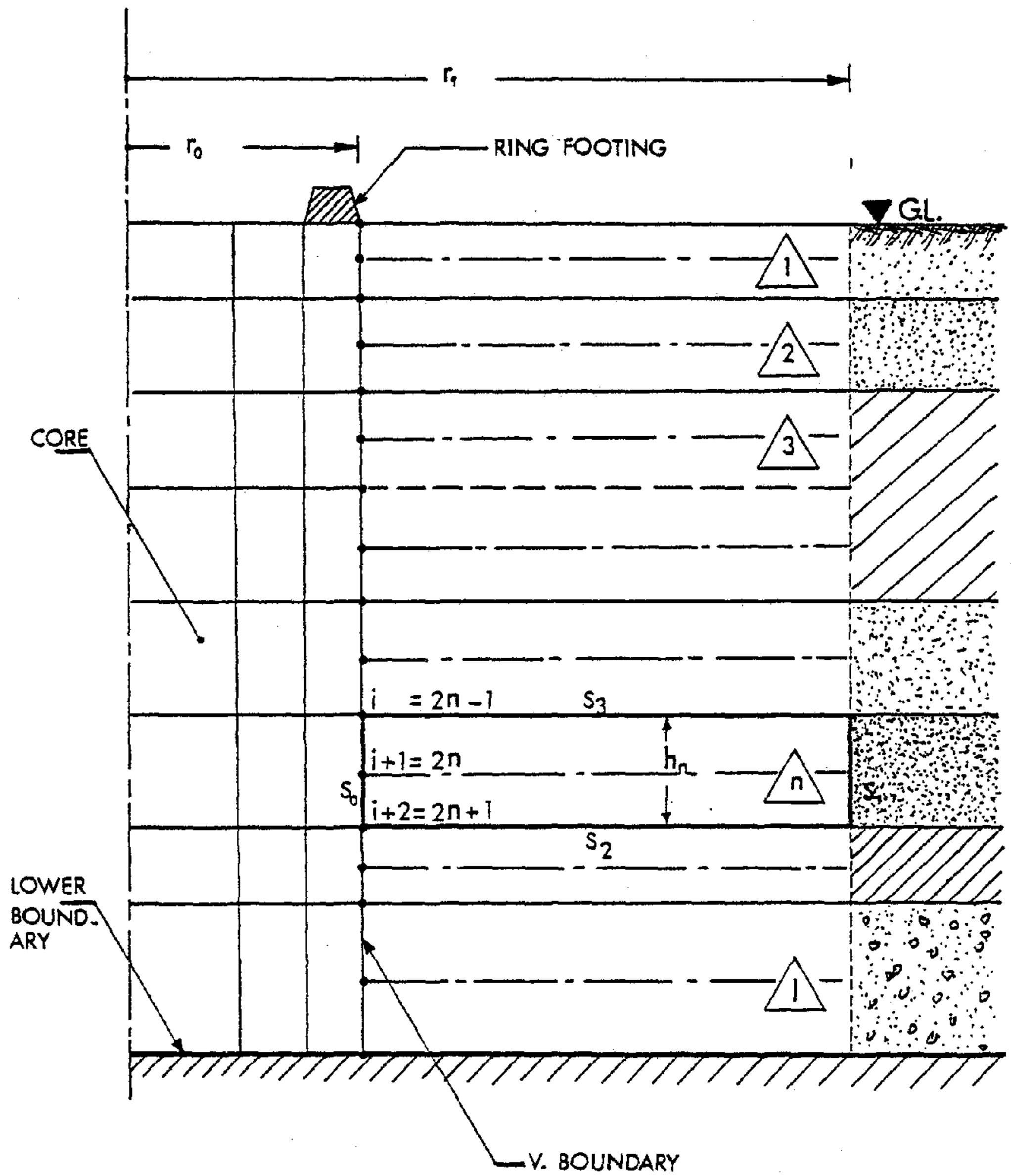

Figure 4. Toroidal Section of the Far Field

$$F_i = N\,X_i \tag{3-22}$$

where

$$N = [g_1 I, g_2 I, g_3 I]_{3\times 9} \tag{3-23}$$

in which I is a 3×3 identity matrix, and g_i represents the expansion coefficients. For a quadratic expansion,

$$g_1 = \frac{1}{2}(\eta^2-\eta),\ g_2 = 1-\eta^2 \text{ and } g_3 = \frac{1}{2}(\eta^2+\eta) \tag{3-24}$$

Combining Equations (3-20) to (3-24) yield

$$U_{app_n} = N\,U_{o_n} \tag{3-25a}$$

= the approximate nodal displacements for the nth layer

and

$$U_{o_n} = \begin{bmatrix} x_{1_i} H'_j + \frac{j}{r_o} x_{3_i} H_j \\ k x_{2_i} H_j \\ \frac{j}{r_o} x_{1_i} H_j + x_{3_i} H'_j \\ x_{1_{i+1}} H'_j + \frac{j}{r_o} x_{3_{i+1}} H_j \\ k x_{2_{i+1}} H_j \\ \frac{j}{r_o} x_{1_{i+1}} H_j + x_{3_{i+1}} H'_j \\ x_{1_{i+2}} H'_j + \frac{j}{r_o} x_{3_{i+2}} H_j \\ k x_{2_{i+2}} H_j \\ \frac{j}{r_o} x_{1_{i+2}} H_j + x_{3_{i+2}} H'_j \end{bmatrix}_n \tag{3-25b}$$

Using the same basic procedure for the finite element formulation as previously employed, an approximate solution is obtained by substituting the displacement expansion into the expression of the principle of virtual displacements (2-43), integrating over the region, and requiring the result to vanish for an arbitrary δu.

Substituting the above approximate displacements in (2-43) and summing over the ℓ layers yields

$$\sum_{n=1}^{\ell} \left[\iint \delta\bar{u}^T \cdot H \cdot Z \cdot r dr dz + \int_{s_o} \delta\bar{u}^T (\bar{p}-\bar{\sigma}^*) r ds + \int_{s_1} \delta\bar{u}^T (\bar{p}-\bar{\sigma}^*) r ds \right.$$

$$\left. + \int_{s_2} \delta\bar{u}^T (\bar{p}-\bar{\sigma}^*) r ds + \int_{s_3} \delta\bar{u}^T (\bar{p}-\bar{\sigma}^*) r ds \right] = 0 \qquad (3\text{-}26)$$

In the above equation, consistent nodal forces $\bar{p}_o$ and $\bar{p}_1$ are applied at each of the boundaries r_o and r_1 such that the integrands over s_o and s_1 vanish

$$\sum_{n=1}^{\ell} \left[\delta\bar{u}_o^T \bar{P}_o = \int_{s_o} \delta\bar{u}^T \bar{p} r ds = \int_{s_o} \delta\bar{u}^T \bar{\sigma}^* \, r ds \right]$$

$$\sum_{n=1}^{\ell} \left[\delta\bar{u}_1^T \bar{P}_1 = \int_{s_1} \delta\bar{u}^T \bar{p} r ds = \int_{s_1} \delta\bar{u}^T \bar{\sigma}^* \, r ds \right] \qquad (3\text{-}27)$$

with no external prescribed forces acting at the layer interfaces;

$$\sum_{n=1}^{\ell} \left[\iint \delta \bar{u}^T \; H \; Z \; rdrdz - \int_{s_2} \delta \bar{u}^T \bar{\sigma}^* rds - \int_{s_3} \delta \bar{u}^T \bar{\sigma}^* rds \right] = 0 \tag{3-28}$$

in which

$$\bar{\sigma}^* = \begin{cases} \{\bar{\sigma}_{rz}, \; \bar{\sigma}_{zz}, \; \bar{\sigma}_{\theta z}\} & \text{for } s_2 \\ -\{\bar{\sigma}_{rz}, \; \bar{\sigma}_{zz}, \; \bar{\sigma}_{\theta z}\} & \text{for } s_3 \end{cases} \tag{3-29}$$

From Equations (2-29), (2-30) and (2-31)

$$\bar{\sigma}^* = \begin{bmatrix} \bar{\sigma}_{rz} \\ \bar{\sigma}_{zz} \\ \bar{\sigma}_{\theta z} \end{bmatrix} = \begin{bmatrix} \mu\{(f_1'+kf_2)H_j' + \frac{j}{r} H_j f_3'\} \\ kH_j\{(\lambda+2\mu)f_2'-\lambda k f_1\} \\ \mu\{(f_1'+kf_2) \frac{j}{r} H_j + f_3' \; H_j'\} \end{bmatrix} \tag{3-30-a}$$

$$\text{or} \qquad \bar{\sigma}^* = H \cdot \bar{Z}_2 \cdot F \tag{3-30-b}$$

where $\bar{Z}_2$ is an operator matrix

$$\bar{Z}_2 = \begin{bmatrix} \mu \frac{\partial}{\partial z} & \mu k & 0 \\ -\lambda k & (\lambda+2\mu)\frac{\partial}{\partial z} & 0 \\ 0 & 0 & \mu\frac{\partial}{\partial z} \end{bmatrix} \tag{3-31}$$

The wave equation H·Z, Equation (2-32), may be written as;

$$W = H \cdot \bar{Z}_1 \cdot F \tag{3-32}$$

in which $\bar{Z}_1$ is an operator matrix

$$\bar{Z}_1 = \begin{bmatrix} \rho\Omega^2+\mu\frac{\partial^2}{\partial z^2} - k^2(\lambda+2\mu) & k(\lambda+\mu)\frac{\partial}{\partial z} & 0 \\ -k^2(\lambda+\mu)\frac{\partial}{\partial z} & \rho\Omega^2-\mu k^2+(\lambda+2\mu)\frac{\partial^2}{\partial z^2} & 0 \\ 0 & 0 & \rho\Omega^2-\mu k^2+\mu\frac{\partial^2}{\partial z^2} \end{bmatrix} \tag{3-33}$$

With $\delta\bar{u} = H\cdot N\cdot\delta X$ and $F = N\cdot X$, Equation (3-28) becomes

$$\sum_{n=1}^{\ell} \int_r \left\{ \int_z \delta X^T N^T H^T H(\bar{Z}_1-\bar{Z}_2')NXdz - \int_z \delta X^T N'^T H\bar{Z}_2 NXdz \; rdr \right\} = 0 \tag{3-34}$$

In the above equation,

$$N^T N = [g_i \cdot g_k] \;, \quad N' = \frac{\partial N}{\partial z} = [g_i' \; I_i]$$

in which i = 1, 2, 3 and k = 1, 2, 3.

Also, in Equation (3-34);

$$N^T H^T H = \bar{H}N^T \quad \text{and} \quad N'^T H^T H = \bar{H}N'^T, \text{ where}$$

$$\bar{H} = \left[\begin{array}{ccc|ccc|ccc} H_1 & 0 & H_2 & & & & & & \\ 0 & H_3 & 0 & & 0 & & & 0 & \\ H_2 & 0 & H_1 & & & & & & \\ \hline & & & H_1 & 0 & H_2 & & & \\ & 0 & & 0 & H_3 & 0 & & 0 & \\ & & & H_2 & 0 & H_1 & & & \\ \hline & & & & & & H_1 & 0 & H_2 \\ & 0 & & & 0 & & 0 & H_3 & 0 \\ & & & & & & H_2 & 0 & H_1 \end{array}\right] \qquad (3\text{-}35)$$

in which

$$H_1 = H_j'^2 + \left(\frac{j}{r}\right)^2 H_j^2$$

$$H_2 = \frac{2j}{r} H_j' H_j$$

$$H_3 = k^2 H_j^2$$

Factoring out the $\bar{H}$ matrix, which is independent of z, from Equation (3-34) and rearranging the equation yields

$$\sum_{n=1}^{\ell} \delta X^T \left[\int_{r_o}^{r_1} \bar{H} r dr\right] \left[\int_0^{h_n} N^T (\bar{Z}_1 - \bar{Z}_2') N dz - \int_0^{h_n} N'^T \bar{Z}_2 N dz\right] X = 0 \qquad (3\text{-}36)$$

For an arbitrary δX and with $\int_{r_o}^{r_1} \bar{H} r dr \neq 0$ (non singular matrix) which is the same for all layers in the case of vertical boundaries, the following equation must hold:

$$\sum_{n=1}^{\ell} \left[\int_0^{h_n} N^T(\bar{Z}_1 - \bar{Z}_2')\,N\,dz - \int_0^{h_n} N'^T \bar{Z}_2 N\,dz \right] X = 0 \qquad (3\text{-}37)$$

and with

$$\int_0^h g_i g_k \,dz = \frac{h}{30} \begin{bmatrix} 4 & 2 & -1 \\ 2 & 16 & 2 \\ -1 & 2 & 4 \end{bmatrix}$$

$$\int_0^h g_i g_k' \,dz = \frac{1}{6} \begin{bmatrix} -3 & 4 & -1 \\ -4 & 0 & 4 \\ 1 & -4 & 3 \end{bmatrix} \qquad (3\text{-}38)$$

and $$\int_0^h g_i' g_k' \,dz = \frac{1}{3h} \begin{bmatrix} 7 & -8 & 1 \\ -8 & 16 & -8 \\ 1 & -8 & 7 \end{bmatrix}$$

equation (3-37) becomes

$$\sum_{n=1}^{\ell} \left([S]_n - k^2 [A]_n\right)\{X\} = 0 \qquad (3\text{-}39)$$

in which

$$[S]_n = \frac{1}{3h_n}\begin{bmatrix}
0.4h_n^2\rho\Omega^2+7\mu & 0 & 0 & 0.2h_n^2\rho\Omega^2+8\mu & 0 & 0 & -0.1h_n^2\rho\Omega^2-\mu & 0 & 0 \\
 & 0.4h_n^2\rho\Omega^2+7(\lambda+2\mu) & 0 & 0 & 0.2h_n^2\rho\Omega^2+8(\lambda+2\mu) & & & -0.1h_n^2\rho\Omega^2-(\lambda+2\mu) & \\
 & & 0.4h_n^2\rho\Omega^2+7\mu & 0 & 0 & 0.2h_n^2\rho\Omega^2+8\mu & 0 & 0 & -0.1h_n^2\rho\Omega^2-\mu \\
 & & & 1.6h_n^2\rho\Omega^2+16\mu & 0 & 0 & 0.2h_n^2\rho\Omega^2+8\mu & & 0 \\
 & & & & 1.6h_n^2\rho\Omega^2+16(\lambda+2\mu) & 0 & & 0.2h_n^2\rho\Omega^2+8(\lambda+2\mu) & 0 \\
 & \text{SYM.} & & & & 1.6h_n^2\rho\Omega^2+16\mu & 0 & 0 & 0.2h_n^2\rho\Omega^2+8\mu \\
 & & & & & & 0.4h_n^2\rho\Omega^2+7\mu & 0 & 0 \\
 & & & & & & & 0.4h_n^2\rho\Omega^2+7(\lambda+2\mu) & 0 \\
 & & & & & & & & 0.4h_n^2\rho\Omega^2+7\mu
\end{bmatrix}$$

(3-40-a)

and

$$[A]_n = \frac{h_n}{30}\left[\begin{array}{ccc|ccc|ccc}
4(\lambda+2\mu) & 15(\lambda-\mu) & 0 & 2(\lambda+2\mu) & -20(\lambda+\mu) & 0 & -(\lambda+2\mu) & 5(\lambda+\mu) & 0 \\
 & 4\mu & 0 & 20(\lambda+\mu) & 2\mu & 0 & -5(\lambda+\mu) & -\mu & 0 \\
 & & 4\mu & 0 & 0 & 2\mu & 0 & 0 & -\mu \\
\hline
 & & & 16(\lambda+2\mu) & 0 & 0 & 2(\lambda+2\mu) & -20(\lambda+\mu) & \\
 & & & & 16\mu & 0 & 20(\lambda+\mu) & 2\mu & 0 \\
 & \text{SYM} & & & & 16\mu & 0 & 0 & 2\mu \\
\hline
 & & & & & & 4(\lambda+2\mu) & -15(\lambda-\mu) & 0 \\
 & & & & & & & 4\mu & 0 \\
 & & & & & & & & 4\mu
\end{array}\right] \tag{3-40-b}$$

For the whole stratum, the assembled matrices of (3-40) leads to

$$(S-k^2A)X = 0 \tag{3-41}$$

which is an eigenvalue problem in k_i^2, the wave number of the propagation mode X_i. The order of this eigenvalue problem is 6ℓ, where ℓ is the total number of layers in the stratum.

3.3.2 Dynamic Stiffness Matrix of the Energy Absorbing Boundary

Consider Equation (3-27) with ds = dz and $r = r_o$, i.e.

$$\sum_{n=1}^{\ell} \left[P_o = r_o \int_0^{h_n} N^T \bar{\sigma}^* dz \right]$$ for an arbitrary variation of the nodal displacements. But

$$P_s = \alpha_s r_o \int_0^{h} N^T \bar{\sigma}_s^* \, dz \tag{3-42}$$

where P_s = the nodal forces for the $s^{\underline{th}}$ propagation mode

α_s = the participation factor for the $s^{\underline{th}}$ propagation mode

$\bar{\sigma}_s^*$ = the $s^{\underline{th}}$ modal boundary stresses vector (Figure 5)

$= \{-\sigma_{rr}, -\sigma_{zr}, -\sigma_{\theta r}\}_s$

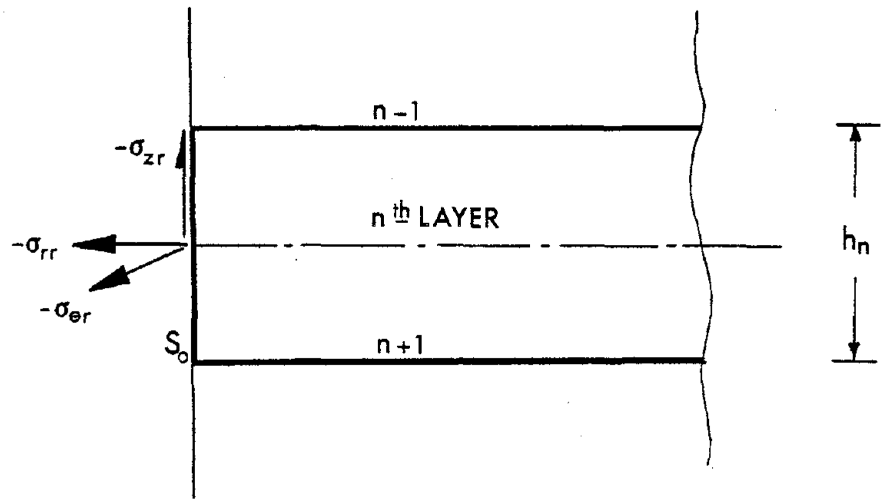

Figure 5. Modal Boundary Stress Vector for the nth Layer

Therefore, from Equations (2-31) and (2-29)

$$\bar{\sigma}_s^* = -\begin{bmatrix} 2\mu H_j'' - \lambda k^2 H_j & (\lambda k H_j)\frac{\partial}{\partial z} & 2\mu\frac{j}{r_o}(H_j' - H_j/r_o) \\ (\mu H_j')\frac{\partial}{\partial z} & \mu k H_j & (\mu\frac{j}{r_o}H_j)\frac{\partial}{\partial z} \\ 2\mu\frac{j}{r_o}(H_j' - H_j/r_o) & 0 & \mu(H_j'' - \frac{H_j'}{r_o} + (\frac{j}{r_o})^2 H_j) \end{bmatrix} \begin{bmatrix} f_1 \\ f_2 \\ f_3 \end{bmatrix}$$

$$= -\begin{bmatrix} s_1 & 0 & s \\ 0 & s_3 & 0 \\ s_2 & 0 & s_4 \end{bmatrix} \begin{bmatrix} f_1 \\ f_2 \\ f_3 \end{bmatrix} - \begin{bmatrix} 0 & T_1 & 0 \\ T_2 & 0 & T_3 \\ 0 & 0 & 0 \end{bmatrix} \begin{bmatrix} f_1' \\ f_2' \\ f_3' \end{bmatrix}$$

$$= -[s]\{f\} - [T]\{f'\} \tag{3-43}$$

where;

$$\begin{aligned} s_1 &= 2\mu H_j'' - \lambda k^2 H_j \\ s_2 &= 2\mu \frac{j}{r_o}(H_j' - \frac{1}{r_o} H_j) \\ s_3 &= \mu k \ H_j' \\ s_4 &= \mu(H_j'' - \frac{1}{r_o} H_j' + \frac{j^2}{r_o^2} H_j) \\ T_1 &= \lambda k H_j \\ T_2 &= \mu H_j' \end{aligned} \tag{3-44}$$

and $$T_3 = \mu \frac{j}{r_o} H_j$$

With $\{f\} = [N]\{X\}$ and $\{f'\} = [N']\{X\}$

$$N^T\bar{\sigma}_s^* = (N^TN\bar{S} + N^TN'\bar{T})x \tag{3-45}$$

where

$$\bar{S} = \begin{bmatrix} S & & \\ & S & \\ & & S \end{bmatrix}_{9\times 9} \quad \text{and } \bar{T} = \begin{bmatrix} T & & \\ & T & \\ & & T \end{bmatrix}_{9\times 9} \tag{3-46}$$

which leads to the following equation for the nodal forces in the $s\underline{th}$ mode:

$$P_s = \alpha_s r_o([\int_0^h N^TNdz]\bar{S} + [\int_0^h N^TN'dz]\bar{T})X \tag{3-47}$$

Matrices S and T may be simplified by taking advantage of the property of Hankel functions (37)

$$\begin{aligned} H_j'' &= -\frac{1}{r}H_j' - [k^2 - \frac{j^2}{r^2}]H_j \\ H_j' &= k\, H_{j-1} - \frac{j}{r}H_j \\ H_{-1} &= -H_1 \end{aligned} \tag{3-48}$$

which yields

$$S = k^2\, S1 + kS2 + S3$$

and

$$T = kT1 + T2 \tag{3-49}$$

with

$$S1 = \begin{bmatrix} \lambda+2\mu & 0 & 0 \\ 0 & \mu & 0 \\ 0 & 0 & \mu \end{bmatrix} \begin{bmatrix} H_j & 0 & 0 \\ 0 & -H_{j-1} & 0 \\ 0 & 0 & H_j \end{bmatrix} \tag{3-50a}$$

$$S2 = \frac{\mu}{r_o} \begin{bmatrix} -2 & 0 & 2j \\ 0 & j & 0 \\ 2j & 0 & -2 \end{bmatrix} \begin{bmatrix} -H_{j-1} & 0 & 0 \\ 0 & H_j & 0 \\ 0 & 0 & -H_{j-1} \end{bmatrix} \tag{3-50b}$$

$$S3 = \frac{2\mu j(j+1)}{r_o^2} \begin{bmatrix} 1 & 0 & -1 \\ 0 & 0 & 0 \\ -1 & 0 & 1 \end{bmatrix} \begin{bmatrix} H_j & 0 & 0 \\ 0 & -H_{j-1} & 0 \\ 0 & 0 & H_j \end{bmatrix} \tag{3-50c}$$

$$T1 = \begin{bmatrix} 0 & -\lambda & 0 \\ \mu & 0 & 0 \\ 0 & 0 & 0 \end{bmatrix} \begin{bmatrix} -H_{j-1} & 0 & 0 \\ 0 & H_j & 0 \\ 0 & 0 & -H_{j-1} \end{bmatrix} \tag{3-50d}$$

and

$$T2 = -\frac{\mu j}{r_o} \begin{bmatrix} 0 & 0 & 0 \\ -1 & 0 & 1 \\ 0 & 0 & 0 \end{bmatrix} \begin{bmatrix} H_j & 0 & 0 \\ 0 & -H_{j-1} & 0 \\ 0 & 0 & H_j \end{bmatrix} \tag{3-50e}$$

Defining the modal vectors XA_s and XB_s

where

$$\begin{aligned} XA_s &= \{XA_1^T\ XA_2^T \ldots .XA_i^T \ldots XA_{2\ell}^T\} \\ XB_s &= \{XB_1^T\ XB_2^T \ldots .XB_i^T \ldots XB_{2\ell}^T\} \end{aligned} \qquad (3\text{-}51)$$

$$\{XA_i\}_s = \begin{bmatrix} H_j & & \\ & -H_{j-1} & \\ & & H_j \end{bmatrix} \begin{bmatrix} x_1 \\ x_2 \\ x_3 \end{bmatrix}_i$$

$$\{XB_i\}_s = \begin{bmatrix} -H_{j-1} & & \\ & H_j & \\ & & -H_{j-1} \end{bmatrix} \begin{bmatrix} x_1 \\ x_2 \\ x_3 \end{bmatrix}_i$$

and the boundary load vector P_{bs} as

$$P_{bs} = \alpha_s r_o \{[A]\{XA\}_s k_s^2 + [G]\{XB\}_s\} k_s$$

$$+ [E]\{XA\}_s\} \qquad (3\text{-}52)$$

the nodal load vector for the whole stratum assembled from P_s for each discrete layer where matrices A, E and G are formed from the layer matrices A_n, E_n and G_n in a similar fashion as in the eigenvalue problem.

A_n is the matrix given by Equation (3-40-b)

$$E_n = \int_0^{h_n} \frac{\mu j}{r_o^2} \left[\begin{bmatrix} 2(j+1)g_i g_m & 0 & -2(j+1)g_i g_m \\ r_o g_i g_m' & 0 & -r_o g_i g_m' \\ -2(j+1)g_i g_m & 0 & 2(j+1)g_i g_m \end{bmatrix}_{3\times 3} \right]_{9\times 9} \tag{3-53}$$

and

$$G_n = \int_0^{h_n} \frac{2}{r_o} \left[\begin{bmatrix} -\mu g_i g_m & -\frac{\lambda r_o}{2} g_i g_m' & j g_i g_m \\ \frac{\mu r_o}{2} g_i g_m' & \frac{j\mu}{2} g_i g_m & 0 \\ j g_i g_m & 0 & -\mu g_i g_m \end{bmatrix}_{3\times 3} \right]_{9\times 9}$$

with $i = 1, 2, 3$

$m = 1, 2, 3$

Adding up the contributions of each mode gives for the boundary load vector

$$P_b = \sum_{s=1}^{6\ell} \alpha_s r_o \{[A]\{XA\}_s k_s^2 + [G]\{XB\}_s k_s + [E]\{XA\}_s\}$$

or

$$P_b = r_o \left[[A][XA][K^2] + [G][XB][K] + [E][XA]\right]\{\alpha\} \tag{3-54}$$

In (3-54)

$$[XA] = [\{XA\}_1 \{XA\}_2 \ldots \{XA\}_s \ldots \{XA\}_{6\ell}]_{6\ell \times 6\ell}$$

$$[XB] = [\{XB\}_1 \{XB\}_2 \ldots \{XB\}_s \ldots \{XB\}_{6\ell}]_{6\ell \times 6\ell}$$

$[K^2]$ and $[K]$ are diagonal matrices with k_s^2 and k_s on the main diagonal respectively ($s=1$ to 6ℓ)

and $\{\alpha\} = \{\alpha_1, \alpha_2, \alpha_3, \ldots, \alpha_s, \ldots, \alpha_{6\ell}\}$

The modal participation factors $\{\alpha\}$ are the only unknown vector in the RHS of Equation (3-54). The next step, then, is to calculate the boundary displacement vector in terms of the modal participation factors, and to relate the boundary load vector to the boundary displacement vector to form the boundary matrix.

At any particular node i, the displacement vector is given by

$$u_i = \sum_{s=1}^{\ell} \alpha_s \, H(s) X_i(s) \tag{3-55}$$

or

$$u_i = \sum_{s=1}^{\ell} \alpha_s \begin{bmatrix} uI_s \\ uJ_s \\ uK_s \end{bmatrix}_i$$

where

$$\begin{bmatrix} uI_s \\ uJ_s \\ uK_s \end{bmatrix}_i = \begin{bmatrix} H_j'(k_s r_o) X_1(s) + \frac{j}{r_o} H_j(k_s r_o) X_3(s) \\ k_s H_j(k_s r_o) X_2(s) \\ \frac{j}{r_o} H_j(k_s r_o) X_1(s) + H_j'(k_s r_o) X_3(s) \end{bmatrix}_i$$

Therefore

$$\begin{bmatrix} \bar{u} \\ \\ \bar{w} \\ \\ \bar{v} \end{bmatrix}_i = \begin{bmatrix} uI(1) & uI(2) \ldots uI(s) \ldots uI(6\ell) \\ \\ uJ(1) & uJ(2) \ldots uJ(s) \ldots uJ(6\ell) \\ \\ uK(1) & uK(2) \ldots uK(s) \ldots uK(6\ell) \end{bmatrix}_i \begin{bmatrix} \alpha_1 \\ \alpha_2 \\ \vdots \\ \alpha_s \\ \vdots \\ \alpha_{6\ell} \end{bmatrix} = [\bar{u}u]_i \{\alpha\} \tag{3-56}$$

Defining $\{u_b\}_{6\ell\times 1}$ as the boundary displacement vector, and with u_i as a general nodal vector, $\{u_b\}$ may be written as

$$u_b = \begin{bmatrix} [\bar{u}u]_1 \\ [\bar{u}u]_2 \\ \vdots \\ [\bar{u}u]_i \\ \vdots \\ [\bar{u}u]_{2\ell} \end{bmatrix}_{6\ell\times 6\ell} \{\alpha\} = [\bar{u}u]\cdot\{\alpha\} \tag{3-57}$$

$$\therefore \quad \{\alpha\} = [\bar{u}u]^{-1}\, u_b \tag{3-58}$$

The dynamic stiffness matrix of the energy absorbing boundary R_b is defined through the following relation:

$$P_b = R_b\, u_b \tag{3-59}$$

Substituting (3-58) into (3-54) for $\{\alpha\}$ and equating the resulting RHS to the RHS of (3-59) for an arbitrary u_b, it follows that

$$R_b = r_o \left[[A][XA][K^2] + [G][XB][K] + [E][XA] \right] [\bar{u}u]^{-1} \tag{3-60}$$

3.4 TOTAL DYNAMIC STIFFNESS MATRIX OF THE SOIL MEDIUM

Consider the boundary load vector of Equation (3-59) as an external load vector acting with negative sign on the finite element region, Equation (3-19) becomes;

$$(K - \Omega^2 M)u = P - R_b u_b$$

and by increasing the size of R_b by adding zero rows and columns to match the dimension of K and M, one can get

$$(K - \Omega^2 M + R)u = P \qquad \text{(3-61\_}$$

or

$$K_c u \qquad = P$$

where K_c is the total dynamic stiffness matrix of the soil medium,

$$\underline{K_c = K - \Omega^2 M + R} \tag{3-62}$$

Equation (3-61) may be solved by the conventional numerical methods to obtain the nodal displacements. Although neither the total dynamic stiffness matrix of Equation (3-62) nor the formula of Equation (3-61) is going to be used in its present form in the structure-soil system of the next chapter, these are very useful in checking the finite element model of the soil medium and the effectiveness of the vertical energy absorbing boundaries. The checking of the model presented in this chapter is part of the parametric study which is to be carried out later.

4. SHELL-SOIL MODEL

4.1 GENERAL APPROACH

One of the most challenging points in the soil-structure interaction problems is the interface between the soil medium and the structure. For rotational shells-soil system, the problem becomes more complicated as the number of degrees of freedom in the shell side is not the same as those in the soil side at the common nodal points connecting the structure model to the soil. Furthermore, the soil model is essentially a three dimensional problem, whereas the shell model is a two dimensional model. Apart from the geometrical difficulty, one must overcome the problem of dealing with two different materials, where the soil model is frequency dependent while the shell model is not. Also, the soil material has no tensile capacity which may cause uplift of the shell structure under the effect of major earthquakes or wind loads.

To overcome the difficulty of the connection problem, one may take advantage of the physical properties of the structure components and the overall behavior of the system. As an example, if the shell is founded over ring footing, the assumption of a rigid footing in the radial and vertical direction may simplify the connection problem, although the ring footing may be flexible in the circumferential direction. Also, the separation between the foundation and the soil may be considered only with the first two Fourier harmonics (J=0 and J=1) as the higher harmonics correspond to local deformations which cannot cause total uplift of the superstructure. However, the uplift problem may be neglected altogether for certain types of shells when the non-structure elements are tied to the foundation, adding to the overall stability. For example, at the bottom of the cooling tower shells the water basin and the fill structure may be tied to the ring footing (38).

In this chapter the connection model is presented and the shell-soil model is explained. The approach presented herein is restricted to shell structures modeled by axisymmetric elements and founded over concentric ring footing. The computer program used in calculating the connection model is explained and a flowchart is provided. For obvious reasons the connecting model is named the Equivalent Boundary System (EBS). The EBS is frequency dependent and must be updated for each Fourier harmonic. To account for the possibility of foundation uplift, an iterative procedure is presented in which the problem is run again after modifying Fourier coefficients of EBS according to the angle of separation.

In Figure 6 the proposed model is given for a cooling tower shell.

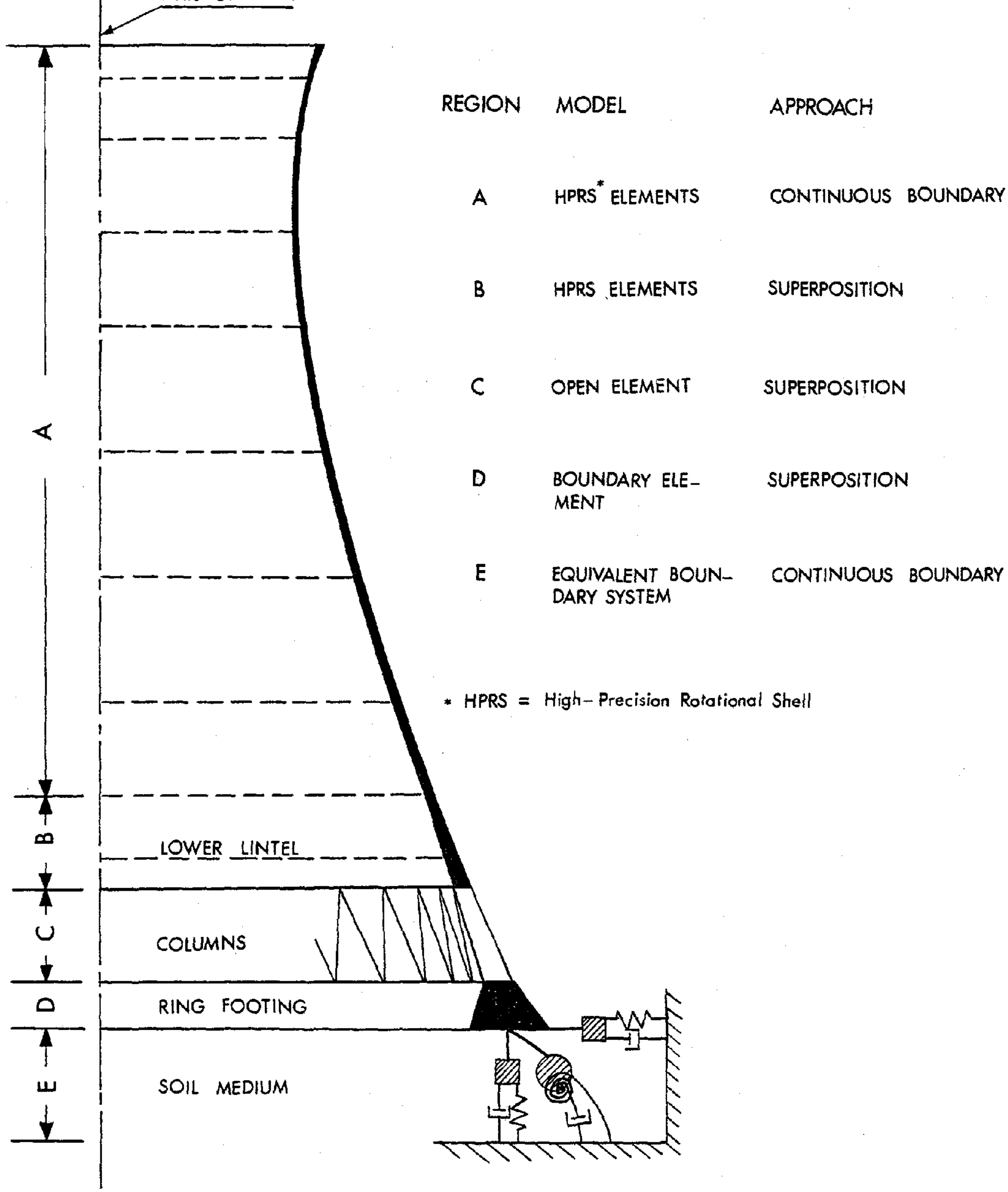

Figure 6. Proposed Model for a Cooling Tower Shell

4.2 EQUIVALENT BOUNDARY SYSTEM (EBS)

In the previous chapter the total dynamic stiffness matrix K_c of Equation (3-62) is of order 3n by 3n where n is the total number of nodes in the finite element mesh. When only one degree of freedom per node on the axis of symmetry is not restrained (vertical displacement) and with the lower boundary fixed, the order of the total stiffness matrix K_c will drop to $\bar{n}$ by $\bar{n}$, where

$$\bar{n} = 3n - 3m - 4\ell \tag{4-1}$$

in which

m = number of nodes at the lower boundary

ℓ = number of layers.

Since the prime degrees of freedom are those at the foundation level (in Figure 7, node number 1 to node number m), one may reduce the problem by carrying out the well known condensation procedure to get

$$K_c^* u^* = P^* \tag{4-2}$$

where

$$\begin{aligned} K_c^* &= K_{11} - K_{12} K_{22}^{-1} K_{21} \\ P^* &= P_1 \\ u^* &= u_1 \end{aligned} \tag{4-3}$$

and K_{11}, K_{12}, K_{21}, K_{22}, u_1 and P_1 can be obtained from the original matrices K_c, u and P of Equation (2-61).

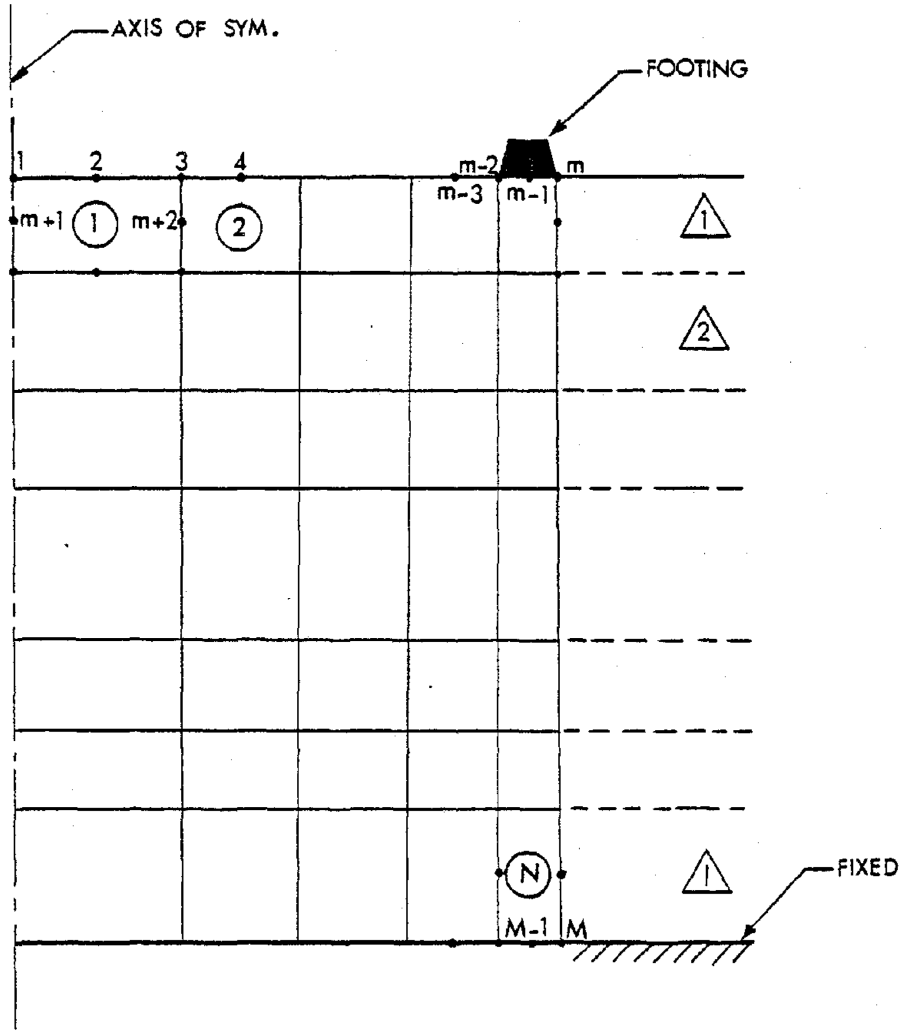

Figure 7. Soil Mesh with the Ring Footing

$$\left[\begin{array}{c|c} K_{11\,n1\times n1} & K_{12\,n1\times n2} \\ \hline K_{21\,n2\times n1} & K_{22\,n2\times n2} \end{array}\right] \left[\begin{array}{c} u_{1\,n1} \\ \hline u_{2\,n2} \end{array}\right] = \left[\begin{array}{c} P_{1\,n1} \\ \hline P_{2\,n2} \end{array}\right] \qquad (4\text{-}4)$$

where $n_1 = 3m - 2$ and $n_2 = \bar{n} - n_1$.

In Equation (4-3), P^* is taken equal to P_1 since P_2 is assumed to be a null vector (no external loads could be applied at the nodes inside the soil stratum).

4.2.1 Impedance Matrix

The impedance matrix is the dynamic stiffness to be added to the superstructure matrices to complete the structure-soil dynamic model. It is, thus, composed of the dynamic stiffness coefficients corresponding to the common degrees of freedom between the superstructure and the soil model. In Figure 7 these degrees of freedom are associated with nodes m-2, m-1 and m.

Using Equation (4-2) with the RHS all zero's except for the value at one of the common d.o.f. which is set to unity and solving for u*, the flexibility matrix F can be obtained. The impedance matrix K_s is obtained by inverting the flexibility matrix F

$$K_s = F^{-1} \qquad (4\text{-}5)$$

The above method is the conventional approach to obtain K_s, however, there is an alternative approach in which one may make use of the condensed stiffness matrix K_s^* by simply inverting K_c^* and then eliminating the columns and rows not corresponding to the common d.o.f. to form F. Equation (4-5) may be used, then, to obtain K_s.

In general, the resulting impedance matrix K_s will be a complex matrix even for an elastic soil medium. This is because of the radiation of the waves toward infinity. While the real part of the impedance matrix represents the soil stiffness elements at the common degrees of freedom (nodes m-2, m-1 and m in Figure 7), the imaginary part represents the part of the damping corresponding to the radiation at the energy transmitting boundary. In the case of complex Lame' constants for the soil material, the imaginary part of the impedance matrix represents both radiational damping in the far field and the viscous damping in the viscoelastic soil material. The viscous damping is due to the phase angle between the stress and strain vectors in the soil.

In the following section the connection problem between the soil medium and the shell foundation is formulated. The frequency dependent stiffnesses of the impedance matrix (the real part of K_s) are used to formulate the stiffness elements of the EBS. The damping elements of the EBS are computed from the imaginary part of K_s plus a linear combination of the stiffness and mass elements of the EBS (proportional damping). Here, the proportional damping matrix represents the material damping for the elastic soil medium.

4.2.2 The Ring Footing

Consider the cross section of Figure 8 to be the concentric ring footing supporting the shell which may have an open element (columns) atop the footing. The ring footing is modelled as a shell element with a constant radius (cylindrical element) with the same shell theory assumptions of no deformation in the normal direction and linear deformations in the meridional direction, which imply that the footing lower boundary has the property of being rigid. This property does not contradict the physical nature of the problem in which the ring footing is rigid relative to the soil, i.e., the line FED must remain a straight line after deformation (Figure 8). It should be noted here that the area bounded by the straight lines AC, CD, DF and FA is the area which will be considered in the finite element formulations.

To introduce the soil effect at the ring footing base level, the following factors must be considered:

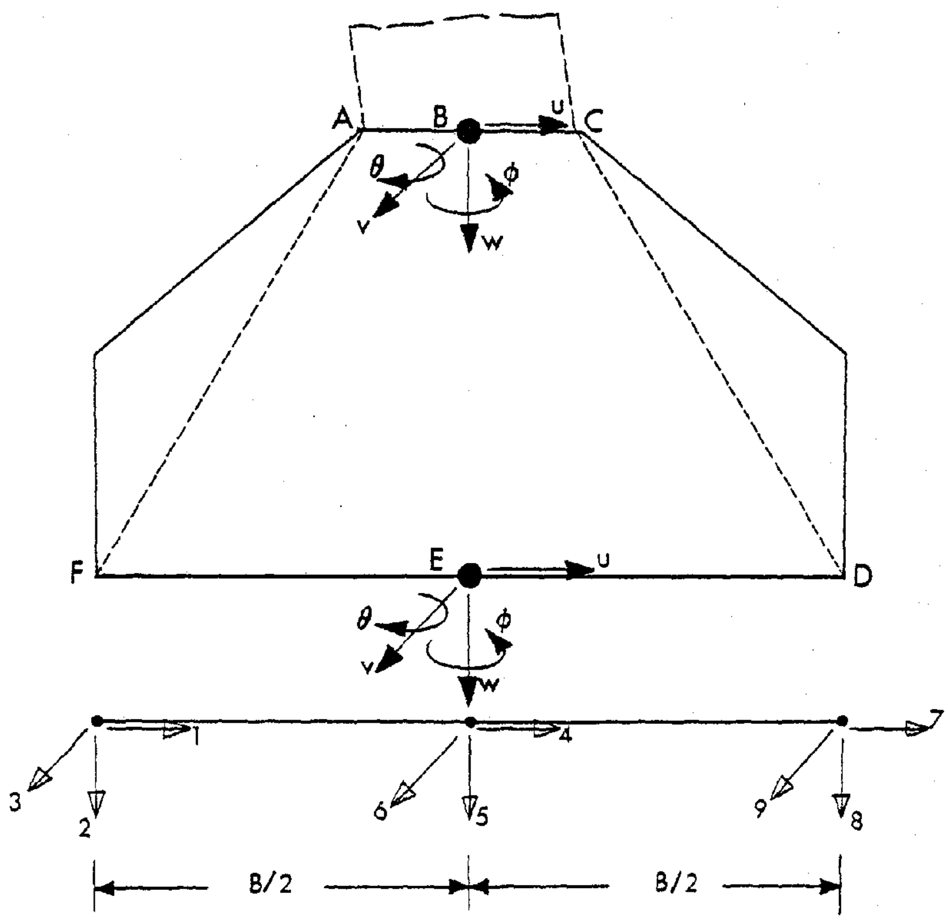

Figure 8. Ring Footing Cross Section

i. The six degrees of freedom at the base edges D and F must be eliminated and, at the same time, the rotational d.o.f. at E must be formed from the eliminated degrees of freedom; in other words, the nine d.o.f. should be lumped in five d.o.f. at the midpoint of the footing base.

ii. The contact stress between the soil and the footing may be compressive or shear stress, but not tensile stress.

iii. As this is a dynamic problem, not only the stiffness of the soil has to be considered, but the damping and inertial effects of the soil have to be taken into account as well.

The nine stiffness elements of Figure 9 are obtained from the impedance matrix by considering each stiffness element on the main diagonal as a linear spring in the corresponding direction. Once these stiffness elements are computed, the rest of the connection model can be formulated, with the aid of the rigid base assumption and with factors (i) and (ii) in mind, by solving for the resultant in the five degrees of freedom at the central point E.

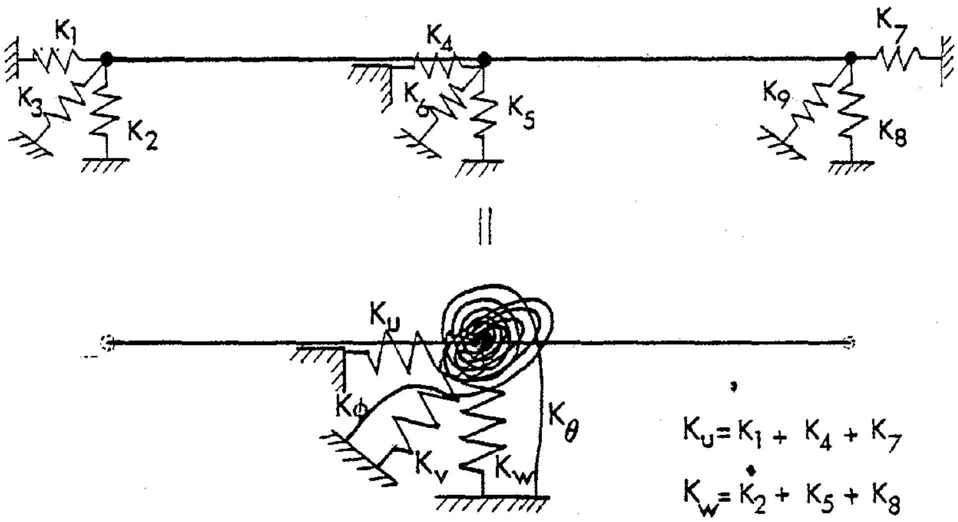

$$K_u = K_1 + K_4 + K_7$$

$$K_w = K_2 + K_5 + K_8$$

$$K_v = K_3 + K_6 + K_9$$

$$K_\theta = [K_2 + K_8]\,B/2$$

$$K_\phi = [K_3 + K_9]\,B/2$$

Figure 9. Equivalent Boundary Stiffnesses

$$
\begin{aligned}
K_u &= K_1 + K_4 + K_7 \\
K_w &= K_2 + K_5 + K_8 \\
K_v &= K_3 + K_6 + K_9 \\
K_\theta &= \frac{B}{2}\,(K_2 + K_8) \\
K_\phi &= \frac{B}{2}\,(K_3 + K_9)
\end{aligned}
\qquad (4\text{-}6)
$$

In the connecting model of Equation (4-6) only force continuity between the shell footing and the soil elements are satisfied while the kinematic continuity may not be satisfied due to the rigid base assumption. However, this problem of incompatibility may be ignored as the analysis is not a combined type of analysis. In the combined finite element models, the kinematic continuity at the points between adjacent elements is necessary and sufficient for the convergence of solution, which is not the case here.

It may be of interest to compare the connection model just described in this section and a recent research study carried out by Karadeniz (39). The model presented in Karadeniz's work is the alternative to the approach chosen herein where two dummy nodes are added to the last node in the shell model to match the dimensions of the adjacent solid element. These dummy nodal points are connected to the shell by horizontal weightless arms. In that model, at the point of connection between the shell and solid elements, only the kinematic continuities are satisfied as stated by Karadeniz. While the the model used by Karadeniz is suitable for combined finite element analysis, it necessitates the modification of the last element in the shell in a way which complicates the dynamic analysis of the shell if the substructure model is to be used, as in the present analysis. This complication arises from the presence of three nodal points at the shell base, one real and two dummy; furthermore, a transformation for the displacements as well as for the input base motion due to the geometrical discontinuities is required. Moreover, adding two dummy nodes increases the size of the problem while the rotational degrees of freedom at all three nodes are still indeterminate.

Proceeding with the present connection model and in consideration of factor (iii) as discussed earlier, an approach for calculating the inertial effects which is similar to that used in deriving the stiffness elements is used, whereby the elements on the diagonal of the condensed mass matrix are considered as lumped masses in the corresponding degrees of freedom, and the resultant in the five degrees of freedom at the central point E of Figure 9 are evaluated as follows:

$$m_u = m_1 + m_4 + m_7$$

$$m_w = m_2 + m_5 + m_8$$

$$m_v = m_3 + m_6 + m_9$$

$$m_\theta = (m_2 + m_8)\cdot B/2 \qquad (4\text{-}7)$$
$$m_\phi = (m_3 + m_9)\cdot B/2$$

The damping system is formulated from the imaginary part of the impedance matrix K_s in a way similar to the stiffness elements of the EBS as discussed previously. The resulting dampers in the five degrees of freedom of point E (Figure 9) represent the complete damping system in the case of a viscoelastic material but only the radiation damping at the energy transmitting boundary for an elastic soil material. For the latter soil case the material damping needs to be considered as well and one possible approach is to construct a proportional damping matrix from the final stiffness elements and the corresponding lumped masses, such that

$$\bar{d}_i = C_o m_i + C_1 K_i \qquad (4\text{-}8)$$

where

$$C_o = 2\,\omega_1\omega_5(\xi_1\omega_5 - \xi_5\omega_1)/(\omega_5^2 - \omega_1^2)$$

and

$$C_1 = 2(\xi_5\omega_5 - \xi_1\omega_1)/(\omega_5^2 - \omega_1^2) \qquad (4\text{-}9)$$

In Equation (4-9), ω_1 and ω_5 are the lowest and the highest frequencies of the system (see Figure 8), ξ_1 and ξ_5 are the corresponding damping ratios. Due to the uncoupling between the five degrees of freedom at point E, the frequencies ω_1 to ω_5 may be calculated from the simple relation

$$\omega_i = (K_i/m_i)^{1/2} \tag{4-10}$$

It should be noted here, that ω_5 and ξ_5 are used in forming C_o and C_1 of Equation (4-9) instead of ω_2 and ξ_2 due to the fact that the band of ω_i is limited as will be seen later and in most cases ω_1 and ω_2 are very close in value which may cause numerical instability while calculating C_o and C_1.

The complete damping system for the elastic soil system is the sum of the material and radiation damping

$$d_i = \bar{d}_i + \bar{C}_i \tag{4-11}$$

where

$$\bar{C}_i = \{\bar{C}_u, \bar{C}_w, \bar{C}_v, \bar{C}_\theta, \bar{C}_\phi\} \tag{4-12}$$

= the radiation damping of the soil medium

and

$$\begin{aligned} \bar{C}_u &= \bar{C}_1 + \bar{C}_4 + \bar{C}_7 \\ \bar{C}_w &= \bar{C}_2 + \bar{C}_5 + \bar{C}_8 \\ \bar{C}_v &= \bar{C}_3 + \bar{C}_6 + \bar{C}_9 \\ \bar{C} &= (\bar{C}_2 + \bar{C}_8)B/2 \\ \bar{C} &= (\bar{C}_3 + \bar{C}_9)B/2 \end{aligned} \tag{4-13}$$

where $\bar{C}_1$ to $\bar{C}_9$ are the main diagonal elements for the imaginary part of matrix K_s of Equation (4-5)

Figure 10 gives the translational and the rotational stiffnesses, lumped masses and damping elements at the midpoint of the footing base. These are the modal values and they are expressed in Fourier series in the θ direction.

4.3 COMPUTER IMPLEMENTATION

In an attempt to use SHORE-III program (40) after introducing the necessary modifications to some subroutines, the authors of this report have developed a computer program (SUBASE), in which the Equivalent Boundary System for a rotational shell is computed. The EBS is to be supplied as input for the modified SHORE-III program. This approach has the advantage of reducing the computer storage area as SHORE-III requires 300K in high speed storage to solve a normal size problem. Furthermore, by this approach, the dynamic analysis capability of SHORE-III program which includes the consideration of the effects of wind, earthquake, and blast loading in deterministic sense is unaltered.

4.3.1 SUBASE Program

The SUBASE program is designed to develop the stiffness, mass and damping elements which represent the soil medium under a ring footing supporting shell of revolution. It has the capability of analyzing layered strata over actual or assumed rock of infinite horizontal extent. The program is limited, however, to soil materials with real modulii (no phase angle between the stress and strain vectors) and with cross-anisotropy, i.e., the constitutivity

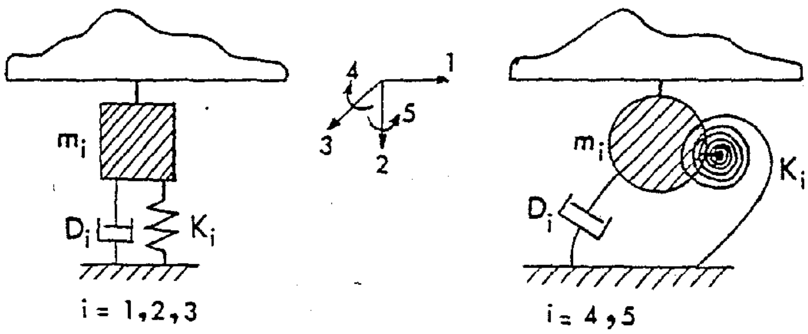

Figure 10. Equivalent Boundary System (EBS)

matrix is restricted to be a function of the radius from the axis of symmetry of the shell and the depth from the foundation level.

The SUBASE program is a new development. It is written in FORTRAN IV language and has been implemented on an IBM 370/145 computer. The program requires 300K in high speed storage and the single precision is used in the calculations.

As can be seen from the flow diagram for SUBASE, shown in Figure 11, the Equivalent Boundary System is obtained, harmonic-wise, for a given excitation frequency Ω through the following steps:

a - Input Data

The input data for geometry, nodal locations, material, number of layers, control data, etc. are read and additional data are generated.

b - Generation of Element Matrices

Corresponding to the current harmonic, the stiffness matrix and the mass matrix for each element are generated.

c - Generation of Layer Matrices

For each harmonic, the layer matrices, required for the eigenvalue problem of the wave propagation problem in the far-field, are generated.

d - Eigenvalue Solution

For each harmonic, the wave numbers and the mode shapes for the propagating wave are obtained.

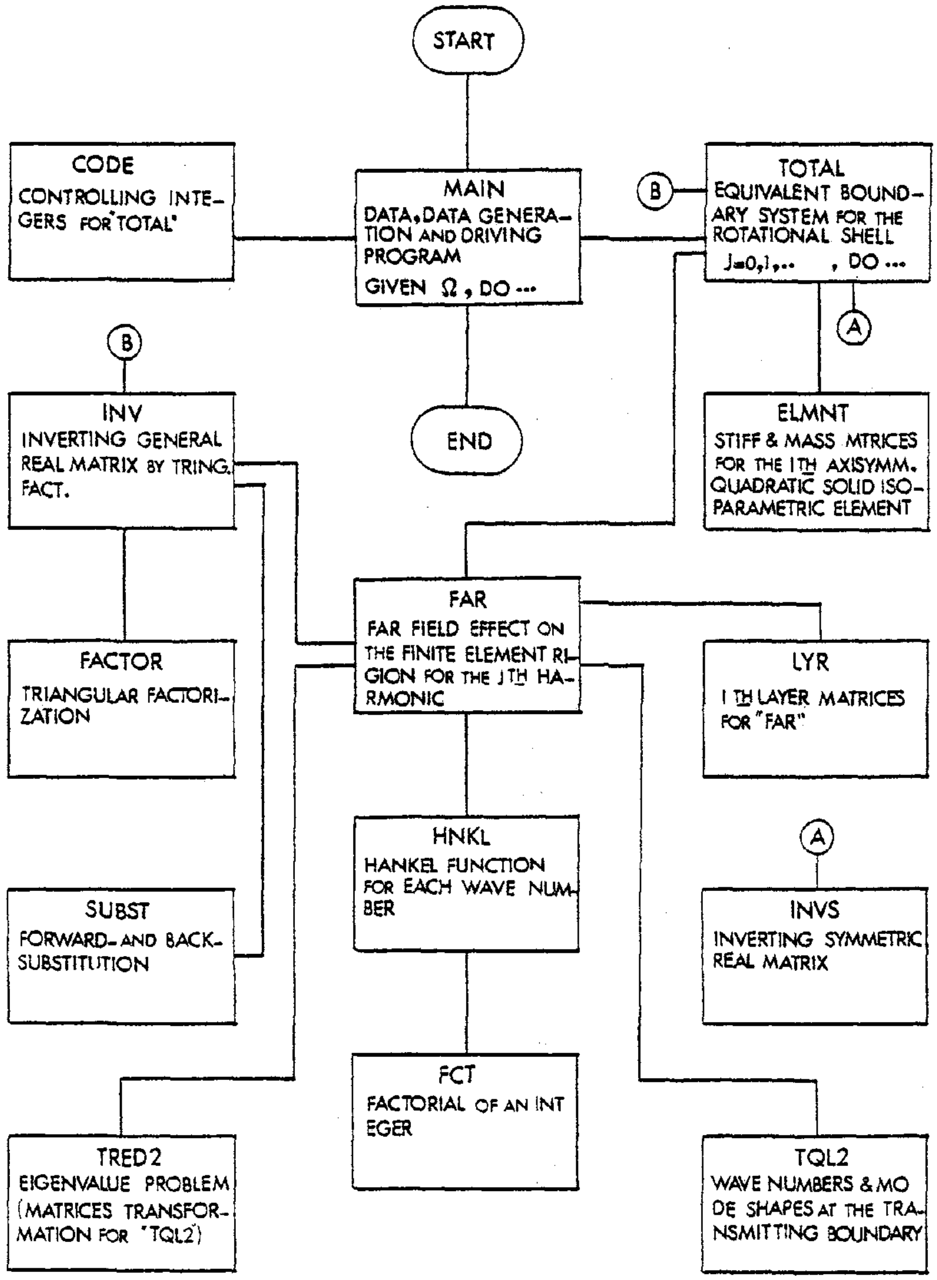

Figure 11. Flow Diagram for SUBASE Program

e - Assembly of Global Matrices

The boundary matrix, together with the matrices of the F.E. region, form the dynamic stiffness matrix of the stratum.

f - Equivalent Boundary System

For each harmonic, the equivalent stiffness elements, mass elements and damping elements at the lower five degrees of freedom of the ring footing are calculated and printed out.

A complete listing of the program is given in Appendix 8. 3. The listing contains further details about the program through the heading comments in each subroutine.

4.3.2 SHORSS Program

The SHORSS program is a finite element program for the linear static and dynamic analysis of axisymmetric shells (and shell-like structures) and plates. The dynamic analysis includes the soil effects which are introduced with the aid of SUBASE program. It is an extension of the static and dynamic analysis program SHORE-III (41).

The SHORSS program is written in FORTRAN IV language and has been implemented on an IBM 370/145 computer. It has the same storage area as SHORE-III and the overlay structure shown in Figure 12 must be used for running the program. All the details about the program as well as the flow diagram are omitted here since they are almost the same as those describing SHORE-III program (35,40). However, the

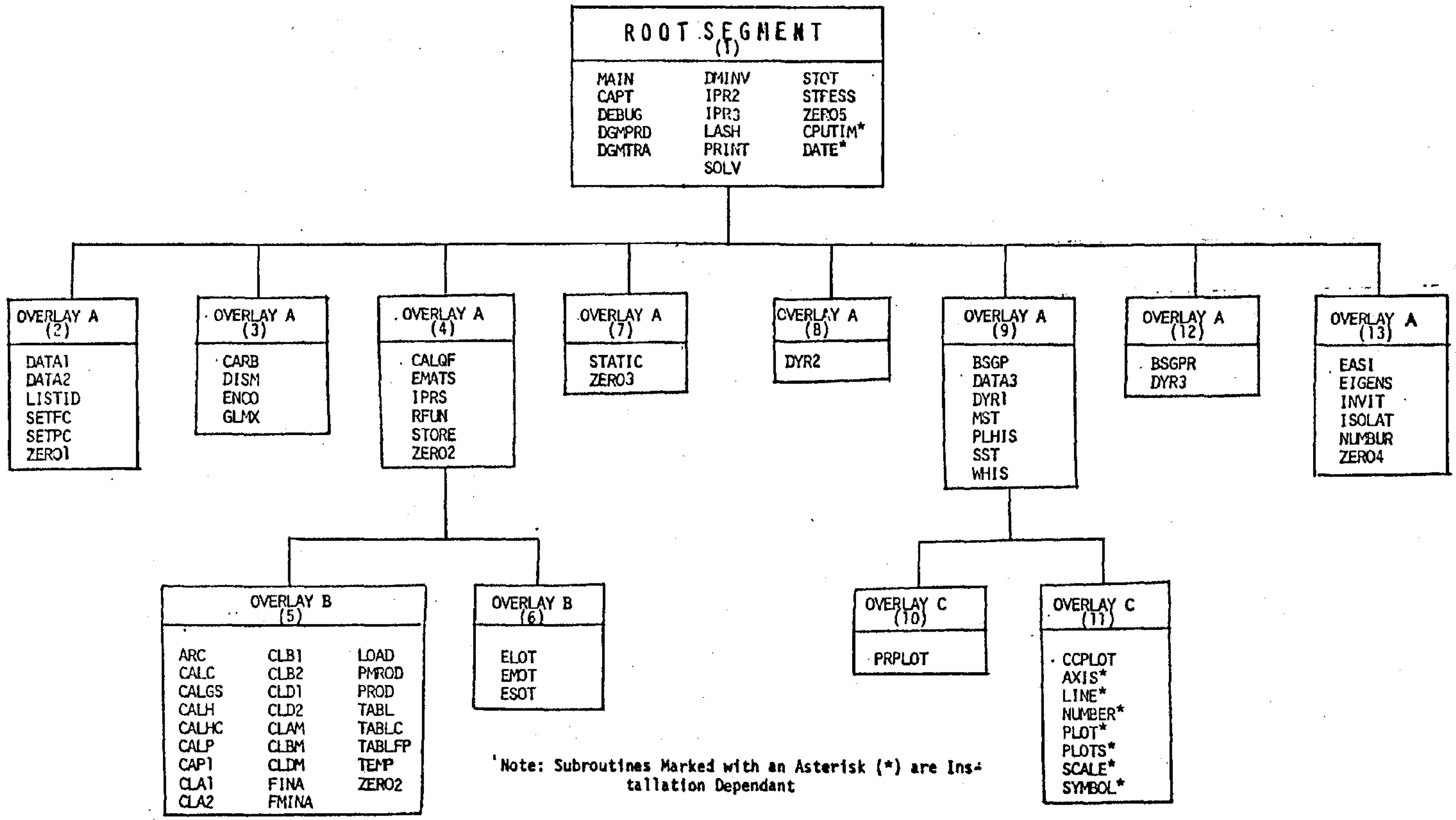

Figure 12. Overlay Structure of SHORSS Program

necessary modifications to the User's Manual of SHORE-III are given in Appendix 8.4.

4.3.3 Scheme of Computation

In this section the overall scheme of the analysis is described. The master flow chart of the computation is presented in Figure 13. In this model the computation for the displacements and stresses in a shell of revolution subjected to a general loading (static or dynamic loading which may be symmetrical, antisymmetrical or with any distributed pattern around the axis of symmetry of the shell). The simplest case of loading is the static loading, in which no soil effect should be considered in the analysis; however, the load may be complicated and requires a Fourier series expansion to carryout the analysis harmonicwise. The SHORSS program, with a fixed lower boundary, becomes SHORE-III program in this case.

In case of dynamic analysis, the problem becomes more involved and the soil effect becomes an important factor for a more realistic model. With the aid of the SUBASE program the equivalent boundary system (EBS) can be calculated and introduced at the foundation level, then the analysis is to be carried out harmonicwise using the SHORSS program. To account for the possibility of foundation uplift the stresses at the foundation level should be checked and any net tensile stresses will correspond to uplift; however, the dead load stresses as well as the

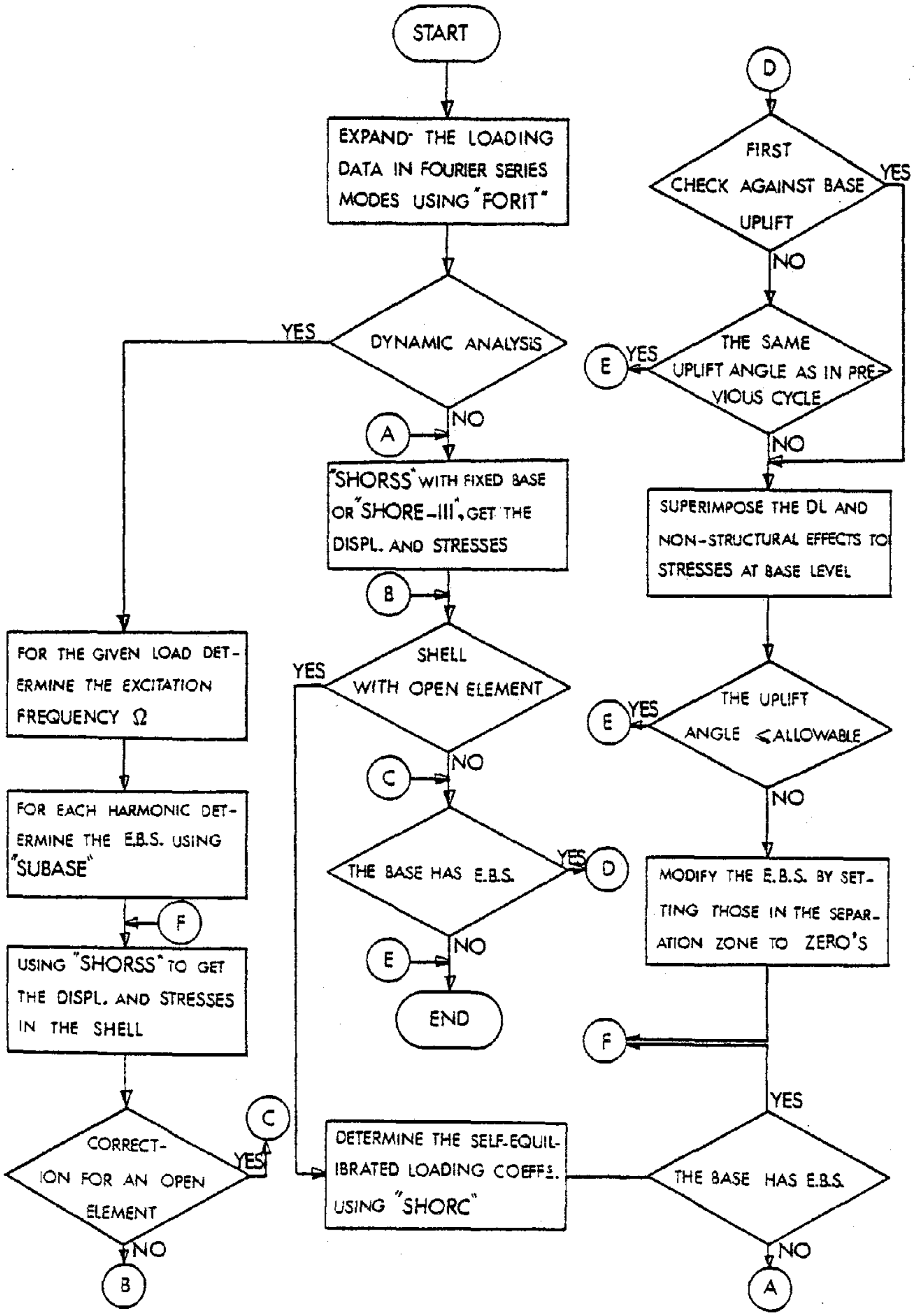

Figure 13. Computational Scheme

effect of any non-structural elements tied to the shell foundation must be included in calculating the net tensile stress at the soil-foundation interface. If the separation zone is significant, the analysis should be carried out again with new EBS with zero stiffnesses, masses and dampers in the separation zone. The modification may be done by expanding the new EBS in Fourier series and the resulting modal values should then be introduced to the ring footing. The analysis is completed if the resulting separation angle, Figure 14, is the same as in the previous cycle.

For any type of analysis, static or dynamic, the local stresses near the base, for shells with column supports, need to be corrected. The superposition technique is to be used. The solution is composed of the continuous boundary case and a self-equilbrated line load case, both of which are represented in Fourier series, Figure 15. The necessary computer program to evaluate the Fourier coefficients is developed by the authors of this report, SHORC program, and is described and listed elsewhere (42). As the ring footing is in the vicinity of the discrete supports the correction should be carried out at both sides of the discrete supports. It should be noted here that FORIT program is capable of evaluating the Fourier coefficient for any loading distribution, but not for the particular case of self-equilibrated line load.

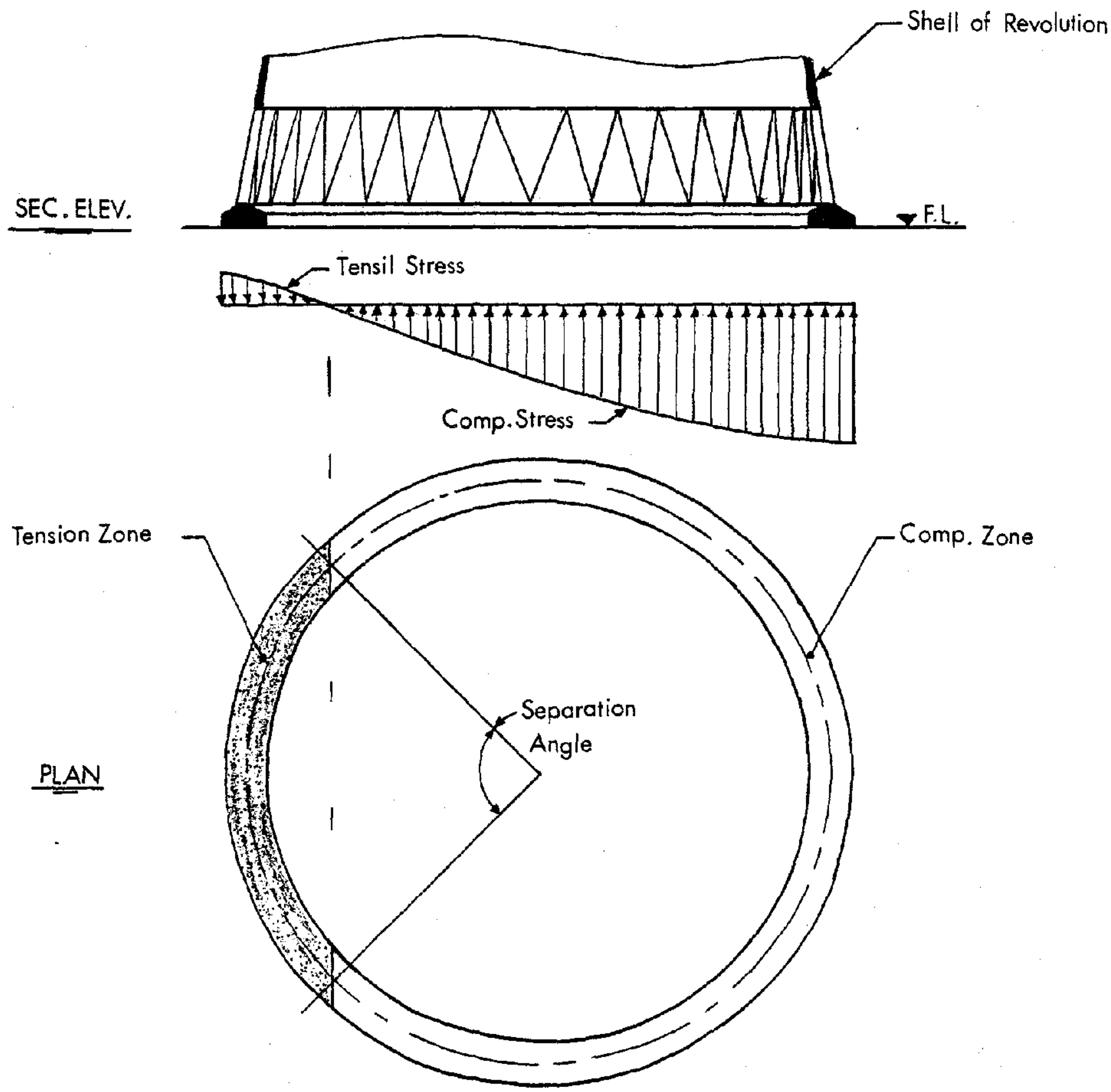

Figure 14. Base Uplift

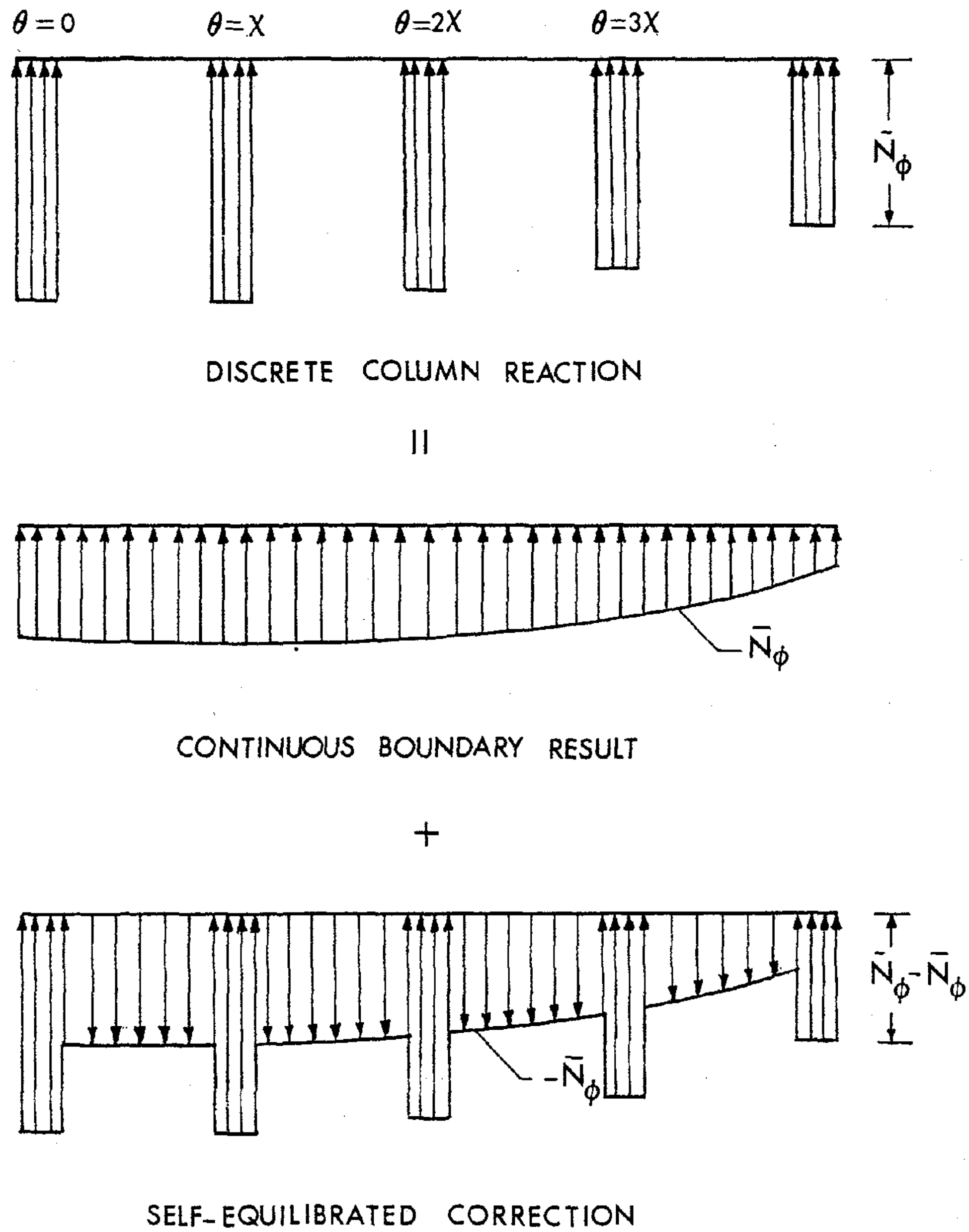

Figure 15. Discrete Column Analysis

5. PARAMETRIC STUDIES AND APPLICATIONS

5.1 INTRODUCTION

The influence of the geometry and material properties of a soil stratum on the response of a shell of revolution founded atop the stratum and subjected to forced excitations will be studied in this chapter. The main objectives are: to check the applicability and accuracy of the model presented in the previous chapter; to present results for cases for which no known analytical solution exists; and to assess the importance of the soil on the shell response to dynamic loads.

The study is divided into two main sections: the first is the study of the soil model which may be examined through the equivalent boundary system and the second is the dynamic analysis of shells of revolution in which the soil effect on the dynamic response is discussed. In the first section, the soil model study, dimensionless analysis is used throughout and the results are plotted against the non-dimensional excitation frequency a_o, where

$$a_o = \frac{\Omega r_o}{v_s} \qquad (5\text{-}1)$$

in which Ω is the excitation frequency, r_o is the radius of the energy absorbing boundary and v_s is the shear wave velocity in the stratum.

In order to check the applicability and effectiveness of the energy absorbing boundary based on the theory presented in Chapters 2 and 3, a time history analysis is carried out for two cycles of a sinusoidal ground acceleration applied at the lower boundary of the finite element region of Figure 16. The sinusoidal ground acceleration has a maximum amplitude of 20% g and a frequency equal to 10 radians per second. To perform the time history analysis, numerical integration is needed which, in turn, depends on the highest period of the system and requires the evaluation of the eigenvalues of the finite element model. However, one may sometimes avoid a time consuming eigenvalue analysis by choosing a most accurate unconditionally stable numerical integration scheme. Among the different numerical schemes, such as the Newmark β method (43), Wilson θ method (44) and the direct step-by-step integration method (45), the Newmark method was found to be the most stable method by Wilson and Bathe (45). The accuracy of the integration increases by decreasing the time step Δt. For large values of Δt, the errors in period are increased and the percentage amplitude decay also is increased. From Wilson and Bathe's Analysis (46), the Newmark technique proved to be the only one which gives no errors either in the period or in amplitude alternation for $\beta = 1/4$.

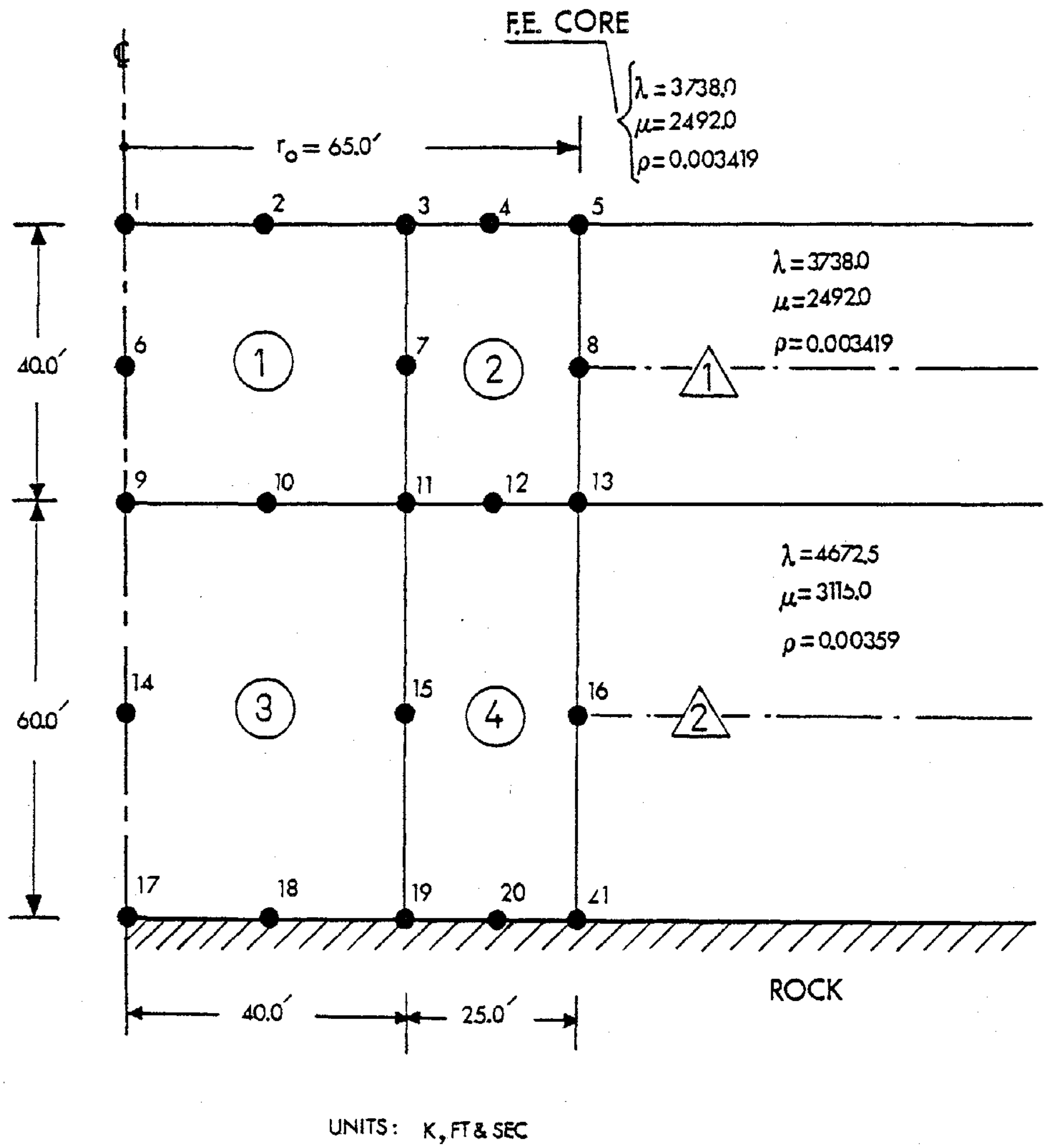

Figure 16. F.E. Mesh for the Time History Analysis of Two Cycles of a Sinusoidal Acceleration

For J = 1, the dynamic analysis is carried out using two models which are the same except for the vertical boundaries. The first model has an energy absorbing boundary which is represented by the boundary matrix R_b of Equation (3-60) while the second has a roller boundary, which alows the nodal points along the vertical boundary to move freely in the vertical and circumferential directions. Numerical computations herein are conducted using the Newmark method with $\beta = 1/4$ and a time step of 0.005 sec.

The three components of the response accelerations of node 4 $\ddot{u}$, $\ddot{w}$ and $\ddot{v}$ are given in Figure 17. This particular node is chosen because of the importance of its nodal degrees of freedom when computing the EBS. In Figure 17 the response accelerations show that, in contrast to the undamped response in the model with a roller boundary (solid lines), the model with an energy absorbing boundary produced a damped response (dotted lines). This indicates that the energy absorbing boundary, which is developed in Chapters 2 and 3, absorbs the energy of the waves. Further, it is indicated in Figure 17 that the response of the roller boundary model builds up around t = 2.5 sec.; thus, it follows that the roller vertical bounary produces reflected waves.

The above numerical illustrations provide a check on the applicability and the effectiveness of the energy absorbing boundary.

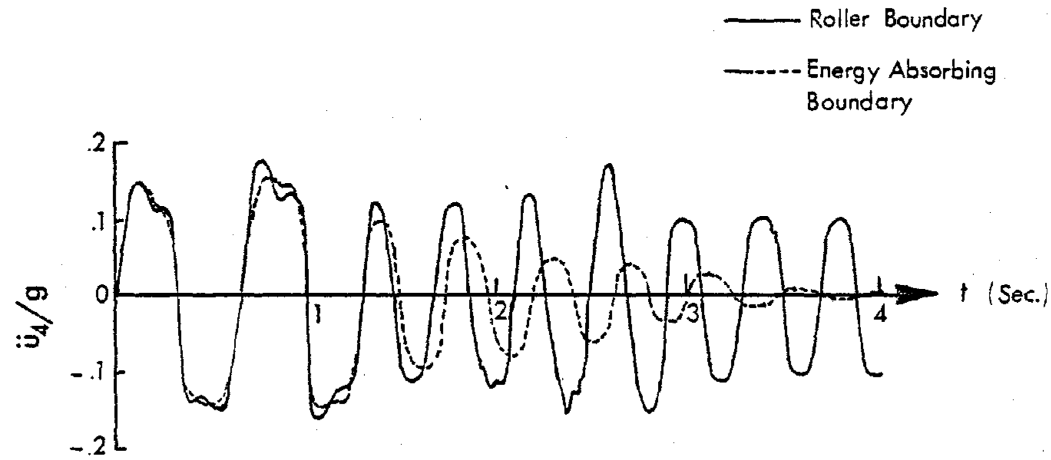

Fig. 17-a

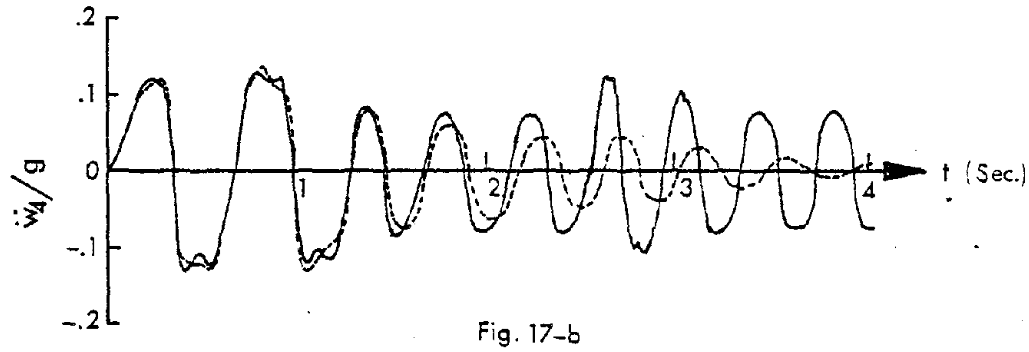

Fig. 17-b

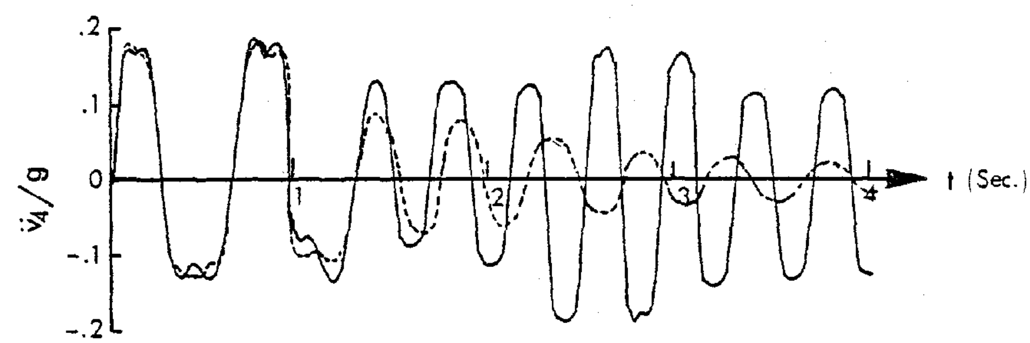

Fig. 17-c

Figure 17. Response Accelerations of
4 Sec. Time History Analysis

5.2 PARAMETERS AFFECTING THE EBS

In this section the convergence of the finite element solution which is used in the equivalent boundary system calculation is evaluated. To evaluate the convergence of the F.E. solution, two parameters should be studied; the first is the effect of the lower boundary location which is assumed to be totally fixed and the second is the mesh effect. The natural frequencies, stiffnesses and damping of the EBS are then studied for a range of the excitation frequency Ω. Also, the EBS quantities for the higher Fourier harmonics are compared to those for the first two harmonics ($J = 0$ and 1), in order to extrapolate the values of the soil constants for the very high harmonics and to assess the usefulness of the present theory in obtaining solutions for a general harmonic, which is a quite new development.

5.2.1 Effect of the Stratum Depth

The depth of the stratum for a given ring footing dimension, influences the results for the stiffnesses and damping of the EBS since the dynamic response of the nodes at the foundation level is significantly influenced by the natural modes of vibration of the stratum as well as by reflections at the rock-soil interface.

To evaluate the convergence of the EBS quantities for the case of a very deep stratum, six meshes with the same element size throughout the mesh were considered. Figure 18 gives the dimensions of the six meshes which start with a shallow stratum and end with a very deep one. Table 2 gives the soil material properties which are used with all meshes. With the vertical boundary radius r_o = 80 ft. and the dimensionless frequency a_o=5.0, Ω is calculated from Equation (5-1) and it is found to be 53.36 radians per second.

The results for the six meshes are summarized in Table 3 in which the natural frequencies, stiffnesses and damping of the EBS are presented. Also, the dimensionless $\omega/\bar{\omega}$, $K/\bar{K}$ and $D/\bar{D}$ are plotted in Figures 19 to 21 against the depth ratio H/r_o, where $\bar{\omega}$, $\bar{K}$ and $\bar{D}$ are the EBS quantities for the very deep stratum which may be considered to be the half-space solution as the reflections at the rock-soil interface are expected to be very small. The percentage damping ratios ξ_1 and ξ_5 are assumed to be 5% and 10% respectively.

The approximate CPU time in the IBM 370 computer to run the SUBASE program is 5 seconds per layer per harmonic for each driving frequency. However, only one Fourier harmonic is used in the analysis (J = 1) for a single driving frequency (Ω = 53.36 radian per second).

The results given by Table 3 and Figures 19,20 indicate the importance of the stratum depth factor for the

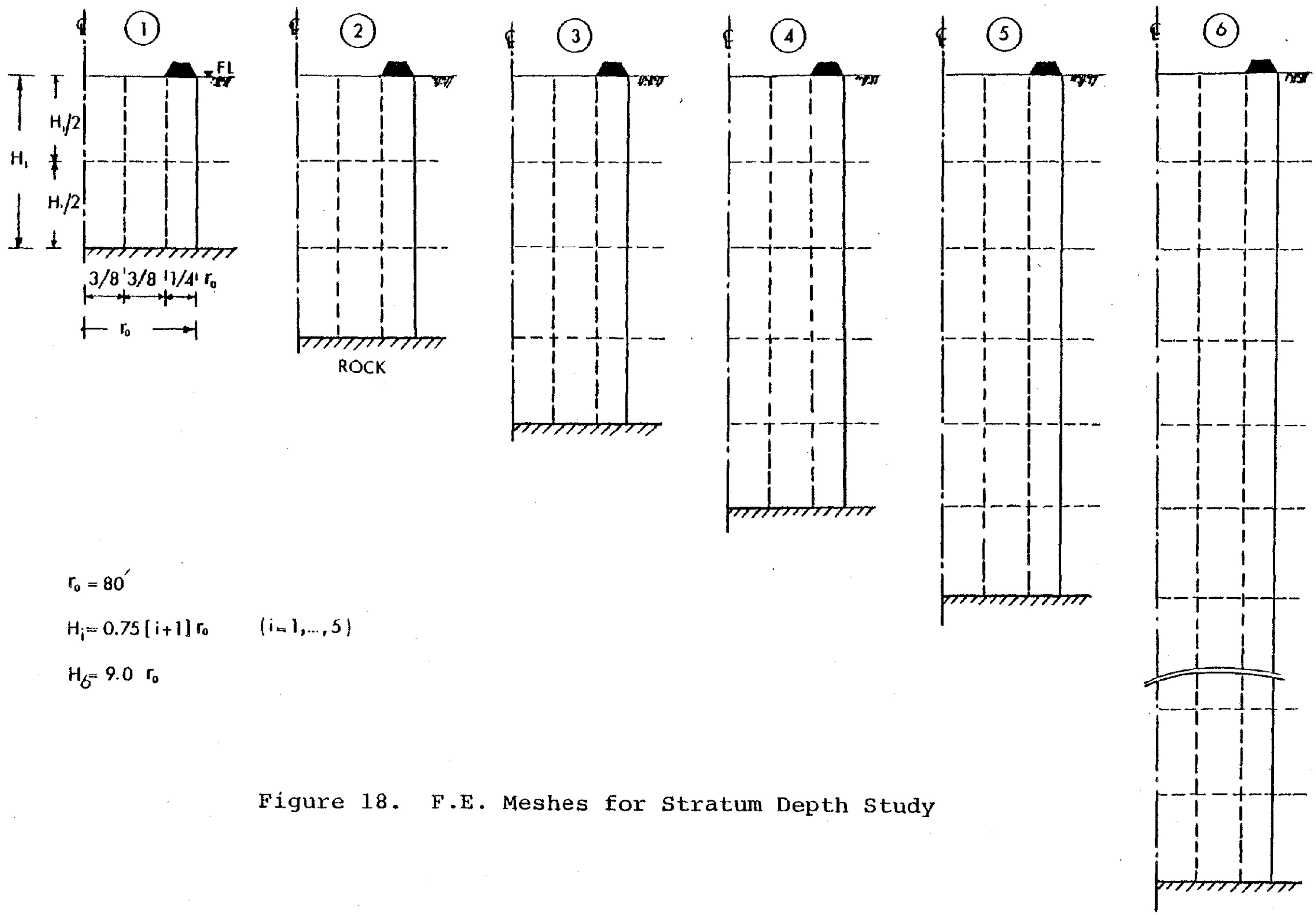

Figure 18. F.E. Meshes for Stratum Depth Study

Table 2. Soil Material Properties

Soil Properties	λ	μ	ρ	a_o	v_s	v_p
All Finite Elements	3738.0	2492.0	0.003419	5.0	853.74	1599.71
All Layers	3738.0	2492.0	0.003419	5.0	853.74	1599.71

Units: K, Ft and Sec.

Table 3. EBS Quantities for the Stratum Depth Analysis (J=1)

H/r_o	u			w			v		
	ω	$K_{\times 10^5}$	$D_{\times 10^3}$	ω	$K_{\times 10^5}$	$D_{\times 10^3}$	ω	$K_{\times 10^5}$	$D_{\times 10^3}$
1.5	49.318	22.654	11.913	51.837	34.046	9.443	40.751	18.184	6.951
2.25	40.816	16.262	13.514	39.623	19.082	10.524	31.465	10.630	7.661
3.0	38.434	14.064	14.210	35.502	16.132	11.381	27.975	8.568	8.354
3.75	36.223	12.785	14.851	33.446	13.872	11.652	26.370	7.771	8.631
4.5	35.713	12.341	15.003	32.705	13.370	11.800	25.987	7.428	8.722
9.0	34.012	11.215	15.233	31.698	12.554	12.061	25.478	7.081	8.916

All units are: Kips, Ft and seconds

Table 3 (continued)

H/r_o	θ			ϕ		
	ω	$K_{\times 10^5}$	$D_{\times 10^3}$	ω	$K_{\times 10^5}$	$D_{\times 10^3}$
1.5	54.071	186.979	31.744	81.188	138.286	27.074
2.25	37.443	83.128	36.124	55.864	75.859	30.541
3.0	32.697	66.711	38.411	53.007	60.398	33.347
3.75	30.810	58.372	39.787	50.599	54.841	34.450
4.5	30.515	55.870	40.012	49.740	51.217	35.117
9.0	29.483	52.118	40.971	47.735	48.318	35.512

All units are: Kips, Ft and seconds

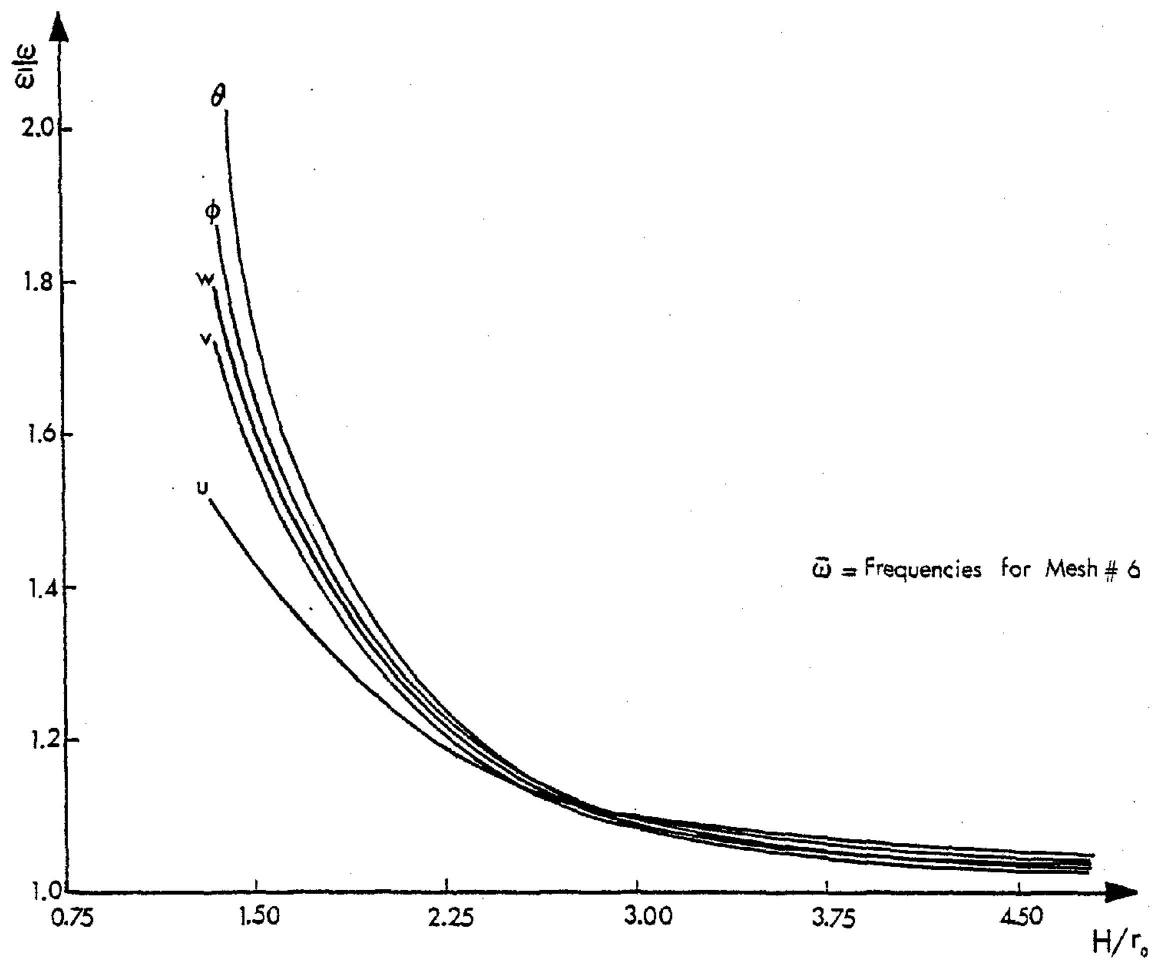

J = 1

$a_o = 5$

$r_o = 80'$

$\lambda = 3738$ ksf

$\mu = 2492$ ksf

$\rho = 0.003419$ $K.Sec.^2 Ft.^{-4}$

Figure 19. Effect of Stratum Depth on the Frequency

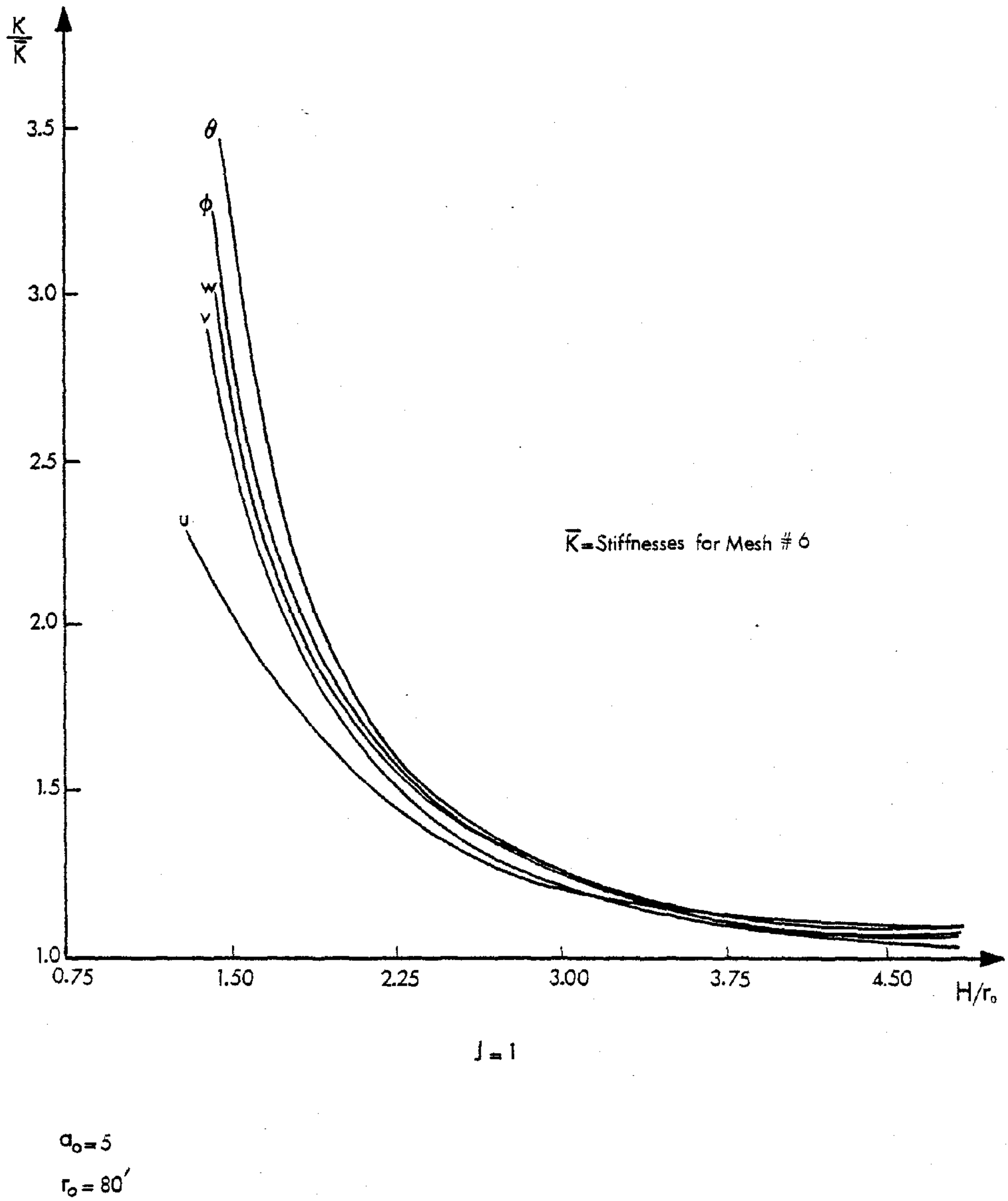

Figure 20. Effect of Stratum Depth on the Stiffnesses

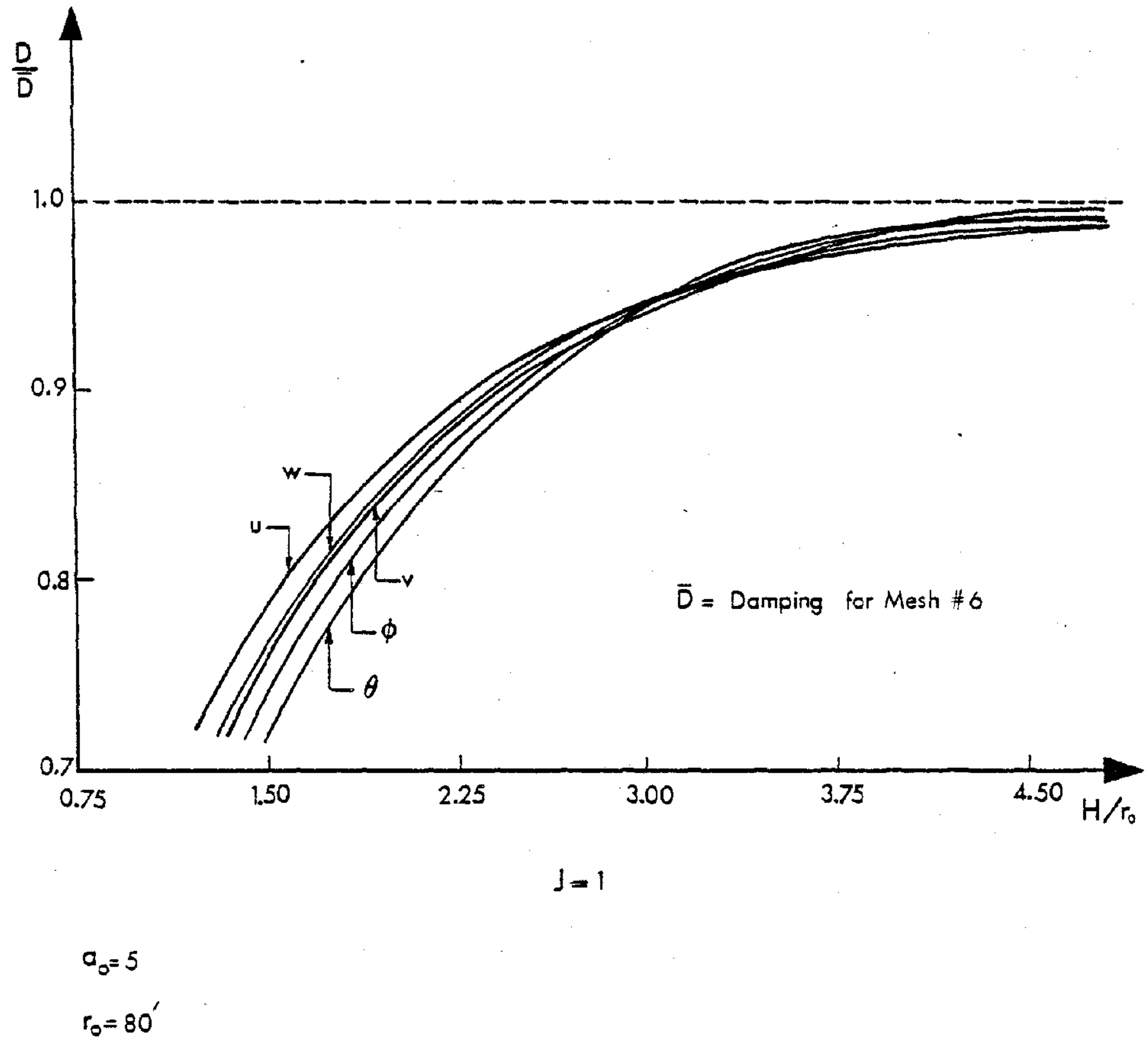

Figure 21. Effect of Stratum Depth on the Damping

natural frequencies and stiffnesses. On the other hand, the damping elements are less sensitive to the depth factor as one can notice from Table 3 and Figure 21. It is interesting to notice that the error in the stiffness elements as the stratum gets shallower is proportional to the square of the error in the corresponding natural frequency. This is because the mass elements did not change with the change of the lower boundary location. It is also interesting to notice that at some depth ratio ($H/r_o \simeq 3$) the error in the five components of the EBS became very close to each other and, morover the EBS quantities at such depth ratios approach the half-space solution which is represented here by the depth ratio $H/R_o = 9$.

The insensitivity of the damping elements to the stratum depth suggests that the damping is mainly due to the radiation of the waves horizontally in the far-field and that the vertical radiation of the waves is not a major factor. However, the reflected waves on the rock-soil interface for the shallow strata ($H/r_o < 3$), caused the damping to decrease by about 15% as may be observed from Figure 21.

It may be noted from Table 3 that the EBS components which correspond to the rotational degrees of freedom (θ and ϕ) are more sensitive for the stratum depth. This may be due to the reflection of the waves on the lower boundary which tends to redistribute the response at the foundation level, mainly affecting the rotational components. This explanation is consistent with the results since for deep strata ($H/r_o \geq 3$), there is no predominant sensitivity of the different components of the EBS.

The study of the stratum depth presented in this section suggests some useful guidelines which may help to reduce the size of the parametric study. One very important finding is that the stiffness elements are the most sensitive of the EBS components; as a result, the remaining parametric studies may concentrate on the stiffness elements only. Also the study reveals that the assumption of fixed lower boundary at a depth $H = 3r_o$ is reasonable for most practical uses. This means that the dynamic influence region is defined through this study which brings forth the idea of a dynamic pressure bulb.

5.2.2 Mesh Size Effect

The dynamic pressure bulb is a generalization of the concept of a pressure bulb as defined in statics, in the study of pressure distributions under footings. It represents the zone of influence under the footing which affects its dynamic response and beyond which coarser finite elements may be employed without significantly influencing the dynamic behavior of the system. It is desirable, in order to ensure the efficiency and economy of the finite element solution, to use larger elements away from the zone of influence provided that such a zone exists.

Earlier studies on the finite element method applied to dynamic problems indicate that the size of the largest element in a system should be smaller than a certain fraction, usually 1/8 to 1/10, of the shortest wave length that is expected to be reasonably reproduced. In the case of a layered system and particularly for a deep one, it is often economically unfeasible to cover the whole depth with a fine mesh and it becomes necessary to investigate the possibility of using narrower (longer) elements with increasing depth away from the dynamic pressure bulb. At the same time, it is of interest to check the rate of convergence towards the continuum solution as the mesh is refined.

To evaluate the convergence of the finite element solution with decreasing element size, four meshes with a depth ratio $H/r_o = 3$ were considered: coarse, medium, medium-fine and fine. Soil material properties used in the analysis are those presented in Table 2. The four meshes along with the results are shown in Figure 22. Only the dimensionless stiffness elements K/Gr_o are plotted against the element size ratio ℓ/Λ, where ℓ is the longest element dimension in the mesh, and Λ is the shear wave length, which is obtained from the relation (27).

$$\Lambda = \frac{2\Pi\ r_o\omega}{\Omega} \qquad (5\text{-}2)$$

with ω = the fundamental frequency of the soil stratum.

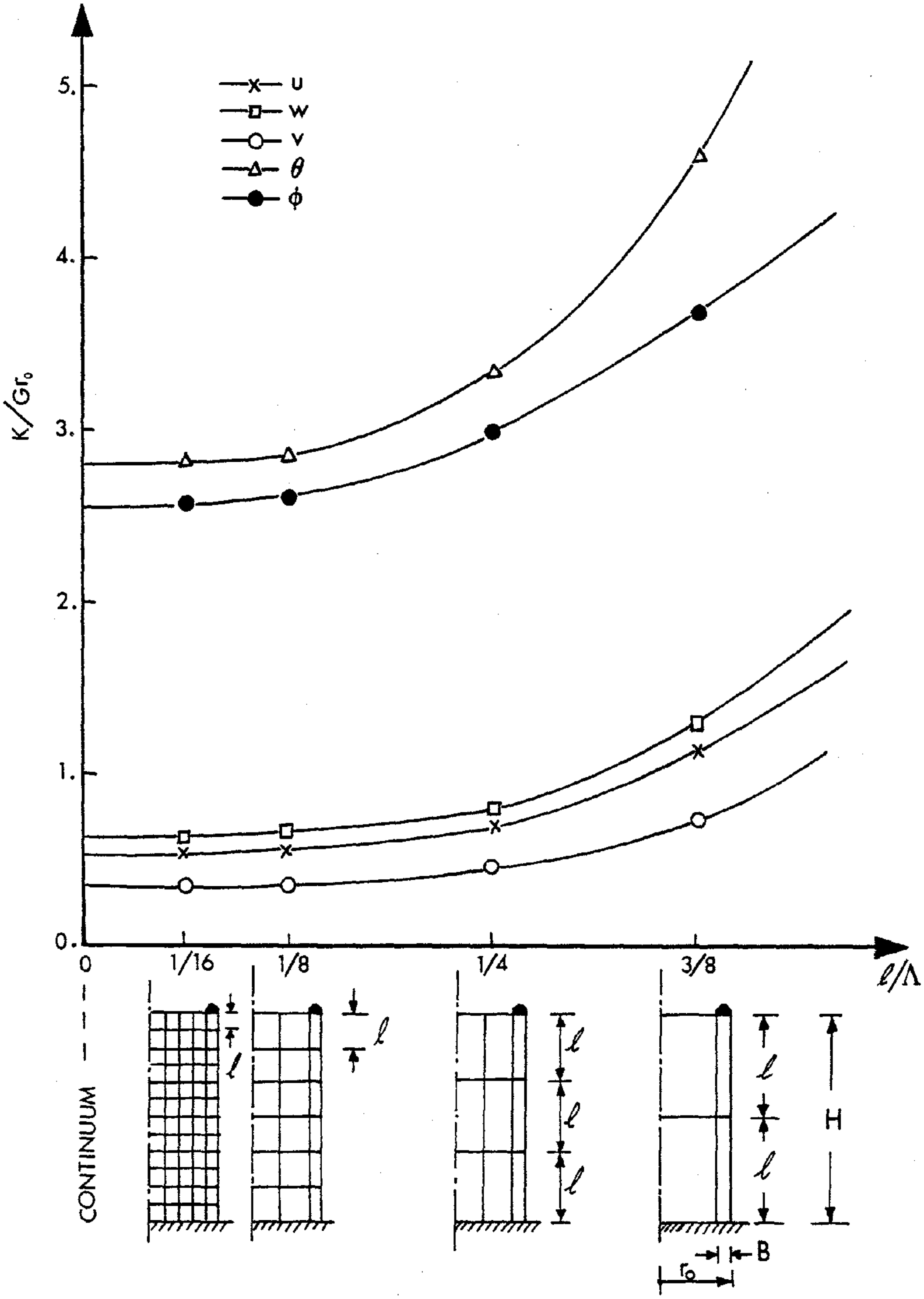

$J=1$

$a_o = 5$

$H/r_o = 3.$ $B/r_o = .2$ $r_o = 80'$

$G = 2492$ ksf $\Lambda = 317.3'$

Figure 22. Element Size Effect (Uniform Layers)

For the present analysis ω was considered to be the average frequency of the EBS with a very deep stratum ($\omega = \bar{\omega}_{av}$ = 33.68 rps) as considered in the previous section.

In Figure 22 the continuum solution could be extrapolated by the intersection of the curves with the vertical axis ($\ell/\Lambda = 0$). The results indicate that the largest element dimension in the mesh should not exceed $\Lambda/6$ for satisfactory results in case of a uniform mesh. Also, it may be noticed that the rate of convergence for the five components is approximately the same and that it is very slow for element size ratio less than 1/8.

In order to investigate the possibility of using larger elements with increasing depth, another four meshes are considered with same soil properties and depth ratio as those used in the convergence study. Knowing the continuum solution for the EBS from the convergence study, the errors in the finite element solution of the four meshes are calculated and plotted against the ratio 100/n, where n is the total number of elements in a mesh, Figure 23. Also, the four meshes used in the study are shown in the same figures.

It is interesting to notice that the mesh with twenty elements produced results with error as small as 0.7% of the continuum solution, although elements with dimensions equal to $\Lambda/4$ are used. Also, the results presented indicate that only negligible differences are noticed between the two

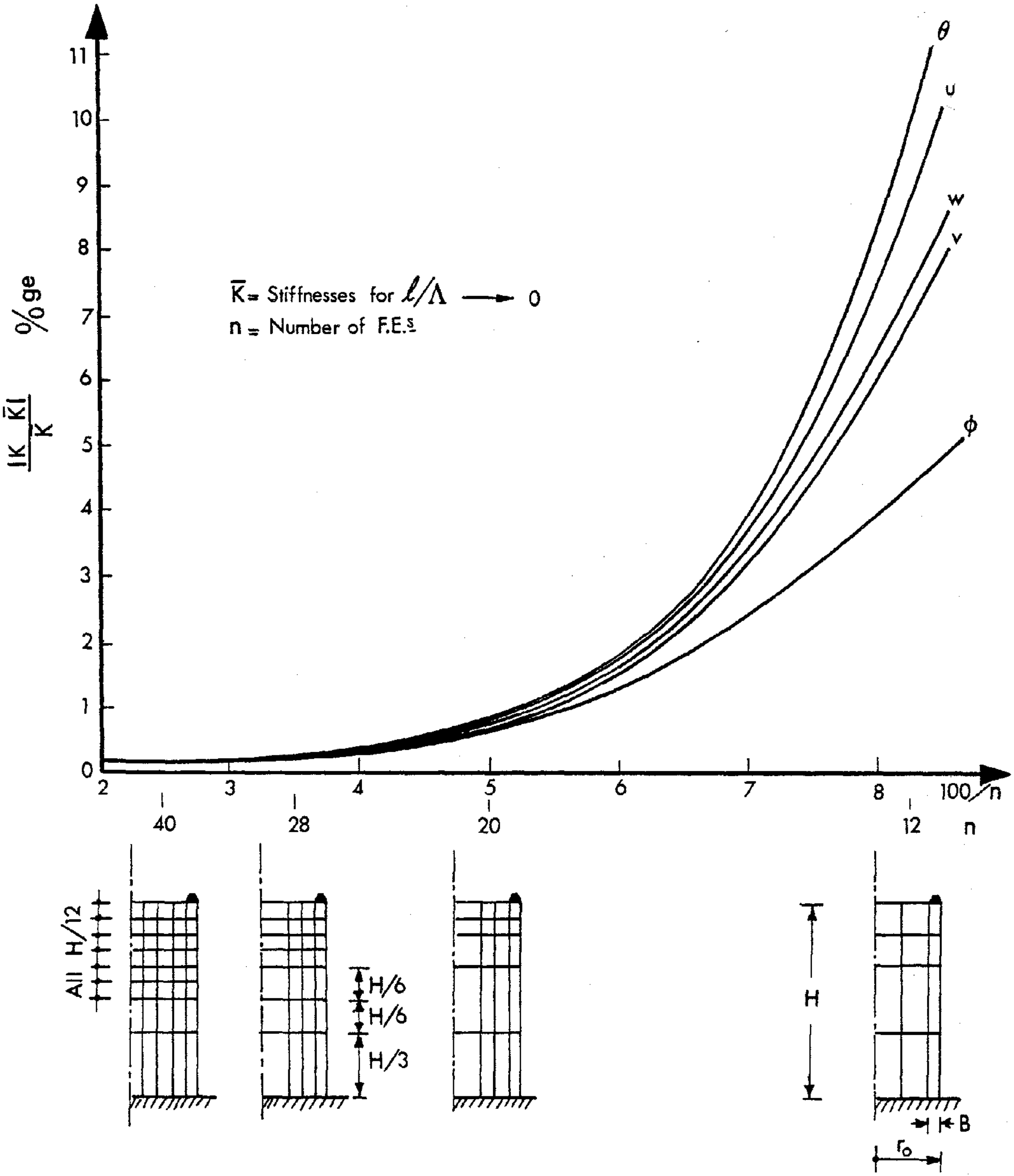

J = 1

$a_o = 5$

$H/r_o = 3.0$ $B/r_o = 0.2$ $r_o = 80'$

Figure 23. Mesh Effect
(Non-Uniform Layers)

meshes with twenty eight and forty elements. These results for the economical (non-uniform meshes) and those for the uniform meshes used in the convergence study are tabulated, for the purpose of comparison, in Table 4. This table indicates that the four meshes with non-uniform elements produced very close results for most practical applications.

Based on the studies of the finite element meshes, it is concluded that the zone of influence under the footing, which may be called the pressure bulb, is about 1.5 r_o and within this zone the size of the elements have an effect on the dynamic behavior. However, it should not be inferred from this conclusion that it is permissible to completely suppress the lower (long element) portion, as this results in increased values for the stiffness element due to the reflections of the waves on the assumed rock-soil interface, as discussed in the previous section. From this it is felt that the elements between the pressure bulb and the assumed lower fixed horizontal boundary may exceed the limitation $\ell/\Lambda < 1/6$ (say). At the same time, the limitations on the size of the finite elements within the dynamic pressure bulb must be enforced.

It should be noted here that the geometry of the foundation, which is a ring footing, affects the mesh size and the elements refinement near the foundation level. As the ratio B/r_o, the ratio of the base width to the radius

Table 4. Mesh Size Effect

Parameter		Stiffness Ratio K/Gr_o u	w	v	θ	ϕ
Max. Element Size Ratio ℓ/Λ (Uniform Meshes)	3/8	115.81	125.39	75.28	460.03	368.75
	1/4	70.63	80.72	46.88	327.67	300.28
	1/8	57.46	66.21	37.89	282.90	262.31
	1/16	55.80	62.09	36.03	280.11	261.08
1/n (Non-Uniform Meshes)	1/40	55.80	62.09	36.03	280.12	261.10
	1/28	55.97	62.28	36.07	280.87	261.69
	1/20	56.32	62.59	36.38	281.90	262.16
	1/12	60.91	66.68	38.51	309.42	274.00

of the energy absorbing boundary gets smaller, the dynamic pressure bulb may be confined to the ring footing vicinity with elements near the axis of symmetry having less effect. In such extreme cases, the zone of influence will take a toroidal shape below the ring footing and, consequently, more economical finite element meshes may be used with large elements away from the footing, radially towards the axis of symmetry and downwards away from the dynamic pressure bulb towards the lower boundary. Large towers, like reinforced concrete cooling towers, often have a large base diameter which results in small B/r_o ratios and possible use of the super-economical mesh like that shown in Figure 24.

5.2.3 Effect of the Driving Frequency

After the mesh size and the lower boundary location have been established it is useful to compare the present model results with existing elastic half space results. Due to the limitations of the half space solution, only a few cases of axisymmetric problems have been solved; one of these is the dynamic analysis of a rigid circular footing on an elastic half space (47). In this paper the axisymmetric vertical footing is considered and the vertical displacement δ of the footing is calculated from the relation (see Figure 25).

$$\delta = \frac{P_o}{K} F e^{i\Omega t} \qquad (5\text{-}3)$$

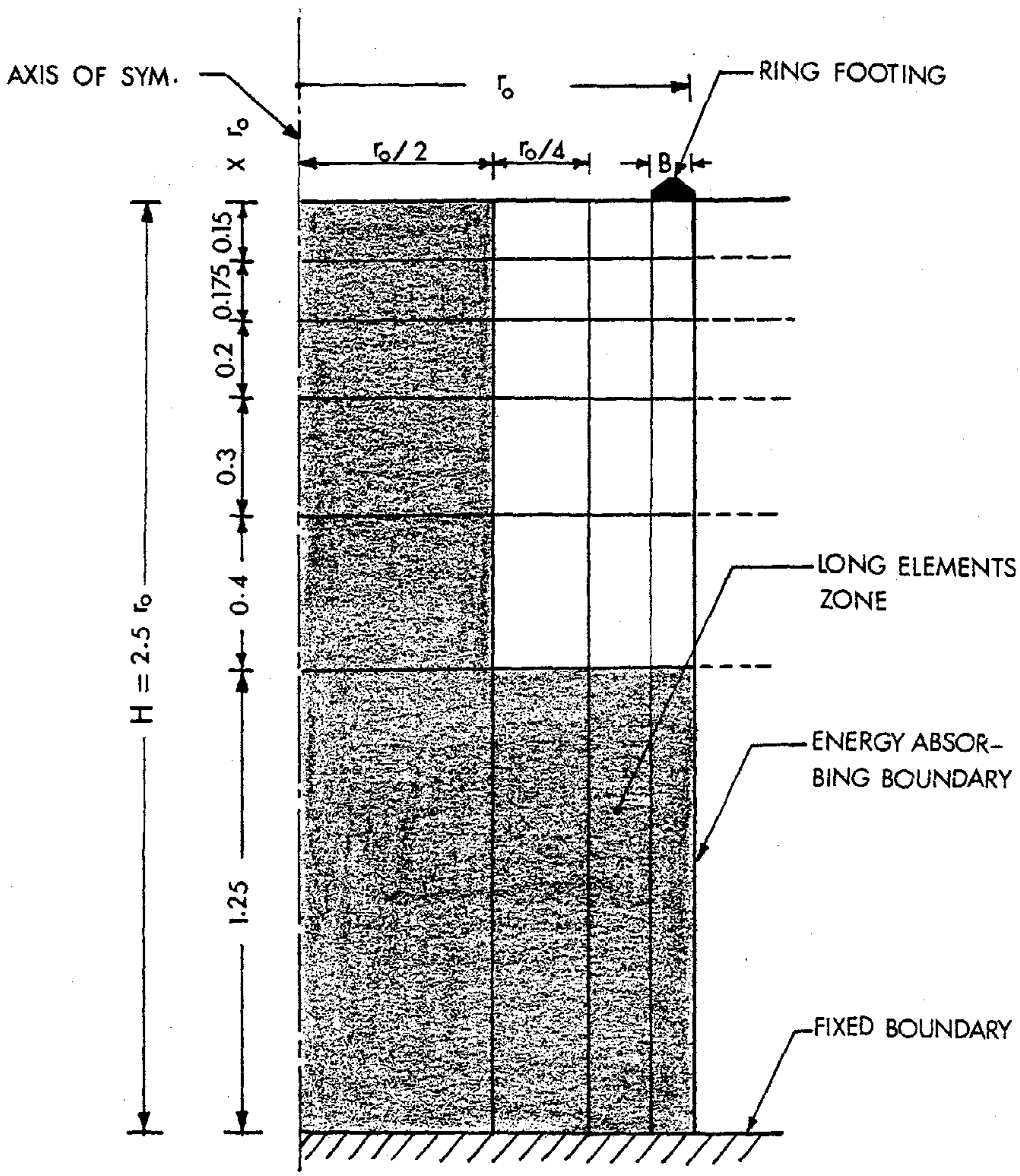

Figure 24. Super-Economical Mesh ($B/r_o \leq 0.1$)

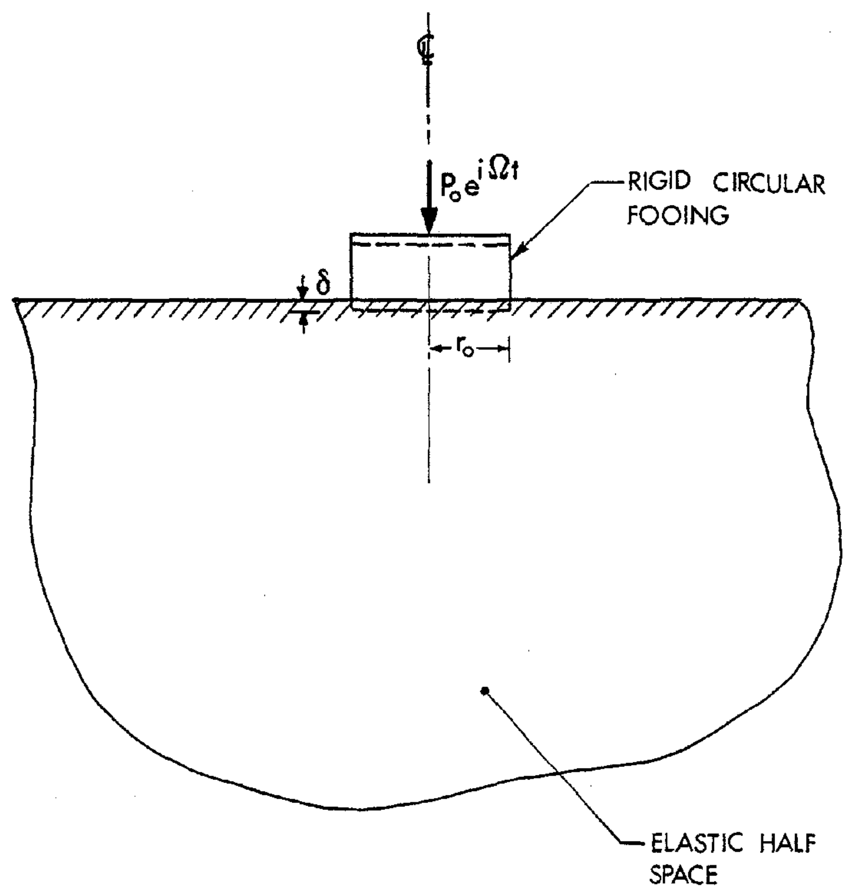

Figure 25. Foundation Vibration Problem

in which P_o and Ω = the amplitude and frequency, respectively, of the exciting force; t = time; and K = the static spring constant. It may be shown that

$$K = \frac{4Gr_o}{1-\nu} \qquad (5\text{-}4)$$

The dimensionless quantity F, herein designated the displacement function is a function of Poisson's ratio ν and the dimensionless frequency ratio a_o.

The rigid circular plate is idealized by a row of massless finite elements of very high rigidity (10^6 times higher than that of the stratum). The equivalent value for the force amplitude in the finite element model is taken $P_o/2\Pi r_o$ and is concentrated along the founction edge, see Figure 26. Also, in the same figure, the displacement in the w direction is plotted against the dimensionless frequency ratio a_o, for P_o = 1.0 K, r_o = 10', G = 2492 K/Ft^2 and $\nu = 1/3$.

The results of the finite element model with an energy absorbing boundary show good agreement, especially in the lower frequency range in which the shear wave velocity Λ becomes longer and the element size ratio ℓ/Λ becomes smaller. The results for the same problem as carried out by Lysmere and Kuhlemeyer (48) are also plotted. It can be seen that the present model with only 10 elements gave results comparable to those of Lysmere and Kuhlemeyer for

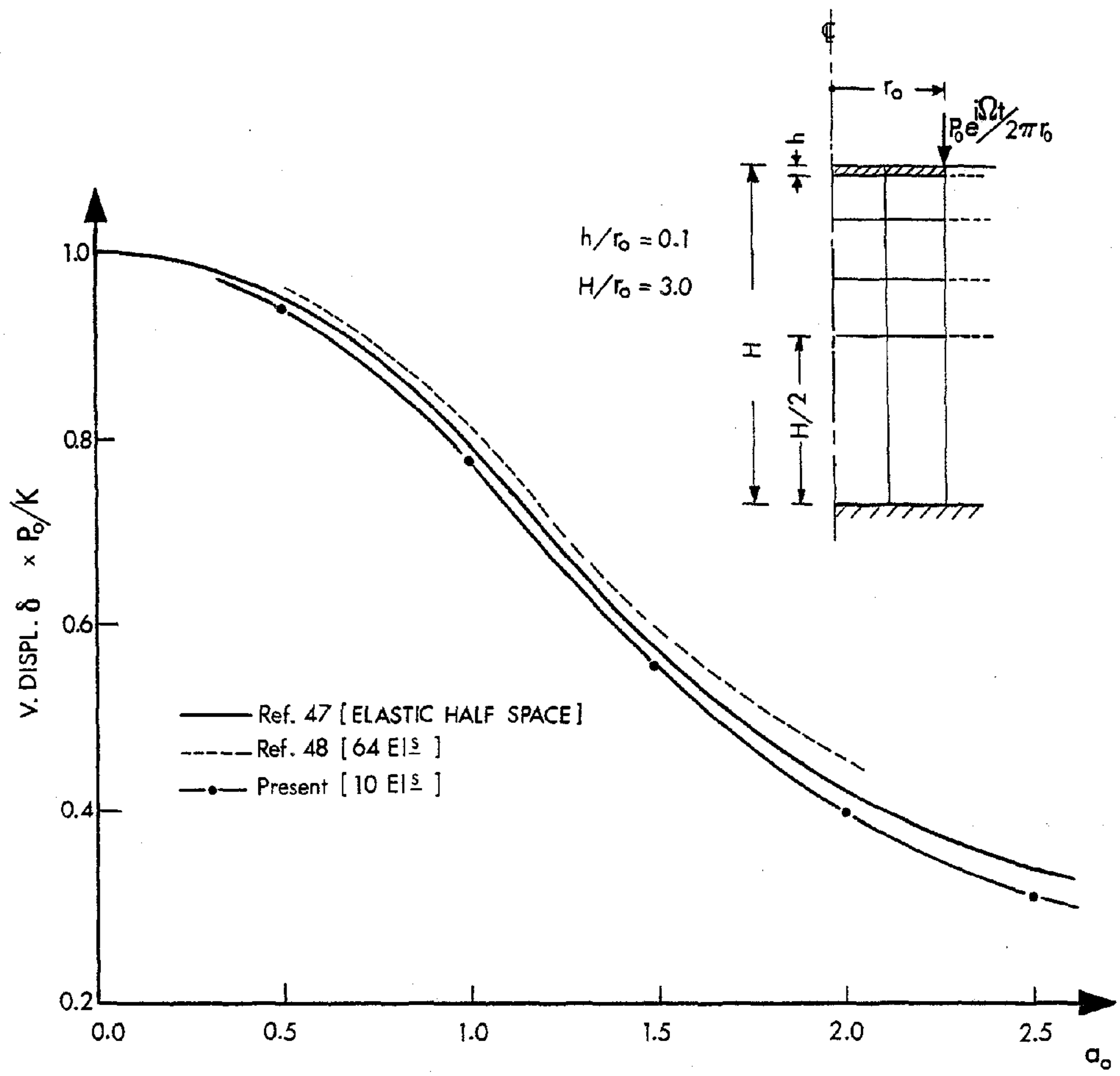

Figure 26. Vertical Displacement for Rigid Circular Footing on Elastic Half Space

which 64 elements were used. This provides a check for the correctness of the present model and suggests its applicability for very deep stratums.

To study the effect of the driving frequency on the EBS components, the frequency ratio a_o is considered for the range $a_o = 1.0$ to 2Π (8) with the first two Fourier harmonics ($J = 0$ and $J = 1$). The super-economical mesh of Figure 24, with $H/r_o = 2.5$, $B/r_o = 0.1$ and $r_o = 100$ feet, is chosen to represent the soil medium. The natural frequencies of the EBS are plotted against the driving frequency ratio for the symmetrical and untisymmetrical nodes in Figures 27 and 28. It can be seen that the translational mode frequencies are less sensitive to the change of a_o than the rotational mode frequencies. Further, it can be noticed that the five frequencies have a limited band for a given driving frequency ratio, especially for $a_o \geq \Pi$. For this reason the smallest and largest values of ω are considered in forming the proportional damping matrix as discussed in Chapter 4.

Figures 29 and 30 show the dependence of the stiffness elements on the driving frequency. It is also noticeable that both translational and rotational stiffnesses are very sensitive to the change of a_o. The sensitivity of the stiffness elements may be explained by examining Equation (3-62), where the second and third terms of the RHS of the equation are functions of the driving frequency Ω.

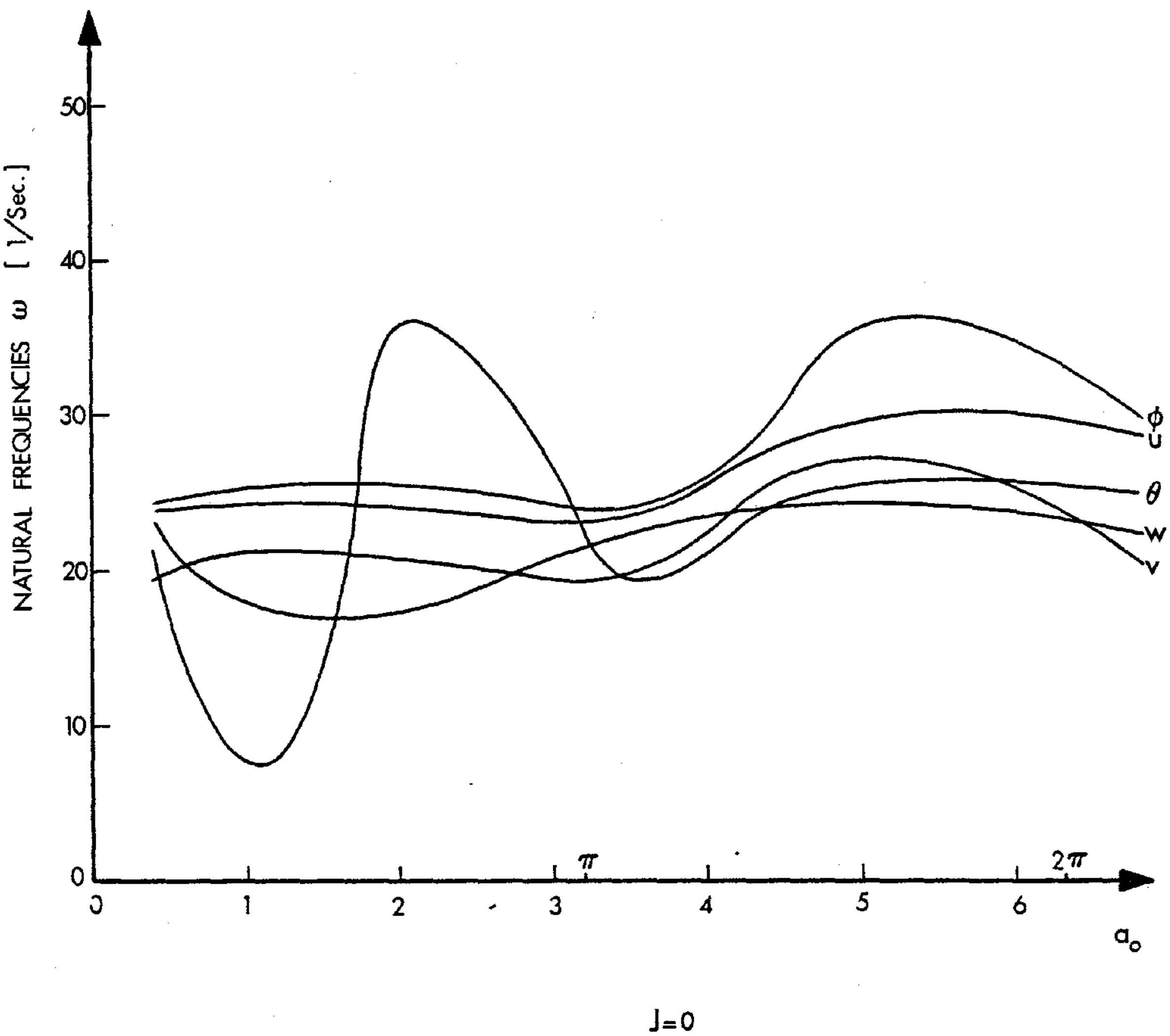

Figure 27. Driving Frequency Effect on the Symmetrical Mode Frequencies

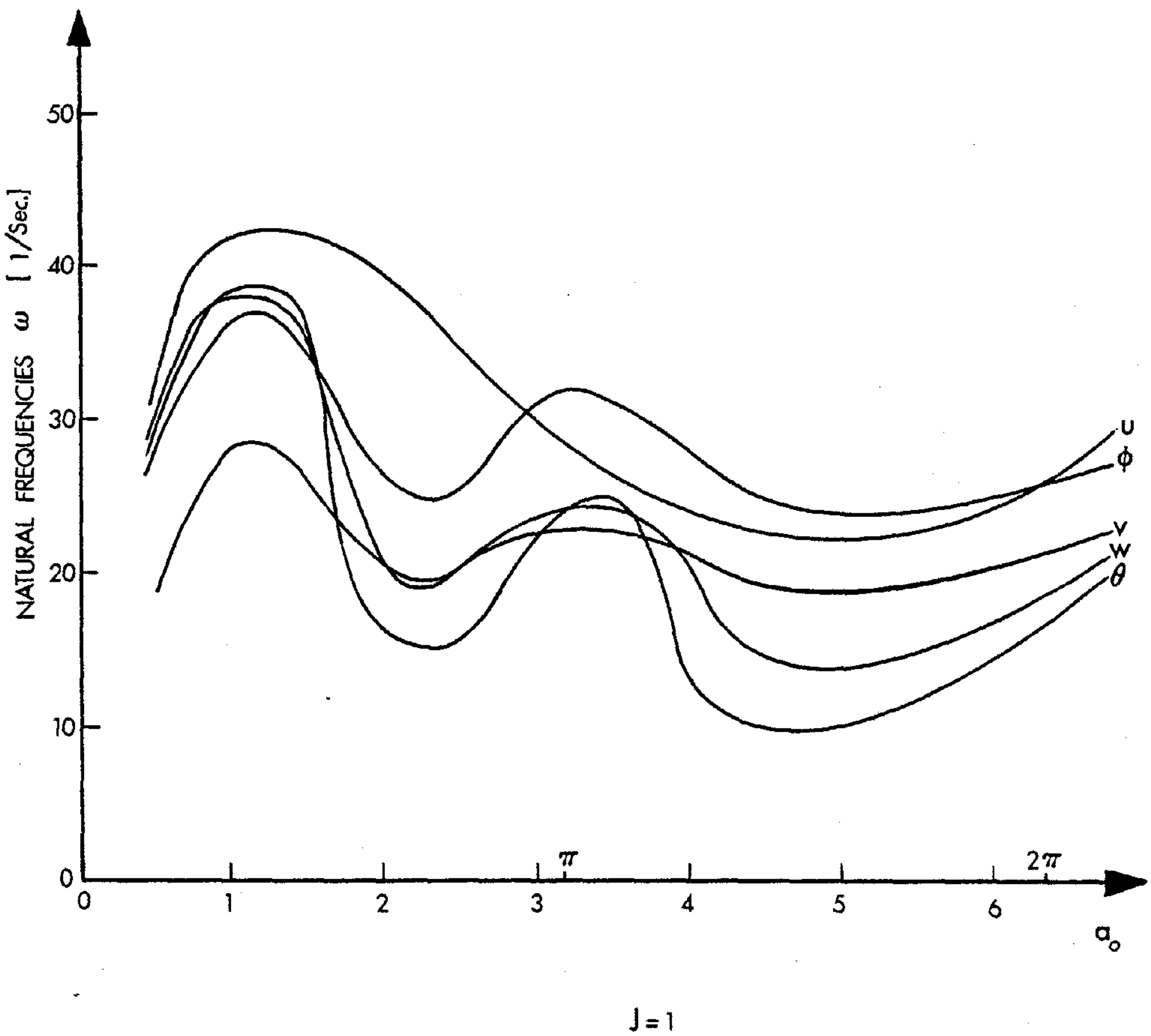

Figure 28. Driving Frequency Effect on the Untisymmetrical Mode Frequencies

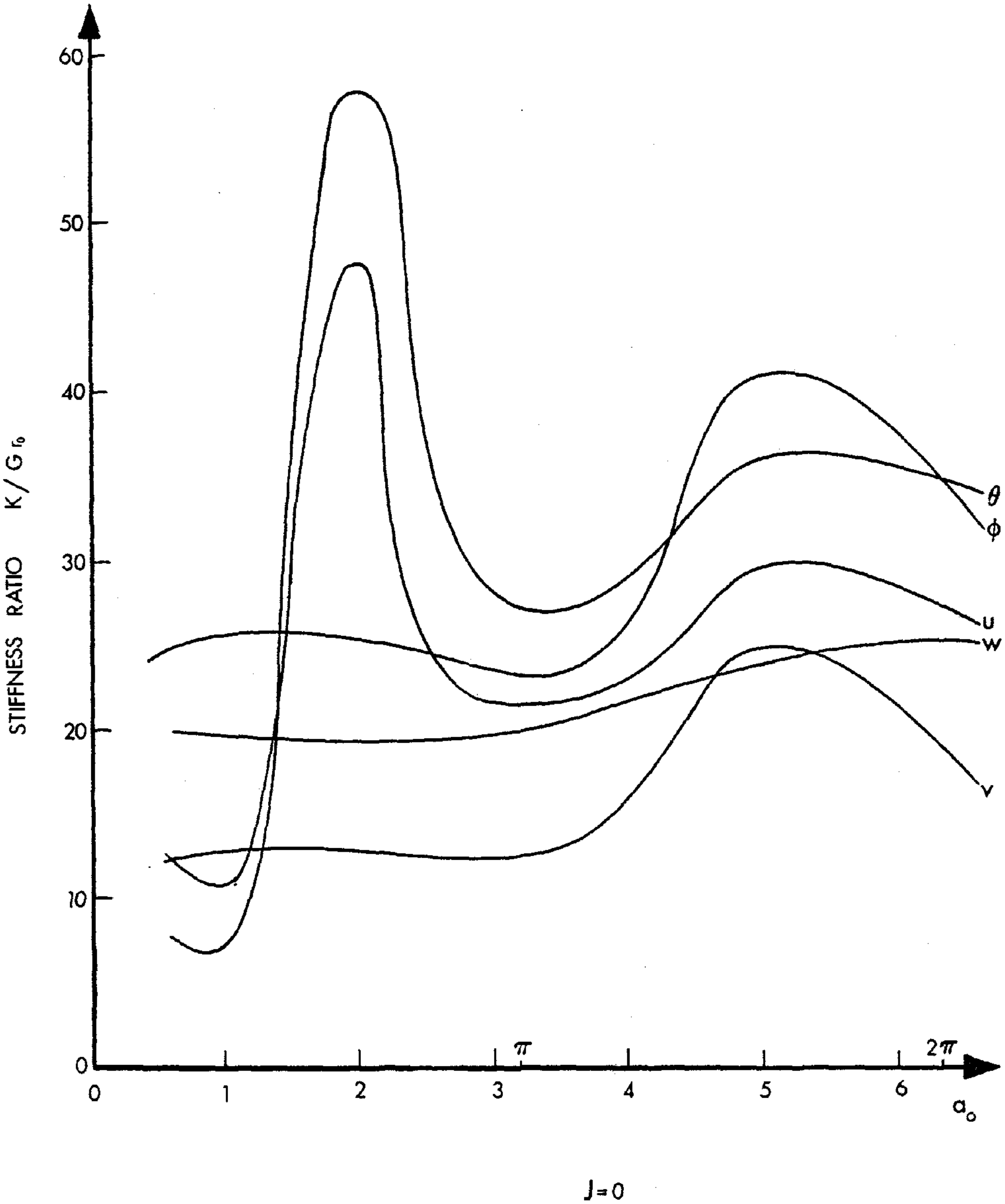

Figure 29. Driving Frequency Effect on Stiffnesses in Symmetrical Modes

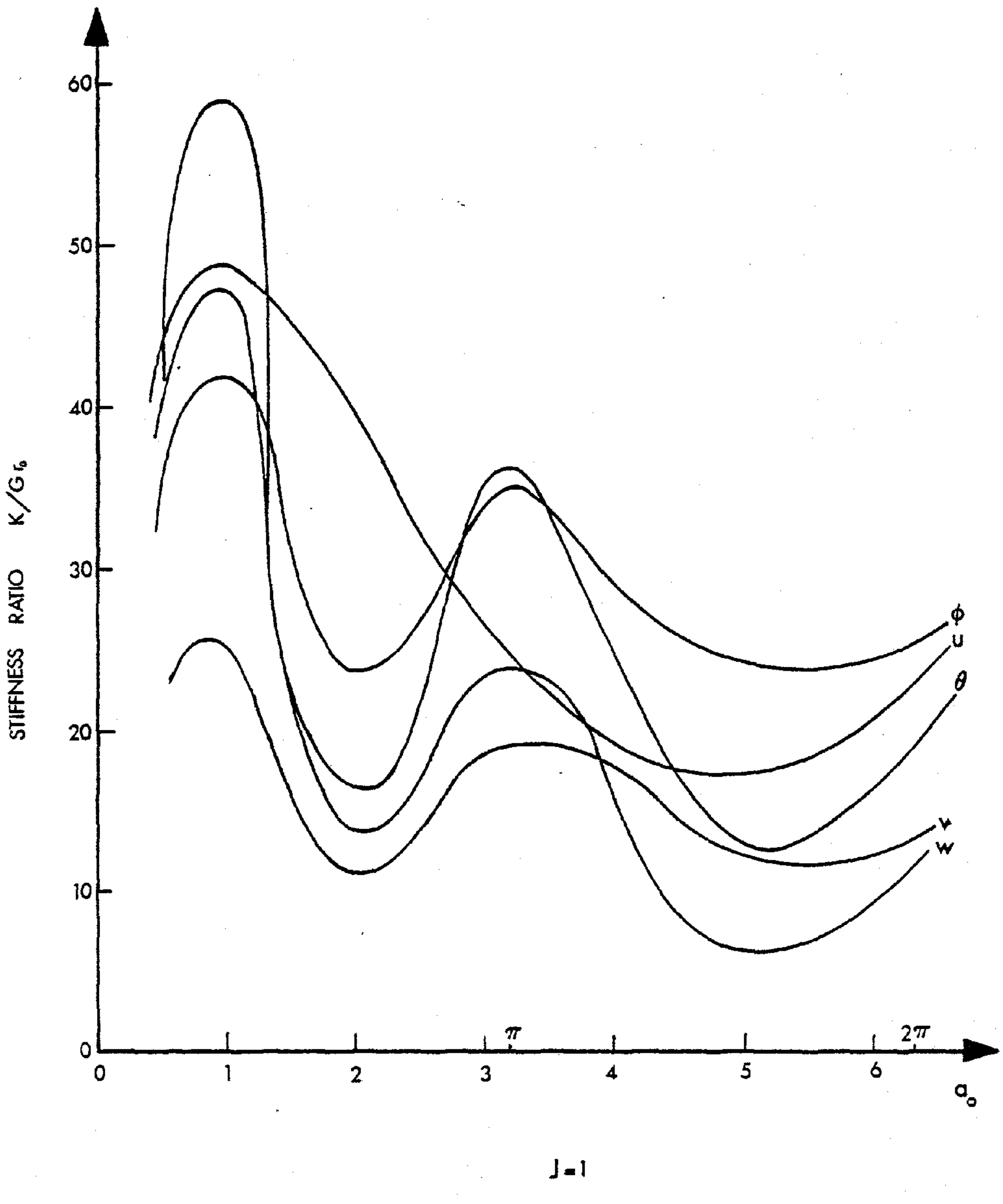

Figure 30. Driving Frequency Effect on Stiffnesses in Untisymmetrical Modes

It is interesting to notice from Figures 29 and 30 that for a given value of a_o either J = 0 or J = 1 gives maximum stiffness value, but not with both Fourier harmonics. This observation suggests the importance of a sensitivity study to the EBS components for a range of Fourier harmonics.

Similar observations may be applied to the damping elements in Figures 31 and 32. In these figures the average effect of a_o on the two harmonic behaves similarly to that in Figures 29 and 30. However, the damping elements are less dependent on the excitation frequency than the stiffness elements which is expected since the proportional damping matrix contains the mass matrix which is independent of the excitation frequency. This conclusion agrees with the results presented in References 8 and 49.

5.2.4 Higher Harmonics

For earthquake analysis, the first two Fourier harmonics are sufficient to carry out a complete dynamic analysis of the structure; thus the EBS components for $J > 1$ are not required with the usual earthquake type of loading. However, the EBS components for the higher harmonics are needed when the dynamic loading distribution in the circumferential angle θ has a general shape. Wind force is one dynamic load which requires more than the first two Fourier harmonics to be fully represented. A typical design wind pressure distribution for circular towers is presented in Reference 50, along with

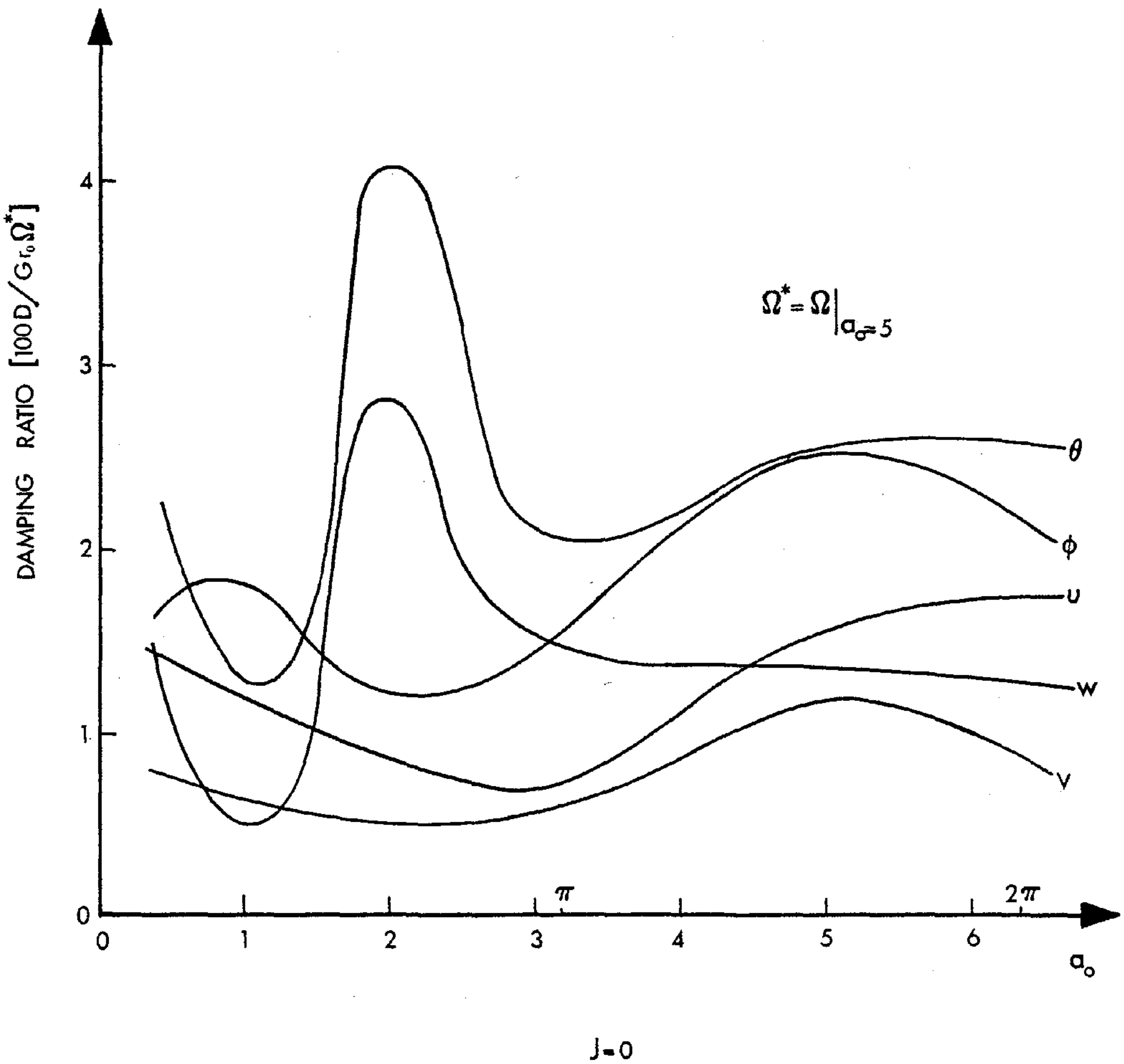

Figure 31. Driving Frequency Effect on Damping in Symmetrical Modes

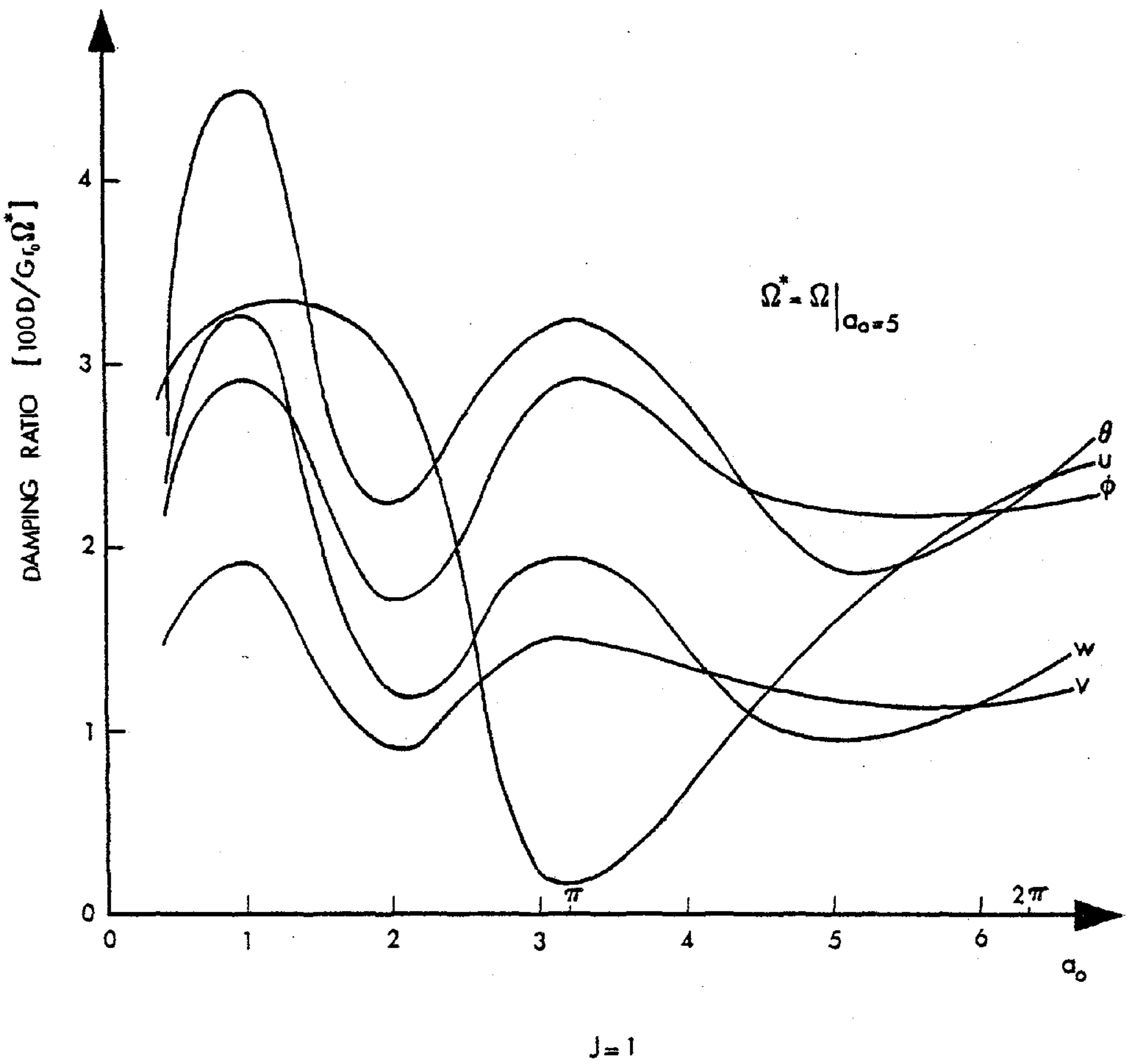

Figure 32. Driving Frequency Effect on Damping in Untisymmetrical Modes

the corresponding Fourier coefficients. Such a circumferential distribution of wind pressure may be represented by,

$$\sum_{j=0}^{\infty} A_j \cos j\theta$$

The Fourier coefficients A_j, for the first eight harmonics, are generally sufficient for the analysis (51). It is worth noting that the very high Fourier harmonics associated with the self-equilbrated correcting line loads of Figure 15 are required in any type of dynamic or static analysis of discretely supported rotational shells (42); however, as these loads are self-equilbrated-local forces, the static analysis of such loads is sufficient and, therefore, there is no need to compute the EBS components for these very high harmonics. Thus, only the first eight or even the first six harmonics need to be considered in this section to study the behavior of the natural frequencies, stiffnesses and damping elements of the soil system in higher Fourier harmonics ($J = 0,1,\ldots 5$). These higher Fourier harmonics are also needed if a non-uniform earthquake excitation is to be considered.

In Figures 33 to 35 the results of the first six Fourier harmonics are shown. The same mesh of Section 5.2.3 is used and the excitation frequency ratio a_o is taken equal to 5.0. It is interesting to notice that the EBS, for $J > 1$,

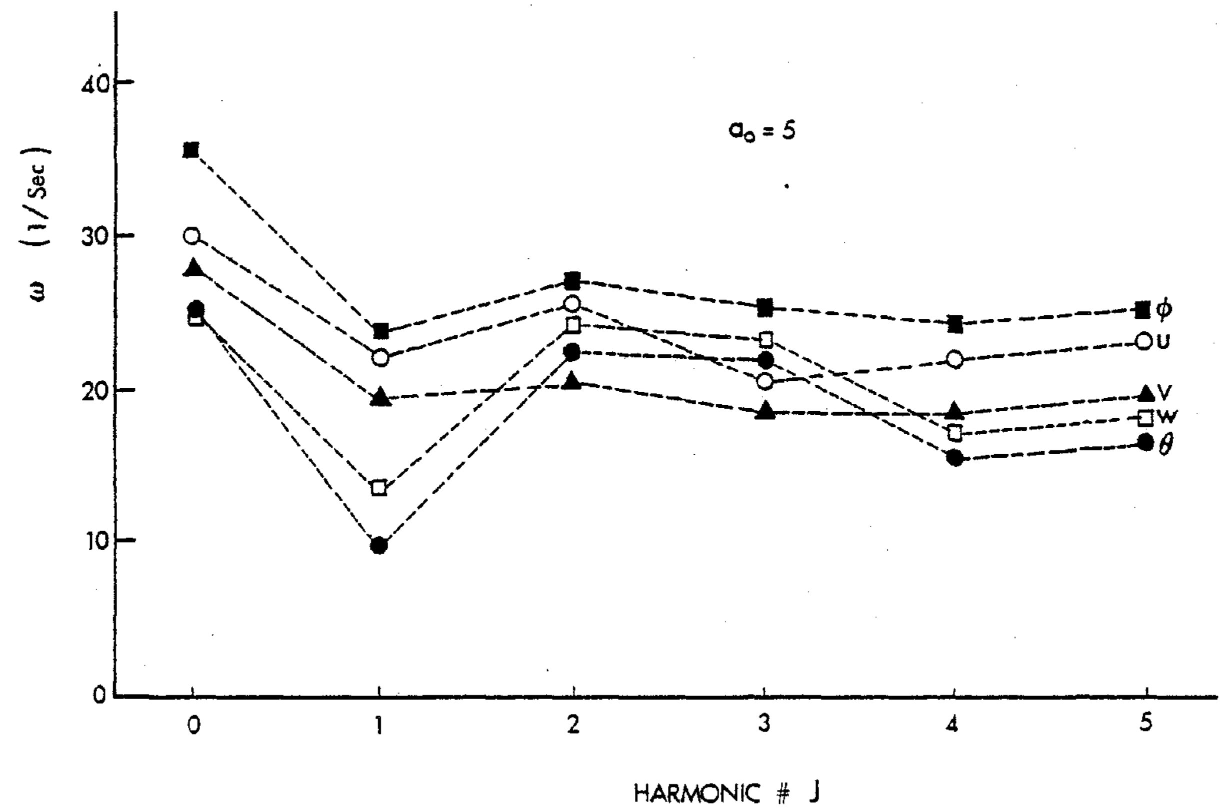

Figure 33. Natural Frequencies of EBS in Higher Fourier Harmonics

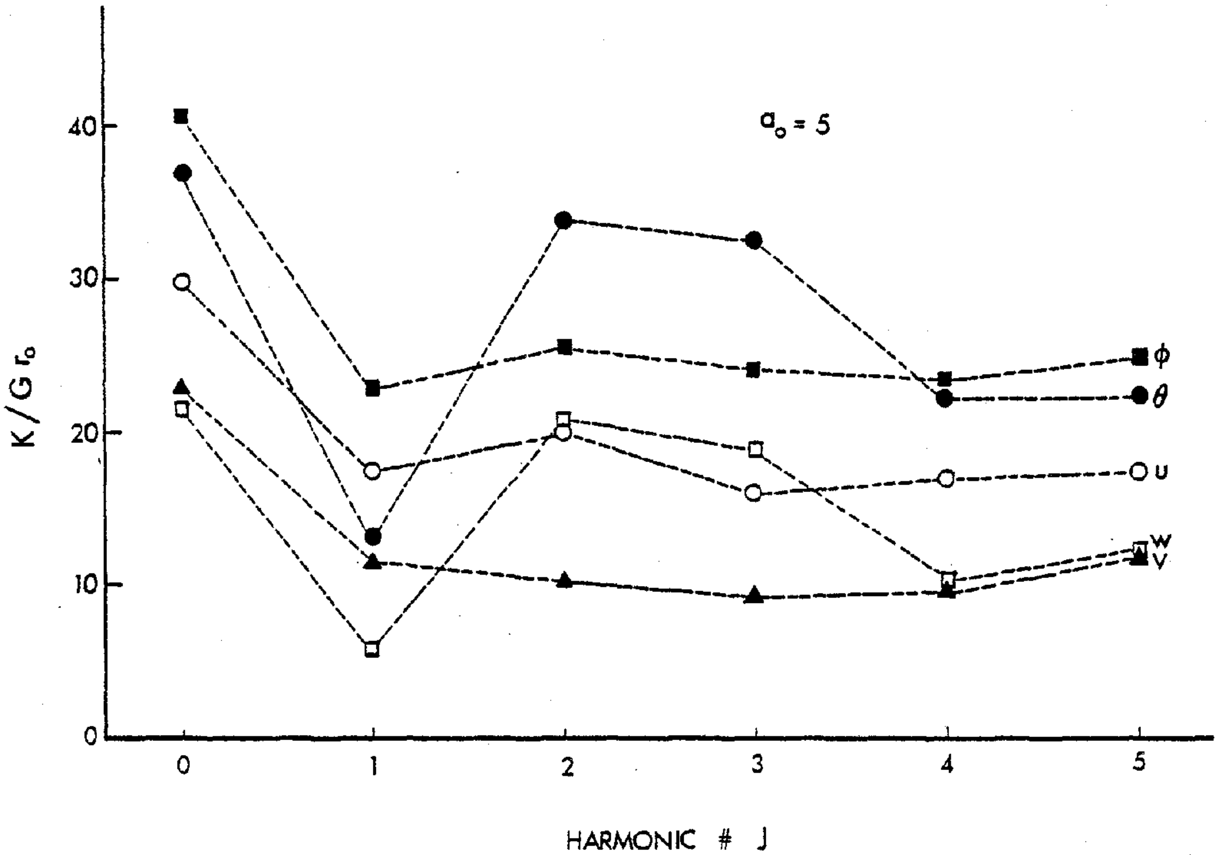

Figure 34. Stiffness Elements in Higher Fourier Harmonics

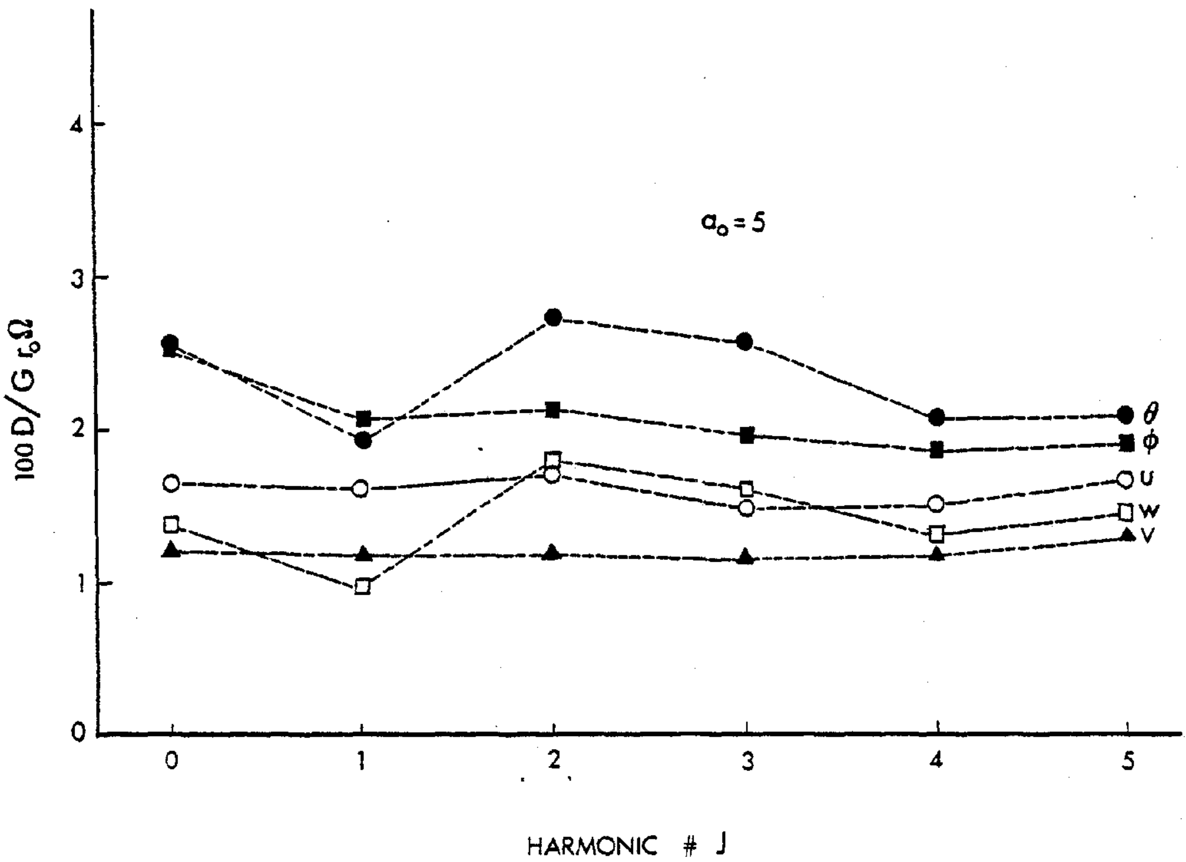

Figure 35. Damping Elements in Higher Fourier Harmonics

are approximately constants for the u, v and ϕ components, while the w and θ components (vertical and rocking) show more variation as shown in Figures 33, 34 and 35. This observation may be useful in reducing the size of the problem if the stiffnesses and damping elements of the higher harmonics are considered to be independent of the Fourier number J and suggests a helpful procedure to determine the EBS components for $J > 1$ with the aid of one harmonic No J, $(J \geq 2)$. By comparing the stiffness and damping elements in Figures 34 and 35, we find that the damping is less dependent on the harmonic number J than the stiffness elements. Again, this is because of the mass elements, which is independent of J, and are contained in the damping, see Equation (4-8).

5.3 DYNAMIC ANALYSIS OF SHELLS OF REVOLUTION

The main aim of this research has been to develop a more realistic mathematical model for rotational shells by including the soil effect in the dynamic model of such structures. Further, it is desired to assess the importance of the new component of the model, the surrounding soil medium, on the dynamic behavior of this class of structures.

The structure under study is the reinforced concrete cooling tower shell shown in Figure 36. The tower is assumed to have a shallow foundation in the form of a ring footing with the ratio $B/r_o < 0.1$. The shell meridian consists of

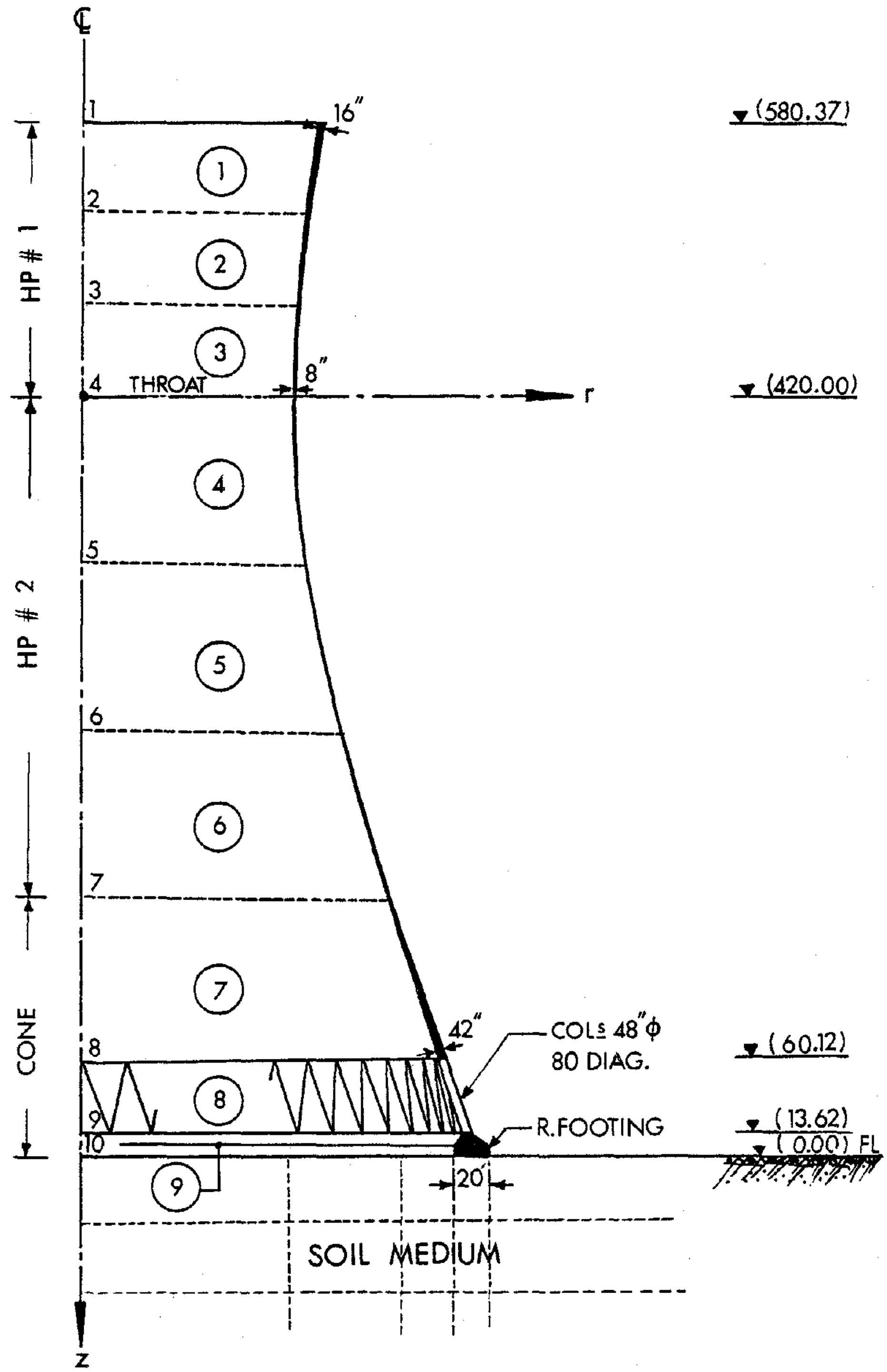

Figure 36. Cooling Tower on a Hypothetical Foundation

three curves with slope continuity at the junction points (nodal points #4 and #7). The equations of the shell meridian are given in Table 5.

In the present study, the following three soil and one rock founded (fixed base) cases are considered. These cases were selected to provide a wide variation of site conditions and also to permit the establishment of trends in the structural response as suggested by Pandya and Setlur (16).

CASE I. The soil consists of 500 ft. of uniform medium sand with 75 percent relative density. The value of the shear modulus coefficient (52) is taken as 1827 K/ft^2 with the value of Poisson's ratio as 0.35. This case is representative of a soft to intermediate soil condition.

CASE II. To study the effect of a stiff and shallow soil condition, the soil depth was reduced to 250 ft. The soil is assumed to be dense sand and gravel with $G = 2675\ K/ft^2$ (52) and Poisson's ratio as 0.4. This case is representative of an intermediate to stiff soil condition.

CASE III. This case is formulated such that fundamental frequency of the soil layer is close to that of the structure. Strong amplification due to resonance effects, if present, would show up.

Table 5. Shell Meridian of the Structure Under Study

Shell Type	Nodes		Equation
	From	To	
HP #1	1	4	$z^2 - 123.68377\ r^2 + 27587.5165\ r - 1536846.5 = 0$
HP #2	4	7	$z^2 - 9.40153\ r^2 + 1302.5923\ r - 25462.9 = 0$
CONE	7	10	$0.3z - r + 87.2112 = 0$

The soil is assumed to be stiff clay with depth of 600 ft. The values of the shear modulus coefficient and Poisson's ratio are taken as 2315 K/ft^2 and 0.4 respectively.

CASE IV. The structure is directly founded on competent rock and, therefore, the soil structure interaction effect is negligible. This case represents an important convergence point for the solution technique.

The super-economical mesh of Figure 24 is considered to model the first and the third cases. Because of the shallow soil condition of Case II, a special finite element mesh is presented in Figure 37 to represent the soil medium.

The EBS of the three cases are computed using the SUBASE program with a driving frequency Ω = 12.3441 rad./sec. (the fundamental frequency of the shell on a fixed foundation) for the antisymmetrical mode (J = 1). Also, the EBS of CASE I is recalculated for a driving frequency Ω = 32.7485 rad./sec., which is the fundamental frequency of the structure on a fixed foundation for the symmetrical mode (J = 0). The values of the EBS are presented in Table 6 along with the soil frequencies for the four cases. Although the values of the EBS of CASE IV are not required, they are shown in the table for completeness.

It should be noted that the coordinate system of Figure 10 is not same as the coordinate system used in the shell

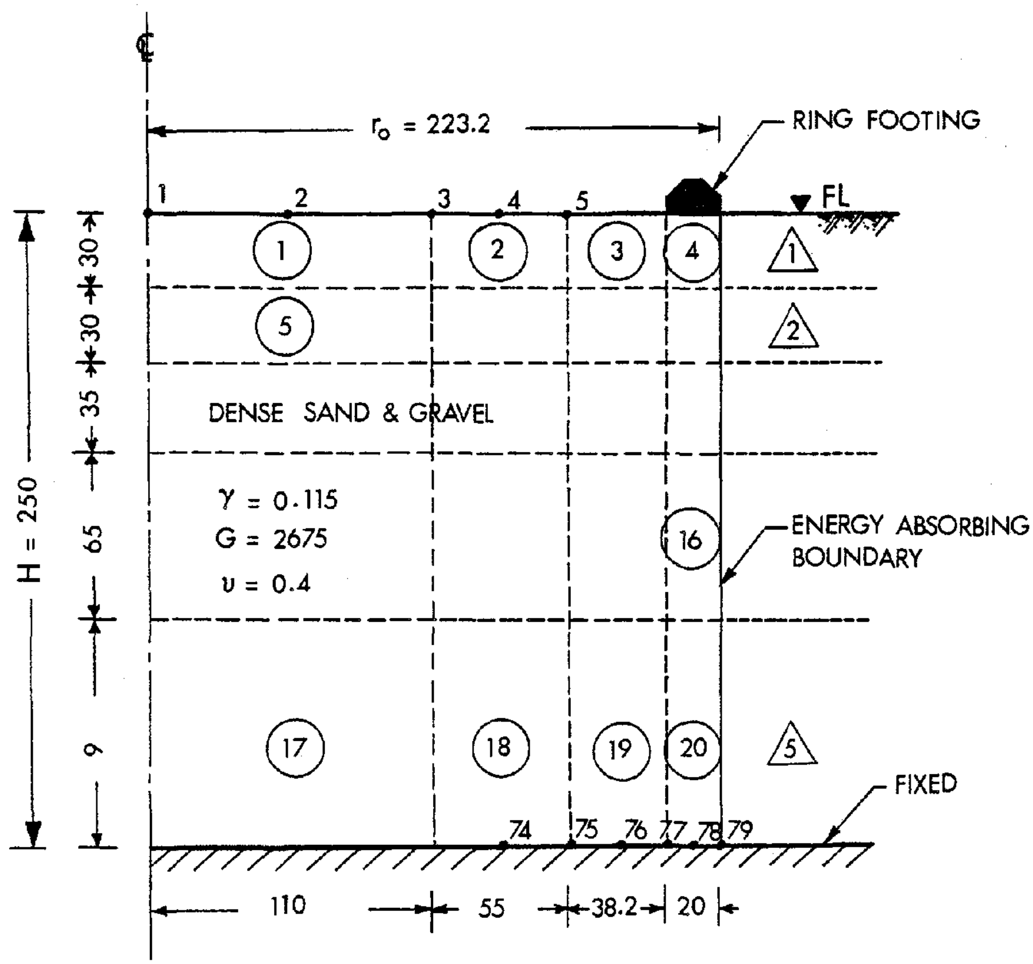

UNITS : K, FT

Figure 37. F.E. Mesh of Case II

Table 6. EBS for the Cases of Study

Soil Case	J	EBS* Comp.	u	ẅ	v	θ	φ
I	0	K	51114.6	80012.8	70410.4	469832.0	784321.0
		D	6320.7	8532.3	3245.7	58692.2	32003.7
		M	100.2	91.0	84.3	798.9	201.4
		ω	22.6	29.7	29.0	24.3	62.6
	1	K	9882.5	58204.8	7780.0	787732.0	289741.0
		D	2000.9	898.8	2145.7	8936.0	12342.7
		M	100.2	91.0	84.3	798.9	201.4
		ω	9.9	25.3	9.6	31.4	38.0
II	1	K	301375.0	912368.0	217140.0	8667110.0	5617950.0
		D	727.1	742.2	574.1	7336.0	6532.8
		M	126.4	96.8	90.2	883.5	268.8
		ω	49.0	97.5	49.2	98.8	145.5
III	1	K	15268.7	82403.0	15365.3	1025780.0	4210990.0
		D	1972.3	821.3	2008.0	8785.7	11135.8
		M	100.4	91.0	84.3	798.9	201.4
		ω	12.1	30.1	13.5	35.8	144.5
IV	-	K	∞	∞	∞	∞	∞
		D	0	0	0	0	0
		M	0	0	0	0	0
		ω	∞	∞	∞	∞	∞

*Units: Kip, Ft, sec.

analysis, see Figures 38 and 39, and the input data must be supplied to SHORSS program after transforming the components in u direction to w direction and vice versa.

5.3.1 Free Vibration Analysis

To investigate the soil effect on the dynamic properties, free vibration analysis of the shell of Figure 36 with the four soil cases is carried out using the SHORSS program. The first three modes of vibration are considered in each case for the antisymmetrical Fourier mode J = 1 (horizontal vibration). For J = 0 (vertical vibration), only the first and fourth cases are considered for the first three modes of vibration, as those are the extremes of the soil conditions.

The results of the study are given in Figures 40 to 47. In Figures 40 to 45 the computer output of the eigenvalue analysis of the lowest two frequencies are given along with the corresponding normalized eigenvectors for the four cases. A comparison between the first three eigenvectors of vibration (vertically and horizontally) for the first and fourth cases can be held from the plotted modes in Figures 46 and 47.

The change in the fundamental frequency is only in the band of 5% of the fixed base frequency for both vertical and horizontal vibration as shown in Figures 40 to 45. The small change in the fundamental frequency for the interactive system makes any further approximation in the EBS using the resulting interactive frequencies unnecessary. On the other hand, the decrease in the frequency of the second mode reaches 25% of the fixed base case (Case IV) for J = 0 and J = 1. The

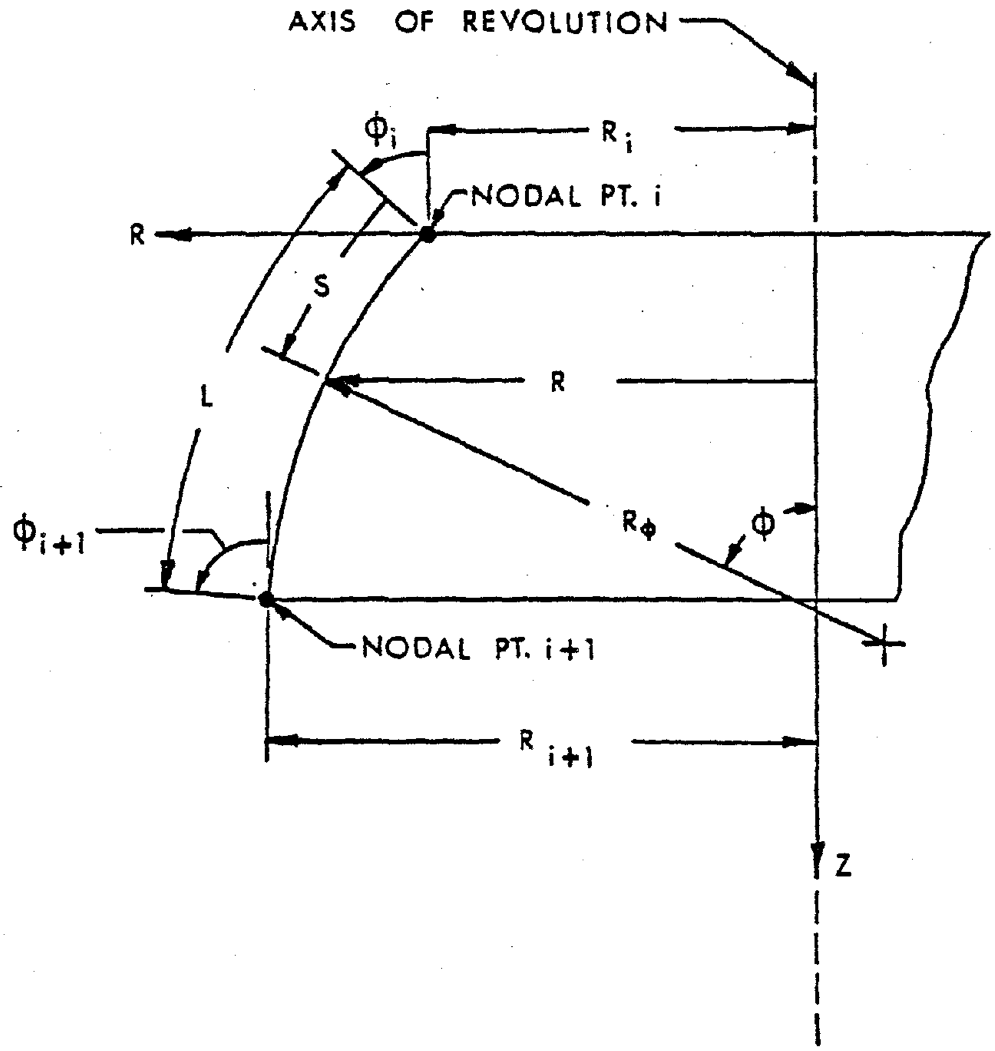

Figure 38. F.E. Geometry

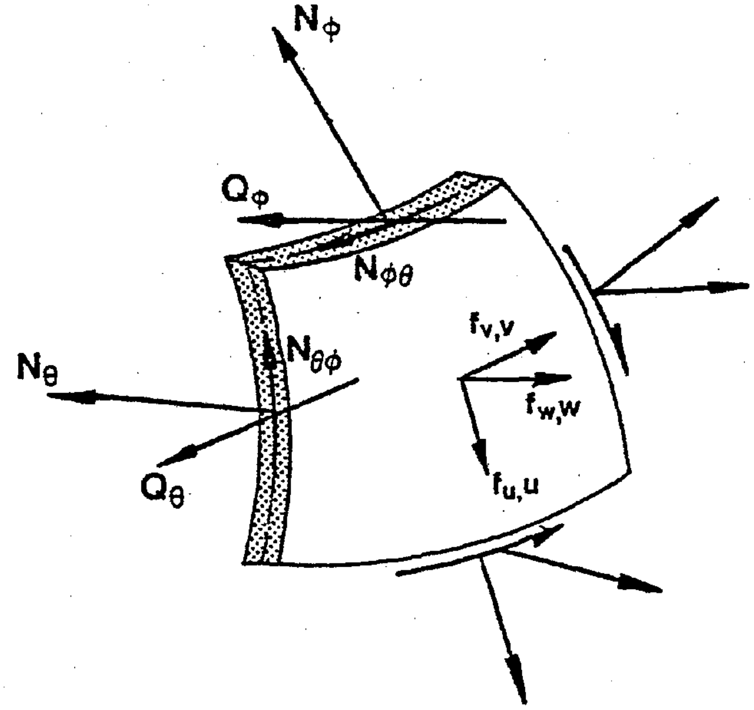

Stress Resultants

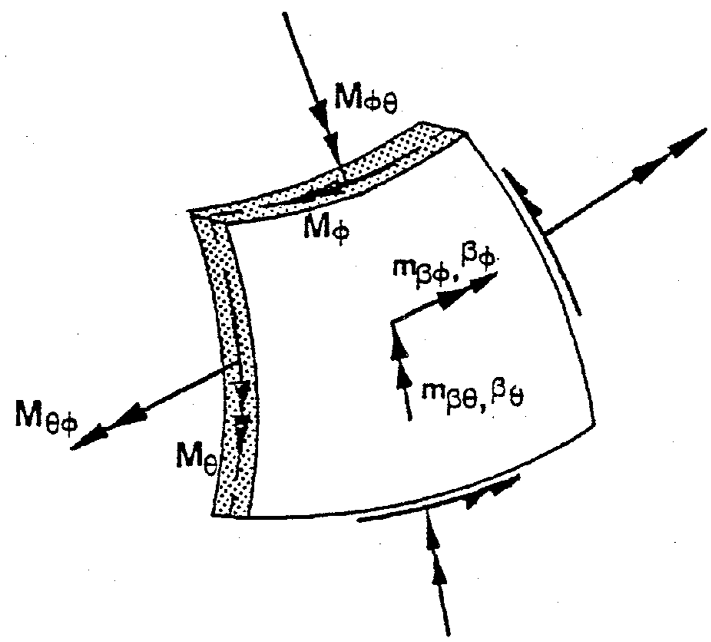

Stress-Couple Resultants

Figure 39. Sign Conventions

RESULTS OF EIGENVALUE ANALYSIS FOR MODE NO. = 1

EIGENVALUE, LAMDA = 0.10076533E-02
CIRCULAR FREQUENCY= 0.31502457E 02 (RAD./SEC)
CYCLIC FREQUENCY = 0.50137758E 01 (CYCLES/SEC)

EIGENVECTOR NO.= 1

NODE NUMBER	U	V	W	BETA(PHI)	BETA(THETA)
1	1.000000		0.101994	-0.000131	
2	0.984922		0.108281	-0.000178	
3	0.932968		0.100328	-0.000007	
4	0.845691		-0.023218	0.000563	
5	0.639444		-0.129421	-0.000876	
6	0.429466		-0.098668	-0.000982	
7	0.249906		-0.053773	-0.000828	
8	0.167460		-0.062370	-0.000140	
9	0.098472		-0.066892	-0.000369	
10	0.099033		-0.061315	-0.000386	

RESULTS OF EIGENVALUE ANALYSIS FOR MODE NO. = 2

EIGENVALUE, LAMDA = 0.79845404E-03
CIRCULAR FREQUENCY= 0.35389542E 02 (RAD./SEC)
CYCLIC FREQUENCY = 0.56324253E 01 (CYCLES/SEC)

EIGENVECTOR NO.= 2

NODE NUMBER	U	V	W	BETA(PHI)	BETA(THETA)
1	0.049781		0.005275	-0.000001	
2	0.048848		0.005721	-0.000003	
3	0.045643		0.005348	0.000012	
4	0.040275		-0.001478	0.000054	
5	0.027966		-0.006056	-0.000011	
6	0.015705		-0.003952	0.000086	
7	0.005593		-0.009460	0.000754	
8	0.002352		-0.221705	0.013642	
9	-0.010634		1.000000	0.098528	
10	-0.013856		-0.406408	0.098832	

Figure 40. Eigenvalues and Eigenvectors for $J = 0$ (Case I)

RESULTS OF EIGENVALUE ANALYSIS FOR MODE NO. = 1

EIGENVALUE, LAMDA = 0.71325339E-02
CIRCULAR FREQUENCY= 0.11840719E 02 (RAD./SEC)
CYCLIC FREQUENCY = 0.18845100E 01 (CYCLES/SEC)

EIGENVECTOR NO.= 1

NODE NUMBER	U	V	W	BETA(PHI)	BETA(THETA)
1	0.124014	-0.965083	1.000000	0.001768	0.000317
2	0.124346	-0.868164	0.899629	0.002037	0.000297
3	0.125937	-0.750468	0.778350	0.002497	0.000267
4	0.156602	-0.617706	0.623203	0.002664	0.000060
5	0.189184	-0.416068	0.397046	0.001687	-0.000090
6	0.143729	-0.278687	0.268689	0.000904	0.000005
7	0.083647	-0.199219	0.201477	0.000634	0.000070
8	0.053765	-0.170953	0.162710	0.001397	0.000010
9	0.028572	-0.111183	0.110519	-0.000568	0.000052
10	0.028489	-0.111558	0.118683	-0.000560	0.000047

RESULTS OF EIGENVALUE ANALYSIS FOR MODE NO. = 2

EIGENVALUE, LAMDA = 0.45256391E-02
CIRCULAR FREQUENCY= 0.14864833E 02 (RAD./SEC)
CYCLIC FREQUENCY = 0.23658133E 01 (CYCLES/SEC)

EIGENVECTOR NO.= 2

NODE NUMBER	U	V	W	BETA(PHI)	BETA(THETA)
1	0.402563	-0.929145	1.000000	0.004063	0.000585
2	0.400645	-0.711271	0.772668	0.004427	0.000526
3	0.393141	-0.466283	0.516339	0.004950	0.000436
4	0.385017	-0.208014	0.205424	0.005019	-0.000023
5	0.299203	0.165859	-0.227703	0.003153	-0.000521
6	0.179069	0.416403	-0.481978	0.001710	-0.000546
7	0.088382	0.561387	-0.630089	0.000319	-0.000540
8	0.056026	0.653323	-0.703627	-0.003427	-0.000401
9	0.027734	0.670246	-0.746116	0.007086	-0.000724
10	0.028707	0.686782	-0.846037	0.007019	-0.000640

Figure 41. Eigenvalues and Eigenvectors
for J = 1 (Case I)

RESULTS OF EIGENVALUE ANALYSIS FOR MODE NO. = 1

EIGENVALUE, LAMDA = 0.69194660E-02
CIRCULAR FREQUENCY= 0.12021640E 02 (RAD./SEC)
CYCLIC FREQUENCY = 0.19133043E 01 (CYCLES/SEC)

EIGENVECTOR NO.= 1

NODE NUMBER	U	V	W	BETA(PHI)	BETA(THETA)
1	0.140465	-0.963007	1.000000	0.001895	0.000326
2	0.140682	-0.858935	0.892190	0.002171	0.000304
3	0.141790	-0.733636	0.762919	0.002637	0.000271
4	0.170226	-0.593197	0.598411	0.002802	0.000051
5	0.195731	-0.380398	0.359148	0.001780	-0.000120
6	0.145501	-0.234857	0.222151	0.000959	-0.000031
7	0.083054	-0.149759	0.148782	0.000628	0.000032
8	0.052613	-0.116457	0.107601	0.001102	-0.000013
9	0.024312	-0.037500	0.034946	0.000833	-0.000028
10	0.024261	-0.036487	0.023088	0.000839	-0.000019

RESULTS OF EIGENVALUE ANALYSIS FOR MODE NO. = 2

EIGENVALUE, LAMDA = 0.32805044E-02
CIRCULAR FREQUENCY= 0.17459412E 02 (RAD./SEC)
CYCLIC FREQUENCY = 0.27787542E 01 (CYCLES/SEC)

EIGENVECTOR NO.= 2

NODE NUMBER	U	V	W	BETA(PHI)	BETA(THETA)
1	0.544576	-0.904702	1.000000	0.005272	0.000740
2	0.540423	-0.623414	0.703271	0.005718	0.000638
3	0.524717	-0.309035	0.370914	0.006308	0.000497
4	0.489152	0.015826	-0.027983	0.006223	-0.000142
5	0.327507	0.460040	-0.547342	0.003460	-0.000759
6	0.162145	0.721639	-0.817148	0.001448	-0.000858
7	0.057494	0.834824	-0.942160	-0.000694	-0.000866
8	0.028826	0.900239	-0.985862	-0.006274	-0.000673
9	0.000036	0.399523	-0.485680	-0.009753	-0.000160
10	-0.000064	0.406724	-0.345779	-0.009865	-0.000220

Figure 42. Eigenvalues and Eigenvectors for J = 1 (Case II)

RESULTS OF EIGENVALUE ANALYSIS FOR MODE NO. = 1

EIGENVALUE, LAMDA = 0.71198605E-02
CIRCULAR FREQUENCY= 0.11851253E 02 (RAD./SEC)
CYCLIC FREQUENCY = 0.18861866E 01 (CYCLES/SEC)

EIGENVECTOR NO.= 1

NODE NUMBER	U	V	W	BETA(PHI)	BETA(THETA)
1	0.125714	-0.964890	1.000000	0.001772	0.000309
2	0.126035	-0.867231	0.898855	0.002041	0.000289
3	0.127578	-0.748758	0.776758	0.002501	0.000258
4	0.158020	-0.615220	0.620663	0.002667	0.000050
5	0.189900	-0.412460	0.393173	0.001687	-0.000102
6	0.143988	-0.274253	0.263918	0.000899	-0.000008
7	0.083698	-0.194210	0.196054	0.000622	0.000056
8	0.053779	-0.165401	0.156987	0.001355	-0.000002
9	0.028470	-0.104221	0.103242	-0.000439	0.000034
10	0.028396	-0.104445	0.109428	-0.000431	0.000031

RESULTS OF EIGENVALUE ANALYSIS FOR MODE NO. = 2

EIGENVALUE, LAMDA = 0.44562295E-02
CIRCULAR FREQUENCY= 0.14980152E 02 (RAD./SEC)
CYCLIC FREQUENCY = 0.23841667E 01 (CYCLES/SEC)

EIGENVECTOR NO.= 2

NODE NUMBER	U	V	W	BETA(PHI)	BETA(THETA)
1	0.410103	-0.927992	1.000000	0.004127	0.000594
2	0.408094	-0.706791	0.769098	0.004494	0.000533
3	0.400240	-0.458217	0.508899	0.005021	0.000441
4	0.390838	-0.196455	0.193501	0.005084	-0.000026
5	0.301345	0.181620	-0.244714	0.003181	-0.000533
6	0.178944	0.433903	-0.501019	0.001715	-0.000561
7	0.087440	0.578745	-0.649472	0.000289	-0.000556
8	0.055151	0.670608	-0.722904	-0.003545	-0.000415
9	0.026675	0.670690	-0.749073	0.006445	-0.000713
10	0.027622	0.687110	-0.839817	0.006373	-0.000634

Figure 43. Eigenvalues and Eigenvectors for J = 1 (Case III)

RESULTS OF EIGENVALUE ANALYSIS FOR MODE NO. = 1

EIGENVALUE, LAMDA = 0.93242992E-03
CIRCULAR FREQUENCY= 0.32748535E 02 (RAD./SEC)
CYCLIC FREQUENCY = 0.52120962E 01 (CYCLES/SEC)

EIGENVECTOR NO.= 1

NODE NUMBER	U	V	W	BETA(PHI)	BETA(THETA)
1	1.000000		0.103296	-0.000103	
2	0.983676		0.110498	-0.000146	
3	0.927492		0.102794	0.000051	
4	0.833184		-0.025291	0.000658	
5	0.612774		-0.125589	-0.000869	
6	0.390008		-0.086023	-0.000908	
7	0.201447		-0.035353	-0.000550	
8	0.116397		-0.027112	-0.000178	
9	0.001222		0.000072	0.000040	
10	0.0		0.0	0.0	

RESULTS OF EIGENVALUE ANALYSIS FOR MODE NO. = 2

EIGENVALUE, LAMDA = 0.45404444E-03
CIRCULAR FREQUENCY= 0.46930023E 02 (RAD./SEC)
CYCLIC FREQUENCY = 0.74691515E 01 (CYCLES/SEC)

EIGENVECTOR NO.= 2

NODE NUMBER	U	V	W	BETA(PHI)	BETA(THETA)
1	0.041706		0.004900	0.000049	
2	0.040280		0.006091	0.000099	
3	0.035458		0.005462	0.000218	
4	0.027547		-0.002940	0.000518	
5	0.010783		-0.009216	0.001064	
6	-0.004524		-0.025900	0.004119	
7	-0.015659		-0.121383	0.016784	
8	-0.034695		1.000000	-0.009449	
9	-0.000315		-0.000035	-0.000409	
10	0.0		0.0	0.0	

Figure 44. Eigenvalues and Eigenvectors for J = 0 (Case IV)

RESULTS OF EIGENVALUE ANALYSIS FOR MODE NO. = 1

EIGENVALUE, LAMDA = 0.65626837E-02
CIRCULAR FREQUENCY= 0.12344095E 02 (RAD./SEC)
CYCLIC FREQUENCY = 0.19646254E 01 (CYCLES/SEC)

EIGENVECTOR NO.= 1

NODE NUMBER	U	V	W	BETA(PHI)	BETA(THETA)
1	0.150540	-0.960994	1.000000	0.001964	0.000325
2	0.150597	-0.852253	0.887208	0.002252	0.000301
3	0.151097	-0.721275	0.751923	0.002737	0.000266
4	0.177272	-0.574626	0.579734	0.002905	0.000033
5	0.195715	-0.353469	0.331573	0.001818	-0.000145
6	0.139890	-0.203930	0.191523	0.000948	-0.000053
7	0.073887	-0.118482	0.118339	0.000581	0.000012
8	0.042228	-0.086644	0.078310	0.001037	-0.000033
9	0.000441	-0.000243	0.000070	0.000004	-0.000012
10	0.0	0.0	0.0	0.0	0.0

RESULTS OF EIGENVALUE ANALYSIS FOR MODE NO. = 2

EIGENVALUE, LAMDA = 0.26967025E-02
CIRCULAR FREQUENCY= 0.19256775E 02 (RAD./SEC)
CYCLIC FREQUENCY = 0.30648136E 01 (CYCLES/SEC)

EIGENVECTOR NO.= 2

NODE NUMBER	U	V	W	BETA(PHI)	BETA(THETA)
1	-0.589482	0.831177	-0.936211	-0.005665	-0.000814
2	-0.583910	0.531823	-0.617660	-0.006129	-0.000684
3	-0.563248	0.197905	-0.261878	-0.006708	-0.000511
4	-0.512021	-0.142429	0.162207	-0.006475	0.000210
5	-0.314635	-0.586070	0.684786	-0.003205	0.000907
6	-0.135211	-0.815325	0.923880	-0.000899	0.000971
7	-0.033480	-0.877660	1.000000	0.001770	0.000957
8	-0.011863	-0.905033	0.968144	0.010239	0.000574
9	0.000181	-0.002618	0.000959	0.000223	0.000038
10	0.0	0.0	0.0	0.0	0.0

Figure 45. Eigenvalues and Eigenvectors for J = 1 (Case IV)

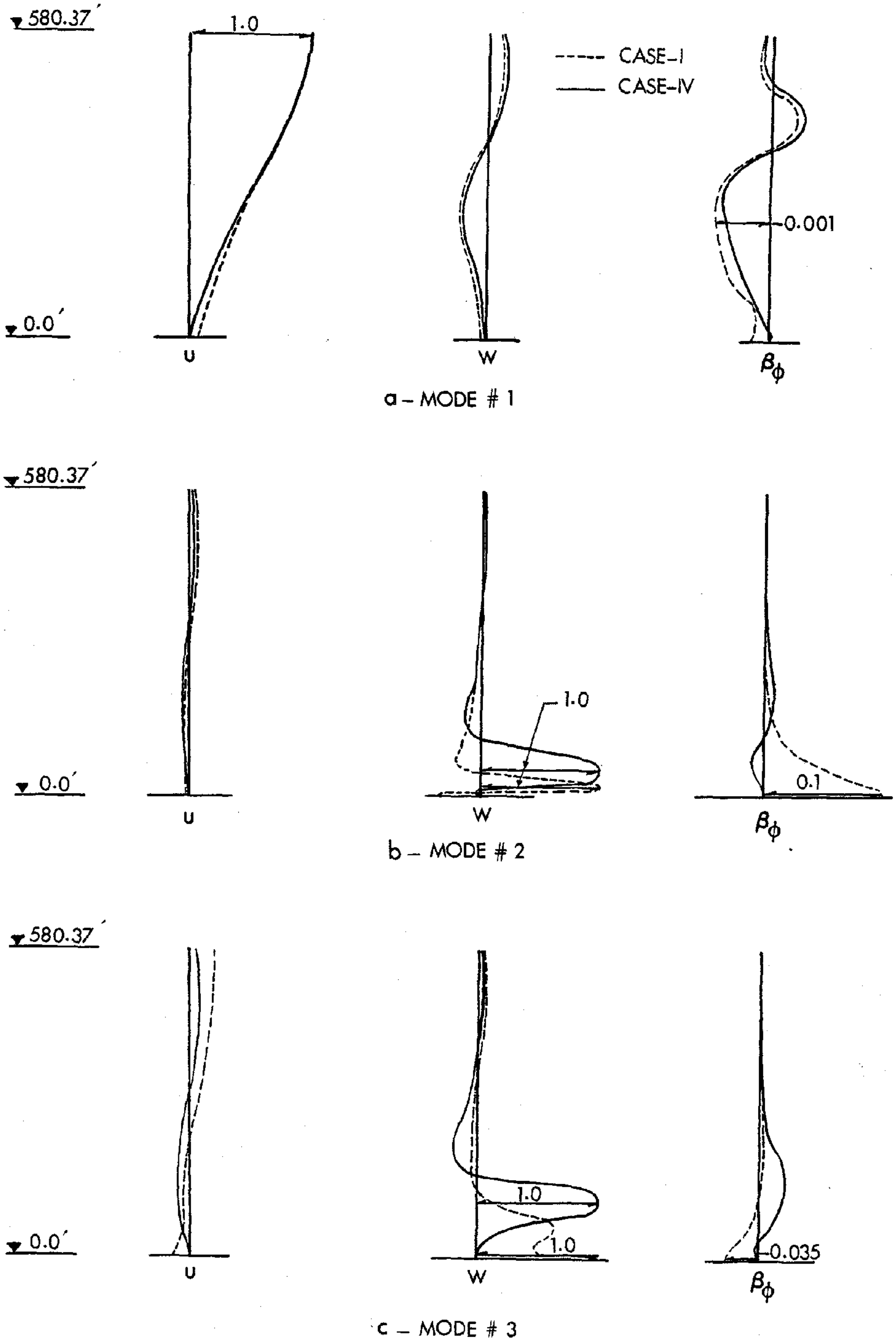

Figure 46. Soil Effect on the Symmetrical Eigenvectors of a Cooling Tower

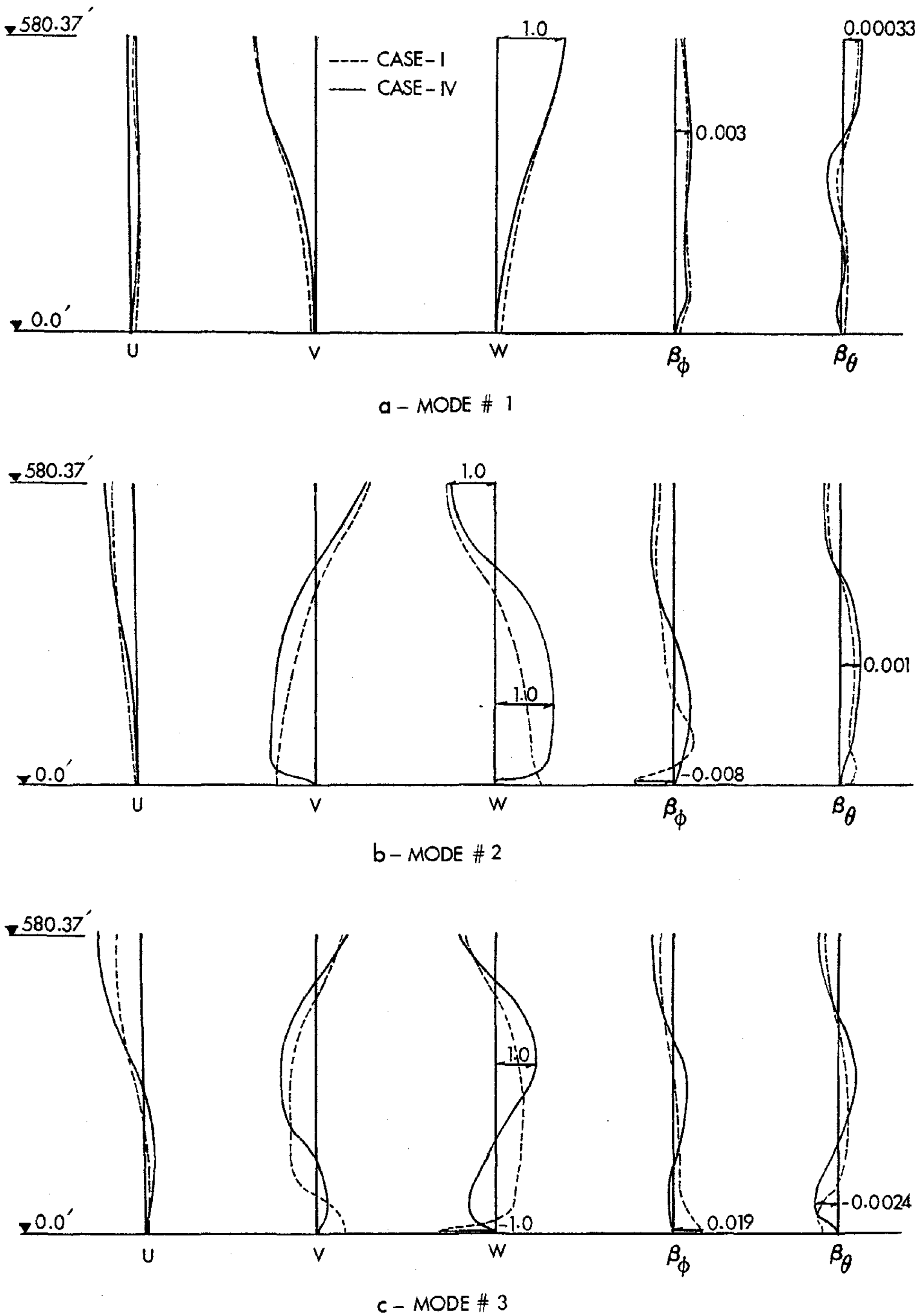

Figure 47. Soil Effect on the Antisymmetrical Eigenvectors of a Cooling Tower

change decreases as the soil gets stiffer as one may notice by comparing the frequencies of the four cases for the horizontal vibration results.

For the soft to intermediate soil case (Case I), the interactive eigenvectors of the second mode are drastically different than the fixed case (Case IV) for both vertical and horizontal vibrations, whereas there is not much difference between the eigenvectors of the first mode for the two soil cases. A similar but less predominant influence of the soil on the interactive eigenvectors is seen in Case II (the stiff-shallow soil case). The eigenvectors of Case III are very similar to those of Case I. This may be attributed to the combined effect of the soil depth and the shear modulus producing very similar compliances for the first and third soil cases.

In spite of the insensitivity of the first mode of vibration to the soil effect, the lower region of the shell is expected to be relieved when these eigenvectors are to be used in calculating the stresses. This is due to the less severe changes in the eigenvectors near the base for the interactive modes as compared to the fixed base modes. However, a bigger gain will accrue from the second mode of vibration which is expected to reduce the stresses near the base dramatically due to the smoothing of the eigenvectors at this region as can be observed from Figure 47b. The soil flexibility has little effect on the third modes, but the small energy in this mode makes it inconsequential when calculating the stress resultants and stress couples in the shell. As expected, the overall flexibility of the shell increases with decreasing soil stiffness as shown by the comparison of the eigenvalues of the first three cases to the stiff base case (Case IV). These reductions in the modal frequencies may increase or decrease the internal stresses when the response spectrum analysis is carried out, according to the peaks of the spectrum.

This study shows that the soil flexibility or compliance is a very important parameter in the soil-structure interaction phenomenon and that a given flexibility can be realized by a non-unique combination of the basic parameters, e.g., soil depth, shear modulus. This observation is in agreement with the conclusions of Pandya and Setlur (16).

5.3.2 Response Spectrum Analysis

To assess the importance of soil-structure interaction on the stress resultant and stress couples in the shell, a response spectrum analysis is carried out using the SHORSS program with the same EBS of the four cases given in Table 6. The structure-soil systems for the four cases are subjected to a horizontal response spectrum with 20% g ground acceleration (Response Spectrum, Figure 48). The soft to intermediate soil case (Case I) and the fixed base case (Case IV) are subjected to 13% g vertical ground acceleration, Figure 49. A damping ratio of 5% is considered for the first three modes

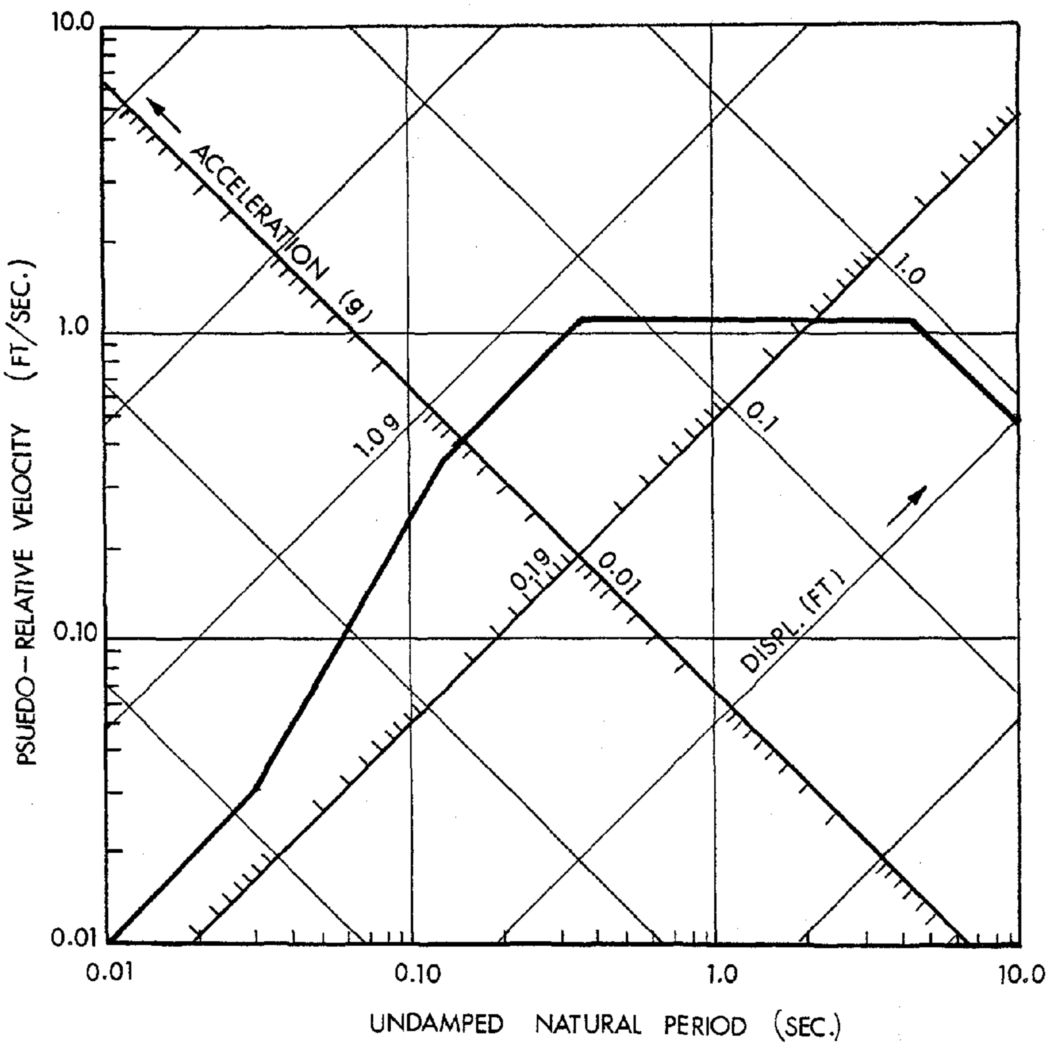

HORIZONTAL [0.20 g , 5% Damping]

Figure 48. Horizontal Response Spectrum

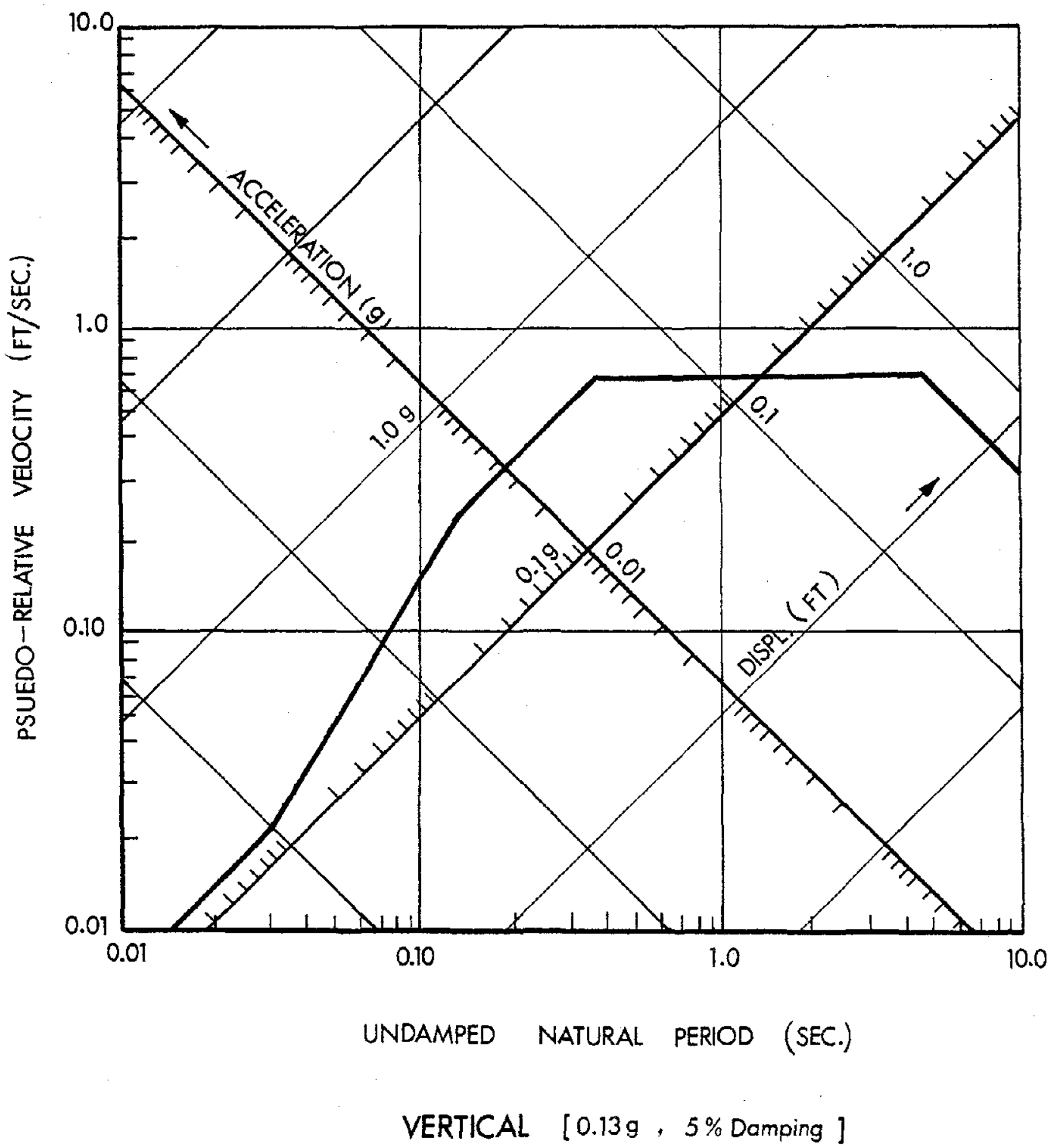

Figure 49. Vertical Response Spectrum

of vibration in all cases. The high intensity of the ground motion is chosen for the purpose of approaching the case of foundation uplift, if present.

The stress resultants and stress couples at $\theta = 0°$ for the shell are given in Figures 50 to 54. It can be seen that the fixed base or stiff soil case produces resultant forces which envelope all soil cases, except for N_ϕ component where the soft soil case (Case I) is the critical case. Therefore the site parameters are indirectly accounted for, except for N_ϕ, when fixed base condition (Case IV) is used.

No significant amplification due to suspected resonance effects is seen in the stress resultants and stress couples for Case III. This is due to the fact that the rocking and swaying motions tend to suppress the response of the structure at the fundamental frequency of the fixed base structure. This observation is in accord with the Pandaya and Setlur results (16).

The increase in the meridional stress resultant N_ϕ as the soil stiffness decreases can be explained by comparing the u-component of the eigenvectors in Figures 46 and 47 for the soft and stiff soil cases. It can be seen that the u-displacement in the lower half of the structure increases as the soil stiffness decreases, which brings about the higher values of N_ϕ for the soft soils compared to the stiff soils. Although the shell thickness may not be affected by

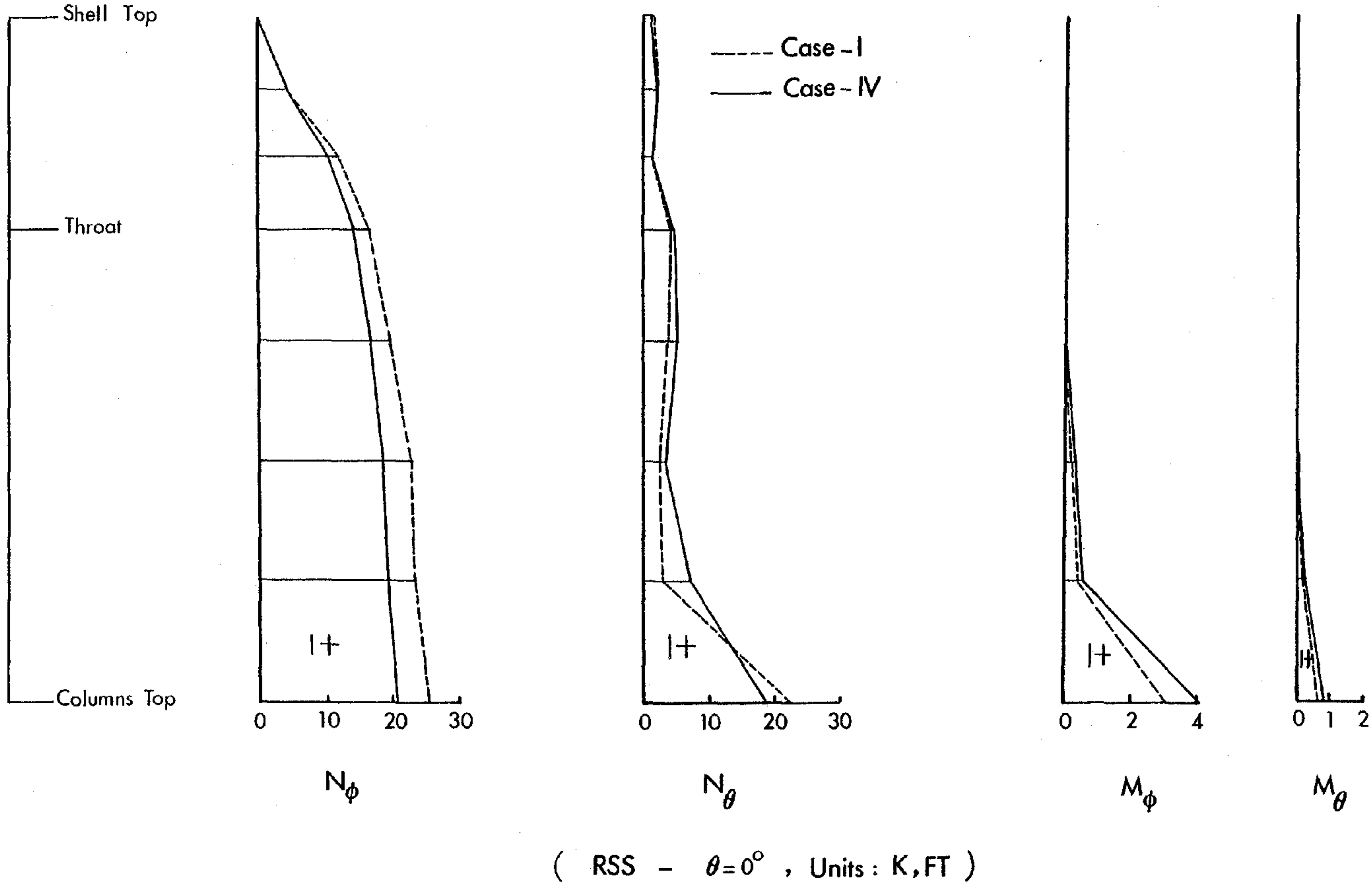

Figure 50. Vertical Response Spectrum Shell Results (J = 0)

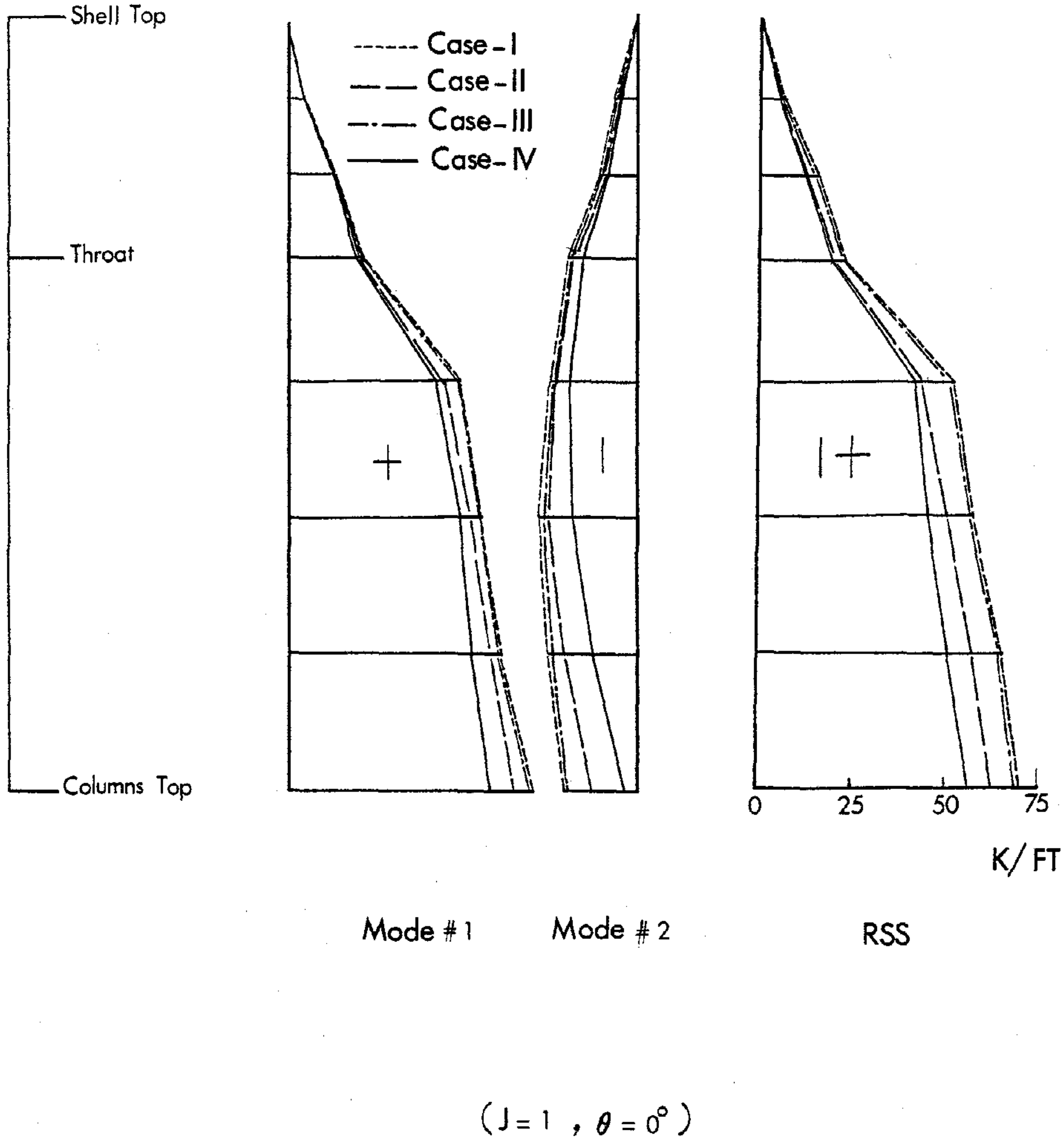

Figure 51. N_ϕ-Component, Earthquake Load

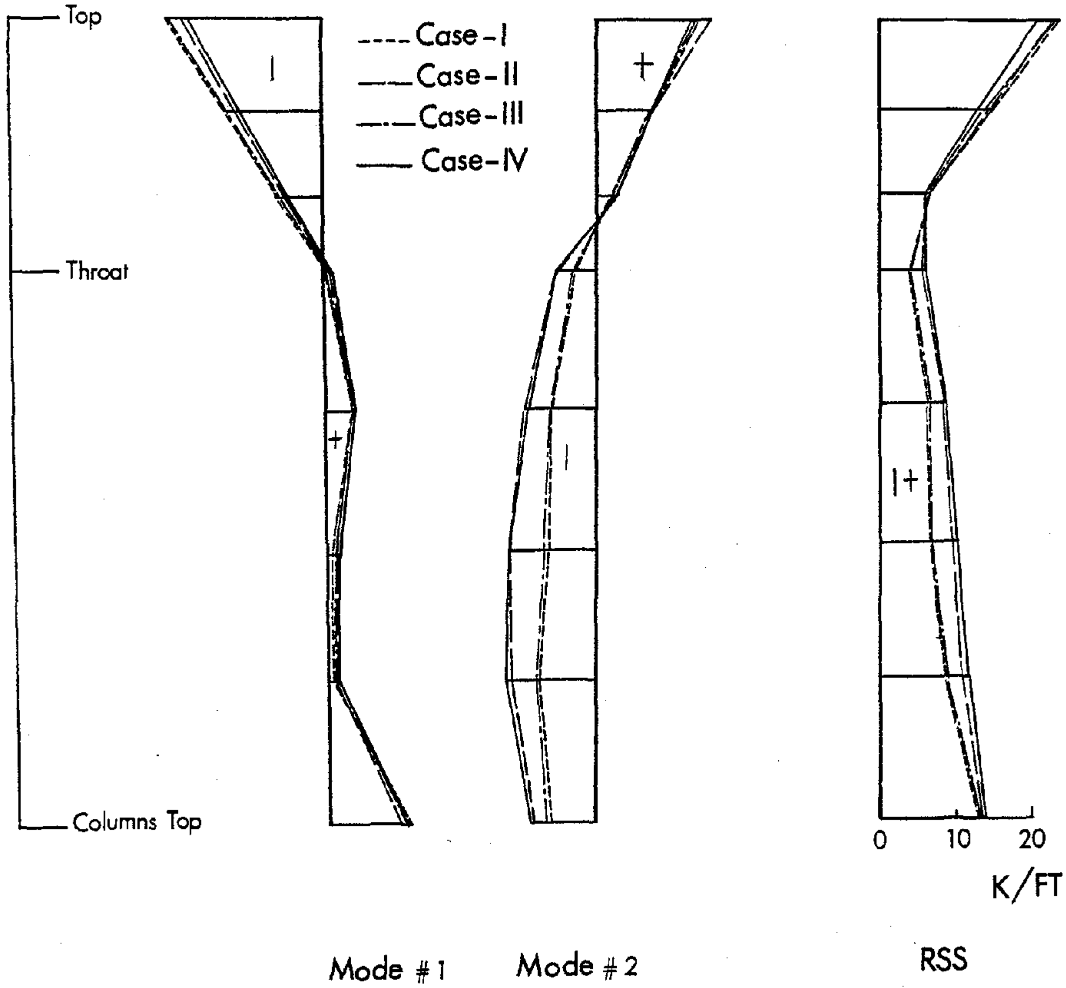

(J=1 , $\theta = 0°$)

Figure 52. N_θ-Component, Earthquake Load

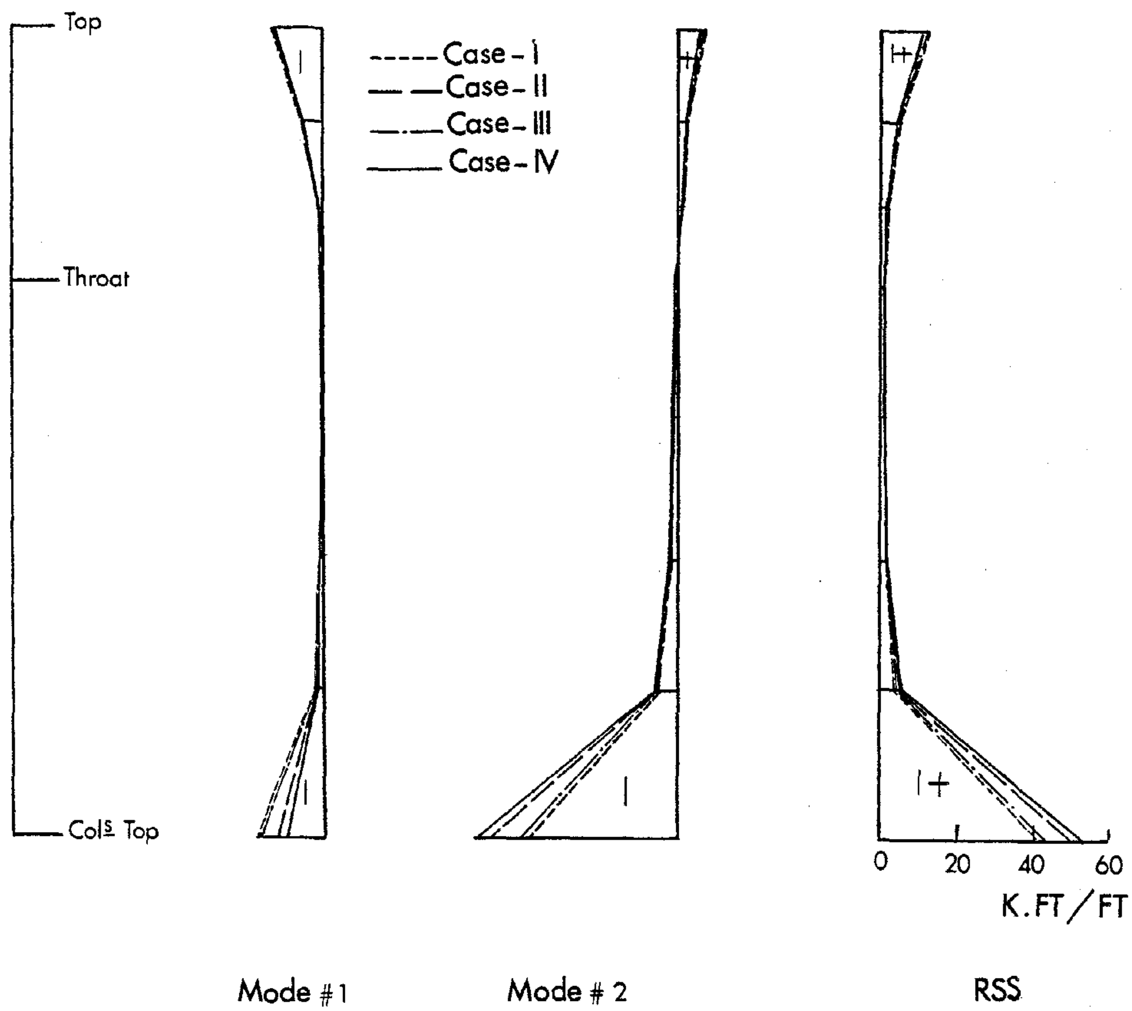

(J = 1 , θ = 0°)

Figure 53. M_ϕ-Component, Earthquake Load

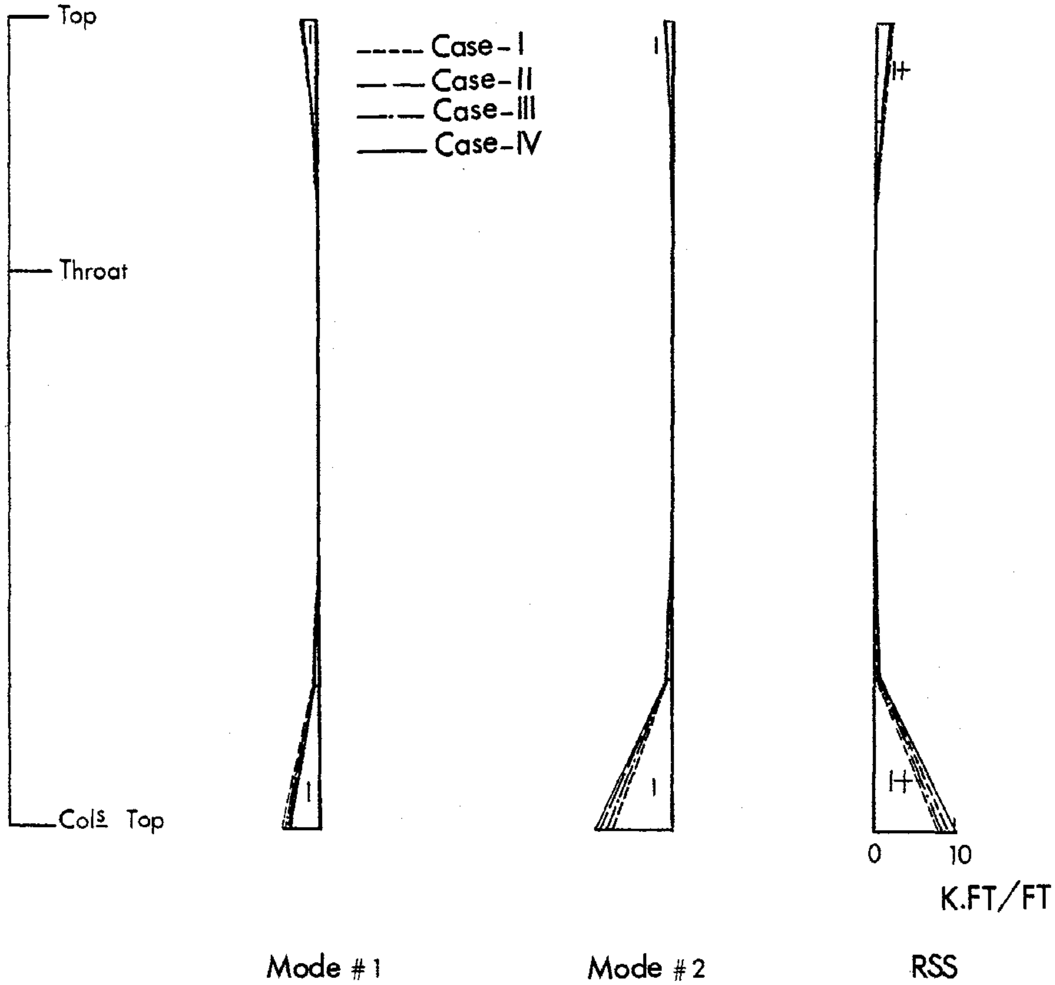

(J = 1 , $\theta = 0^\circ$)

Figure 54. M_θ-Component, Earthquake Load

this higher meridional stress, special attention should be directed to the adequacy of the vertical steel in the lower half of the shell.

As predicted in the previous section the reduction of the square root of the sum of squares (RSS) stress resultants and couples in the responses as the stiffness of the soil decreases is due mainly to the second mode of vibration as can be observed from Figures 52 to 54. This reduction, which is of the range of 20 percent of the fixed base solution, may reduce the thickness of the shell as well as the horizontal steel in the shell and thereby may cut considerably in the structure cost.

The axial forces, bending moments and twisting moments in the columns are calculated using SHORSS program at $\theta = 0°$. Tables 7 and 8 show these responses for the four cases. For the vertical ground motion the effect is mixed, while the axial forces are reduced for the soft soil case (Case I), the moments for the same case are increased compared to the fixed base case (Case IV), see Table 7. It may be seen from Table 8 that there is a sharp decrease in the axial forces and bending moments as the soil stiffness decreases. The decrease in the bending moment may be attributed to the smoothing of the second mode shape (Figure 47b) in the lower region, whereas the 15 percent reduction of the axial forces may be due to the reduction in the total base shear as a result of a smaller input motion.

Table 7. Maximum Column Forces at $\theta = 0°$ (Vertical Ground Motion)

Mode	Axial Force (K)		Bending Moment (K.ft)		Twisting Moment (K.ft)	
	Fixed	Case I	Fixed	Case I	Fixed	Case I
1	351.8	256.3	17.1	13.5	0.19	-0.25
2	9.9	-1.8	47.0	79.9	-0.76	-3.44
3	32.3	-24.0	5.9	92.7	-0.17	3.08
RSS	±352.0	±256.5	±50.1	±126.0	±0.80	±4.65

Table 8. Maximum Column Forces at θ = 0°(Horizontal Ground Motion)

Mode	Axial Force (K)				Bending Moment (K.ft)				Twisting Moment (K.ft)			
	Case I	Case II	Case III	Fixed	Case I	Case II	Case III	Fixed	Case I	Case II	Case III	Fixed
1	539.7	592.9	543.3	826.8	160.2	88.8	153.6	160.5	-14.4	-1.7	-13.1	-6.1
2	-450.1	-364.4	-451.2	-141.3	166.5	143.4	157.9	615.1	-30.3	7.8	-28.6	-17.2
3	0.2	-42.2	1.1	-19.6	1.0	398.8	9.4	17.5	-0.1	16.4	-0.3	-0.1
RSS	±702.2	±697.2	±706.2	±838.9	±240.3	±432.9	±220.5	±636.0	±33.7	±18.2	±31.5	±18.2

The twisting moment in the columns increases as the soil stiffness decreases. However, the values of the twisting moments are not large enough to be a controlling factor in the column design as can be seen from Tables 7 and 8.

The response of the concentric ring footing for the vertical and horizontal ground motions is given in Tables 9 and 10 respectively. The results presented in these two tables are the complete solution which consists of the continuous boundary solution and self-equilibrated correction, see Figure 15. In the self-equilibrated correction, the SHORC program is used to calculate the Fourier coefficients for the loads and the resulting self-equilibrated loads are applied as line loads at the top of the beam which is modeled as two rotational shell elements. The highest harmonic number used in expanding the self-equilibrated loads was 440. The lower boundary of the footing consisted of static springs with zero masses and damping, i.e., the correction is carried out as static self-equilibrated forces as explained in Section (4-3-3) using SHORSS program.

Table 9 shows that the soft soil case (Case I) gives higher values for the axial force and bending moments, vertically and horizontally, compared to the fixed base case (Case IV). The values of the fixed base response are unrealistically small due to the restriction imposed by the

Table 9. Foundation Response to Vertical Ground Motion (RSS)

Soil Case		Axial Force (K)	V. Moment (K.ft)	H. Moment (K.ft)	Torsion (K.ft)
Case I	Col.	±269.7	±387.0	∓117.1	±207.3
	Field	±270.2	∓436.6	±120.3	±172.9
Case IV	Col.	±47.6	±68.2	∓20.4	±575.1
	Field	±47.3	∓69.8	±27.5	±491.2

Sign Convention:

Axial Force: (+ve) for tension

Bending Mom.: (+ve) for tension in bottom or inside fibers

Torsion: (+ve) clock-wise rotation

Table 10. Foundation Response to Horizontal Ground Motion (RSS)

Soil Case	θ	Axial Force (K) Col.	Axial Force (K) Field	V. Moment (K.Ft) Col.	V. Moment (K.Ft) Field	H. Moment (K.Ft) Col.	H. Moment (K.Ft) Field	Torsion (K.Ft) Col.	Torsion (K.Ft) Field
Case I	0°	±1867.4	±1805.7	±10953.2	∓11837.4	∓809.2	±911.6	±3767.7	±4340.5
	90°	±152.4	±157.9	±715.7	∓731.6	∓32.7	±64.4	±7762.0	±7699.3
Case II	0°	±1385.0	±1361.6	±6705.0	∓7007.8	∓620.7	±701.0	±5013.1	±4897.6
	90°	±141.6	±150.7	±682.3	∓695.9	∓24.1	±54.9	±9267.4	±9226.3
Case III	0°	±1751.1	±1691.8	±9817.4	∓10911.1	∓752.5	±839.6	±4266.1	±4703.8
	90°	±146.7	±152.2	±700.5	∓715.9	∓30.8	±62.8	±8117.7	±8100.4
Case IV	0°	±392.4	±388.8	±745.7	∓699.0	∓110.0	±118.1	±6946.2	±5988.1
	90°	±23.0	±27.7	±47.7	∓50.6	∓6.7	±7.2	±11207.0	±11200.6

The sign convention as in the vertical ground motion, Table 9 fixed boundary assumption. However, the torsional moment for the fixed base case is higher than that for the soft soil case, which could be due to the same reason discussed in connection with the axial force and bending moments response in the footing. Similar observations could be made for the results shown in Table 10. The three cases of soil structure interaction give responses for the axial forces and bending moments sharply higher than the fixed base response, while the torsional moment gets smaller as the soil becomes softer. The convergence to the fixed base results, as the soil gets stiffer, is evident from Table 10. Incidentally, the values presented for the vertical moment are computed from N_θ results along the footing depth, since the vertical bending moment corresponds to the rotational degree of freedom about the normal axis which is neglected in shell theories (50).

The analysis of the ring footing is repeated for the intermediate to stiff soil case (Case II) using the RSS of the column reactions given in Table 8. The STRUDL-II program (53) has been used for computing the forces and displacements at different nodal points along the circumference. The ring footing with the soil is modeled as a space frame with six degrees of freedom per nodal point, Figure 55. The bearing stiffness and the horizontal frictional stiffness

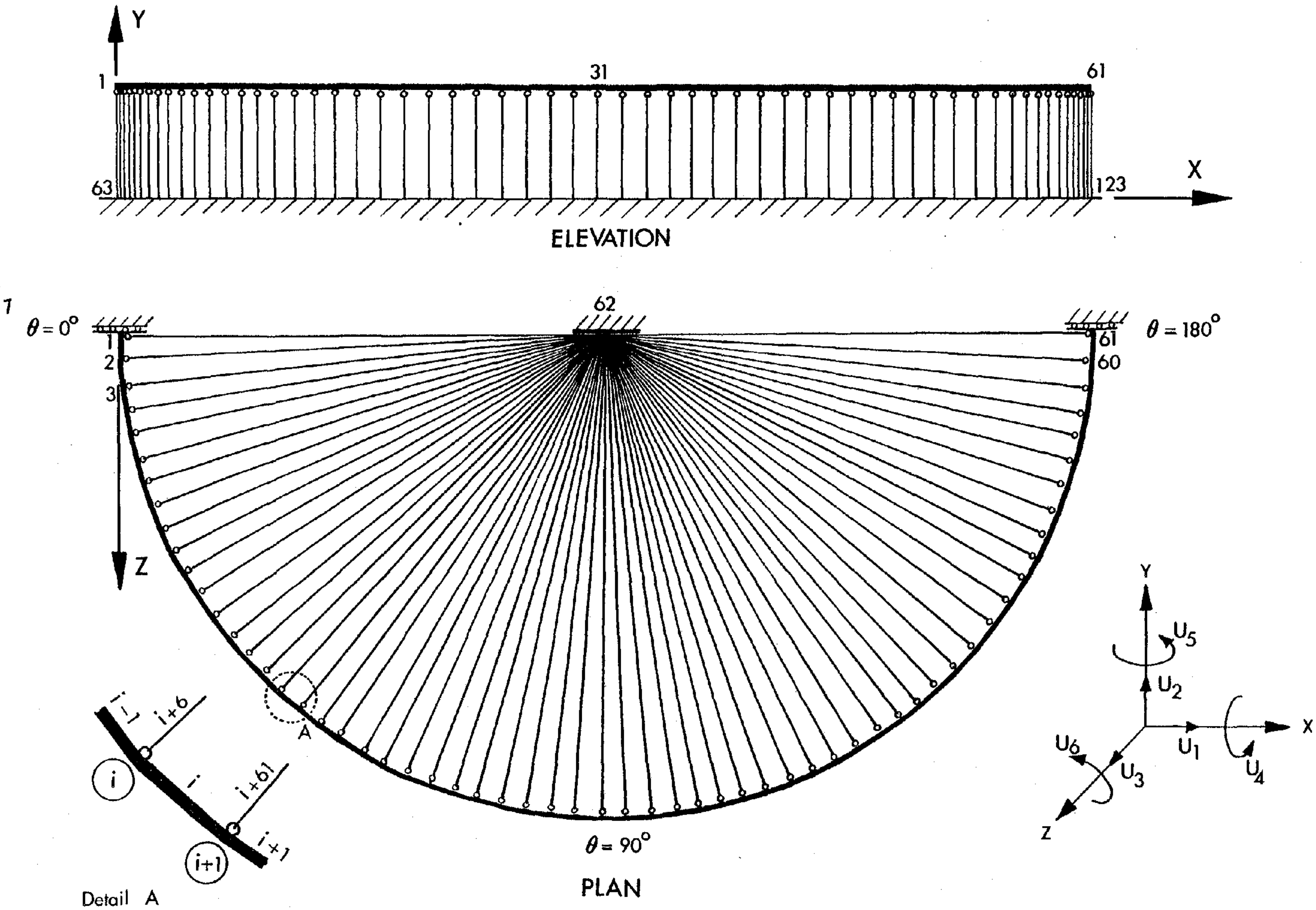

Figure 55. Ring Footing Soil Model for STRUDL Program

of the soil are modeled by axial members with the same stiffness of the corresponding soil component such that:

for vertical members

$$\frac{EA_v}{L} = (\text{Bearing Stiffness}) \times \text{Nodal point spacing}$$

and for horizontal members

$$\frac{EA_h}{r_o} = (\text{Avg. Frictional Stiffness}) \times \text{Nodal point spacing}$$

The connection between these axial members are designed to allow for only axial forces in the soil model by releasing the other five degrees of freedom at the start of each member (u_2 to u_6 in Figure 55). The release is done on the local level for the member with u_1 parallel to the member axis.

The results of the space frame analysis are presented in Figures 56 to 59 for the axial forces and the moments. On the same figures the ring forces at θ equals 0°, 4°, 40°, 45°, 86° and 90°, using SHORC and SHORSS programs,are plotted for comparison.

It may be seen from Figures 56 to 59 that the rotational shell element model gives smaller response than that obtained using space frame model with straight elements. This may be due to the approximation used to expand the self equilibrated forces in Fourier series modes for the rotational element model. This approximation might underestimate the actual

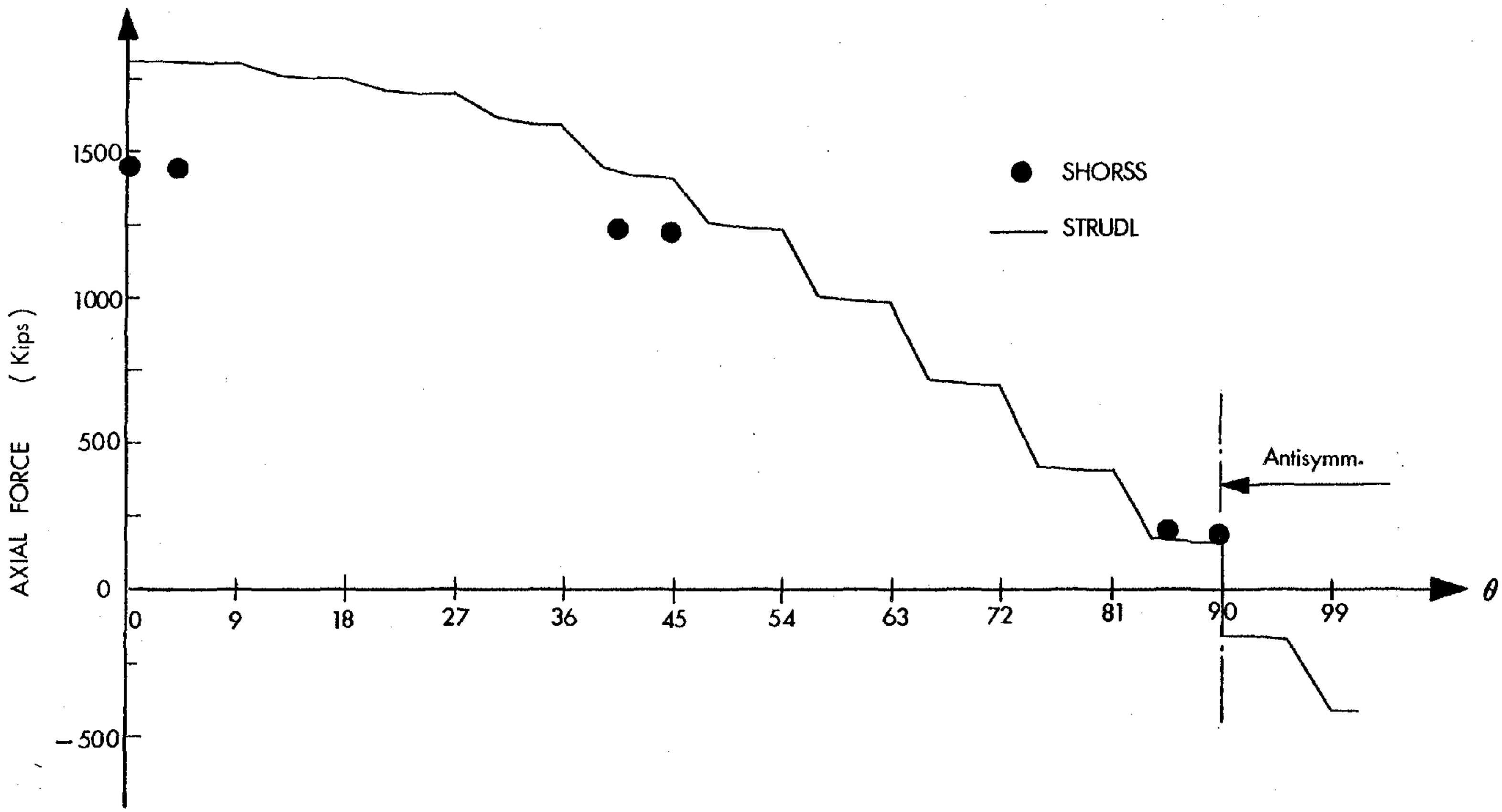

Figure 56. Axial Force in the Ring Footing for Soil Case II (J = 1)

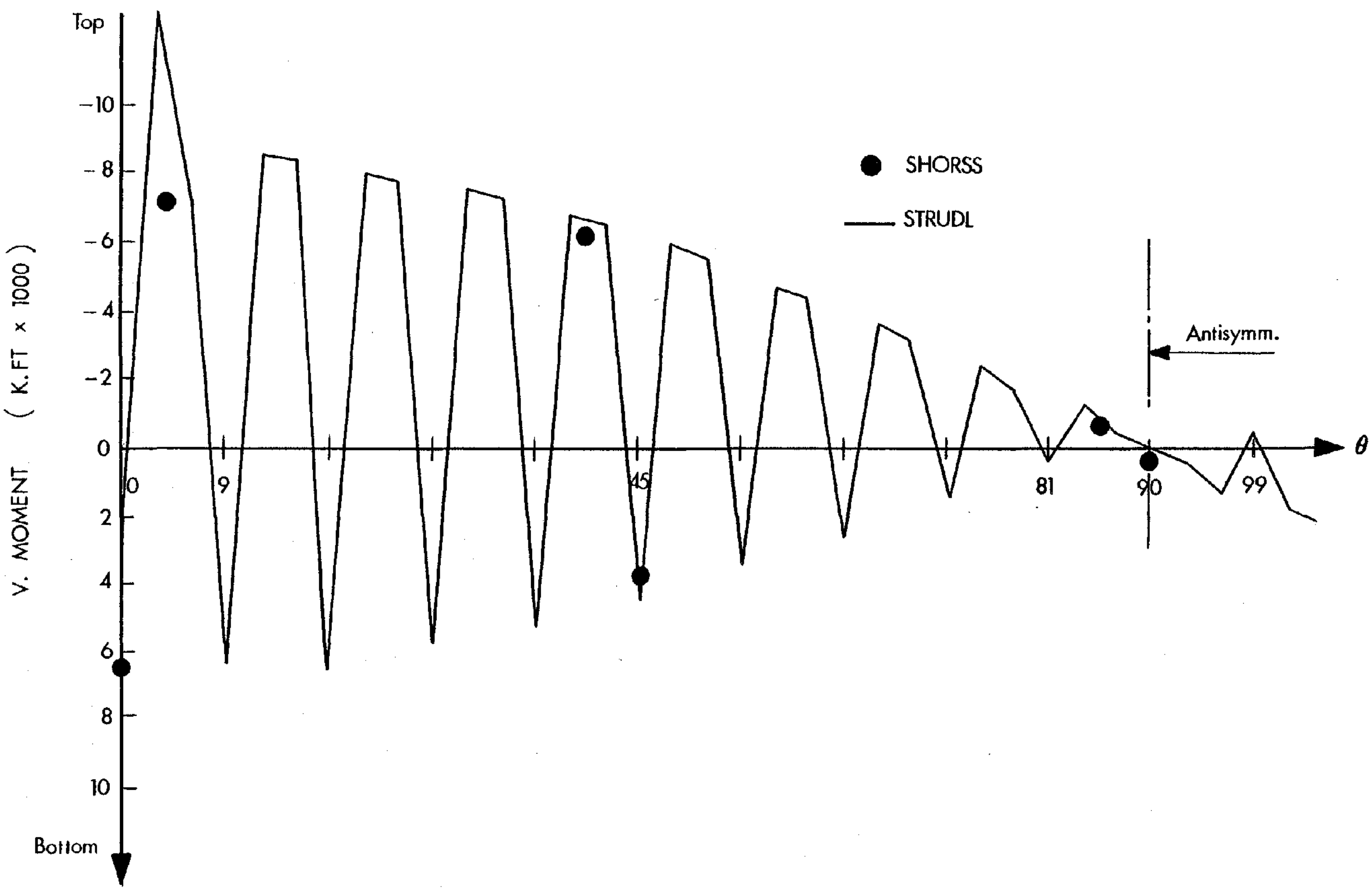

Figure 57. V. Moment in the Ring Footing for Soil Case II (J = 1)

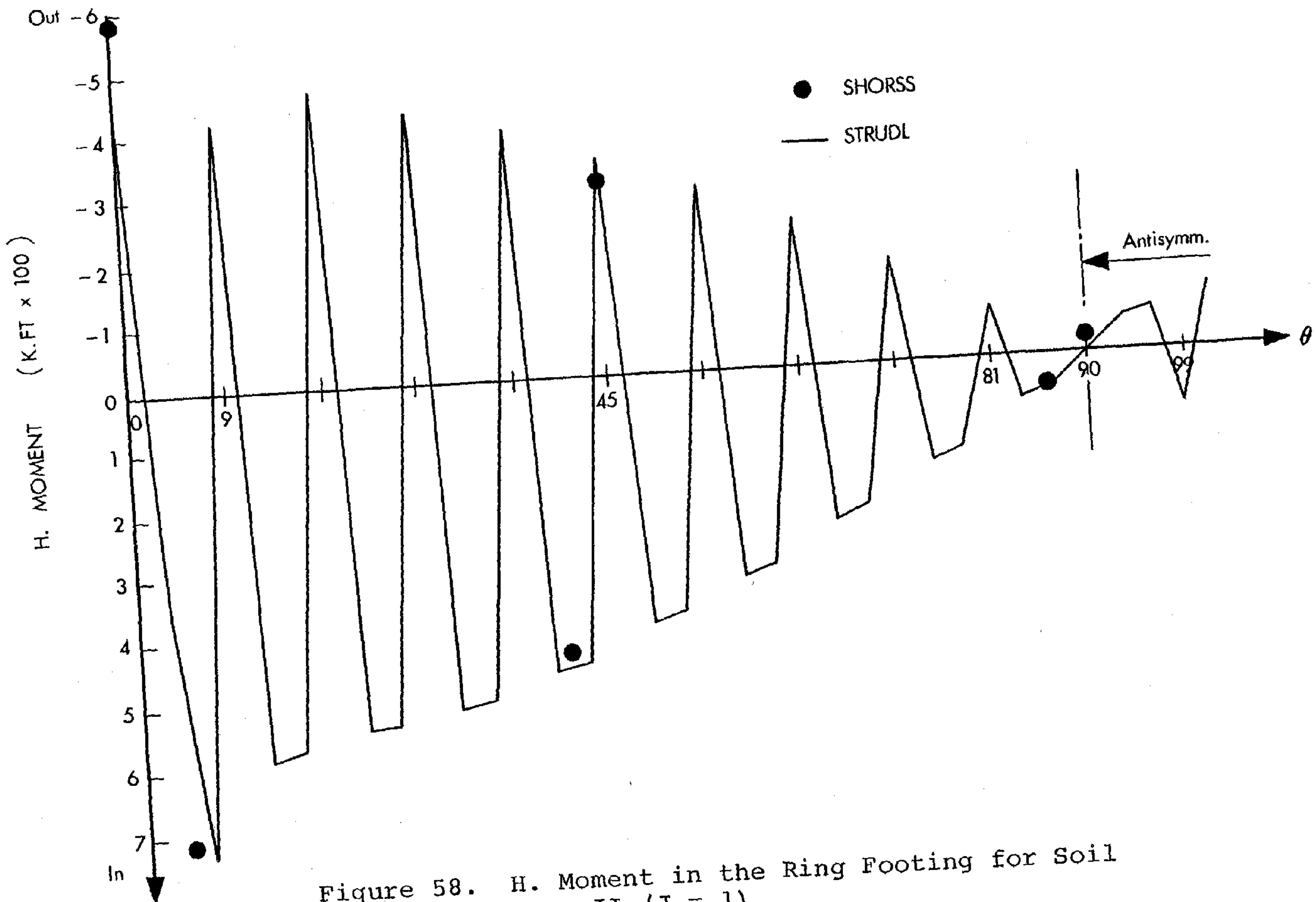

Figure 58. H. Moment in the Ring Footing for Soil Case II (J = 1)

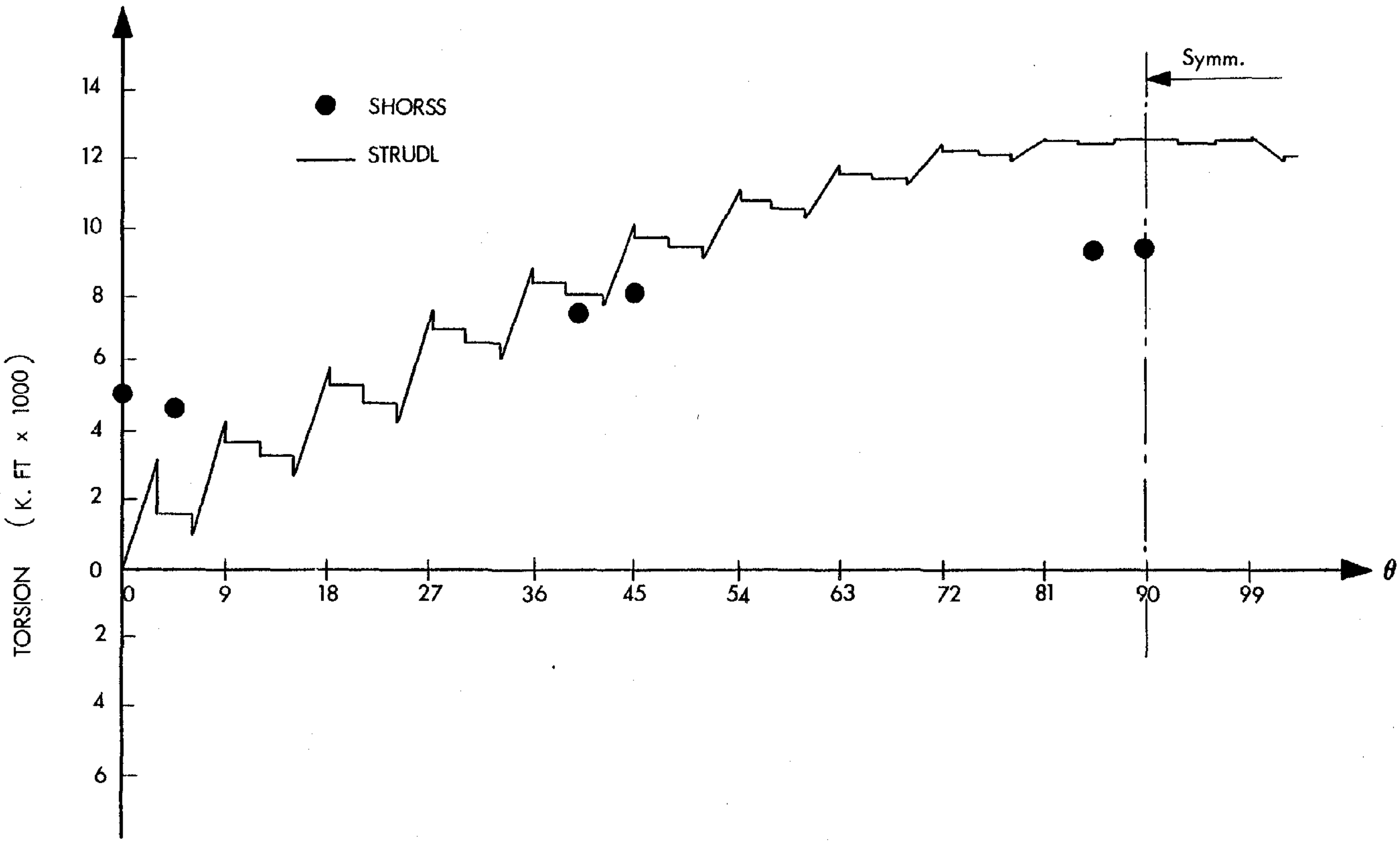

Figure 59. Torsion in the Ring Footing for Soil Case II (J = 1)

forces from the columns on the ring footing and, as a result, produce smaller ring forces, especially the axial force and torsion, Figures 56 and 59. The difference of the results may be explained by comparing the lower boundaries of the footing in the two models. While the boundaries are continuous in the axisymmetric element model, program, they correspond to a point bearing (discrete) boundary in the space frame model. Furthermore, the use of straight elements in STRUDL program is expected to increase the bending moment in the ring footing which can be observed from Figures 57 and 58.

From the results the big difference between the response of the two models around the second node is noticeable. The disagreement could be due to the deviation of the first two elements in the space frame model from the equation of the circle since node number 2 is shifted in the x-direction such that the global value of the x-coordinate of node number 2 becomes zero to allow the boundary condition at the first node to be parallel to the global axes. These boundary conditions at the line of symmetry ($z = 0$), which allow for the rotation about the z-axis, are responsible for the unrealistic zero torsion at $\theta = 0°$, see Figure 59.

In spite of the above boundary, geometry and loading differences in the two models used for the analysis, the results are fairly close and give some confidence in both models while eliminating the possibility for gross errors.

As mentioned in Chapter 4, the model is correct only after a check for the foundation uplift is carried out. This check could be performed at the continuous boundary result level without the need for the self-equilibrated correction. This is because the overall behavior of the foundation is shown from the continuous boundary results alone, which may then be combined with the dead load results to check against the possibility of foundation uplift.

To check against foundation uplift, the N_ϕ component of the stress resultants is computed at the foundation level for D.L., factored by 0.9 and then added to the unfactored earthquake response. The results are tabulated in Table 11.

It can be seen from Table 11 that the net stress at the F.L. for all cases is compression and no uplift occurs for the severe 20% g spectrum used in the analysis. However, we can see that the softer the soil the more likely the uplift to occur. To investigate this possibility more closely the vertical component of the earthquake may be included. The RSS of N_ϕ at the foundation level for the vertical and horizontal ground motions for Case I is computed and the net value for N_ϕ is found by combining the resulting RSS value of N_ϕ with the factored D.L. value. The net value of N_ϕ is computed from the equation:

Table 11. N_ϕ - Component at F.L. (J = 1)

D.L.	0.9(D.L.)	Case I		Case II		Case III		Case IV	
		EQ	Net	EQ	Net	EQ	Net	EQ	Net
-77.8	-70.0	64.8	-5.2	59.2	-10.8	61.9	-8.1	58.3	-11.7

Units: K/ft.

$$N_\phi(\text{net}) = (N^2_{\phi_h} + N^2_{\phi_v})^{1/2} - 0.9\, N_{\phi_d} \tag{5-5}$$

where

$N_{\phi_h} = N_\phi$ at the F.L. due to horizontal ground motion

$N_{\phi_v} = N_\phi$ at the F.L. due to vertical ground motion

and $N_{\phi_d} = N_\phi$ at the F.L. due to the dead load

For Case I N_ϕ(net) is computed from Equation (5-5), with N_{ϕ_v} = 29.8 K/ft, and the resulting value of N_ϕ(net) is found to be a tensile stress of 1.3 K/ft which can cause uplift. However, N_ϕ(net) is probably too small to cause a real uplift as this net stress could be counteracted by the soil friction on the sides of the footing.

6. SUMMARY AND CONCLUSIONS

A numerical method to determine the response of axi-symmetric shell structure soil systems to arbitrary non-axisymmetric dynamic loads was developed and applied to some particular cases. The method carried out with finite element analysis using high-precision rotational shell elements to represent the axisymmetric shell and isoparametric solid elements with an energy transmitting boundary to represent the soil medium. The connection problem between the three dimensional soil medium and the two dimensional shell-elements is solved by introducing a frequency dependent dynamic boundary system at the common degrees of freedom between the shell foundation and the underlaying soil. The Fourier expansion technique is used in the finite element analysis. The soil model components were computed at the fundamental frequency of the shell structure without the soil system for the free vibration and the response spectrum analysis, whereas the dominant driving frequency of the time history excitations (54) should be used with the time history analysis which has not been carried out.

It was shown that the size of the finite element mesh is controlled throughout the dynamic pressure bulb by the shortest shear wave length and that such bulb exists through a depth of one and half times the footing radius. The influence of the lower boundary on the soil model components is significant only for depths less than three times the footing radius due to the reflections of the waves on the assumed rock-soil interface which tends to increase the stiffness elements and decrease the damping elements (convergence to the fixed base cases). Based on the dynamic pressure bulb study an economical finite element mesh for the soil medium was suggested for use with shells having a small B/r_o ratio.

The sensitivity study of the equivalent boundary system to the driving frequency showed that the stiffness elements are more sensitive than the damping elements, and among the different components, the rotational ones are the most sensitive to the driving frequency. A similar conclusion may be drawn for the sensitivity of the EBS to Fourier harmonic number J. It is also concluded that the EBS components are fairly independent of the harmonic number J for $J > 1$, which suggests a useful procedure to determine the EBS components for $J > 1$ with the aid of a single harmonic number ($J \geq 2$) analysis.

The free vibration analysis of a cooling tower on a shallow foundation showed that the overall flexibility of the shell increases with the decrease of the soil stiffness and consequently, gives a reduction in the inertial forces on the shell. The study also revealed a dramatic change in the second mode of vibration as the soil gets more flexible. This relieves the lower region of the shell (column supports in cooling towers) from the high stresses which often occur when the soil interaction is neglected. It is concluded from this study that the soil flexibility or compliance is a very important parameter in the soil-structure interaction phenomenon and that a given flexibility can be realized by a non-unique combination of the basis paramaters. This finding is in agreement with Pandya and Setlur conclusions (16).

The importance of the soil-structure interaction on the stress resultants and the stress couples in the shell was shown by response spectrum analysis of the cooling tower used in the free vibration analysis. It was shown that the fixed base or very stiff soil case produces resultant forces which envelope all soil cases, except for N_ϕ component. The reduction, which is of the range of 20% of the fixed base solution, may permit reduction of the shell cross section and the horizontal steel in the shell resulting in a considerable cost savings. Perhaps, the segment in the shell structure most affected by soil-structure interaction are the column supports as may be seen from Tables 7 and 8. The saving in the stresses may reach 50% for certain soil flexibilities.

The analysis of the concentric ring footing, which has not been studied previously so far as the authors can determine, showed a tremendous twisting moment on the footing which increases with increasing the soil stiffness. On the contrary, the axial force and bending moments increase with decreasing the soil stiffness. With the present model, the footing can be analyzed as a ring resting on a continuous elastic foundation, bringing forth the axial forces and the torsion which were not possible to obtain with the continuous beam over point support model used before. Confidence in the ring footing response is established by comparing the present model results to the results of a space frame model.

The possibility of foundation uplift increases with increasing the soil flexibility. In the design earthquake considered here, uplift could occur only if the two components of the ground motions were considered simultaneously (vertical and horizontal components). However, the net tensile stress after adding the dead load effect is too small to cause a real uplift as shown in the analysis.

The free vibration and the response spectrum analysis for the shell of revolution-soil system may be adequate for linear analysis under uniform earthquake excitation. However, the damping ratio for the response spectrum should be chosen such that the radiation damping in the far field is represented. The relationship between this damping ratio and the radiation damping needs further study. Further investigations are also required to study the relationship between the damping ratio and the viscous damping where complex Lamé constants of the soil material are used.

The effect of non-uniform earthquake excitation may yield further reduction in the structure response due to the inherent self-diminishing feature to this type of earthquake excitation as suggested by Scanlan (19). Time-history analysis may be necessary with non-uniform earthquakes and for better understanding to the damping phenomenon of soil-structure system. These two topics need further investigation as well.

7. ACKNOWLEDGMENT

The material presented in this report is based on research supported by the National Science Foundation under Grant No. PFR-7900012. However, any opinions, findings, conclusions or recommendations expressed herein are those of the authors and do not necessarily reflect the views of NSF.

8. APPENDICES

APPENDIX 8.1

High Precision Rotational Shell Elements

In this appendix, the outlines of the derivation of the high-precision rotational shell finite elements is presented. These may be classified into four main groups: curved rotational elements, cap elements, plate elements and special open type elements (see Figure 60).

For the shell elements, the strain-displacement relationships used in the formulation include the effect of transverse shear deformations. In forming the element stiffness and mass matrices, displacement fields of arbitrary order, i.e., linear to sixth order, can be used, and because only C° continuity is required to be satisfied, the extra coefficients in quadratic and higher order displacement-fields are eliminated by kinematic condensation at the element level. Proportional damping is assumed and the damping matrix is arrived at through a linear combination of the condensed stiffness and mass matrices.

To overcome the singularity problem in the case of a cap element, $R = 0$ and $R' = \infty$ at the center, a suitable rotation of the coordinate axes into the $\bar{R}$-$\bar{Z}$ system as shown in Figure 61 is considered (6).

In case of the open type elements, the displacement fields are taken as Hermetian polynomials. The stiffness and mass matrices are formed by distributing the properties of the individual members around the circumference.

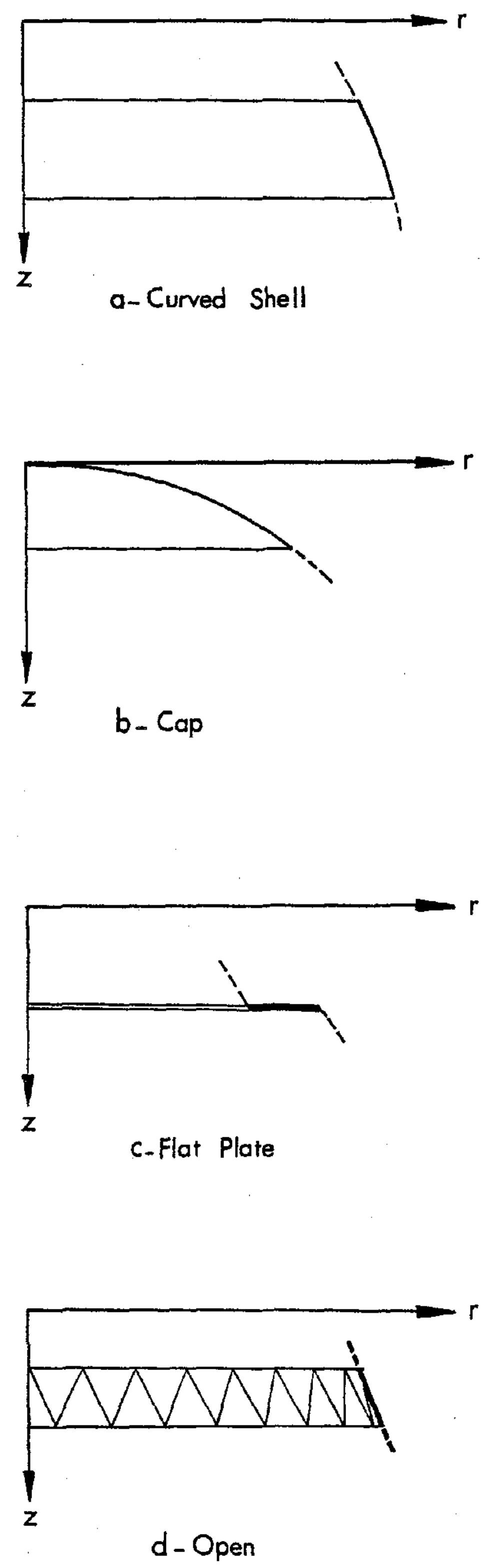

Figure 60. High Precision Rotational Shell Element Groups

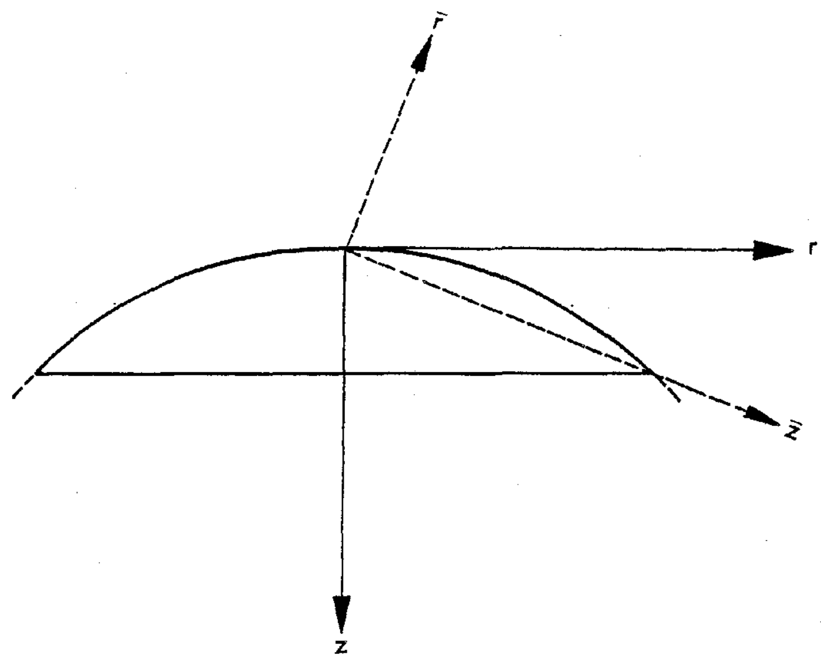

Figure 61. Rotation of Axes for Cap Element

8.1.1 Geometry of Elements

The geometry of a general rotational shell element is shown in Figure 38. Points on the meridian of the element are defined in terms of the non dimensional parameter s such that:

$$\frac{\partial}{\partial s} = \frac{1}{L}\frac{\partial}{\partial s} \qquad (8.1.1)$$

where

L = the length of the meridian of element "i"

$$= \int_{z_i}^{z_{i+1}} \left[1 + \left(\frac{dR}{dZ}\right)^2\right]^{1/2} dZ \qquad (8.1.2)$$

in which z_i and z_{i+1} = the nodal stations for element i. The above equation must be evaluated numerically. In order to arrive at the terms of the element matrices in explicit forms, definitive geometric parameters, like $1/R_\phi$, $1/R$, $\cos\phi$, etc. are expressed by fourth degree Lagrangian polynomials (41) which satisfy the value of these parameters exactly at five equidistant points along the meridian, including the ends.

8.1.2 Displacement Fields

Each displacement component shown in Figure 39 is considered a product of the meridional and circumferential fields. The meridional field is a polynomial in s and the circumferential field is represented by a finite Fourier series. For a typical harmonic

$$\{D^j(s,\theta)\} = \lceil\theta\rfloor \{\bar{D}^j(s) \qquad (8.1.3)$$

where

$$\lceil\theta\rfloor = \lceil g^j(\theta) \;\; \bar{g}^j(\theta) \;\; g^j(\theta) \;\; g^j(\theta) \;\; \bar{g}^j(\theta)\rfloor \qquad (8.1.4)$$

and

$$\begin{aligned}\{\bar{D}^j(s)\} &= \{u^j(s) \;\; v^j(s0 \;\; w^j(s) \;\; \beta_\phi^j(s) \;\; \beta_\theta^j(s)\} \\ &= \{\bar{d}^1(s) \;\; \bar{d}^2(s) \;\; \bar{d}^3(s) \;\; \bar{d}^4(s) \;\; \bar{d}^5(s)\}\end{aligned} \qquad (8.1.5)$$

In Equation (8.1.4),

$$\begin{aligned}g^j(\theta) &= \cos j\theta && \text{for } j \geq 0 \\ &= -\sin j\theta && \text{for } j < 0 \\ \bar{g}^j(\theta) &= -\sin j\theta && \text{for } j \geq 0 \\ &= \cos j\theta && \text{for } j < 0\end{aligned}$$

and in Equation (8.1.5)

$$\begin{aligned}\bar{d}^i(s) &= \text{an interpolation polynomial} \\ &= \sum_{k=1}^{m_i} \bar{d}_k^i N_k \qquad (i=1,\ldots,5)\end{aligned} \qquad (8.1.6)$$

where N_k are the shape functions, as defined below

$$\begin{aligned}N_1 &= (1-s) \\ N_2 &= s \\ N_k &= s^{k-2}(1-s) \qquad \text{for } k > 2\end{aligned} \qquad (8.1.7)$$

Also,

$\bar{d}_1^i$ = the displacement at s = 0

$\bar{d}_2^k$ = the displacement at s = 1

For further details see Reference (35).

8.1.3 Element Stiffness and Mass Matrices

On substituting the assumed displacement fields into the strain-displacement relationships the following expressions are obtained:

The membrane strain components,

$$\{\varepsilon\} = \sum_{j=-m_1}^{m_2} [E_1^j \; E_2^j \; E_3^j \; E_4^j \ldots]\{\Delta^{[j]},\Omega^{[j]}\}$$

$$= \sum_{j=-m_1}^{m_2} [G_1^j]\{\Delta^{[j]},\Omega^{[j]}\} \qquad (8.1.8)$$

The curvature components,

$$\{\chi\} = \sum_{j=-m_1}^{m_2} [x_1^j \; x_2^j \; x_3^j \; x_4^j \ldots]\{\Delta^{[j]},\Omega^{[j]}\}$$

$$= \sum_{j=-m_1}^{m_2} [G_2^j]\{\Delta^{[j]},\Omega^{[j]} \qquad (8.1.9)$$

The transverse shear strain components,

$$\{\gamma^j\} = \sum_{j=-m_1}^{m_2} [Y_1^j \; Y_2^j \; Y_3^j \; Y_4^j \ldots]\{\Delta^{[j]},\Omega^{[j]}\}$$

$$= \sum_{j=-m_1}^{m_2} [G_3^j]\{\Delta^{[j]},\Omega^{[j]}\} \qquad (8.1.10)$$

where

$$\{\varepsilon\} = \{\varepsilon_\phi \ \varepsilon_\theta \ \varepsilon_{\phi\theta}\}$$

$$\{\chi\} = \{\chi_\phi \ \chi_\theta \ \chi_{\phi\theta}\}$$

$$\{\gamma^j\} = \{\gamma^j_\phi \ \gamma^j_\theta\}$$

$$\{\Delta^j,\Omega^j\} = \lceil\theta_j\rfloor\{\Delta^j,\Omega^j\}$$

$$\{\Delta^j\} = \{u^j_0 \ v^j_0 \ w^j_0 \ \beta^j_{\phi 0} \ \beta^j_{\theta 0} \ u^j_1 \ v^j_1 \ w^j_1 \ \beta^j_{\phi 1} \ \beta^j_{\theta 1}\}$$

$$\{\Omega^j\} = \{a^j_1 \ b^j_1 \ c^j_1 \ d^j_1 \ e^j_1 \ \ a^j_2 \ b^j_2 \ c^j_2 \ldots\ldots\}$$

Expressing

$$G^j = \begin{bmatrix} [G^j_1] \\ [G^j_2] \\ [G^j_3] \end{bmatrix}_{8\times M} \lceil\theta_j\rfloor \tag{8.1.11}$$

where

$$M = 2 + \sum_{i=1}^{5} (2+n_i), \text{ and}$$

n_i = the number of internal nodal variables for the i<u>th</u> field

The matrices E^j_i, x^j_i and y^j_i contain the shape function N_i and are given in (41).

The element stiffness matrix for the j<u>th</u> harmonic becomes

$$[K^j] = L \int_0^1 \int_{-\Pi}^{\Pi} [G^j]^T[H][G^j]Rd\theta ds \tag{8.1.12}$$

The kinematically consistent mass matrix (35) corresponding to any harmonic is expressed by

$$[m] = \Pi L \int_0^1 [G^m]^T [H^m] [G^m] R ds \qquad (8.1.13)$$

8.1.4 Constitutive Relationships

The relationship between the force resultants and the strain components are expressed by

$$\{N\} = [H]\{\varepsilon\} - \{N_t\} \qquad (8.1.14)$$

where

$$\{N\} = \{N_\phi, N_\theta, N_{\theta\phi}, M_\phi, M_\theta, M_{\phi\theta}, Q_\phi, Q_\theta\}$$

$$\{\varepsilon\} = \{\varepsilon_\phi, \varepsilon_\theta, \varepsilon_{\theta\phi}, \chi_\phi, \chi_\theta, \chi_{\phi\theta}, \gamma_\phi, \gamma_\theta\}$$

$[H]$ = the (8×8) elasticity matrix

and

$\{N_t\}$ = the initial stress-resultants and stress-couples due to thermal effects

$$= \{N_{t\phi}, N_{t\theta}, 0, M_{t\phi}, M_{t\theta}, 0, 0, 0\}$$

For an isotropic shell material (50),

$$N_{t\phi} = N_{t\theta} = \frac{E\alpha}{1-\nu} \int_{-h/2}^{h/2} T(\xi) d\xi$$

$$M_{t\phi} = M_{t\theta} = \frac{E\alpha}{1-\nu} \int_{-h/2}^{h/2} T(\xi) \xi d\xi \qquad (8.1.15)$$

where

α = the coefficient of thermal expansion

$T(\xi)$ = the temperature difference from the reference value for any point located at a distance ξ from the middle surface.

The constitutive relationships for the open type elements is presented in (35).

8.1.5 Element Load Vectors

The consistent load vector (35) for an element due to distributed loads, f_ϕ^j, f_θ^j, and f_ξ^j acting along the ϕ, θ, and ξ directions corresponding to harmonic j is expressed as

$$\{P_s^j\} = L\int_0^1 [G^m]^T[G^f]\{F_s^j\}Rds \tag{8.1.16}$$

where

$$[G^m] = [\tilde{n}_1, \tilde{n}_2, \tilde{n}_3, \tilde{n}_4, \ldots.]$$

$$\tilde{n}_i = [N_i, N_i, N_i, 0, 0]$$

$$[G^f] = [\bar{n}_1, \bar{n}_2]$$

$$\bar{n}_i = \Pi[\bar{N}_i, \bar{N}_i, \bar{N}_i, 0, 0]$$

$$\bar{N} = (1-s)$$

$$\bar{N}_2 = s$$

$$\{F_s^j\} = \{f_{\phi 1}^j, f_{\theta 1}^j, f_{\xi 1}^j, f_{\phi 2}^j, f_{\theta 2}^j, f_{\xi 2}^j\}$$

The consistent load vector due to the thermal effect is expressed as

$$\{P_T^j\} = \Pi L(\int_0^1 [G^j]^T[H^t][G^t]ds)\{T^j\} \tag{8.1.17}$$

where

$$\{T^j\} = \{T^j_{00}, T^j_{10}, T^j_{01}, T^j_{11}\}$$

$\underset{8\times 2}{[H^t]}$ = a matrix contains the material constants and the shell thickness

$\underset{2\times 4}{[G^t]}$ = a matrix of the shape functions

The details of H^t and G^t are given in Reference (41).

APPENDIX 8.2

Details Of Stiffness Matrix For An Isoparametric Solid Element

This appendix presents the details of the 24×24 stiffness matrix components of a quadratic isoparametric solid element for a general Fourier harmonic J. The shape function ϕ_i and first derivatives are given in Table 1 , which are chosen to represent the element geometry as well as the displacements within the element. From Equations (3-6) to (3-9), using the partitioned form of B, D and Φ matrices one can get

$$K_k = \iint \left[\begin{array}{c|c} \underset{16\times 16}{(b_{11}^T D_1 b_{11} + b_{21}^T D_2 B_{21})} & \underset{16\times 8}{(b_{11}^T D_1 b_{12} + b_{21}^T D_2 b_{22})} \\ \hline \underset{8\times 16}{(b_{11}^T D_1 b_{12} + b_{21}^T D_2 b_{22})^T} & \underset{8\times 8}{(b_{22}^T D_2 b_{22} + b_{12}^T D_1 b_{12})} \end{array} \right]_{24\times 24} \qquad (8\text{-}2\text{-}1)$$

= the stiffness matrix of the k<u>th</u> element.

and with Equation (2-11) we can write

$$
\begin{array}{llll}
b_{1n} = \dfrac{\partial g_n}{\partial r} , & b_{1m} = 0 & & \\
b_{2n} = b_{2s} = 0 & , b_{2\ell} = \dfrac{\partial g(\ell-8)}{\partial z} & & \\
b_{3n} = \dfrac{g_n}{r} & , b_{3\ell} = 0 & , b_{3s} = \dfrac{-jg(s-16)}{r} & \\
b_{4n} = \dfrac{\partial g_n}{\partial z} & , b_{4\ell} = \dfrac{\partial g(\ell-8)}{\partial r} & , b_{4s} = 0 & \\
b_{5n} = \dfrac{jg_n}{r} & , b_{5\ell} = 0 & , b_{5s} = r \dfrac{\partial}{\partial r} \left(\dfrac{g(s-16)}{r}\right) & \\
b_{6h} = 0 & , b_{6\ell} = \dfrac{j}{r} g(\ell-8) & , b_{6s} = \dfrac{\partial g(s-16)}{\partial z} &
\end{array}
\tag{8-2-2}
$$

where

$(n = 1,\ldots,8)$

$(m = 9,\ldots,24)$

$(\ell = 9,\ldots,16)$

$(s = 17,\ldots,24)$

Using the above values of the B matrix in Equation 8.2.1 yields,

$$
* \quad b_{11}^{T} D_1 b_{11} + b_{21}^{T} D_2 b_{21} = \left[\begin{array}{c|c} \bar{K}_{11} & \bar{K}_{12} \\ \hline \bar{K}_{12}^{T} & \bar{K}_{22} \end{array}\right]_{16\times16} \tag{8.2.3}
$$

where each of $\bar{K}_{11}$, $\bar{K}_{12}$ and $\bar{K}_{22}$ are submatrices of order 8×8.

$$
* \quad b_{21}^{T} D_2 b_{22} + b_{11}^{T} D_1 b_{12} = \left[\begin{array}{c} \bar{K}_{13} \\ \hline \bar{K}_{23} \end{array}\right]_{16\times8} \tag{8.2.4}
$$

$$* \quad (b_{21}^T \; D_2 \; b_{22} + b_{11}^T \; D_1 \; b_{12})^T = \underset{8\times 16}{\left[\bar{K}_{13}^T \; \vdots \; \bar{K}_{23}^T\right]} \tag{8-2-5}$$

$$* \quad b_{22}^T \; D_2 \; b_{22} + b_{12}^T \; D_1 \; b_{12} = \underset{8\times 8}{\left[\bar{K}_{33}\right]} \tag{8-2-6}$$

In Equations (8-2-3) to (8-2-6) the elements of the sub-matrices are defined as:

$$\begin{aligned}
\bar{K}_{11mn} &= (\lambda+2\mu)\,[g_{m,r}\; g_{n,r} + g_m\; g_n/r] \\
&\quad + \frac{\lambda}{r}(g_m\; g_{n,r} + g_n\; g_{m,r}) + \mu g_{m,z}\; g_{n,z} \\
&\quad + \mu\left(\frac{j}{r}\right)^2 g_m\; g_n \\
\bar{K}_{12mn} &= \lambda\,[g_{n,z}(g_{m,r} + g_m/r)] + \mu g_{m,z}\; g_{n,r} \\
\bar{K}_{13mn} &= j\mu g_m (g_n/r)_{,r} - \frac{j}{r}\, g_n\,[\lambda g_{m,r} + (\lambda+2\mu)\, g_m/r] \\
\bar{K}_{22mn} &= (\lambda+2\mu)\,[g_{m,z}\; g_{n,z}] + \mu\,[g_{m,r}\; g_{n,r}] + \mu\left(\frac{j}{r}\right)^2 g_m\; g_n \\
\bar{K}_{23mn} &= \mu\,\frac{j}{r}\, g_m\; g_{n,z} - \frac{j}{r}\,\lambda g_n\; g_{m,z} \\
\bar{K}_{33mn} &= (\lambda+2\mu)\left(\frac{j}{r}\right)^2 g_m\; g_n + \mu\left[r\left(\frac{g_m}{r}\right)_{,r}\; r\left(\frac{g_n}{r}\right)_{,r} + g_{m,z}\; g_{n,z}\right]
\end{aligned} \tag{8-2-7}$$

where $(m = 1,\ldots,8)$, and $(n = 1,\ldots,8)$

Now, the element stiffness element K_k can be written as:

$$K_k = \iint \left[\begin{array}{c|c|c} \bar{K}_{11} & \bar{K}_{12} & \bar{K}_{13} \\ \hline \bar{K}_{12}^T & \bar{K}_{22} & \bar{K}_{23} \\ \hline \bar{K}_{13}^T & \bar{K}_{23}^T & \bar{K}_{33} \end{array}\right] rdrdz \qquad (8\text{-}2\text{-}8)$$

and with the transformation of Equation (3-12) together with (3-17), the submatrices of Equation (8-2-7) can be expressed in terms of the natural coordinates ξ and η, as follows:

$$\begin{aligned} \bar{K}_{11mn} = {} & (\lambda+2\mu)(IJ_{11}\, g_{m,\xi} + IJ_{12}\, g_{m,\eta})(IJ_{11}\, g_{n,\xi} + IJ_{12}\, g_{n,\eta}) \\ & + \frac{\lambda}{RG}[g_m(IJ_{11}\, g_{n,\xi} + IJ_{12}\, g_{n,\eta}) + g_n(IJ_{11}\, g_{m,\xi} + IJ_{12}\, g_{m,\eta})] \\ & + \mu(IJ_{21}\, g_{m,\xi} + IJ_{22}\, g_{m,\eta})(IJ_{21}\, g_{n,\xi} + IJ_{22}\, g_{n,\eta}) \\ & + \left(\frac{j}{RG}\right)^2 \mu\, g_m\, g_n \end{aligned} \qquad (8\text{-}2\text{-}9)$$

$$\begin{aligned} \bar{K}_{12mn} = {} & \lambda(IJ_{21}\, g_{n,\xi} + IJ_{22}\, g_{n,\eta})(IJ_{11}\, g_{m,\xi} + IJ_{12}\, g_{m,\eta} + g_{m/RG}) \\ & + \mu(IJ_{21}\, g_{m,\xi} + IJ_{22}\, g_{m,\eta})(IJ_{11}\, g_{n,\xi} + IJ_{12}\, g_{n,\eta}) \end{aligned}$$

$$(8\text{-}2\text{-}10)$$

$$\bar{K}_{13mn} = \frac{\mu j}{RG} g_m (IJ_{11}\ g_{n,\xi} + IJ_{12}\ g_{n,\eta} - g_{n/RG}) - \frac{\lambda j}{RG} g_n \cdot$$

$$(IJ_{11}\ g_{m,\xi} + IJ_{12}\ g_{m,\eta}) - \frac{j(\lambda+2\mu)}{(RG)^2} g_m\ g_n \tag{8-2-11}$$

$$\bar{K}_{22mn} = (\lambda+2\mu)(IJ_{21}\ g_{m,\xi} + IJ_{22}\ g_{m,\eta})(IJ_{21}\ g_{n,\xi} + IJ_{22}\ g_{n,\eta})$$

$$+ \mu(IJ_{11}\ g_{m,\xi} + IJ_{12}\ g_{m,\eta})(IJ_{11}\ g_{n,\xi} + IJ_{12}\ g_{n,\eta})$$

$$+ (\frac{j}{RG})^2 \mu\ g_m\ g_n \tag{8-2-12}$$

$$\bar{K}_{23mn} = \frac{\mu j}{RG} g_m (IJ_{21}\ g_{n,\xi} + IJ_{22}\ g_{n,\eta}) - \frac{\lambda j}{RG} \cdot$$

$$g_n (IJ_{21}\ g_{m,\xi} + IJ_{22}\ g_{m,\eta}) \tag{8-2-13}$$

$$\bar{K}_{33mn} = (\frac{j}{RG})^2\ (\lambda+2\mu) g_m\ g_n + \mu[(IJ_{21}\ g_{m,\xi} + IJ_{22}\ g_{m,\eta}) \cdot$$

$$(IJ_{21}\ g_{n,\xi} + IJ_{22}\ g_{n,\eta}) + (IJ_{11}\ g_{m,\xi} + IJ_{12}\ g_{m,\eta}$$

$$- g_{m/RG})(IJ_{11}\ g_{n,\xi} + IJ_{12}\ g_{n,\eta} - g_n/RG)] \tag{8-2-14}$$

In the above equations IJ_{11}, IJ_{12}, IJ_{21} and IJ_{22} are defined by Equation (3-11), and;

$(m = 1,...,8)$

$(n = 1,...,8)$

The final stiffness matrix K_k is obtained by substituting Equations (8-2-9) to (8-2-14) in Equation (8-2-8), and with Equation (3-18), one can write

$$K_k = \int_{-1}^{1}\int_{-1}^{1} \left[\begin{array}{c|c|c} \bar{K}_{11_{mn}} & \bar{K}_{12_{mn}} & \bar{K}_{13_{mn}} \\ \hline \bar{K}^T_{12_{mn}} & \bar{K}_{23_{mn}} & \bar{K}_{23_{mn}} \\ \hline \bar{K}^T_{13_{mn}} & \bar{K}^T_{23_{mn}} & \bar{K}_{33_{mn}} \end{array}\right]_{24\times 24} RG\det.Jac\,d\xi d\eta \qquad (8\text{-}2\text{-}15)$$

$(m = 1,...,8)$ and $(n = 1,...,8)$

The integration in the above equation is carried out by means of four points Gaussian integration with the natural cooredinates ξ, η.

APPENDIX 8.3

Listing of SUBASE Program

```
C
C     *****************************************************************
C
C     SUBASE IS A SPICIAL PROGRAM TO BE USED IN SHELLS OF REVOLUTION-SOIL
C     SYSTEM MODEL UNDER DYNAMIC LOADS
C
C
C
C     PROGRAMMED BY OSAMA MOUSTAFA EL-SHAFEE  ...  FEB. 1978
C
C     *****************************************************************
C
C     MAIN PROGRAM  ( DATA AND DATA GENERATION )
C
C
C     INPUT DATA NOTATIONS
C
C
C     AO            DIMENSIONLESS FACTOR FOR THE INPUT FREQUENCY
C
C     NJF           TOTAL NUMBER OF FOURIER HARMONICS
C     NL            TOTAL NUMBER OF LAYERS
C     NCOL          NUMBER OF COLUMNS IN THE FINITE ELEMENT MESH
C     NOE           PRINT OUT PARAMETER   IF NOE = 0 NO INTERMIDIAT RESULTS
C                   TO BE PRINTED OUT
C
C     RCOL(I)       THE OUTER RADIUS OF THE I-TH. COLUMN
C
C     ALAMDA(I),AMUE(I),RUE(I)   ARE THE MATERIAL PROPERTIES OF ELEMENT I
C
C     ALA(I),AMU(I),RU(I)   ARE THE MATERIAL PROPERTIES OF LAYER I
C     H(I)          THE THICKNESS OF LAYER I
C
C     NOTE ...      IF TWO OR MORE ELEMENTS(LAYERS) WITH SUCCESSIVE NUMBERS
C                   HAVE THE SAME PROPERTIES , ONLY THOSE OF THE FIRST OF
C                   THEM NEED TO BE GIVEN , WITH THE LAST ELEMENT'S(LAYER'S)
C                   PROPERTIES MUST ALWAYS BEEN GIVEN.
C
C     DR(1),DR(2)   THE PERCENTAGE DAMPING RATIO OF THE FIRST TWO MODES
C
C
C
C     LIMITATIONS   *****
C
C                   MAXIMUM NUMBER OF ELEMENTS IS 20
C                   MAXIMUM NUMBER OF LAYERS IS 6
C                   MAXIMUM NUMBER OF COLUMNS IN THE F.E. MESH IS 4
C
C
C
C
      COMMON EM1(24,24),SM1(24,24),AA(9,9),AD(9,9),AE(9,9),AS(9,9),
     $       AAA(36,36),ADD(36,36),AEE(36,36),AGG(36,36),ASS(36,36),
     $       RSS(36,36),Y(36,36),Z(36,36),HO(36),H1(36),E(36),DD(36),
     $       RX(24,8),ZX(24,8),ALAMDA(24),AMUE(24),RUE(24),ALA(6),RU(6),
     $       RCOL(4),AMU(6),H(6),DR(2),SM(190,190),NO(80,3),N1(20,8),
     $       NV(12),NRS(36),MP(20,24)
      WRITE(6,1000)
      READ(5,25) AO
      READ(5,15) NJF,NL,NCOL,NOE
      IF ( NL . GT . 6. OR . NCOL . GT . 4) GO TO 200
      READ(5,25) (RCOL(I),I=1,NCOL)
C
C      NN=TOTAL NUMBER OF NODES  ,  NE=TOTAL NUMBER OF ELEMENTS  ,
C     NC1=FIRST COMMON NODE BETWEEN THE SOIL AND THE FOUNDATION
C     RO            THE VERTICAL BOUNDARY RADIUS
C
      NN = (3*NCOL + 2)*NL + 2*NCOL + 1
      NE = NCOL * NL
      IF ( NE . GT . 20) GO TO 200
      NC1= 2*NCOL - 1
      RO = RCOL(NCOL)
C
C     READ THE ELEMENTS AND THE LAYERS PROPERTIES
C
      J = 0
    4 READ(5,35) I,ALAMDA(I),AMUE(I),RUE(I)
      L = J
      J = J + 1
      K = I - 1
      IF(J . EQ . NE) GO TO 9
      IF(J . EQ . I)  GO TO 4
      DO 8  N = J,K
      ALAMDA(N) = ALAMDA(L)
      AMUE(N)   =   AMUE(L)
    8 RUE(N)    =    RUE(L)
      J = I
      IF(I . LT . NE) GO TO 4
C
    9 J = 0
   10 READ(5,35) I,ALA(I),AMU(I),RU(I),H(I)
      L = J
      J = J + 1
      K = I - 1
      IF(J . EQ . NL) GO TO 12
      IF(J . EQ . I)  GO TO 10
      DO 11 N = J,K
      ALA(N) = ALA(L)
      AMU(N) = AMU(L)
      RU(N)  =  RU(L)
   11 H(N)   =   H(L)
      J = I
      IF(I . LT . NL) GO TO 10
C
C     NO(I,J)       CODE NO. OF THE NODE I IN THE THREE DIRECTIONS  J
C                   J = 1      FOR U
C                       2      FOR W
C                       3      FOR V
C                   NO = 0         FREE
C                        1         FIXED
C
   12 DO 5 I = 1,NN
      DO 5 J = 1,3
    5 NO(I,J) = 0
C
C     OM            FRIQUANCY OF THE EXCITING MOTION
C
      U1U = 0.
      R1R = 0.
      DO 77 I = 1,NL
      U1U = U1U + AMU(I)
   77 R1R = R1R + RU(I)
      OM = AO * SQRT(U1U/R1R) / RO
      ZZX = 0.
C
C     N1(I,J)       NODE NUMBER OF ELEMENT  I  STARTING FROM THE UPPER
C                   LEFT CORNER IN CLOCKWISE DIRECTION
C
      DO 100 I = 1,NL
      NIN = (I-1)*(3*NCOL + 2)
      DO 90 J = 1,NCOL
      JJ = J - 1
      K = (I-1)*NCOL + J
      DO 80 L = 1,8
      LL = L - 1
      N1(K,L) = NIN + L
      IF(L . EQ . 4) N1(K,L) = N1(K,L) + 2*NCOL - J
      IF(L . EQ . 5) N1(K,L) = N1(K,L) + 3*NCOL
      IF(L . GT . 5) N1(K,L) = N1(K,LL) - 1
   80 IF(L . EQ . 8) N1(K,L) = N1(K,L) - (NCOL + J - 1)
      NIN = N1(K,2)
      IF(J . GT . 1) GO TO 85
      L1 = N1(K,1)
      L8 = N1(K,8)
      NO(L1,1) = 1
      NO(L1,3) = 1
      NO(L8,1) = 1
      NO(L8,3) = 1
C
C     RX(I,J),ZX(I,J) ARE THE RADIAL AND THE AXIAL COORDINATES OF NODE J
C                     IN ELEMENT I
C
      RX(K,1) = 0.
      RX(K,7) = 0.
      RX(K,8) = 0.
      RX(K,2) = RCOL(1) / 2.
      RX(K,6) = RCOL(1) / 2.
      GO TO 86
   85 RX(K,1) = RCOL(JJ)
      RX(K,7) = RCOL(JJ)
      RX(K,8) = RCOL(JJ)
      RX(K,2) = (RCOL(JJ) + RCOL(J)) / 2.
      RX(K,6) = RX(K,2)
   86 RX(K,3) = RCOL(J)
      RX(K,4) = RCOL(J)
      RX(K,5) = RCOL(J)
      ZX(K,1) = ZZX
      ZX(K,2) = ZZX
      ZX(K,3) = ZZX
      ZX(K,4) = ZZX + H(I) / 2.
      ZX(K,8) = ZZX + H(I) / 2.
      ZX(K,5) = ZZX + H(I)
      ZX(K,6) = ZZX + H(I)
   90 ZX(K,7) = ZZX + H(I)
  100 ZZX = ZX(K,7)
      READ(5,25) DR(1),DR(2)
C
C     NV(I)         THE I TH. V. BOUNDARY NODE NUMBER (I=1 AT G. LEVEL)
C
      DO 95 I = 1,NL
      K = I * NCOL
      DO 94 J = 1,2
      L = (I-1) * 2 + J
      M = J + 2
   94 NV(L) = N1(K,M)
   95 CONTINUE
      NO1 = NN - 2*NCOL
      DO 96 I = NO1,NN
      DO 96 J = 1,3
   96 NO(I,J) = 1
      NL2 = 2 * NL
C
C     PRINT OUT THE DATA AND THE GENERATED DATA
C
      WRITE(6,66) OM,AO
      WRITE(6,106)
      WRITE(6,107) NJF,NL,NCOL,NOE,NN,NE,NC1
      WRITE(6,108)(RCOL(I),I=1,NCOL)
      WRITE(6,109)
      WRITE(6,108)(ALA(I),RU(I),AMU(I),I=1,NL)
      WRITE(6,109)
      WRITE(6,108)(ALAMDA(I),RUE(I),AMUE(I),I=1,NE)
      WRITE(6,109)
      WRITE(6,108) DR(1),DR(2)
      WRITE(6,106)
      WRITE(6,107)((N1(I,J),J=1,8),I=1,NE)
      WRITE(6,109)
      WRITE(6,107)(NV(I),I=1,NL2)
      WRITE(6,109)
      WRITE(6,107)((NO(I,J),J=1,3),I=1,NN)
      WRITE(6,106)
      WRITE(6,108)((RX(I,J),ZX(I,J),J=1,8),I=1,NE)
C
C
      CALL CODE(NN,NE,NL,NB,NUM)
      CALL TOTAL(NUM,NC1,NE,NJF,NL,OM,RO,NOE)
C
  200 WRITE(6,666)
      STOP
C
C     FORMAT STATEMENT
C
   15 FORMAT(16I5)
   25 FORMAT(8F10.0)
   35 FORMAT(I5,4F10.0)
   66 FORMAT(1H1,2X,//////////30X,'OMIGA =',F12.6,10X,'AO =',F8.4///  )
  106 FORMAT(1H1,2X //  )
  107 FORMAT(/24I5)
  108 FORMAT(/8F15.6)
  109 FORMAT(////5X,'      '  )
  666 FORMAT(1H1,2X,/////////////////////////////46X,'***  STOP  ***'///////
     $/////////  )
 1000 FORMAT(1H1,2X,///////////////////////47X,'** SUBASE **'/48X,' -------
     $-'//35X,'EQV. BOUNDARY SYSTEM OF THE SUB-BASE'//31X,'FOR DYNAMIC A
     $NALYSIS OF SHELLS OF REVOLUTION'/////38X,'PROGRAMMED BY  OSAMA EL-
     $SHAFEE'//48X,'FEB.  1978' //     )
```

```
C
      END
      SUBROUTINE CODE(NN,NE,NL,NB,NUM)
C
C     ******************************************************************
C
C
C     THIS SUBROUTINE GENERATES THE CONTROLING INTEGERS FOR SUBROUTINE
C     TOTAL
C
C     NN           TOTAL NUMBER OF NODES
C     NE           TOTAL NUMBER OF ELEMENTS
C     NL           TOTAL NUMBER OF LAYERS
C
      COMMON EM1(24,24),SM1(24,24),AA(9,9),AD(9,9),AE(9,9),AS(9,9),
     $       AAA(36,36),ADD(36,36),AEE(36,36),AQQ(36,36),ASS(36,36),
     $       RSS(36,36),Y(36,36),Z(36,36),HO(36),H1(36),E(36),DD(36),
     $       RX(24,8),ZX(24,8),ALAMDA(24),AMUE(24),RUE(24),ALA(6),RU(6),
     $       RCOL(4),AMU(6),H(6),DR(2),SM(190,190),ND(80,3),NI(20,8),
     $       NV(12),NRS(36),MP(20,24)
C
      K = 1
      DO 8 I = 1,NN
      DO 8 J = 1,3
      IF(ND(I,J) . EQ . 0) GO TO 9
      ND(I,J) = 0
      GO TO 8
    9 ND(I,J) = K
      K = K + 1
    8 CONTINUE
C
C     CALCULATION OF BOUNDARY CODE NUMBERS
C
      NL2 = 2 * NL
      DO 18 J = 1,NL2
      J1 = (J - 1) * 3 + 1
      J2 = (J - 1) * 3 + 2
      J3 = (J - 1) * 3 + 3
      NRS(J1) = (NV(J) - J) * 3  +  (J - 2)
      NRS(J2) = NRS(J1) + 1
      NRS(J3) = NRS(J2) + 2
   18 CONTINUE
C
C     CALCULATION OF CODE NUMBERS
C
      NB = 0
      DO 13 N = 1,NE
      DO 10 I = 1,8
      J = I + 8
      K = I + 16
      L = NI(N,I)
      MP(N,I) = ND(L,1)
    . MP(N,J) = ND(L,2)
      MP(N,K) = ND(L,3)
   10 CONTINUE
C
C     CALCULATION OF BAND WIDTH
C
      MAX = 0
      MIN = 1000
      DO 11 I = 1,24
      IF(MP(N,I) . EQ . 0) GO TO 11
      IF(MP(N,I) . LE . MAX) GO TO 12
      MAX = MP(N,I)
   12 IF(MP(N,I) . GE . MIN) GO TO 11
      MIN = MP(N,I)
   11 CONTINUE
      NB1 = MAX -MIN
      IF(NB1 . GT . NB) NB = NB1
   13 CONTINUE
      NB = NB + 1
      NUM = MAX
      WRITE(6,16) NN,NE,NL,NB,NUM
C
      RETURN
C
   16 FORMAT(1H1,4X,'NO OF NODES IS',I4,3X,'NO OF ELEMENTS IS',I4,3X,
     $'NO OF LAYERS IS',I4//,5X,'HALF BAND WIDTH IS',I4,3X,'NO OF UNKNOW
     $NS IS',I4///    )
      END
      SUBROUTINE ELMNT(N,JA)
C
C
C     THIS SUBROUTINE GENERATES THE CONSISTANT MASS MATRIX AND THE ST9FF E
C     MATRIX FOR THE N-TH. ELEMENT    (4-POINTS GAUSS INTEGRATION)
C
C
C     N        ELEMENT  NUMBER
C     JA       HARMONIC NUMBER
C
C
      DIMENSION AIJ(4),DM(36),DS1(36),DS2(36),DS3(36),DS4(64),DS5(64),
     $       DS6(64),G(8),GX(8),GY(8)
      COMMON EM1(24,24),SM1(24,24),AA(9,9),AD(9,9),AE(9,9),AS(9,9),
     $       AAA(36,36),ADD(36,36),AEE(36,36),AQQ(36,36),ASS(36,36),
     $       RSS(36,36),Y(36,36),Z(36,36),HO(36),H1(36),E(36),DD(36),
     $       RX(24,8),ZX(24,8),ALAMDA(24),AMUE(24),RUE(24),ALA(6),RU(6),
     $       RCOL(4),AMU(6),H(6),DR(2),SM(190,190),ND(80,3),NI(20,8),
     $       NV(12),NRS(36),MP(20,24)
C
      AJ = JA
      P1 = ALAMDA(N)
      P2 = AMUE(N)
      P3 = P1 + 2.*P2
      DO 98 I = 1,36
      DM(I)  = 0.
      DS1(I) = 0.
      DS2(I) = 0.
   98 DS3(I) = 0.
      DO 99 I = 1,64
      DS4(I) = 0.
      DS5(I) = 0.
   99 DS6(I) = 0.
C
C     JACOBIAN
C
      DO 100 I = 1,4
      AM = 1.
      AN = 1.
      AJ1 = 0.
      AJ2 = 0.
      AJ3 = 0.
      AJ4 = 0.
      RG  = 0.
      IF ( I . EQ .2. OR . I . EQ .3) AM = -1.
      IF ( I . EQ .3. OR . I . EQ .4) AN = -1.
      AX = AM * 0.57735027
      AY = AN * 0.57735027
C
      G(1)  =-.2500*(1.00-AX)*(1.00-AY)*(1.00+AX+AY)
      GX(1) = .2500*(1.00-AY)*(2.00*AX+AY)
      GY(1) = .2500*(1.00-AX)*(2.00*AY+AX)
C
      G(2)  = .5000*(1.00-AX*AX)*(1.00-AY)
      GX(2) =-AX*(1.00-AY)
      GY(2) =-.5000*(1.00-AX*AX)
C
      G(3)  = .2500*(1.00+AX)*(1.00-AY)*(AX-AY-1.00)
      GX(3) = .2500*(1.00-AY)*(2.00*AX-AY)
      GY(3) = .2500*(1.00+AX)*(2.00*AY-AX)
C
      G(4)  = .5000*(1.00+AX)*(1.00-AY*AY)
      GX(4) = .5000*(1.00-AY*AY)
      GY(4) =-AY*(1.00+AX)
C
      G(5)  = .2500*(1.00+AX)*(1.00+AY)*(AX+AY-1.00)
      GX(5) = .2500*(1.00+AY)*(2.00*AX+AY)
      GY(5) = .2500*(1.00+AX)*(2.00*AY+AX)
C
      G(6)  = .5000*(1.00-AX*AX)*(1.00+AY)
      GX(6) =-AX*(1.00+AY)
      GY(6) = .5000*(1.00-AX*AX)
C
      G(7)  = .2500*(1.00-AX)*(1.00+AY)*(AY-AX-1.00)
      GX(7) = .2500*(1.00+AY)*(2.00*AX-AY)
      GY(7) = .2500*(1.00-AX)*(2.00*AY-AX)
C
      G(8)  = .5000*(1.00-AX)*(1.00-AY*AY)
      GX(8) =-.5000*(1.00-AY*AY)
      GY(8) = -AY*(1.00-AX)
C
      DO 101 J = 1,8
      AJ1 = AJ1 + GX(J) * RX(N,J)
      AJ2 = AJ2 + GX(J) * ZX(N,J)
      AJ3 = AJ3 + GY(J) * RX(N,J)
      AJ4 = AJ4 + GY(J) * ZX(N,J)
      RG = RG + G(J)  *  RX(N,J)
  101 CONTINUE
      DETJAC = AJ1 * AJ4 -AJ2 * AJ3
      GSTF   = RG * DETJAC
      GMAS   = RUE(N) * GSTF
      AIJ(1) = AJ4 / DETJAC
      AIJ(2) =-AJ2 / DETJAC
      AIJ(3) =-AJ3 / DETJAC
      AIJ(4) = AJ1 / DETJAC
C
C     ARRAY  DM(JJ) IS TO BE USED IN STORING THE 36 INDEPENDENT ELEMESTO
C     OF THE MASS MATRIX
C     ARRAY DS1(JJ) TO ARRAY DS6(KK) ARE TO BE USED IN STORING THE 300
C     INDEPENDENT ELEMENTS OF THE STIFFNESS MATRIX
C
      JJ = 0
      KK = 0
      DO 102 J = 1,8
      JD = JJ
      DO 103 K = J,8
      JJ = JD + K -(J-1)
C
      DM(JJ) = DM(JJ) + GMAS*G(J)*G(K)
C
      DS1(JJ)=DS1(JJ) + GSTF*(P3*(AIJ(1)*GX(J) + AIJ(2)*GY(J))*(AIJ(1)*
     $        GX(K) + AIJ(2)*GY(K)) + (P1/RG)*(G(J)*(AIJ(1)*GX(K) +
     $        AIJ(2)*GY(K)) + G(K)*(AIJ(1)*GX(J) +AIJ(2)*GY(J))) + P2*
     $        (AIJ(3)*GX(J) + AIJ(4)*GY(J))*(AIJ(3)*GX(K) + AIJ(4)*GY(K)
     $        ) + (AJ/RG)**2*P2*G(J)*G(K))
C
      DS2(JJ)=DS2(JJ) + GSTF*(P3*(AIJ(3)*GX(J) + AIJ(4)*GY(J))*(AIJ(3)*
     $        GX(K) + AIJ(4)*GY(K)) + P2*(AIJ(1)*GX(J) + AIJ(2)*GY(J))*(
     $        AIJ(1)*GX(K) + AIJ(2)*GY(K)) + (AJ/RG)**2*P2*G(J)*G(K))
C
      DS3(JJ)=DS3(JJ) + GSTF*((AJ/RG)**2*G(J)*G(K)*P3 + P2*((AIJ(3)*GX(J
     $        ) + AIJ(4)*GY(J))*(AIJ(3)*GX(K) + AIJ(4)*GY(K)) + (AIJ(1)*
     $        GX(J) + AIJ(2)*GY(J) - G(J)/RG)*(AIJ(1)*GX(K) + AIJ(2)*
     $        GY(K) - G(K)/RG)))
  103 CONTINUE
C
      KD = KK
      DO 104 K = 1,8
      KK = KD + K
C
      DS4(KK)=DS4(KK) + GSTF*(P1*(AIJ(3)*GX(K) + AIJ(4)*GY(K))*(AIJ(1)*
     $        GX(J) + AIJ(2)*GY(J) + G(J)/RG) + P2*(AIJ(3)*GX(J) +AIJ(4)
     $        *GY(J))*(AIJ(1)*GX(K) + AIJ(2)*GY(K)))
C
      IF ( AJ . EQ . 0. ) GO TO 105
      DS5(KK)=DS5(KK) + GSTF*((AJ*P2/RG)*(G(J)*(AIJ(3)*GX(K) + AIJ(4)*
     $        GY(K))) - (AJ*P1/RG)*G(K)*(AIJ(3)*GX(J) + AIJ(4)*GY(J)))
C
      DS6(KK)=DS6(KK) + GSTF*((AJ*P2/RG)*G(J)*(AIJ(1)*GX(K) + AIJ(2)*
     $        GY(K) - G(K)/RG) - (AJ*P1/RG)*G(K)*(AIJ(1)*GX(J) + AIJ(2)
     $        *GY(J)) - (AJ*P3/RG**2)*G(J)*G(K))
      GO TO 104
  105 DS5(KK) = 0.
      DS6(KK) = 0.
  104 CONTINUE
  102 CONTINUE
  100 CONTINUE
      DO 18 I = 1,24
      DO 18 J = 1,24
      EM1(I,J) = 0.
   18 SM1(I,J) = 0.
      K = 0
      DO 19 I = 1,8
      KD = K
      DO 19 J = 1,8
      K = KD + J - (I-1)
```

```
      EM1(I,J) = DM(K)
      EM1(I+8,J+8) = DM(K)
      EM1(I+16,J+16) = DM(K)
      SM1(I,J) = DS1(K)
      SM1(I+8,J+8) = DS2(K)
      SM1(I+16,J+16) = DS3(K)
   19 CONTINUE
      K = 0
      DO 20 I = 1,8
      KD = K
      DO 20 J = 1,8
      K = KD + J
      SM1(I,J+8) = DS4(K)
      SM1(I+8,J+16) = DS5(K)
      SM1(I,J+16) = DS6(K)
   20 CONTINUE
      DO 21 I = 2,24
      DO 21 J = 1,I
      IF(J . EQ . I) GO TO 21
      EM1(I,J) = EM1(J,I)
      SM1(I,J) = SM1(J,I)
   21 CONTINUE
      RETURN
C
      END
      SUBROUTINE FACTOR(A,W,IPIVOT,S,N,IFLAG)
C
      DIMENSION A(N,N),W(N,N),IPIVOT(N),S(N)
      IFLAG = 1
C     INITIALIZE W,IPIVOT,S
      DO 10 I = 1,N
      IPIVOT(I) = I
      ROWMAX = 0.
      DO 9 J = 1,N
      W(I,J) = A(I,J)
    9 ROWMAX= AMAX1(ROWMAX,ABS(W(I,J)))
      IF(ROWMAX.EQ.0.) GO TO 999
   10 S(I) = ROWMAX
C     GAUSS ELIMINATION WITH SCALED PARTIAL PIVOTING.
      NM1 = N - 1
      IF(NM1 . EQ . 0) RETURN
      DO 20 K = 1,NM1
      J = K
      KP1 = K + 1
      IP = IPIVOT(K)
      COLMAX = ABS(W(IP,K))/S(IP)
      DO 11 I = KP1,N
      IP = IPIVOT(I)
      AWIKOV = ABS(W(IP,K))/S(IP)
      IF(AWIKOV . LE . COLMAX) GO TO 11
      COLMAX = AWIKOV
      J = I
   11 CONTINUE
      IF(COLMAX.EQ.0.) GO TO 999
C
      IPK = IPIVOT(J)
      IPIVOT(J) = IPIVOT(K)
      IPIVOT(K) = IPK
      DO 20 I = KP1,N
      IP = IPIVOT(I)
      W(IP,K) = W(IP,K)/W(IPK,K)
      RATIO = -W(IP,K)
      DO 20 J = KP1,N
   20 W(IP,J) = RATIO*W(IPK,J) + W(IP,J)
      IF(W(IP,N) . EQ . 0.) GO TO 999
      RETURN
  999 IFLAG = 2
      RETURN
      END
      SUBROUTINE FAR(JF,NL,OM,RO,NOE)
C
C
C     THIS SUBROUTINE GENERATES THE FAR FIELD EFFECT ON THE  FE  RIGION
C
      COMMON EM1(24,24),SM1(24,24),AA(9,9),AD(9,9),AE(9,9),AS(9,9),
     $       AAA(36,36),ADD(36,36),AEE(36,36),AQQ(36,36),ASS(36,36),
     $       RSS(36,36),Y(36,36),Z(36,36),HO(36),H1(36),E(36),DD(36),
     $       RX(24,8),ZX(24,8),ALAMDA(24),AMUE(24),RUE(24),ALA(6),RU(6),
     $       RCOL(4),AMU(6),H(6),DR(2),SM(190,190),ND(80,3),NI(20,8),
     $       NV(12),NRS(36),MP(20,24)
C
      NT = NL * 6
      DO 2 I = 1,NT
      DO 2 J = 1,NT
      AAA(I,J) = 0.
      ADD(I,J) = 0.
      AEE(I,J) = 0.
    2 ASS(I,J) = 0.
      DO 1 N = 1,NL
      CALL LYR(JF,N,OM,RO)
      NM1 = N - 1
      DO 3 K = 1,9
      IF(N . EQ . NL . AND . K . EQ . 7) GO TO 4
      I = NM1 * 6 + K
      DO 3 L = 1,9
      IF(N . EQ . NL . AND . L . GE . 7) GO TO 3
      J = NM1 * 6 + L
      AAA(I,J) = AAA(I,J) + AA(K,L)
      ADD(I,J) = ADD(I,J) + AD(K,L)
      AEE(I,J) = AEE(I,J) + AE(K,L)
      ASS(I,J) = ASS(I,J) + AS(K,L)
    3 CONTINUE
    1 CONTINUE
    4 DO 5 I = 2,NT
      II = I - 1
      DO 5 J = 1,II
      AAA(I,J) = AAA(J,I)
    5 ASS(I,J) = ASS(J,I)
      DO 22 I = 1,NT
      DO 22 J = 1,NT
   22 AQQ(I,J) = AAA(I,J)
      CALL INV(NT)
      DO 6 I = 1,NT
      DO 6 J = 1,NT
      Y(I,J) = 0.
      DO 7 K = 1,NT
    7 Y(I,J) = Y(I,J) + AAA(I,K) * ASS(K,J)
    6 CONTINUE
```

```
      CALL TRED2(36,NT,Y,DD,E,Z)
      CALL TQL2(36,NT,DD,E,Z,IERR)
      IF (IERR .NE. 0) GO TO 99
      DO 9 I = 1,NT
      DO 9 J = 1,NT
      AAA(I,J) = 0.
      ASS(I,J) = 0.
    9   Y(I,J) = 0.
C
      CALL HNKL(NT,RO)
      IF (JF . EQ . 1) GO TO 13
      DO 12 K = 1,NT
      IZ = 2
      DO 11 I = 1,NT
      IF ( I . NE . IZ) GO TO 10
      IZ = IZ + 3
      ASS(I,K) = Z(I,K) * H1(K)
        Y(I,K) = Z(I,K) * HO(K)
      GO TO 11
   10 ASS(I,K) = Z(I,K) * HO(K)
        Y(I,K) = Z(I,K) * H1(K)
   11 CONTINUE
   12 CONTINUE
      GO TO 17
   13 DO 16 K = 1,NT
      IZ = 2
      DO 15 I = 1,NT
      IF ( I . NE . IZ) GO TO 14
      IZ = IZ + 3
      ASS(I,K) = Z(I,K) * HO(K)
        Y(I,K) = Z(I,K) * H1(K)
      GO TO 15
   14 ASS(I,K) = Z(I,K) * H1(K)
        Y(I,K) = Z(I,K) * HO(K)
   15 CONTINUE
   16 CONTINUE
C
   17 IF (NOE . EQ . 0) GO TO 18
      DO 8 I = 1,NT
      WRITE(6,56)I,DD(I),HO(I),H1(I)
      WRITE(6,46)(Z(I,J),ASS(I,J),Y(I,J),J=1,NT)
    8 CONTINUE
C
   18 UJ = JF
      NU = NT/3
      DO 21 K = 1,NT
      X =  ABS(DD(K))
      S =  SQRT(X)
      KU = 0
      U1 = -S * H1(K)
      U2 =  S * HO(K)
      U3 =   H1(K) / RO
      DO 21 KK = 1,NU
      DO 20 IU = 1,3
      I = KU + IU
      IF (JF . EQ . 1) GO TO 19
      IF (IU . NE . 2) AAA(I,K) = U1 * Z(I,K)
      IF (IU . EQ . 2) AAA(I,K) = U2 * Z(I,K)
      GO TO 20
   19 IF (IU . EQ . 1) AAA(I,K) = U2 * Z(I,K) + U3 * Z(I+2,K)
      IF (IU . EQ . 2) AAA(I,K) =-U1 * Z(I,K)
      IF (IU . EQ . 3) AAA(I,K) = U3 * Z(I-2,K) + U2 * Z(I,K)
   20 CONTINUE
      KU = KU + 3
   21 CONTINUE
      CALL INV(NT)
C
      DO 23 I = 1,NT
      DO 23 J = 1,NT
      Z(I,J) = 0.
      DO 23 K = 1,NT
   23 Z(I,J) = Z(I,J) + AQQ(I,K) * ASS(K,J)
C
      DO 24 J = 1,NT
      DO 24 I = 1,NT
   24 Z(I,J) = Z(I,J) * DD(J) * RO
C
      DO 25 I = 1,NT
      DO 25 J = 1,NT
   25 RSS(I,J) = Z(I,J)
C
      DO 26 I = 1,NT
      DO 26 J = 1,NT
      Z(I,J) = 0.
      DO 26 K = 1,NT
   26 Z(I,J) = Z(I,J) + ADD(I,K) * Y(K,J)
C
      DO 27 J = 1,NT
      DO 27 I = 1,NT
   27 Z(I,J) = Z(I,J) *  SQRT( ABS(DD(J))) * RO
C
      DO 28 I = 1,NT
      DO 28 J = 1,NT
   28 RSS(I,J) = RSS(I,J) + Z(I,J)
C
      DO 29 I = 1,NT
      DO 29 J = 1,NT
      Z(I,J) = 0.
      DO 29 K = 1,NT
   29 Z(I,J) = Z(I,J) + AEE(I,K) * ASS(K,J) * RO
C
      DO 30 I = 1,NT
      DO 30 J = 1,NT
   30 RSS(I,J) = RSS(I,J) + Z(I,J)
C
      DO 31 I = 1,NT
      DO 31 J = 1,NT
   31 Z(I,J) = RSS(I,J)
C
      DO 32 I = 1,NT
      DO 32 J = 1,NT
      RSS(I,J) = 0.
      DO 32 K = 1,NT
   32 RSS(I,J) = RSS(I,J) + Z(I,J) * AAA(K,J)
      DO 33 I = 2,NT
      K = I - 1
      DO 33 J = 1,K
   33 RSS(I,J) = RSS(J,I)
```

```
      IF (NOE . EQ . 0) GO TO 100
C
      WRITE(6,96)
      WRITE(6,66)((RSS(I,J),J=1,NT),I=1,NT)
C
      GO TO 100
   99 WRITE(6,76)
  100 RETURN
C
   46 FORMAT(/21X,3E15.7)
   56 FORMAT(1H1,5X,'MODE NO.',I5,5X,'EIGENVALUE =',E15.7,5X,'HO=',E15.7
     $,5X,'H1=',E15.7///24X,'EIGENVECTOR',8X,'XA',13X,'XB'/// )
   66 FORMAT(/4X,6E15.7)
   76 FORMAT(1H1,5X,'IERR IS GT ZERO    ...    STOP')
   96 FORMAT(1H1,5X,'BOUNDARY STIFFNESS MATRIX'////  )
C
      END
      SUBROUTINE FCT(N,AN)
C
C
C     THIS SUBROUTINE CALCULATES THE FACTORIAL OF AN INTEGER  N
C
      NN = 1
      IF ( N . LE . 1) GO TO 2
      DO 1 I = 2,N
    1 NN = NN * I
    2 AN = NN
      RETURN
      END
      SUBROUTINE HNKL(NT,RO)
C
C
C     THIS SUBROUTINE CALCULATES HANKEL FUNCTIONS FOR THE WAVE NUMBSR
C
C     NT        TOTAL NO. OF THE WAVE NUMBERS
C     RO        RADIUS OF THE VERTICAL BOUNDARIES
C
      COMMON EM1(24,24),SM1(24,24),AA(9,9),AD(9,9),AE(9,9),AS(9,9),
     $       AAA(36,36),ADD(36,36),AEE(36,36),AQQ(36,36),ASS(36,36),
     $       RSS(36,36),Y(36,36),Z(36,36),HO(36),H1(36),E(36),DD(36),
     $       RX(24,8),ZX(24,8),ALAMDA(24),AMUE(24),RUE(24),ALA(6),RU(6),
     $       RCOL(4),AMU(6),H(6),DR(2),SM(190,190),ND(80,3),NI(20,8),
     $       NV(12),NRS(36),MP(20,24)
C
      DO 100 JA = 1,2
      J = JA - 1
      DO 90 I = 1,NT
      X = ABS(DD(I))
      S = SQRT(X) * RO
      P = 1.
      Q = 0.
      IF (J . EQ . 1) GO TO 50
      DO 40 KK = 2,8,2
      K = KK - 1
      KP= 2*KK - 1
      KQ= 2*K  - 1
      L = KK/2
      SN= (-1.)**L
      FP= 1.
      DO 10 N = 1,KP,2
      AN = N
   10 FP = FP * AN*AN
      FQ = 1.
      IF (KQ . EQ . 1) GO TO 30
      DO 20 N = 1,KQ,2
      AN = N
   20 FQ = FQ * AN*AN
   30 CALL FCT(KK,AP)
      CALL FCT(K,AQ)
      P = P + SN * FP / (AP * (8.00*S)**KK)
      Q = Q + SN * FQ / (AQ * (8.00*S)**K)
   40 CONTINUE
      BJ    =   SQRT(2.00/(S*3.141592654)) * (P*COS(S-.7853981634)
     $                                       -Q*SIN(S-.7853981634))
      BY    =   SQRT(2.00/(S*3.141592654)) * (P*SIN(S-.7853981634)
     $                                       +Q*COS(S-.7853981634))
      HO(I) = SQRT(BJ**2 + BY**2)
      IF (BJ . LT . 0.) HO(I) = -HO(I)
      GO TO 90
   50 DO 80 KK = 2,8,2
      L = KK/2 - 1
      SN= (-1.)**L
      K = KK - 1
      KP= 2*KK + 1
      KQ= 2*KK - 1
      FP= 1.
      M = KP - 2
      DO 60 N = 1,KP,2
      AN = N
      IF (N . LT . M) FP = FP * AN*AN
      IF (N . GE . M) FP = FP * AN
   60 CONTINUE
      FQ = 1.
      M = KQ - 2
      DO 70 N = 1,KQ,2
      AN = N
      IF (N . LT . M) FQ = FQ * AN*AN
      IF (N . GE . M) FQ = FQ * AN
   70 CONTINUE
      CALL FCT(KK,AP)
      CALL FCT(K,AQ)
      P = P + SN * FP / (AP * (8.*S)**KK)
      Q = Q + SN * FQ / (AQ * (8.*S)**K)
   80 CONTINUE
      BJ    =   SQRT(2.00/(S*3.141592654)) * (P*COS(S-2.356194490)
     $                                       -Q*SIN(S-2.356194490))
      BY    =   SQRT(2.00/(S*3.141592654)) * (P*SIN(S-2.356194490)
     $                                       +Q*COS(S-2.356194490))
      H1(I) = SQRT(BJ**2 + BY**2)
      IF (BJ . LT . 0.) H1(I) = -H1(I)
   90 CONTINUE
C
  100 CONTINUE
C
      RETURN
      END
      SUBROUTINE INV(N)
C
C
C     THIS SUBROUTINE CALCULATES THE INVERSE OF A GIVEN MATRIO
C
C
C     N               THE ORDER OF THE MATRIX TO BE INVERTED
C
      DIMENSION A(1296), AINV(1296), B(36), IPIVOT(36)
      COMMON EM1(24,24),SM1(24,24),AA(9,9),AD(9,9),AE(9,9),AS(9,9),
     $       AAA(36,36),ADD(36,36),AEE(36,36),AQQ(36,36),ASS(36,36),
     $       RSS(36,36),Y(36,36),Z(36,36),HO(36),H1(36),E(36),DD(36),
     $       RX(24,8),ZX(24,8),ALAMDA(24),AMUE(24),RUE(24),ALA(6),RU(6),
     $       RCOL(4),AMU(6),H(6),DR(2),SM(190,190),ND(80,3),NI(20,8),
     $       NV(12),NRS(36),MP(20,24)
C
      NSQ = N * N
      DO 10 J = 1,N
      DO 10 I = 1,N
      K = N * (J-1) + I
   10 A(K) = AAA(I,J)
      CALL FACTOR(A,A,IPIVOT,B,N,IFLAG)
      GO TO (20,11),IFLAG
   11 WRITE(6,611)
      GO TO 1
   20 DO 21 I = 1,N
   21 B(I) = 0.
      IBEG = 1
      DO 30 J = 1,N
      B(J) = 1.
      CALL SUBST(A,B,AINV(IBEG),IPIVOT,N)
      B(J) = 0.
   30 IBEG = IBEG + N
      DO 40 J = 1,N
      DO 40 I = 1,N
      K = N * (J-1) + I
   40 AAA(I,J) = AINV(K)
    1 RETURN
C
  611 FORMAT(1H1,5X,'MATRIX IS SINGULAR')
      END
      SUBROUTINE INVS(N)
C
      DIMENSION KP(165),KR(165),KC(165)
      COMMON EM1(24,24),SM1(24,24),AA(9,9),AD(9,9),AE(9,9),AS(9,9),
     $       AAA(36,36),ADD(36,36),AEE(36,36),AQQ(36,36),ASS(36,36),
     $       RSS(36,36),Y(36,36),Z(36,36),HO(36),H1(36),E(36),DD(36),
     $       RX(24,8),ZX(24,8),ALAMDA(24),AMUE(24),RUE(24),ALA(6),RU(6),
     $       RCOL(4),AMU(6),H(6),DR(2),SM(190,190),ND(80,3),NI(20,8),
     $       NV(12),NRS(36),MP(20,24)
C
      DO 5 I = 1,N
    5 KP(I) = 0
      DO 45 I = 1,N
      T = 0.
      DO 20 J = 1,N
      IF (KP(J) . EQ . 1) GO TO 20
      DO 15 K = 1,N
      IF (KP(K) - 1) 10,15,60
   10 IF (T . GE . ABS(SM(J,K))) GO TO 15
      IR = J
      IC = K
      T  = ABS(SM(J,K))
   15 CONTINUE
   20 CONTINUE
      KP(IC) = KP(IC) + 1
      IF (IR . EQ . IC) GO TO 30
      DO 25 L = 1,N
      T = SM(IR,L)
      SM(IR,L) = SM(IC,L)
   25 SM(IC,L) = T
   30 KR(I) = IR
      KC(I) = IC
      T = SM(IC,IC)
      SM(IC,IC) = 1.
      DO 35 L = 1,N
   35 SM(IC,L) = SM(IC,L) / T
      DO 45 M = 1,N
      IF (M . EQ . IC) GO TO 45
      T = SM(M,IC)
      SM(M,IC) = 0.
      DO 40 L = 1,N
   40 SM(M,L) = SM(M,L) - SM(IC,L) * T
   45 CONTINUE
      DO 55 I = 1,N
      J = N - I + 1
      IF (KR(J) . EQ . KC(J)) GO TO 55
      K = KR(J)
      L = KC(J)
      DO 50 M = 1,N
      T = SM(M,K)
      SM(M,K) = SM(M,L)
   50 SM(M,L) = T
   55 CONTINUE
   60 RETURN
      END
      SUBROUTINE LYR(JF,N,OM,R)
C
C
C     THIS SUBROUTINE GENERATES THE LAYERS MATRICES
C
C     JF        HARMONIC NUMBER
C     N         LAYER NUMBER
C     OM        FRIQUANCY OF THE EXCITING MOTION
C     R         F.E. RIGION RADIUS
C
      COMMON EM1(24,24),SM1(24,24),AA(9,9),AD(9,9),AE(9,9),AS(9,9),
     $       AAA(36,36),ADD(36,36),AEE(36,36),AQQ(36,36),ASS(36,36),
     $       RSS(36,36),Y(36,36),Z(36,36),HO(36),H1(36),E(36),DD(36),
     $       RX(24,8),ZX(24,8),ALAMDA(24),AMUE(24),RUE(24),ALA(6),RU(6),
     $       RCOL(4),AMU(6),H(6),DR(2),SM(190,190),ND(80,3),NI(20,8),
     $       NV(12),NRS(36),MP(20,24)
C
      XA = AMU(N)
      XB = H(N)
      XC = (ALA(N) + 2.00*AMU(N))
      XD = (ALA(N) + AMU(N))
      XE = (ALA(N) - AMU(N))
      XF = RU(N) * OM * OM
      XG = AMU(N) * H(N) / R
```

```
      XH = ALA(N)
      XJ = JF
      XI = H(N) * (XJ + 1.00) / R
      XK = XJ * XA / R
      DO 1 I = 1,9
      DO 1 J = 1,9
      AA(I,J) = 0.
      AD(I,J) = 0.
      AE(I,J) = 0.
    1 AS(I,J) = 0.
      DO 2 I = 1,3
      J = I + 3
      K = I + 6
      IF(I . EQ . 2) GO TO 3
      AS(I,I) = ( 0.400*XA*XB*XF - 7.000*XA) / (3.00*XB)
      AS(I,J) = ( 0.200*XB*XB*XF + 8.000*XA) / (3.00*XB)
      AS(I,K) = (-0.100*XB*XA*XF       -XA) / (3.00*XB)
      AS(J,J) = ( 1.600*XB*XB*XF -16.000*XA) / (3.00*XB)
      GO TO 4
    3 AS(I,I) = ( 0.400*XA*XB*XF - 7.000*XC) / (3.00*XB)
      AS(I,J) = ( 0.200*XB*XB*XF + 8.000*XC) / (3.00*XB)
      AS(I,K) = (-0.100*XB*XB*XF       -XC) / (3.00*XB)
      AS(J,J) = ( 1.600*XB*XB*XF -16.000*XC) / (3.00*XB)
    4 AS(J,K) = AS(I,J)
      AS(K,K) = AS(I,I)
C
      IF(I . EQ . 1) GO TO 5
      AA(I,I) =  4.00*XA*XB/30.00
      AA(I,J) =  2.00*XA*XB/30.
      AA(I,K) =     -XA*XB/30.
      AA(J,J) = 16.00*XA*XB/30.
      GO TO 6
    5 AA(I,I) =  4.00*XC*XB/30.
      AA(I,J) =  2.00*XC*XB/30.
      AA(I,K) =     -XC*XB/30.
      AA(J,J) = 16.00*XC*XB/30.
    6 AA(J,K) = AA(I,J)
      AA(K,K) = AA(I,I)
C
    2 CONTINUE
C
      AA(1,2) = XB*XE/2.
      AA(1,5) = -2.00*XB*XD/3.
      AA(1,8) = XB*XD/6.
      AA(2,4) = -AA(1,5)
      AA(2,7) = -AA(1,8)
      AA(4,8) = AA(1,5)
      AA(5,7) = AA(2,4)
      AA(7,8) = -AA(1,2)
C
      DO 7 I = 2,9
      K = I - 1
      DO 7 J = 1,K
      AS(I,J) = AS(J,I)
    7 AA(I,J) = AA(J,I)
C
      AD(1,1) = -XG / 3.75
      AD(1,3) = -XJ * AD(1,1)
      AD(2,2) = AD(1,3) / 2.
      AD(3,3) = AD(1,1)
      AD(3,1) = AD(1,3)
C
      AE(1,1) = XK *XI / 3.75
      AE(1,3) = -AE(1,1)
      AE(3,1) = AE(1,3)
      AE(3,3) = AE(1,1)
C
      DO 8 I1 = 1,3
      DO 8 J1 = 1,3
      I2 = I1 + 3
      I3 = I1 + 6
      J2 = J1 + 3
      J3 = J1 + 6
      AD(I1,J2) = AD(I1,J1) / 2.
      AE(I1,J2) = AE(I1,J1) / 2.
      AD(I1,J3) =-AD(I1,J1) / 4.
      AE(I1,J3) =-AE(I1,J1) / 4.
      AD(I2,J2) = 4. * AD(I1,J1)
      AE(I2,J2) = 4. * AE(I1,J1)
      AD(I2,J3) = AD(I1,J2)
      AE(I2,J3) = AE(I1,J2)
      AD(I3,J3) = AD(I1,J1)
      AE(I3,J3) = AE(I1,J1)
      AD(I2,J1) = AD(I1,J2)
      AE(I2,J1) = AE(I1,J2)
      AD(I3,J2) = AD(I1,J2)
      AE(I3,J2) = AE(I1,J2)
      AD(I3,J1) = AD(I1,J3)
    8 AE(I3,J1) = AE(I1,J3)
C
      DO 9 I = 1,3
      DO 9 J = 1,3
      I1 = (I-1) * 3 + 1
      I2 = (I-1) * 3 + 2
      J1 = (J-1) * 3 + 1
      J2 = (J-1) * 3 + 2
      J3 = (J-1) * 3 + 3
C
      IF (I . EQ . 1. AND . J . EQ.1) FC = 1.
      IF (I . EQ . 1. AND . J . EQ.2) FC = -4.00 / 3.
      IF (I . EQ . 1. AND . J . EQ.3) FC =  1.00 / 3.
      IF (I . EQ . 2. AND . J . EQ. 1) FC = 4.00 / 3.
      IF (I . EQ . 2. AND . J . EQ.2) FC =  0.
      IF (I . EQ . 2. AND . J . EQ.3) FC = -4.00 / 3.
      IF (I . EQ . 3. AND . J . EQ.1) FC =  1.00 / 3.
      IF (I . EQ . 3. AND . J . EQ.2) FC =  4.00 / 3.
      IF (I . EQ . 3. AND . J . EQ.3) FC = -1.
C
      AD(I1,J2) = FC * XH / 2.
      AD(I2,J1) =-FC * XA / 2.
      AE(I2,J1) =-FC * XK / 2.
      AE(I2,J3) =-AE(I2,J1)
    9 CONTINUE
C
      RETURN
      END
      SUBROUTINE SUBST(W,B,X,IPIVOT,N)
C
      DIMENSION W(N,N),B(N),X(N),IPIVOT(N)
      IF(N . GT . 1) GO TO 10
      X(1) = B(1) / W(1,1)
      RETURN
   10 IP = IPIVOT(1)
      X(1) = B(IP)
      DO 15 K = 2,N
      IP = IPIVOT(K)
      KM1 = K - 1
      SUM = 0.
      DO 14 J = 1,KM1
   14 SUM = W(IP,J) * X(J)  +  SUM
   15 X(K) = B(IP)  -  SUM
C
      X(N) = X(N) / W(IP,N)
      K = N
      DO 20 NPINK = 2,N
      KP1 = K
      K = K - 1
      IP = IPIVOT(K)
      SUM = 0.
      DO 19 J = KP1,N
   19 SUM = W(IP,J)*X(J) + SUM
   20 X(K)= (X(K) - SUM) / W(IP,K)
      RETURN
      END
      SUBROUTINE TOTAL(NUN,NC1,NE,NJF,NL,OM,RO,NOE)
C
C
C     THIS SUBROUTINE GENERATES THE TOTAL DYNAMIC STIFFNESS MATRIX OF
C     THE SOIL MODEL
C
C
C     NUN          TOTAL NUMBER OF UNKNOWNS
C     NC1          FIRST COMMON NODE NUMBER BETWEEN THE SOIL AND THE
C                  FOUNDATION
C     NE           TOTAL NUMBER OF ELEMENTS
C     NJF          TOTAL NUMBER OF FOURIER HARMONICS
C     NL           TOTAL NUMBER OF LAYERS
C     OM           FRIQUANCY OF THE EXCITING MOTION
C     RO           THE VERTICAL BOUNDARY RADIUS
C     NOE          PRINT OUT PARAMETER   IF NOE = 0 NO INTERMIDIAT RESULTS
C                  TO BE PRINTED OUT
C
      DIMENSION SSL(25,25),AMM(9,9),DMM(9,15),STIFF(5),AMASS(5),DAMP(5)
      COMMON EM1(24,24),SM1(24,24),AA(9,9),AD(9,9),AE(9,9),AS(9,9),
     $       AAA(36,36),ADD(36,36),AEE(36,36),AQQ(36,36),ASS(36,36),
     $       RSS(36,36),Y(36,36),Z(36,36),H0(36),H1(36),E(36),DD(36),
     $       RX(24,8),ZX(24,8),ALAMDA(24),AMUE(24),RUE(24),ALA(6),RU(6),
     $       RCOL(4),AMU(6),H(6),DR(2),SM(190,190),ND(80,3),NI(20,8),
     $       NV(12),NRS(36),MP(20,24)
C
      DO 14 JF = 1,NJF
      JA = JF - 1
      WRITE(6,60) JA
C
      DO 16 I = 1,NUN
      DO 16 J = 1,NUN
   16 SM(I,J) = 0.
C
      DO 17 N = 1,NE
      CALL ELMNT(N,JA)
      IF (NI(N,3) . NE . NV(1)) GO TO 13
      BW = RX(N,3) - RX(N,1)
      DO 12 I = 1,15
      II = 9 + I
      DO 12 J = 1,15
      JJ = 9 + J
   12 AAA(I,J) = EM1(II,JJ)
      CALL INV(15)
      DO 11 I = 1,9
      DO 11 J = 1,15
      DMM(I,J) = 0.
      DO 11 K = 1,15
      KK = 9 + K
   11 DMM(I,J) = DMM(I,J) + EM1(I,KK) * AAA(K,J)
      DO 10 I = 1,9
      DO 10 J = 1,9
      AMM(I,J) = 0.
      DO 10 K = 1,15
      KK = 9 + K
   10 AMM(I,J) = AMM(I,J) - DMM(I,K) * EM1(KK,J)
      DO 9 I = 1,9
      DO 9 J = 1,9
    9 AMM(I,J) = AMM(I,J) + EM1(I,J)
C
C     CALCULATION OF TOTAL STIFFNESS MATRIX
C
   13 DO 22 KK = 1,24
      IF(MP(N,KK) . EQ . 0) GO TO 22
      I = MP(N,KK)
      DO 23 KJ = 1,24
      IF(MP(N,KJ) . EQ . 0) GO TO 23
      J = MP(N,KJ)
      SM(I,J)  =  SM(I,J)  +  SM1(KK,KJ) - EM1(KK,KJ) * OM * OM
   23 CONTINUE
   22 CONTINUE
   17 CONTINUE
      IF(JA . EQ . 0) EAII = 10.E-09
      IF(JA . GT . 0) EAII = 10.E-10
      IF(NOE . EQ . 0) GO TO 15
      WRITE(6,62)
      WRITE(6,66)((SM(I,J),J=1,NUN),I=1,NUN)
   15 CALL FAR (JA,NL,OM,RO,NOE)
      NT = 6 * NL
      DO 20 KK = 1,NT
      DO 20 KJ = 1,NT
      I = NRS(KK)
      J = NRS(KJ)
      SM(I,J) = SM(I,J) + RSS(KK,KJ)
   20 CONTINUE
      DO 18 I = 1,NUN
   18 IF (SM(I,I) . LT . 0.) SM(I,I) = -SM(I,I)
      DO 19 I = 2,NUN
      IM1 = I - 1
      DO 19 J = 1,IM1
   19 SM(I,J) = SM(J,I)
      IF (NOE . EQ . 0) GO TO 24
```

```
C
      WRITE(6,61)
      WRITE(6,66)((SM(I,J),J=1,NUN),I=1,NUN)
C
C     CONDENSATION OF THE STIFFNESS MATRIX
C
   24 N11 = NRS(3)
      N22 = NUN - N11
      DO 30 I = 1,N11
      DO 30 J = 1,N11
   30 SSL(I,J) = SM(I,J)
      DO 48 I = 1,N11
      DO 48 J = 1,36
      K = N11 + J
      L = N11 + J + 36
      M = N11 + J + 72
      KK= N11 + J + 108
      LL= N11 + J + 144
      IF (K . GT . NUN) GO TO 48
      AAA(I,J) = SM(I,K)
      IF (L . GT . NUN) GO TO 48
      ADD(I,J) = SM(I,L)
      IF (M . GT . NUN) GO TO 48
      AEE(I,J) = SM(I,M)
      IF (KK . GT . NUN) GO TO 48
      AQQ(I,J) = SM(I,KK)
      IF (LL . GT . NUN) GO TO 48
      ASS(I,J) = SM(I,LL)
   48 CONTINUE
      DO 31 I = 1,N22
      K = N11 + I
      DO 31 J = 1,N22
      L = N11 + J
   31 SM(I,J) = SM(K,L)
C
      CALL INVS(N22)
C
      DO 49 II = 1,N22
      I = N22 - II + 1
      K = N11 + I
      DO 49 JJ = 1,N22
      J = N22 - JJ + 1
      L = N11 + J
   49 SM(K,L) = SM(I,J)
      DO 50 I = 1,N11
      DO 50 J = 1,N11
   50 SM(I,J) = SSL(I,J)
      DO 51 I = 1,N11
      DO 51 J = 1,36
      K = N11 + J
      L = N11 + J + 36
      M = N11 + J + 72
      KK= N11 + J + 108
      LL= N11 + J + 144
      IF (K . GT . NUN) GO TO 51
      SM(I,K) = AAA(I,J)
      IF (L . GT . NUN) GO TO 51
      SM(I,L) = ADD(I,J)
      IF (M . GT . NUN) GO TO 51
      SM(I,M) = AEE(I,J)
      IF (KK. GT . NUN) GO TO 51
      SM(I,KK)= AQQ(I,J)
      IF (LL. GT . NUN) GO TO 51
      SM(I,LL)= ASS(I,J)
   51 CONTINUE
      DO 37 I = 1,N11
      JJ = I
      DO 32 J = 1,N22
      II = N11 + J
      SM(II,JJ) = 0.
      DO 32 K = 1,N22
      KK = N11 + K
   32 SM(II,JJ) = SM(II,JJ) + SM(I,KK) * AAA(K,J)
      DO 33 I = 1,N11
      DO 33 J = 1,N11
      SSL(I,J) = 0.
      DO 33 K = 1,N22
      KK = N11 + K
   33 SSL(I,J) = SSL(I,J) - SM(KK,I) * SM(J,KK)
      DO 34 I = 1,N11
      DO 34 J = 1,N11
   34 SSL(I,J) = SSL(I,J) + SM(I,J)
      IF(NOE . EQ . 0) GO TO 44
C
      WRITE(6,63)
      DO 35 I = 1,N11
   35 WRITE(6,66)(SSL(I,J),J=1,N11)
C
C     IMPEDENCE MATRIX
C
   44 NSTA = (NCI - 1) * 3 - 1
      IF (NCI . EQ . 1) NSTA = 1
      NCOM = N11 - NSTA + 1
C
      DO 36 I = 1,N22
      DO 36 J = 1,N22
   36 AAA(I,J) = 0.
      DO 37 I = 1,N11
      DO 37 J = 1,N11
   37 AAA(I,J) = SSL(I,J)
      CALL INV(N11)
      DO 38 I = 1,N11
      DO 38 J = 1,N11
      SSL(I,J) = AAA(I,J)
   38 AAA(I,J) = 0.
      M = NCOM
      DO 39 I = 1,M
   39 AAA(I,I) = 1.0
C
      CALL LEQTIC(SSL,M,M,AAA,M,M,0,WA,IER)
C
      DO 40 I = 1,M
      DO 40 J = 1,M
      ASS(I,J) = REAL(AAA(I,J))
   40 OMM(I,J) = AIMAG(AAA(I,J)) / OM
C
      WRITE(6,64)
      WRITE(6,69)((AMM(I,J),J=1,NCOM),I=1,NCOM)
C
      WRITE(6,65)
      WRITE(6,69)((SSL(I,J),J=1,NCOM),I=1,NCOM)
C
C
C     STIFF. , MASS AND DAMPING AT THE LOWER FIVE DOF FOR THE RING FOOTING
C
C
      DO 41 I = 1,3
      J = I + 3
      K = I + 6
      STIFF(I) = ASS(I,I) + ASS(J,J) + ASS(K,K)
      DAMP(I)  = OMM(I,I) + OMM(J,J) + OMM(K,K)
   41 AMASS(I) = AMM(I,I) + AMM(J,J) + AMM(K,K)
      STIFF(4) = (ASS(2,2) + ASS(8,8)) * BW / 2.
      DAMP(4)  = (OMM(2,2) + OMM(8,8)) * BW / 2.
      AMASS(4) = (AMM(2,2) + AMM(8,8)) * BW / 2.
      STIFF(5) = (ASS(3,3) + ASS(9,9)) * BW / 2.
      DAMP(5)  = (OMM(3,3) + OMM(9,9)) * BW / 2.
      AMASS(5) = (AMM(3,3) + AMM(9,9)) * BW / 2.
      DO 42 I = 1,5
   42 DD(I) = SQRT(STIFF(I) / AMASS(I))
C
      WRITE(6,67)
      WRITE(6,68)(DD(I),I=1,5)
C
      DO 43 I = 1,5
   43 E(I) = DD(I)
      M = 0
      DO 45 I = 1,5
      SMAL = 0.5E 20
      DO 46 J = 1,5
      IF(J . EQ . M) E(J) = 0.5E 20
      IF (SMAL . GT . E(J)) K = J
      IF (SMAL . GT . E(J)) SMAL = E(J)
   46 CONTINUE
      M = K
      DD(I) = SMAL
   45 CONTINUE
C
C
      DDS = (DD(5) + DD(1)) * (DD(5) - DD(1))
      C0 = 2. * (DD(1)*DD(5)) * (DD(5)*DR(1) - DD(1)*DR(2)) / DDS
      C1 = 2. * (DD(5)*DR(2) - DD(1)*DR(1)) / DDS
      DO 47 I = 1,5
   47 DAMP(I) = C0 * AMASS(I)  +  C1 * STIFF(I)
      WRITE(6,600)
      WRITE(6,68)(STIFF(I),I=1,5)
      WRITE(6,601)
      WRITE(6,68)(AMASS(I),I=1,5)
      WRITE(6,602)
      WRITE(6,68) (DAMP(I),I=1,5)
C
   14 CONTINUE
C
      RETURN
C
C
C     FORMAT STATEMENTS  .....
C
   60 FORMAT(1H1,/////////////////////////40X,'*** HARMONIC NO',I3,' ***'/
     $44X,'---------------'  )
   61 FORMAT(1H1,2X,'TOTAL  STIFFNESS  MATRIX  OF  THE  SOIL  MODEL',///
     $/)
   62 FORMAT(1H1,2X,'STIFFNESS MATRIX OF THE FINITE ELEMENT CORE',////)
   63 FORMAT(1H1,2X,'CONDENSED STIFFNESS MATRIX OF THE SOIL MODEL',////)
   64 FORMAT(1H1,2X,'CONDENSED MASS MATRIX AT THE COMMON DEGREES O. F.'/
     $/// )
   65 FORMAT(1H1,2X,'IMPEDENCE STIFFNESS MATRIX'//// )
   66 FORMAT(/2X,8E13.6)
   67 FORMAT(1H1,3X,'NATURAL FREQUENCIES OF THE SOIL'////10X,'U',14X,'W'
     $,14X,'V',12X,'THITA',11X,'FAY'    )
   68 FORMAT(//2X,5E15.7)
   69 FORMAT(2X,9E14.7///)
  600 FORMAT(///////4X,'STIFFNESSES OF THE EQUIVALENT SPRINGS ...'  )
  601 FORMAT(///////4X,'EQUIVALENT MASSES OF THE SOIL ...'  )
  602 FORMAT(///////4X,'EQUIVALENT DAMPING ELEMENTS OF THE SOIL ...'  )
C
      END
      SUBROUTINE TQL2(NM,N,D,E,Z,IERR)
C
C
      INTEGER I,J,K,L,M,N,II,L1,NM,MML,IERR
      REAL D(N),E(N),Z(NM,N)
      REAL B,C,F,G,H,P,R,S
      REAL SQRT,ABS,SIGN
      REAL MACHEP
C
C     ********* MACHEP IS A MACHINE DEPENDENT PARAMETER SPECIFYING THE
C               RELATIVE PRECISION OF FLOATING POINT ARITHMETIC ******0*
      MACHEP = 6.
C
      IERR = 0
      IF (N .EQ. 1) GO TO 1001
C
      DO 100 I = 2,N
  100 E(I-1) = E(I)
C
      F = 0.
      B = 0.
      E(N) = 0.
C
      DO 240 L = 1,N
      J = 0
      H = MACHEP * (ABS(D(L)) + ABS(E(L)))
      IF (B .LT. H) B = H
C     ********* LOOK FOR SMALL SUB-DIAGONAL ELEMENT *********
      DO 110 M = L,N
      IF (ABS(E(M)) .LE. B) GO TO 120
C     ********* E(N) IS ALWAYS ZERO, SO THERE IS NO EXIT THROUGH THE
C               BOTTOM OF THE LOOP *********
  110 CONTINUE
C
  120 IF (M .EQ. L) GO TO 220
  130 IF (J .EQ. 50) GO TO 1000
      J = J + 1
C     ********* FORM SHIFT *********
      L1 = L + 1
      G = D(L)
```

```
      P = (D(L1) - G) / (2.0 * E(L))
      R = SQRT(P*P + 1.0)
      D(L) = E(L) / (P + SIGN(R,P))
      H = G - D(L)
C
      DO 140 I = L1,N
  140 D(I) = D(I) - H
C
      F = F + H
C     ******** QL TRANSFORMATION ********
      P = D(M)
      C = 1.0
      S = 0.0
      MML = M - L
C     ******** FOR I=M-1 STEP -1 UNTIL L DO -- ********
      DO 200 II = 1,MML
      I = M - II
      G = C * E(I)
      H = C * P
      IF (ABS(P) .LT. ABS(E(I))) GO TO 150
      C = E(I) / P
      R = SQRT(C*C + 1.0)
      E(I+1) = S*P*R
      S = C / R
      C = 1.0 / R
      GO TO 160
  150 C = P / E(I)
      R = SQRT(C*C + 1.0)
      E(I+1) = S * E(I) * R
      S = 1.0 / R
      C = C * S
  160 P = C * D(I) - S * G
      D(I+1) = H + S * (C * G + S * D(I))
C     ******** FORM VECTOR ********
      DO 180 K = 1,N
      H = Z(K,I+1)
      Z(K,I+1) = S * Z(K,I) + C * H
      Z(K,I) = C * Z(K,I) - S * H
  180 CONTINUE
C
  200 CONTINUE
C
      E(L) = S * P
      D(L) = C * P
      IF (ABS(E(L)) .GT. B) GO TO 130
  220 D(L) = D(L) + F
  240 CONTINUE
C     ******** ORDER EIGENVALUES AND EIGENVECTORS ********
      DO 300 II = 2,N
      I = II - 1
      K = I
      P = D(I)
C
      DO 260 J = II,N
      IF (D(J) .GE. P) GO TO 260
      K = J
      P = D(J)
  260 CONTINUE
C
      IF (K .EQ. I) GO TO 300
      D(K) = D(I)
      D(I) = P
C
      DO 280 J = 1,N
      P = Z(J,I)
      Z(J,I) = Z(J,K)
      Z(J,K) = P
  280 CONTINUE
C
  300 CONTINUE
C
      GO TO 1001
C     ******** SET ERROR -- NO CONVERGENCE TO AN EIGENVALUE AFTER 50
C                ITERATIONS * ******
 1000 IERR = L
 1001 RETURN
      END
      SUBROUTINE TRED2(NM,N,A,D,E,Z)
C
C
      INTEGER I,J,K,L,N,II,NM,JP1
      REAL A(NM,N),D(N),E(N),Z(NM,N)
      REAL F,G,H,HH,SCALE
      REAL SQRT,ABS,SIGN
C
      DO 100 I = 1,N
C
      DO 100 J = 1,I
      Z(I,J) = A(I,J)
  100 CONTINUE
C
      IF (N .EQ. 1) GO TO 320
C     ******** FOR I = N STEP -1 UNTIL 2 DO -- ********
      DO 300 II = 2,N
      I = N + 2 - II
      L = I - 1
      H = 0.
      SCALE = 0.
      IF (L .LT. 2) GO TO 130
C     ******** SCALE ROW (ALGOL TOL THEN NOT NEEDED) ********
      DO 120 K = 1,L
  120 SCALE = SCALE + ABS(Z(I,K))
C
      IF (SCALE .NE. 0.) GO TO 140
  130 E(I) = Z(I,L)
      GO TO 290
C
  140 DO 150 K = 1,L
      Z(I,K) = Z(I,K) / SCALE
      H = H + Z(I,K) * Z(I,K)
  150 CONTINUE
C
      F = Z(I,L)
      G = -SIGN(SQRT(H),F)
      E(I) = SCALE * G
      H = H - F * G
      Z(I,L) = F - G
      F = 0.
C
      DO 240 J = 1,L
      Z(J,I) = Z(I,J) / H
      G = 0.
C     ******** FORM ELEMENT OF A*U ********
      DO 180 K = 1,J
  180 G = G + Z(J,K) * Z(I,K)
C
      JP1 = J + 1
      IF (L .LT. JP1) GO TO 220
C
      DO 200 K = JP1,L
  200 G = G + Z(K,J) * Z(I,K)
C     ******** FORM ELEMENT OF P ********
  220 E(J) = G / H
      F = F + E(J) * Z(I,J)
  240 CONTINUE
C
      HH = F / (H + H)
C     ******** FORM REDUCED A ********
      DO 260 J = 1,L
      F = Z(I,J)
      G = E(J) - HH * F
      E(J) = G
C
      DO 260 K = 1,J
      Z(J,K) = Z(J,K) - F * E(K) - G * Z(I,K)
  260 CONTINUE
C
  290 D(I) = H
  300 CONTINUE
C
  320 D(1) = 0.
      E(1) = 0.
C     ******** ACCUMULATION OF TRANSFORMATION MATRICES ********
      DO 500 I = 1,N
      L = I - 1
      IF (D(I) .EQ. 0.) GO TO 380
C
      DO 360 J = 1,L
      G = 0.
C
      DO 340 K = 1,L
  340 G = G + Z(I,K) * Z(K,J)
C
      DO 360 K = 1,L
      Z(K,J) = Z(K,J) - G * Z(K,I)
  360 CONTINUE
C
  380 D(I) = Z(I,I)
      Z(I,I) = 1.0
      IF (L .LT. 1) GO TO 500
C
      DO 400 J = 1,L
      Z(I,J) = 0.
      Z(J,I) = 0.
  400 CONTINUE
C
  500 CONTINUE
C
      RETURN
      END
```

APPENDIX 8.4

Modifications and Additions For User's Manual Of SHORE-III Program

In this appendix, only the necessary modifications and additions to the user's manual of SHORE-III program (40) are presented to make it applicable for SHORSS program. To introduce the soil effects in the form of the Equivalent Boundary System, modifications to number of subroutines in SHORE-III are carried out. These subroutines are: DATA1, DATA2, ESOT, GLMX, LISTID and SOLV (see the overlay structure in Figure 12). These modifications necessitate the input data to be changed in some sections of the twelve data sections of SHORE-III (40). However, new limitations are introduced as a result to the new options in SHORSS program. These limitations are given in this appendix as well.

INPUT DATA

Given below are the modifications and additions to the input data of SHORE-III to suit SHORSS:

B. Problem Control Card

The format of Problem Control Card will be as follows:

Columns	Format	Entry
1-5	I5	Number of finite elements to be used (Maximum 47)
6-40	......UNCHANGED.....	
41-45	I5	1 or 0, refers to EBS

The flag 1 in the ninth field signifies that the soil effect is to be considered in the analysis and the equivalent boundary system values should be supplied for each harmonic. Otherwise, no EBS to be supplied and SHORSS becomes SHORE-III program in this case. It should be noted that the soil effect is limited to the dynamic analysis only, therefore, columns 41 to 45 should be left blank in static analysis problems.

D. Nodal Point Cards

If columns 41-45 in the problem control card are not left blank no geometric constraints at last node are required. Thus, it is necessary to leave columns 16 to 45 blank for the last nodal point card.

I. Loading Information Cards

As the EBS components must be supplied for each Fourier harmonic they are introduced in this section. Thus, for each harmonic, there shall be one title card, the 'load title card', followed by a control card, the 'loading control card', followed by three cards,'the EBS cards' if columns 41-45 in the problem control card are not left blank. These cards are followed by the loading cards as usual.

The format of the first card of the EBS cards, the stiffness elements card, for each harmonic will be as follows:

Columns	Format	Entry
1-15	E15.6	Fourier coefficient for the stiffness element in u-direction at $\theta = 0°$ (or $\theta = 90°$)
16-30	E15.6	Fourier coefficient for the stiffness element in v-direction at $\theta = 90°$ (or $\theta = 0°$)
31-45	E15.6	Fourier coefficient for the stiffness element in w-direction at $\theta = 0°$ (or $\theta = 90°$)
46-60	E15.6	Fourier coefficient for the stiffness element in β_ϕ direction at $\theta = 0°$ (or $\theta = 90°$)
61-75	E15.6	Fourier coefficient for the stiffness element in β_θ direction at $\theta = 90°$ (or $\theta = 0°$)

The format of the second and third cards are like the first card except the entry will be the damping elements in the second and the mass elements in the third. However, the mass elements for all Fourier harmonic are the same, it is necessary to supply the mass card for each harmonic.

OUTPUT

The only change in the output format of the program is in the program title printout at the beginning of the output, SHORSS title instead of SHORE-III title, and a statement to be printed with the nodal point constraints to describe the type of the boundary at the shell base.

SYSTEM CONTROL CARDS

The image of system control cards used to run SHORSS from permanent file (WU650E.SHORSS) at Washington University Computing Facility, using an IBM 370 computer, is the same as those given in Appendix A of Reference (40) except the first two cards should be replaced by:

```
//SHORSTST JOB (65587,1466,20),'OSAMA', CLASS=N, TIME=20
//A EXEC FORTRAN,LIBRARY='WU650E.SHORSS',PROGRAM=SHORSS
```

9. BIBLIOGRAPHY

1. "Analysis for Soil-Structure Interaction Effects for Nuclear Power Plants", Report by the Ad Hoc Group in Soil-Structure International, Nuclear Structures and Material Committee of the Structure Division, ASCE (draft) Dec. 5, 1975.

2. Vaish, A. K. and Chopra, A. K., "Earthquake Finite Element Analysis of Structure-Foundation Systems", Journal of Engineering Mechanics Division, ASCE, Vol. 108, No. EM6, Dec. 1974, pp. 1101-1116.

3. Chopra, A. K. and Gutierrez, J. A., "Earthquake Response Analysis of Multistory Buildings Including Foundation Interaction", International Journal of Earthquake Engineering and Structural Dynamics, Vol. 3, 1974, pp. 65-77.

4. Veletsos, A. S., "Dynamics of Structure-Foundation Systems", Presented at the Symposium on Structural and Geotechnical Mechanics Honoring Nathan M. Newmark, Univ. of Illinois, Urbana, Champaign, Oct. 2 & 3, 1975.

5. Brombolich, L. and Gould, P. L., "High-Precision Finite Element Analysis of Shells of Revolution", Research Report No. 16, Structural Division, Washington University, St. Louis, MO, Feb. 1971.

6. Sen, S., Gould, P. and Suryoutomo, H., "High-Precision Static and Dynamic Finite Element Analysis of Shells of Revolution with Application to Hyperboloidal Shells on Discrete Supports", Research Report No. 23, Structural Division, Washington University, St. Louis, MO., Nov. 1973.

7. Gould, P. L., Szabo, B. A. and Suryoutomo, H. B., "Curved Rotational Shell Elements by the Constraint Method", Proceedings of the International Conference on Variational Methods in Engineering, Vol. II, Southampton University, England, Sept. 1972, pp. 8/33-8/42.

8. Kausel, E., Roesset, J. M. and Waas, G., "Dynamic Analysis of Footing on Layered Media", Journal of Engineering Mechanics Division, ASCE, Vol. 101, No. EM5, Oct. 1975, pp. 679-693.

9. Luco, J. E. and Westmann, R.A., "Dynamic Response of Circular Footing" Journal of Engineering Mechanics Division, ASCE, No. EM5, Oct. 1971, pp. 1381-1395.

10. Novak, M., "Effect of Soil on Structural Response to Wind and Earthquake", International Journal of Earthquake Engineering and Structural Dynamics, Vol. 3, 1974, pp. 79-96.

11. Bielak, J., "Modal Analysis for Building-Soil Interaction", Journal of Engineering Mechanics Division, ASCE, Vol. 102, No. EM5, Oct. 1976, pp. 771-786.

12. Rainer, J. H., "Damping in Dynamic Structure-Foundation Interaction", Canadian Geotechnical Journal, Vol. 12, 1975, pp. 13-22.

13. Roesset, J. M., Whitman, R. V. and Dobry, R., "Modal Analysis for Structure with Foundation Interaction", Journal Structure Division, ASCE, Vol. 99, No. ST3, Proceedings Paper 9603, March 1973, pp. 399-416.

14. Tsai, N. C., "Modal Damping for Soil-Structure Interaction", Journal of the Engineering Mechanics Division, ASCE, Vol. 100, No. EM2, Proceedings Paper 10490, April 1974, pp. 323-341.

15. Clough, R. and Mojtahedi, S., "Earthquake Response Analysis Considering Non-Proportional Damping", International Journal of Earthquake Engineering and Structural Dynamics, Vol. 4, 1976, pp. 489-496.

16. Pandya, V. and Setlar, A. Y., "Seismic Soil-Structure Interaction by Finite Elements: Case Studies", Proceedings of the 2nd ASCE Specialty Conference on Structural Design of Nuclear Plant Facilities, Vol. 1-A, Dec. 1975, pp. 826-848.

17. Penzien, J., "Soil-Pile Foundation Interaction", Earthquake Engineering, Wiegel, Prentice-Hall, 1970.

18. Veletsos, A. S. and Nair, V., "Seismic Interaction of Structures on Hystretic Foundations", Journal of the Structural Division, ASCE, ST1, Jan. 1975, pp. 109-129.

19. Scanlan, R. C., "Seismic Wave Effects on Soil-Structure Interaction", International Journal of Earthquake Engineering and Structural Dynamics, Vol. 4, 1976, pp. 379-388.

20. Akiyoshi, T., "Compatible Viscous Boundary for Discrete Models", Journal of the Engineering Mechanics Division, ASCE, No. EM5, Oct. 1978, pp. 1253-1266.

21. Kausel, E., "Forced Vibration of Circular Foundation on Layered Media", MIT Research Report R74-11, Soils Publication No. 336, Structures Publication No. 38, Massachusetts Institute of Technology, Cambridge, Mass., Jan., 1974.

22. Luco, J. E., Wong, H. L. and Trifunac, M. D., "A Note on the Dynamic Response of Rigid Embedded Foundations", International Journal of Earthquake Engineering and Structural Dynamics, Vol. 4, 1975, pp. 119-127.

23. Arnold, R. N., Bycroft, G. N., Warburton, G. B., "Forced Vibrations of a Body on an Infinite Elastic Solid", Journal of Applied Mechanics, No. 77, pp. 391-401, 1955.

24. Veletsos, A. S. and Verbic, B., "Dynamics of Elastic and Yielding Structure-Foundation Systems", Proceedings Fifth World Conference on Earthquake Engineering, Rome, Italy, pp. 2610-2613.

25. Veletsos, A. and Wei, Y., "Lateral and Rocking Vibration of Footings", Journal of the Soil Mechanics and Foundation Division, ASCE, Vol. 97, Sept. 1971.

26. Veletsos, A. and Meek, J., "Dynamic Behaviour of Building-Foundation Systems", International Journal of Earthquake Engineering and Structural Dynamics, Vol. 3, 1974, pp. 121-138.

27. White, J. E., "Seismic Waves: Radiation, Transmission and Attenuation", McGraw-Hill, 1965.

28. Bullen, K. E., "An Introduction to the Theory of Seismology", Cambridge Press, 1963.

29. Ewing, W. M., Jardetsky, W. S. and Press, F., "Elastic Waves in Layered Media", McGraw-Hill, New York, 1957.

30. Langhaar, H. L., "Energy Methods in Applied Mechanics", J. Wiley and Sons, 1962.

31. Zienkewics, D. C., "The Finite Element Method in Engineering Science", McGraw-Hill, 1971.

32. Wilson, E., "Structural Analysis of Axisymmetric Solids", AIAA Journal, Vol. 3, No. 12, Dec. 1965, p. 2269.

33. Gould, P. L., Sen, S.K. and Suryoutomo, H., "Dynamic Analysis of Column-Supported Hyperboloidal Shells", International Journal of Earthquake Engineering and Structural Dynamics, Vol. 2, No. 3, January-March, 1974, pp. 269-280.

34. Sen, S. K. and Gould, P. L., "Criteria for Finite Element Discretization of Shells of Revolution", International Journal Numerical Methods Engineering, Vol. 6, 1973, pp. 265-274.

35. Basu, P. K., "Dynamic and Non-Linear Analysis of Shells of Revolution", Dissertation presented to Sever Institute of Technology, Washington University, St. Louis, Mo., March 1977.

36. Cook, R. D., "Concepts and Applications of Finite Element Analysis", John Wiley and Sons, Inc., 1974.

37. Wylie, C. R., "Advanced Engineering Mathematics", McGraw Hill, Fourth Edition, 1975.

38. Krätzig, W. B., Personal Communication.

39. Karadeniz, H., "The Theoretical and Experimental Dynamic Analysis of Thin Shells of Revolution", A Dissertation submitted for the Degree of Doctor of Philosophy in Engineering in the University of Bristol, England, May 1976.

40. Basu, P. K. and Gould, P. L., "SHORE-III, Shell of Revolution Finite Element Program - User's Manual", Research Report No. 49, Structural Division, Washington University, St. Louis, Mo., Sept. 1977.

41. Basu, P. K. and Gould, P. L., "SHORE-III, Shell of Revolution Finite Element Program - Theoretical Manual", Research Report No. 48, Structural Division, Washington University, St. Louis, Mo., Sept. 1977.

42. Gould, P. L. and El-Shafee, O. M., "Local Stress Analysis of Discretely Supported Rotational Shells: Method and Computer Program", Engineering Structures (in press).

43. Newmark, N. M., "A Method of Computation for Structural Dynamics", Proceedings ASCE, 85, EM3, 1959, pp. 67-94.

44. Bath, K. J. and Wilson, E. L., "Stability and Accuracy of Direct Integration Methods", International Journal Earthquake Engineering and Structural Dynamics, Vol. 1, 1973, pp. 283-291.

45. Wigel, R., "Earthquake Engineering", Prentice-Hall, Inc., Englewood Cliffs, N. J., 1970.

46. Wilson, E. L., Farhoad, A. and Bathe, K. J., "Non-Linear Dynamic Analysis of Complex Structures", International Journal Earthquake Engineering and Structural Dynamics, Vol. 1, 1973, pp. 241-252.

47. Lysmer, J., and Richart, F. E., Jr., "Dynamic Response of Footings to Vertical Loading", Journal of the Soil Mechanics and Foundations Division, ASCE, Vol. 92, No. SM1, Proceedings Paper 4592, Jan., 1966, pp. 65-91.

48. Lysmer, J. and Kuhlemeyer, R. L., Finite Dynamic Model for Infinite Media", Journal for Engineering Mechanics Division, ASCE, No. EM4, Aug., 1969, pp. 859-877.

49. Wong, H. L. and Luco, J. E., "Dynamic Response of Rigid Foundations of Arbitrary Shape", International Journal Earthquake Engineering and Structural Dynamics, Vol. 4, 1976, pp. 579-587.

50. Gould, P. L., "Static Analysis of Shells", Lexington Books, D. C. Heath and Company, 1977.

51. "Reinforced Concrete Cooling Tower Shells-Practice and Commentary", Report by ACI-ASCE Committee 334, ACI Journal, January 1977.

52. Lambe, T. W. and Whitman, R. V., "Soil Mechanics", John Wiley & Sons, Inc., 1969.

53. ICES STRUDL-II "The Structural Design Language-Engineering User's Manual", Vol. 1, MIT, Department of Civil Engineering, Cambridge, Mass., 1968.

54. Fagel, L. W. and Liu, S-C., "Earthquake Interaction for Multi-story Buildings", Journal for Engineering Mechanics Division, ASCE, Vol. 98, No. EM4, Aug. 1972, pp. 929-945.